The Investigation of Tube Sampling Disturbance using Transparent Soil and Particle Image Velocimetry

by

Eyre deDanaan Fogarty Hover, MEng (Hons)

A thesis submitted in partial fulfilment of the requirements for the degree of Doctor of Philosophy in Engineering

School of Engineering,

University of Warwick

March 2014

Table of Contents

List of Figures

List of Appendix Figures

List of Tables

Acknowledgements

The completion of this research was made possible by a great many people, all of whom I will forever be indebted to.

First and foremost, to my son Belièv, for your patience during these past years, thank you! Many thanks also to Damien for your endless encouragement and (IT) support – to you both I am extremely grateful.

I want to thank Dr Qing Ni, my supervisor, for his encouragement, enthusiasm and support during the past three and a half years, and for the time and effort he has dedicated to this project and to me.

Many thanks also to the following staff in the School of Engineering: to Professor Ian Guymer, for his insightful feedback and opinions, to Colin Banks, for help in the geotechnical laboratory and for getting me involved in teaching, to Richard Kasler for help with CAD design, to Kerrie Hatton for all the help and support, and to the workshop staff for manufacturing the numerous items this project required. I am also grateful to the School of Engineering and the EPSRC for the funding for this work.

And finally, because the completion of a PhD is as much a technical and intellectual exercise as it is a personal challenge, I am grateful to those around me who through their understanding and friendship made the process a little easier. I cannot possibly list them all but especially want to thank Madison Clough, Gareth Weightman, my grandmother, Dr Carol Hover, and once again, Dr Qing Ni.

Declaration

This thesis is submitted to the University of Warwick in support of my application for the degree of Doctor of Philosophy. It has been composed by myself and has not been submitted in any previous application for any degree. The work presented (including data generated and data analysis) was carried out by the author.

Parts of this thesis have been published by the author:

Hover, E.D., Ni, Q. and Guymer, I. (2012). Investigation of tube sampling disturbance using Transparent Soil and Particle Image Velocimetry. In: *Proceedings from the 11th Australia – New Zealand Conference on Geomechanics, Melbourne*

Hover, E.D., Ni, Q. and Guymer, I. (2013). Investigation of Centreline Strain Path during Tube Penetration using Transparent Soil and Particle Image Velocimetry. *Géotechnique Letters*, **3** (2)

Hover, E.D., Ni, Q. and Guymer, I. (2013). Physical Modelling of Tube Sampling Disturbance in Clays. In: *Proceedings of the 5th International Young Engineers' Conference, Paris*, 415-418

Summary

A small-scale physical modelling system was developed and employed to investigate the effects of tube sampling. Amorphous silica and an oil blend of matching refractive index were mixed to form a transparent soil. Black glass beads were embedded within the soil body on the vertical central plane. After consolidation in a Perspex box, a glass model sampler was pushed into the transparent soil. Movements within the soil body were recorded using digital photography; these images were later analysed by Particle Image Velocimetry. The centreline strain path (CSP) of the sample during tube penetration was calculated and compared to existing analytical and numerical models' strain predictions, and some degree of correlation was observed. However, it is shown that the CSP is not constant throughout the sample, but varies with depth below the base of the borehole. It was also noticed that after tube penetration, significant residual extensive strains remain for soil on the centreline of the specimen. Different tube geometries were tested and a correlation was found between strain magnitudes and the Area Ratio, Inside Clearance Ratio and the Outer Cutting Edge Taper Angle. It was also found that samples taken in normally consolidated soils were more heavily disturbed than those in lightly overconsolidated soils. After removal from the soil model, samples were stored for six months and volumetric strains within them, set up by a redistribution of pore fluid pressures, were found to be small, typically less than 1%. Soil at the edge of the sampler wall reduced in volume, while the centre swelled. Specimens were thereafter extruded from the sampling tube and the strain path created by this step was quantified. It was found that extrusion compresses the soil while still inside the tube, with soil closest to the extruder more significantly affected. All of these parts of the sampling process contribute to the overall sample disturbance and can therefore have an effect on the sample's measured properties.

Symbols

a	line gradient
A	Area
A_o	Original Area
A_u	Skempton and Sowa's (1963) pore pressure parameter
B	Tube outer diameter
c	Cohesion
c'	Effective cohesion
C_u	Undrained shear strength
d	Horizontal distance from the centreline of the sampler
D_c	Inner Diameter of the cutting edge
dm	Magnified dimension, in object-space
dmp	Magnified dimension, in image-space
D_o	Outer Diameter of the sampling tube
dr	Real dimension, in object-space
D_s	Inner Diameter of the sampling tube
D_w	Outer Diameter of the cutting edge
E	Young's modulus, rigidity
e	Void ratio
e_o	Original void ratio
F	Frictional force
f	Light intensity 1
g	Light intensity 2
H	Height
k	Single lens distortion coefficient
K	Overall lens distortion coefficient
K_o	Coefficient of earth pressure
L	Length
L_d	Length of sample after driving
l_f	IA spacing, final
L_o	Length of sample before driving
l_o	IA spacing, initial
N	Normal force
n	see RI
p	Mean normal stress
p'	Effective mean normal stress
P	Tensile strength
P'	Preconsolidation pressure
Q	Driving force

q	Deviatoric stress
Q_p	Edge resistance
r_d	Distance to centre, in distorted terms
RI	Refractive Index
R_r	Recovery Ratio
r_u	Distance to centre, in real terms
s'	Effective mean normal stress
t	Thickness
U	Water or air pressure
u	Pore pressure
v	Vertical displacement vector
W	Width
w	Water content
x	x coordinate
x_c	Centre of image, x coordinate
x_d	Distorted x coordinate
x_i	Initial x coordinate
x_f	Final x coordinate
x_u	Corrected or original x coordinate
y	y coordinate
Y1	Yield Surface 1
Y2	Yield Surface 2
Y3	see BS
y_c	Centre of image, y coordinate
y_d	Distorted y coordinate
y_i	Initial y coordinate
y_f	Final y coordinate
y_u	Corrected or original y coordinate
z	depth over tube cutting edge
Δ	Change
ε	Strain
ε_o	Volumetric strain
σ	Total normal stress
σ'	Effective normal stress
σ_h / σ'_h	Total / Effective horizontal normal stress
σ_v / σ'_v	Total / Effective vertical normal stress
ϕ / ϕ'	Angle of friction / Effective angle of friction
θ	Angle

Abbreviations

AR	Area Ratio of sampling tube
BS	Bounding surface
CCD	Charge Coupled Device
CSP	Centreline Strain Path
FPS	Frames Per Second
IA	Interrogation Area
ICR	Inside Clearance Ratio of sampling tube
ISA	Ideal Sampling Approach
LSF	Linear Scale Factor
N-P	Normal-Paraffin
NC	Normally Consolidated
OC	Over Consolidated
OCA	Outer Cutting edge Angle
OCR	OverConsolidation Ratio
OuCR	Outside Clearance Angle of sampling tube
PIV	Particle Image Velocimetry
PSA	Perfect Sampling Approach
SPM	Strain Path Method
TWO	Technical White Oil

Chapter 1: Introduction

1.1 Sampling Disturbance

The biggest source of uncertainty and risk for the construction of civil engineering projects lies in the ground. It has been observed that among projects that were delayed, nearly half of the cases were due to unforeseen ground problems and little improvement has been made on this matter during the past three decades (Tyrell *et al*., 1983; NEDO, 1988; Chapman & Marcetteau, 2004). As a result, projects are often built at costs over the initial budget and it is estimated that across the European Union, about €50b is spent each year due to such problems (Chapman, 2008).

Though it is of critical importance to obtain accurate and representative ground information, the task itself is very challenging for several reasons. Our knowledge of the ground mainly comes from studying soil samples, which by volume are usually less than 1/1,000,000 of the ground affected by construction (Clayton *et al*., 1995). Most of the time, soil samples are retrieved by pushing a tube into the ground, a process called tube sampling. Though better sampling techniques do exist, the required technical and financial support makes them impractical for many projects, so tube sampling is still the most widely used sampling method around the world. It has long been recognised that this sampling process might cause significant disturbance to the soil, so the soil samples obtained do not truly reflect the in-situ soil state, typically with lower strength and stiffness properties. Without understanding the tube sampling disturbances, it is impossible to interpret the laboratory test data accurately and obtain the correct engineering property values. It has been a primary concern among geotechnical engineers, and though extensive research has been done, our understanding on this problem is still incomplete.

The most influential theory on tube-push sampling is the 'ideal sampling approach' (ISA) (Baligh *et al*., 1987). By treating soil as an incompressible fluid and applying the strain path method (Baligh, 1985), the strain field caused by the penetration of the 'simple sampler' was established. In particular, it was shown that along the centre-line of the sampler, a soil

element experienced three phases of compression / extension / compression during tube penetration, and the magnitude of axial strain is mainly governed by the ratio of outer diameter (B) to tube thickness (t). Though the ISA offered valuable insights into the process, the modelled 'simple sampler' was different from the real tube samplers in use. Clayton *et al.* (1998) used finite element methods to investigate the design features of such samplers, and concluded that the cutting-shoe geometry and the inside clearance had significant impacts on the strain path along the centreline. By using well designed sampling tubes they believed it was possible to reduce the centreline axial strain to lower magnitudes than those predicted by Baligh for comparable B/t values. Numerous researchers have studied sampling disturbances with physical models. However, these investigations were mainly comparative studies focusing on the soil's behaviour after it went through in-situ tube sampling or were subjected to an ISA centreline strain path in the triaxial apparatus. No researcher has to date measured the centreline strain path using a physical model.

Disturbance to clay samples does not only occur during tube penetration; it can also happen during sample storage (Hight *et al*.,1992). The tube penetration process generates excess pore water pressures near the tube wall, and a redistribution of moisture can occur during storage, resulting in additional changes in stress and strain even after sampling. Significant disturbances can also happen during the process of extruding soil samples from the tube (Clayton *et al*., 1995). However, in the past most research has focused on disturbances during sampling only, and other aspects were largely ignored.

Ground engineering works are often based on distorted information, which leads to increased risks. The practical difficulties of measuring such deformations in the sample are obvious: tube sampling is conducted underground and there is no means of seeing into the soil. After the process, the soil sample remains obscured by the tube. However, the development of a transparent soil (Iskander *et al*., 2002; Liu *et al*., 2003) has made it possible to observe displacements inside the soil body. The application of Particle Image Velocimetry (PIV, White *et al.*, 2003), a non-intrusive technique using digital photography to record displacements, enables the accurate measurement of whole field soil movements within the soil. A physical modelling system combining these two elements has been

successfully used to model geotechnical problems such as pile penetration (Ni *et al*, 2010), tunnel face stability (Ahmed and Iskander, 2012) and deformations around piling augers (Hird *et al*, 2010).

1.2 Research Aims

The aim of this research project was to study tube sampling disturbance at three stages of the sampling process: during tube driving, storage and extrusion. For this to be possible, a physical model had to be built, which was capable of providing accurate measurements of displacements and strain inside a near-transparent artificial soil body. Specific objectives were set:

- To quantify the centreline strain paths experienced by the soil during sampling with tubes with various geometries.
- To evaluate the effects of sampler design (area ratio, inside clearance and cutting-shoe geometry) on the centreline strain path.
- To investigate the influence of the Overconsolidation Ratio (OCR) of the soil on the extent of sampling disturbance experienced by the soil.
- To measure the soil displacement due to pore pressure re-distribution inside the sampling tube during storage.
- To observe the strain path imposed on soil samples during extrusion

The novelty of the project lies in two aspects. It is the first study to measure the centreline strain path with a physical model. It is also the first study to observe and quantify post-sampling disturbance using strain path measurements, thereby developing a more complete record of sampling disturbance from tube driving until immediately prior to laboratory testing.

1.3 Testing Programme and Challenges

Three series of tests were carried out during this project, one for each of the three main topics: tube penetration, storage and extrusion. Since no standard testing equipment existed to model these, a new physical modelling system had to be developed and built using knowledge gained from previous projects using transparent soil to model clays. One major challenge was increasing the size of the physical model. Transparent soil loses its

transparency with distance and previously, soil depths of 100mm had been used in physical models, but this relatively small size cast doubts upon the influence of boundary conditions. It was aimed to double this depth to 200mm while still maintaining a high result accuracy. Another important development was the switch from laser light to white light to illuminate the model. This came with its own challenges, as will be explained in the Methodology Chapter.

The first eighteen months of the project were dedicated to reviewing the literature, developing the methodology, finding the appropriate materials, and manufacturing the parts required for the testing rigs. Following this, a year was spent preparing the twelve soil models, two at a time (each took 4 to 6 weeks), carrying out the tests and developing the analysis methodology. PIV users have described their method's limitations as "garbage in – garbage out", which perfectly illustrates the difficulties associated with PIV analysis: the settings and parameters used in the analysis must be chosen carefully so that the displacements reflect the real soil movement. Many issues can influence the result of these analyses, yielding different displacement fields for the same image. In this project, the measured strains were observed to differ between PIV runs, and much work was required to obtain strain paths which faithfully described the soil's behaviour.

The success of this research lies not only with the generated strain paths but with a now tried and tested method of analysis, the strengths and weaknesses of which have been investigated. While this technique is extremely labour-intensive, both in terms of model preparation and data processing, it is a viable and relatively cheap approach to the study of displacements within a soil body. Others using this technique in the future will benefit from this work and will be able to generate data much faster than in this project by following recommendations based on experience gained during the development and use of this modelling system.

This piece of work has achieved its original goal of physically modelling the Centreline Strain Path during tube penetration and extrusion, and studying the behaviour of soil samples during storage over a number of months.

1.4 The Thesis

This thesis comprises seven chapters, most of which end with a summary of the main points covered in each section.

Chapter 2 presents the current knowledge on sampling disturbance, from a number of sources spanning 70 years' work. The development of transparent soils in the last twenty years is also covered in this section.

Chapter 3 presents the experimental and analysis methodologies. Since this project required a novel testing approach, this section follows the development process and is in itself a result of this research.

Chapters 4 and 5 present the results of the three test series, based on data corrected in the manner outlined in Chapter 3. Raw data was obtained from the tests in the form of digital photographs, from which displacements could be measured using PIV, while strains could be calculated from these displacements. A number of aspects could have been studied from the data in the photographs, but time restrictions meant that only the main aspects were chosen. Other research aims, which could have been investigated using the photographs, are suggested for future work in Chapter 6, along with the main conclusions from the studies completed in this research project. An Appendix section is also included. It contains:

- Design sheets for manufactured parts (Appendix A)
- Health and Safety COSHH forms (Appendix B)
- A study of camera shake (Appendix C)
- Matlab Scripts (Appendix D)
- Additional details of the lens distortion correction method (Appendix D)
- Additional details of the analysis method (Appendix E)
- Tube Driving Results Graphs (Appendix G)
- Monitoring Results (Appendix H)
- The lens calibration plate which was used to correct the data (Appendix I)
- Costing details (Appendix J)

Chapter 2: Literature Review

2.1 Introduction

The aim of this research project is to investigate tube sampling disturbance in cohesive soils through laboratory modelling of the sampling process, both within a soil body and after recovery of the samples from the ground. Soil distortions within the ground and inside the tube have been tracked and quantified using Particle Image Velocimetry (PIV), a displacement measuring technique which relies on time-controlled photography of the areas under consideration. To use PIV, the soil and sampler must consist of a transparent medium through which good visibility is maintained.

This literature review provides a background on the current understanding of sampling disturbance in saturated clayey soils, the models already developed to predict and quantify this disturbance, and the development of a transparent material with properties similar to those of clay.

2.2 Soil Sampling

Soil sampling is the action of retrieving representative specimens of soil from an area of ground, to study its properties ahead of geotechnical and structural works. Sampling disturbance is a problematic issue affecting site investigation and has been the focus of much interest in recent years. Methods for in-situ testing of ground conditions and soil properties are limited, with much of the investigation into the soil parameters carried out on small soil samples in laboratory settings, where measured soil properties have been found to differ from those in-situ, with typically lowered undrained shear strength and stiffness. The cause of this discrepancy is sampling disturbance, which can take many forms and cause a number of changes to the soil's structure and to its properties. Geotechnical engineers rely on these samples and their test results as a basis for their design decisions, and it is therefore crucial that a method is devised to reliably determine soil properties from extracted samples, either by minimising sampling disturbance, or by quantifying the link between in-situ and recovered sample conditions. In either case a good understanding of the effects of sampling disturbance on each measured soil parameter is essential. This section aims to

introduce the mechanisms behind sampling disturbance and their effects on sample quality with particular respect to clayey soils. While sampling disturbance has many causes, this research aims to quantify those that the engineer, having selected his method of sampling, has no means of reducing.

Samples can be taken from site by a variety of methods, which differ with regard to the equipment used to cut and remove the sample from its location in-situ. Although some samplers have been designed to minimise disturbance to the sample, the variability between soils means that no universal perfect sampler can exist and samplers which are effective on one site may be useless on another, taking heavily disturbed samples despite their optimised design. Even with the best available samplers, extracting a sample with exact in-situ properties is not achievable. Each type of sampler subjects the soil within – and surrounding – the sample to specific distortions, and is therefore associated to a particular sample quality. The options available to the engineer are explained in Figure 2.1 (the focus of this research is shaded).

The starting point for the engineer on site is to consider the end-use of the soil sample. The engineer chooses the sample quality appropriate to the type of test to be carried out, and decides whether the soil is required to be undisturbed. Disturbed samples can easily be collected from boreholes by cutting up the soil with augers, and can be stored in jars or bags, but cannot be used for most types of laboratory tests due to the amount of disturbance caused to their structure. Where undisturbed samples are required (i.e. in most cases), two alternative methods exist: by Non-Displacement, and Displacement techniques. The first option groups all methods by which a sample is isolated from the soil by cutting the surrounding material away, and then retrieved from the ground. This is the case for block sampling, which involves manually isolating a large cube of soil from its surroundings by digging a trench around it, then cutting it free at its base (Figure 2.2a).

Similarly, core-boring samplers (or rotary core samplers, Figure 2.2b) work by rotating or chopping up the soil surrounding the sample, and removing the displaced material to the surface with water or drilling fluid. In this case the sample can be taken at any depth reachable by the borehole equipment.

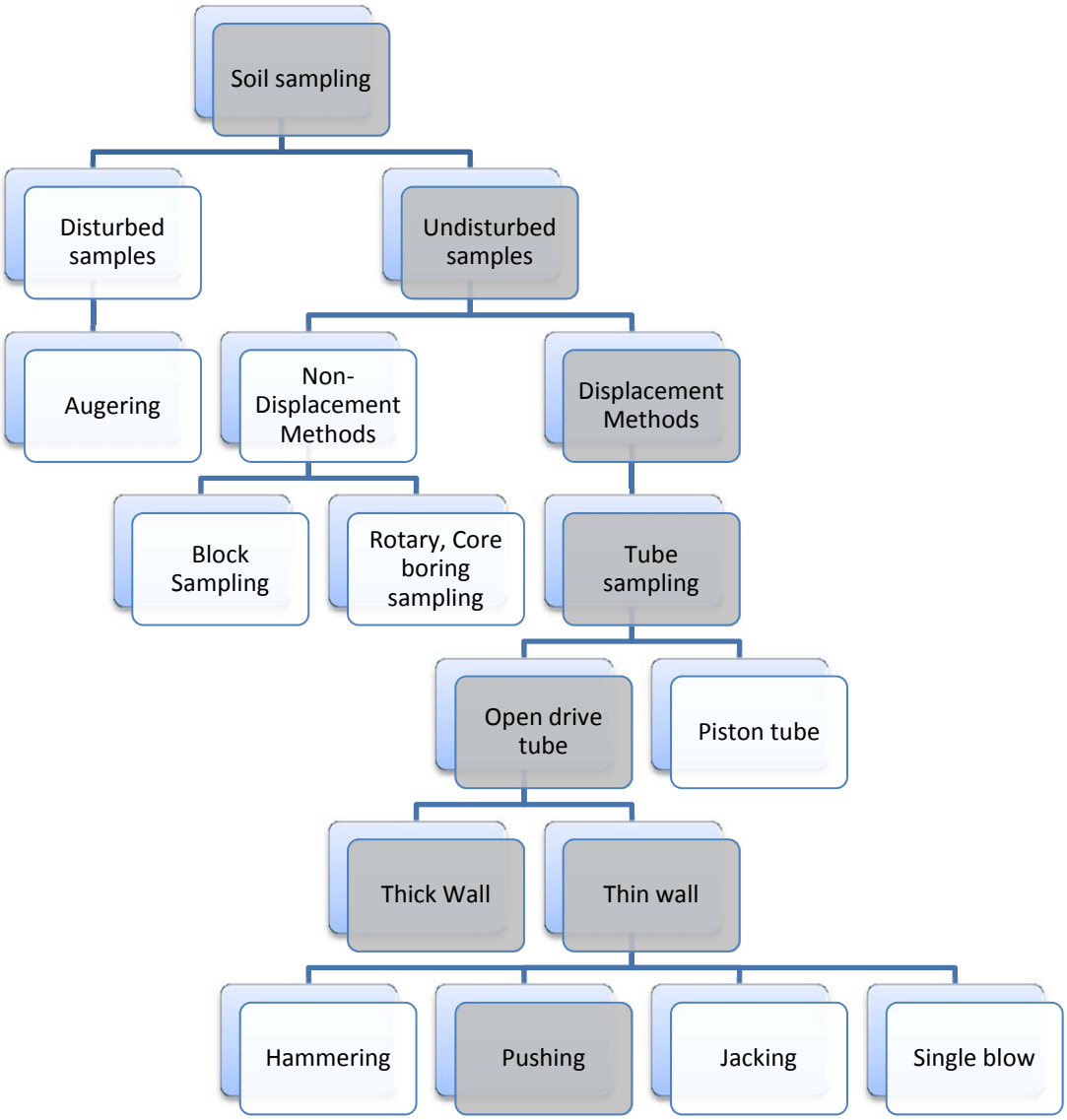

Figure 2.1 - Methods of Sampling

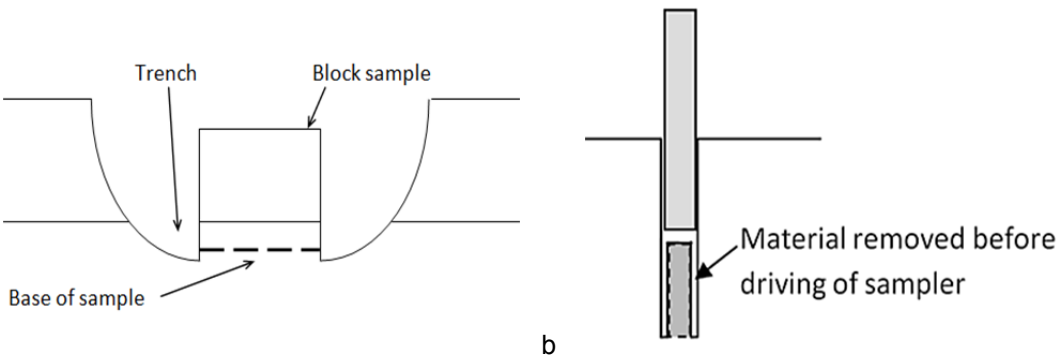

a b

Figure 2.2 - Non-Displacement Sampling: a) Block and b) Coring

Non-Displacement sampling is generally accepted to be the method generating the least disturbance to the sample, since the contact between cutting tool and soil is limited, and the method avoids any shear distortions. It is uncommonly used, especially in soft soils where the samples may poorly support their own weight and may be eroded by the drilling fluid (Fang, 1991). Also, the costs associated with digging, transporting and storing such large samples are prohibitive, and samples generated in this manner are not ready for testing in standard laboratory equipment since this generally requires standard sample sizes.

Sampling by Displacement involves pushing a metal tube into the soil with the aim to collect samples without the soil displaced by the sampler itself. This is the case of tube sampling, where a borehole is created from which soil specimens will be collected at different depths, and their properties recorded. The equipment involved in drilling the borehole is in itself a cause of vibrations and distortions which can be transmitted to the soil below the borehole and affect sample quality. After the borehole has reached the desired depth, the engineer can begin taking samples, either continuously or at chosen depths. In the latter case, the borehole will be cut to the required depths by boring or drilling (potentially causing further disturbance) and cleaned from disturbed material before sampling can take place. Below groundwater level, the borehole may be filled with water or drilling fluid to support the sides against collapse and to alleviate the differences in stress experienced by the soil at the base of the borehole.

In softer soils, the borehole can be fitted with a casing for the same purposes. Samples are taken from the ground either by being cut from the bottom of a pre-prepared borehole with an open tube or, in some soils, by penetrating to the required depth and collecting a sample where chosen using a piston sampler. The tube sampler is fitted or designed with a cutting shoe and driven into the borehole. A differentiation is made between driven samplers which have a sharp cutting shoe and are pushed without rotation into the ground, and rotary samplers which are blunt and are rotated into the soil.

Driving without rotation causes the least disturbance and can be done using one of four different methods, listed below in descending order of disturbance caused (Hvorslev, 1949):

- Hammering: rapid successive hammer blows. This method causes large disturbances to all but the hardest of soils, and should therefore not be used for soft or loose soils.
- Jacking: intermittent slow levering (15-30mm/min). Volume changes can occur, meaning that the water content in the sample is not representative. It cannot produce long samples, and is not adapted for soft soils.
- Pushing: continuous penetration of the tube (10-20m/min). This is recommended for general use and can produce relatively undisturbed samples. No rotation must occur. The movement must be continuous or adhesion will start to occur between the soil and the tube, thereby increasing the penetration resistance.
- Single blow: a single powerful hammer blow. This method has the potential of producing the least disturbance but is impractical.

The choice of sampler type depends on the material being collected and the soil properties being investigated, but it is apparent that each set-up will exert different forces on the ground both within and surrounding the sampler. These forces will cause some extent of disturbance to the soil structure, and hence to its properties. Usually steel or aluminium open-tube samplers are used for extracting cohesive materials. These sample the soil directly from the borehole base, and are fitted at the top with a non-return valve to allow trapped air and water to escape the sampler, while later providing enough suction to aid in the retrieval of the sample from the ground. The diameter of the cutting shoe is generally larger than the internal diameter of the tube to facilitate penetration and later retrieval of the sample. Thin walled versions of open tube samplers (e.g. Shelby tubes) also exist and are extensively used for undisturbed sampling purposes, since they have long been considered the most appropriate choice of sampler for clayey soils. The samplers are typically are up to 610-762mm long, with an ICR of less than 1%, an internal diameter between 42 and 121mm and area ratios between 8 and 15%.

During sampling of glacial till Gosling and Baldwin (2010) compared the U100 and a thin walled version that they were trialling, the Ut100. Dimensions of these tubes are given in Table 2.1. Samples taken with the thinner tube required fewer blows of the driving rig to

attain a specific depth (Figure 2.3), resulting in less mechanical disturbance to the specimen. No differences were noted between the measured undrained shear strengths of U100 and Ut100 below a depth of 9m, although after this, the strength of samples taken with the thin tube was higher.

Large diameter samplers have been developed and can produce samples of quality similar to that of block samples. The Laval sampler (La Rochelle *et al*, 1981) produces cylindrical samples of 208mm diameter from an outer diameter of 218mm. This high quality sampler has a small area ratio (10%) and a sharp cutting edge (5° over a taper length of 60mm). The Sherbrooke sampler produces block samples from a borehole, by cutting with rotating elements cylindrical samples of 250mm diameter and 350 mm length. These tend to be prohibitively expensive for most routine site investigations, but a compromise exists in a short large diameter sampler (Messerklinger and Springman, 2009) which according to its developers can produce samples of comparable quality to the aforementioned options since it reduces the force required for driving the sampler into the soil and reduces the forces upon removal.

Plastic or steel liners can be fitted to the inside of the tube to reduce the friction between the soil and the tube walls. Alternatively, sliding liner samplers can be used. These are made of two tubes, one plastic within the other made of steel, and are fitted with a core-catcher to retain the sample during retrieval. Where recovery of the sample is problematic, in the case of soft and sensitive soils for instance, piston samplers are often used. As their name suggests, these include a piston which is fitted to the bottom of the sampler. Different types of piston sampler exist, which vary in the piston's function which can be fixed in place or free at different parts of the sampling process. In general, the piston sits flush with the end of the cutting edge while the tube is pushed into the ground below the base of the borehole, past the disturbed layers of soil at the base of the borehole, until the desired depth for sampling is reached. Two piston samplers used in the UK are the NGI (Norwegian geotechnical institute) and the Swedish piston sampler. The former is 880mm long, with an outer diameter of 57mm and an Area Ratio of 11-12% and an Inside Clearance Ratio of 1.3%. The latter is

700mm long, with an internal diameter of 50mm, an outer diameter of 60mm and an area ratio of 44%.

Table 2.1 - Dimensions of U100 and Ut00, from Gosling and Baldwin (2010)

Dimension (mm)	U100	Ut100
Outside Diameter	114.3	110.0
Inside Diameter	105.7	104.0
Wall Thickness	4.3	3.0

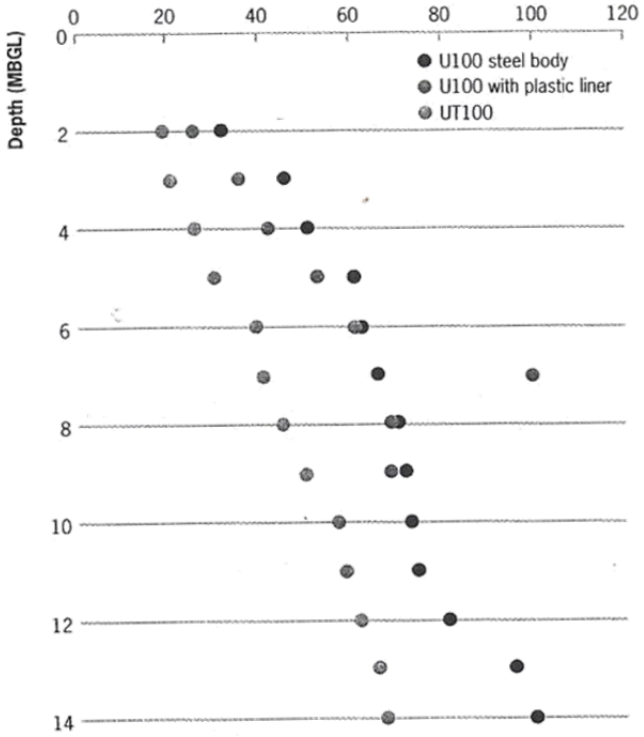

Figure 2.3 - Number of Blows Required to Attain Sample Depth, from Gosling and Baldwin (2010)

When the tube reaches the desired depth, the piston is held in place or left to move with the sample while the tube is pushed down into the ground below it. The retraction of the piston prior to sampling is also an option, and when operated can produce a suction on the sample, useful for retrieving soft soils, but can cause very soft soils to flow into the tube before sampling. The use of a piston sampler generally results in a relatively undisturbed sample. Lubricating or polishing the inside of the tube can help reduce the friction, and gel-push samples (Taylor and Cubrinovski, 2012a and 2012b) are also being developed, which use a lubricating gel to reduce friction between the sample and the sampling tube, resulting in reduced visual disturbances to the sample's structure. In any case, the inside of the tube must be kept free from rust and dirt since these increase the friction between the tube and

the soil (Hvorslev, 1949, Tan *et al*, 2008). Open-tube samplers and piston samplers are illustrated in Figure 2.4a and b respectively.

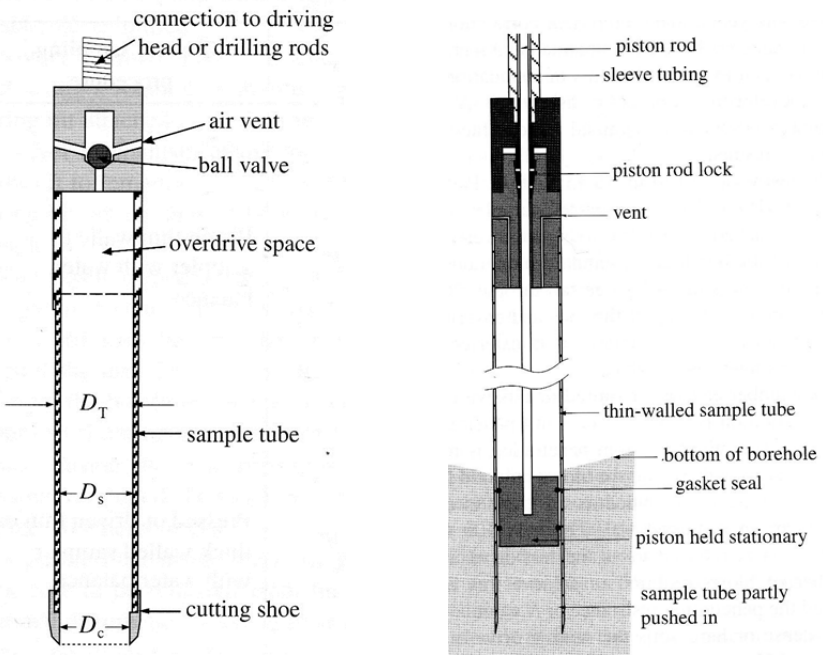

a) Open-Tube Sampler b) Piston Sampler

Figure 2.4- Types of tube samplers (from Barnes, 2000)

The advantages of using the open-drive sampler are its low cost and simplicity of use, while its disadvantages are the possibility of excess soil entering the sample (and the difficulty in evaluating the extent of excess soil recovery), and the sampling of dirt at the base of the borehole. When thin-walled tubes are used, they are easily damaged by the presence of stones in the ground. Piston samplers are generally recognised as more adequate in softer cohesive soils, since they are able to avoid excess soil recovery and can collect soil below the distorted layers directly below the base of the borehole, but the suction caused during their use can severely distort some soils. Piston sampling can also be a difficult process with many time-consuming steps. Hvorslev (1949) stated that of all existing options for tube sampling, piston sampling came the closest to being a universal tool, being well adapted for many soil conditions. Another factor to be taken into account is the borehole itself. Stresses immediately beneath the base of the borehole are affected by previous sampling and this will have an influence on the soil and its properties. This varies with the type of sampler used: for open tube samplers, the base of the borehole is exposed to atmospheric pressure where

the borehole is kept dry, and pressures smaller than the original in-situ stresses where mud is used to support the borehole. This has the effect of relieving stress for some depth under the borehole (Figure 2.5), to the extent that the base of the borehole may fail. For piston samplers, the opposite is true. The layers under the piston are pushed down until they form a plug, which itself causes disturbance to lower layers of soil.

Once removed from the ground, samples are ideally stored within cut sections of the sample tube or liner (if used) until required. The seriously disturbed parts of the sample must be removed, following which the tubes are sealed to ensure long-term air-tightness before being transported to the lab for testing. Most methods for sealing the tubes do not ensure perfect air-tightness, meaning that most samples will have a tendency to lose water over time; however, with the use of appropriate sealing materials changes in water content can be reduced. A four year study by Hvorslev (1949) compared numerous methods of protecting a clay sample against changes in moisture content during storage. The main approaches are presented in Table 2.2.

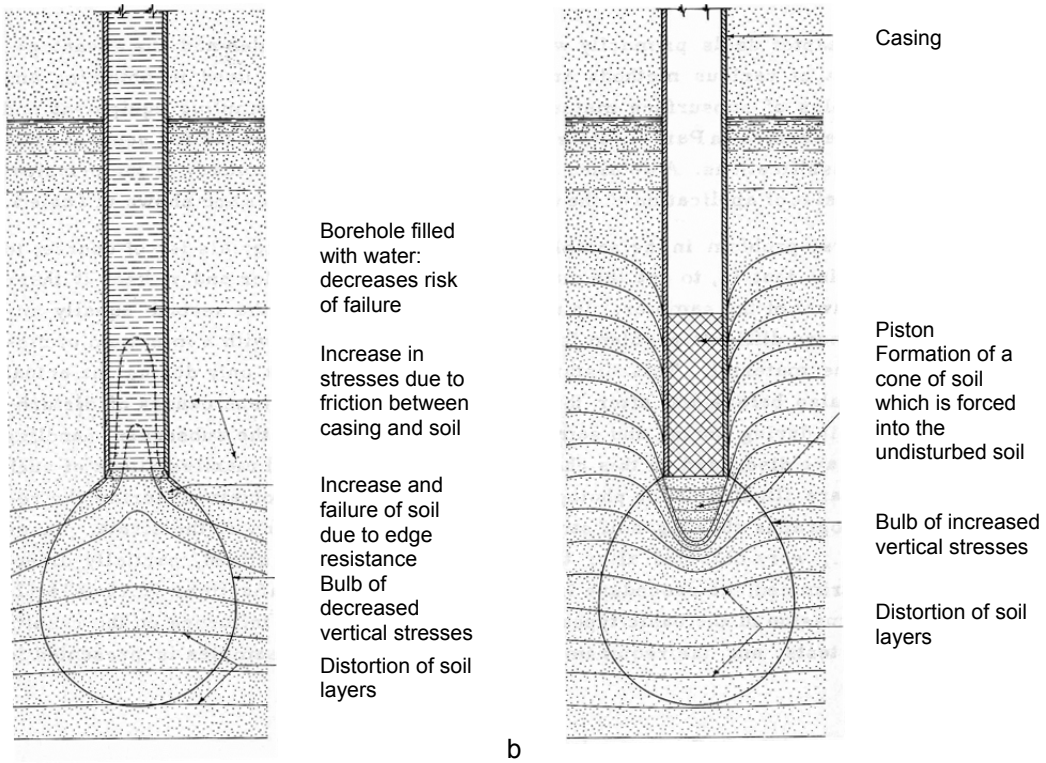

Figure 2.5 - Stress Contours under the Borehole a) with an Open Tube and b) with a Piston Sampler (from Hvorslev, 1949)

Table 2.2- Moisture Loss in Clay Samples with different Methods of Protection (data from Hvorslev, 1949)

Method	Moisture Loss			
	after 1 day	after 7 days	after 32 days	after 6 months
Unprotected	30%	93%	98%	>98%
Wax paper	2%	19%	86%	>94%
Paraffin wax- full coating (thickness= 4 to 13mm)	0%	0%	0.1%	0.4%
Sample left in tube, sealed with paraffin wax plugs (20mm/40mm)	0% / 0%	0% / 0%	0.1% / 0%	10% / 2%
Sample left in tube, sealed with tight fitting caps	0%	0%	0.2%	4%

Sealing the tube provided the best degree of protection against moisture loss, with typical loss over 6 months 4% for caps and 2-10% for wax plugs. Both these methods are cheap solutions for preserving moisture content, although paraffin is known to shrink and crack when cooling, which can affect its ability to provide a seal. Where a poor seal is formed, fungus may develop and cause chemical changes to the sample.

A number of sources provide detailed descriptions of tube samplers, including Clayton *et al* (1995), Hunt (2005), Fang (1991), and Barnes (2000).

2.3 Causes of Sampling Disturbance

2.3.1 Introduction to Sampling Disturbance

Sampling disturbance describes any visible or invisible change from the sample's in-situ state. This can manifest itself very evidently as a deformed sample, with marks or rippling (Figure 2.6), or can be very hard to detect. The behaviour of soil as a material is difficult to predict since it depends on its stress history, void ratio and structure, all of which can easily be disturbed during the taking and handling of samples. The strength of a soil depends on the interaction between its three components (soil particles, pore fluid and air, when present), but since pore water cannot transmit shear stresses, the soil is particularly reliant on its structure. The structure itself depends on two aspects: its fabric, or particle arrangement, and the bond between its particles. The former is governed by the type and shape of the particles present in the soil, while the latter is a result of soil ageing and chemical processes which strengthen the soil over time.

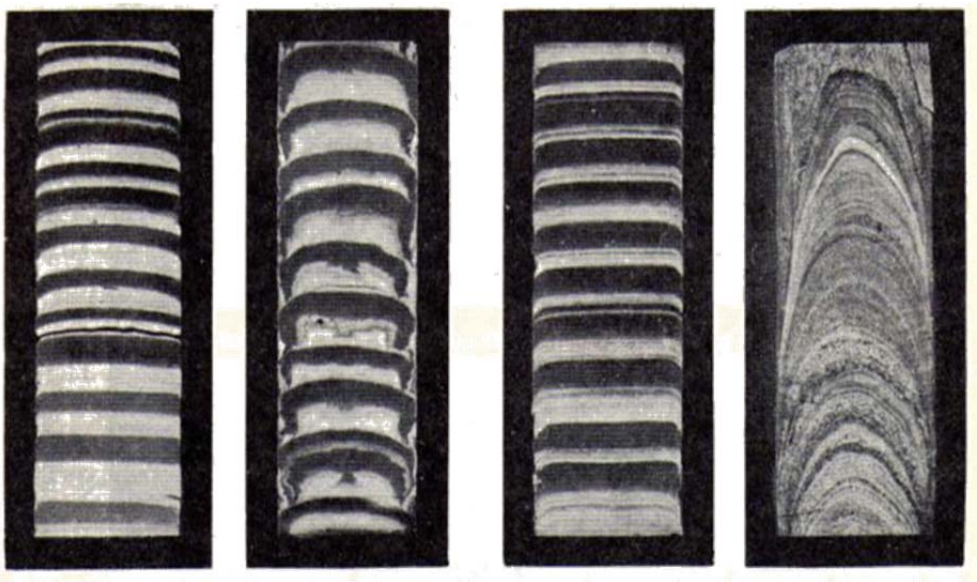

Figure 2.6 – Physical Evidence of Tube Sampling Disturbance, from Hvorslev (1949)

Any rearrangement of the particles (as happens under any new stress conditions) will modify the structural bond and expel pore fluid by consolidation. This will have an effect on the void ratio and water content and hence on the stresses and strains present within the element of soil. This brings to attention the concept of stress changes within the sample. Stress changes are caused by introducing, removing, increasing or reducing forces which act upon the soil at a given point in time. A saturated soil responds by adapting the stresses within its structure from its original point of equilibrium following Terzaghi's (1943) effective stress principle:

$$\sigma = \sigma' + \mathrm{u} \qquad \text{Equation 1}$$

Where: σ=total stress (kN/m^2), σ'=effective stress (kN/m^2), u=pore water pressure (kN/m^2)

This means that any change in external forces during sampling, or any change which influences the value of any of these parameters may modify the stresses carried by the bond between particles, and hence modify its internal (microscopic) structure. In clays, where permeability is low, samples are particularly susceptible to sudden increases in pore pressure which can take a long time to dissipate. Current practice standards (EN ISO-BS22475-1) have considered the ways in which other soil parameters can influence the soil's original equilibrium during sampling and have for this reason proposed some

guidelines to determine firstly what constitutes an “undisturbed” sample, and secondly which tubes are currently available to suit this purpose. A sample will fall into one of five quality classes (1 to 5), where class 1 is considered undisturbed. These quality classes have been linked to three equipment categories (A to C, Table 2.3) which are known, from experience, to produce certain visible disturbances to the soil. The end purpose of a sample will determine which method of sampling and quality class is appropriate for its particular situation. The quality classes are detailed in the following manner and are appropriate for different purposes (Table 2.3):

- Class 1. These may show slight evidence of soil structure disturbance. To be considered “undisturbed”, parameters such as water content, void ratio and chemical content must remain unchanged from the in-situ state. For this reason, only class 1 samples are used for extensive laboratory testing (moisture content, density, porosity, permeability, compressibility, effective and total stress parameters, stress-strain behaviour, coefficient of consolidation, fabric, remoulded properties...)
- Class 2. These will have experienced some extent of distortion and are appropriate for most laboratory tests (although not for properties such as permeability and coefficient of compression)
- Class 3 and 4. These exhibit some degree of structure disturbance but are similar in their composition to the in-situ condition (water content, particle types and proportions). These are suitable for determining the remoulded properties of the investigated soil.
- Class 5. These samples are unsuitable for laboratory testing. These should only be used for obtaining an approximate idea of the strata sequence and moisture content

These quality classes agree with older recommendations (Hvorslev, 1949, Rowe, 1972), the former of which also suggested the correct equipment to be used for different soils (Table 2.4), which are similar to those recommended nowadays by Eurocode 7 (Table 2.5) although the minimum recommended diameter of samples has since increased. Tubes must also be rigid enough to withstand deformations in the soil and need to be perfectly cylindrical, which is not always the case (Tavenas and Leroueil, 1987).

Table 2.3 - Use of Samples of Different Qualities (from BS EN ISO 22475-1)

Property	**Quality 1**	**Quality 2**	**Quality 3**	**Quality 4**	**Quality 5**
Particle size	●	●	●	●	
Water content	●	●	●		
Density	●	●			
Permeability	●	●			
Shear strength	●				
Layer sequence	●	●	●	●	●
Compressibility	●				
Sampling Category	A				
			B		
					C

Table 2.4 - Sampling Equipment for Clays

Sampler type	Sample diameter (mm)	Type of Soil	Condition of samples
Open, Thin-Wall	25-200	Soft to stiff and loose to medium dense soils.	Representative to undisturbed
Open, Thick-Walled	25-175	All except coarse	Top of the sample often non-representative, rest partially disturbed but representative
Piston	15-150	Very soft to stiff soils	Representative to undisturbed, less risk of loss of sample
Core Boring	70-185mm	Stiff to hard clays	Close to undisturbed

Table 2.5 - Sampler Selection for Tube Sampling for Soil recommended in EC7 (BS EN ISO 22475-1:2006)

Type of sampler	Preferred sample dimensions		Recommended for	Achievable quality class
	Diameter (*mm*)	Length (*mm*)		For normal (for favourable) soil conditions
Thin-wall open	70-120	250-1000	Soft to stiff cohesive or organic soils	1
			Medium dense sand below water surface	3 (2)
			Stiff , cohesive or organic soils	2 (1)
Thick-wall open	>100	250-1000	Soft to stiff cohesive or organic soils, and including coarse particles	3 (2)
Thin-wall piston	50-100	600-800	Pasty or stiff, cohesive or organic soils, or sensitive soils	1
			Sand above ground water	3
Thick-wall piston	50-100	600-1000	Soft to stiff cohesive or organic soils, or sensitive soils	2 (1)
Split barrel cylinder	35	450	Sand, silt, clays	4

2.3.2 Mechanical disturbance caused by the sampler

Sections 2.2 and 2.3.1 outlined the basic types of tube samplers currently available. Each type varies not only in their mode of operation, but also in the tube dimensions (diameter and thickness) and cutting edge geometry.

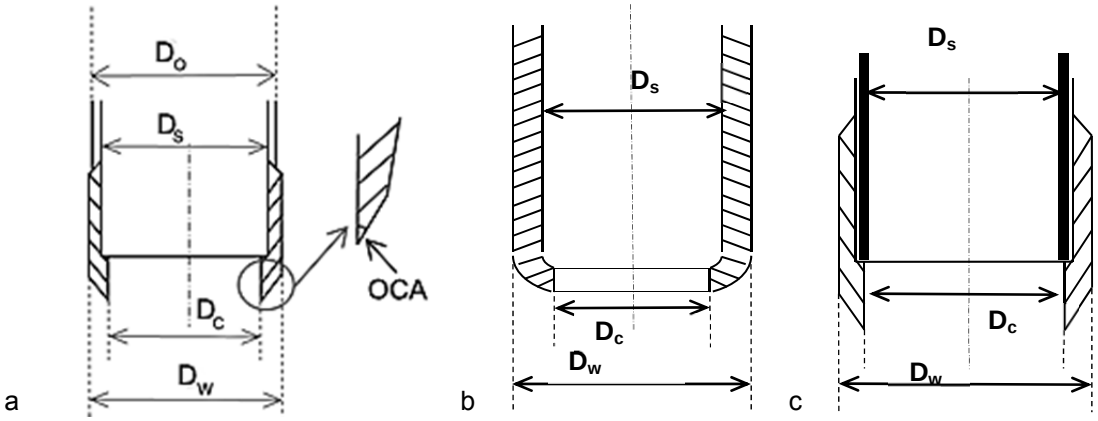

Figure 2.7 - Cutting Shoe Geometry: a) Attachable, b) Built-in and c) with a Liner

This can be created by two methods: using an attachable cutting edge (expensive and makes the tube thicker - Figure 2.7a) or machining the end of the tube to become sharper or curved (Figure 2.7b).

As the sampler cuts into the soil, the tube is subjected to normal and frictional forces, both internal and external (Figure 2.8a) which will govern the extent of mechanical deformation the soil will be subjected to. Hvorslev (1949) states that the inside wall friction is the single most important source of disturbance during sampling. Upon removal, the vertical forces are reversed and therefore cause destructuring in the opposite direction (Figure 2.8b). It is of note that while friction is problematic during sampler driving, during retrieval it is beneficial, since without it sample recovery would not be feasible.

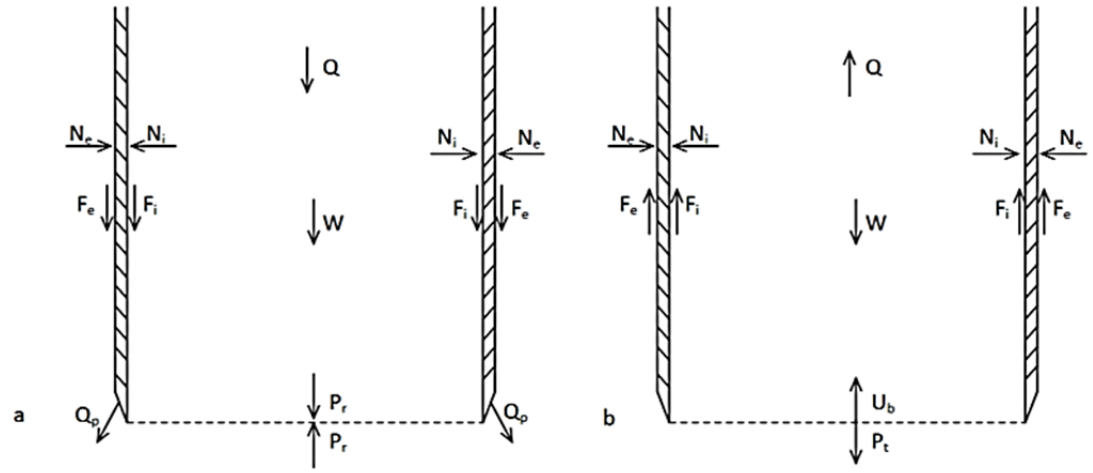

With
N= Normal Force, F= Friction, Q=Driving Force, U_b=Water or Air Pressure, P_t=Tensile Strength, W=Weight of Sample, Qp=Edge Resistance. Subscripts: e=external, i=internal

Figure 2.8 - Forces acting on the Soil in the Sampler: a) during Driving and b) during Retrieval from the Ground (from Hvorslev, 1949)

Friction increases with penetration into the ground and can eventually cause severe mechanical disturbance (Hvorslev, 1949). In its least severe form, samples suffer from significant edge drag-down (Figure 2.6), while where the internal friction between the soil and the tube increases sufficiently to impede the sampling process, a soil plug is formed within the tube, and the forces on the surrounding soil are comparable to those created by a piston sampler (Figure 2.5b). This can result in severe distortions to the soil within and below the sampler. The important sampler dimensions are illustrated in Figure 2.7; these influence

the interaction between the soil and the tube as the sampler is pushed into the ground. Three parameters linked to the sampler geometry in BS EN ISO 22475-1:2006, the Area Ratio (AR), Inside Clearance Ratio (ICR) and Outside Clearance Ratio (OuCR) have been defined as:

$$AR(\%) = \frac{{D_w}^2 - {D_c}^2}{{D_c}^2} \times 100 \quad \text{Equation 2}$$

$$ICR(\%) = \frac{D_s - D_c}{D_c} \times 100 \quad \text{Equation 3}$$

$$OuCR(\%) = \frac{D_w - D_o}{D_o} \times 100 \quad \text{Equation 4}$$

With: D_w= Outer radius of the cutting shoe, D_c= Inner radius of the cutting shoe, D_s= Inner radius of the sampling tube, D_o= Outer radius of the sampling tube. In many sources, D_w (the outer diameter) is referred to as B, and this notation is used in this thesis.

This means that a sampling tube with a high area ratio will have a comparatively thick cutting element which will produce relatively large deformations during its travel due to the large amount of soil being forced out of the way of the tube itself. A tube with a high inside clearance will have a large internal diameter in comparison to the cutting shoe. Since the amount of soil entering the tube is largely dependent on the diameter of the cutting shoe, the soil within the sample will be able to expand upon entry. This reduces the amount of friction between the soil and the tube for some of the travel, but is associated to disturbances caused by stress relief. An additional geometry parameter has a known effect on disturbance: the OCA (Outside Cutting edge Angle). This governs the apparent “sharpness” of the sampler, and hence the extent of deformation caused to the soil on the outside surface of the sampler.

Since some tube geometry parameters govern the amount of friction between the soil and tube walls, and the expansion which the soil is allowed upon entering the sampler, they are directly linked to the extent of mechanical sample deformation during the driving and retrieval of the sampler from the ground and later during extrusion of the soil from the sampler. It must be noted that where these mechanical deformations cause particle rearrangement, the deformations are predominantly plastic, and it is therefore not possible to recover the original shape and particle arrangements by reversing the direction of the sampling tube (Barnes, 2000).

When the sample is removed, it is typically sheared off by rotation from the ground below and retrieved from the borehole. This creates torsional and tensile stresses within the sample and can cause the sample to fail. The retrieval can create a vacuum below the sample which can also create some amount of destructuring, especially in soft and sensitive soils. Extrusion of the sample in the laboratory can be conducted in the same direction as the soil entered the tube, to avoid a complete reversal of stresses on the sample. When a thin tube or liner has been used, this will be cut into small lengths so that the sample can be retrieved from the tube without excessive frictional disturbance. However the cutting of the metal tube causes a significant amount of vibrations which may cause additional damage. All of the above can result in severe mechanical deformation of the sample, which is apparent as a destructuring of the soil and a disturbance at the edges of the sample. The extent of mechanical deformation largely depends on the aforementioned sampler geometry parameters (thickness, area ratio, inside clearance ratio, and edge of cutting element OCA), and as a general rule:

- High values of tube thickness are associated with high disturbance because of the amount of soil displaced during tube penetration.
- High values of Area Ratio are associated with high disturbance due to the amount of excess soil allowed into the sampler. The AR is essentially the ratio between the volume of displaced soil and that of the sample. High values of AR are also linked to higher penetration resistance and therefore disturbance to the sample.
- High values of edge of cutting element, OCA (i.e, blunter tubes) are associated with high sample disturbance.
- High values of Inside Clearance Ratio allow stress relief during tube driving and increase disturbance since the sample is allowed to expand upon entry into the tube.
- A low ICR implies increased friction between the sampling tube and the soil. While friction is undesirable during tube penetration since it results in some extent of edge disturbance, a certain amount of friction is necessary to recover the sample. Friction causes some amount of disturbance, which has been observed to be significantly greater during driving than during sample recovery (Clayton *et al*, 1995). Similarly,

the soil beneath the borehole may be heavily remoulded due to the drag-down effect of the tube sampler.

- Extrusion strains have been found to be small in comparison with penetration induced strains (if strains are due to stress relief, Baligh *et al*, 1987, and if they are due to the mechanical action of the extruder, Chung *et al*, 2004).

It was mentioned previously that liners could be fitted to the inside of the sampling tubes to facilitate transport and handling of the soil once removed from the tube. The effect of installing a liner is illustrated in Figure 2.7c and Table 2.6. The apparent tube diameter is reduced, which has the effect of reducing the inside clearance and increasing the area ratio.

Table 2.6 - AR, ICR and OCA of thick-wall, thick-wall with liner and thin-wall Samplers (from Gosling and Baldwin, 2010)

Feature	Thick Wall open tube (U100)	Thick Wall open tube with plastic liner	Thin-Wall (values required by EC7)
Outer Cutting Edge Angle	10°	7°	< 5°
Area Ratio	29.4%	47.1%	< 15%
Inside Clearance Ratio	1.34%	1.27%	< 0.5%

Current sample quality requirements are such that most types of commonly used open tube samplers such as the U100 (Table 2.5) are rarely able to produce undisturbed specimens. There is an on-going debate as to whether this method of sampling can remain usable (Baldwin and Gosling, 2009, 2010, Gosling and Baldwin, 2010). Thin wall samplers produce less disturbance, but are only used in soft to stiff soils since harder materials and the presence of stones tend to cause damage to the tube. This highlights the need for the development of a resistant tube sampler able to collect stiffer soils.

Table 2.5 shows the complexity of sampling disturbance, which is dependent not only on the chosen sampling method, but on the ground conditions themselves. This is particularly relevant when considering the development of equipment to satisfy strictly defined quality requirements. Hvorslev (1949) recommended the following for sampler design and selection:

- The ICR should be tailored to the soil being sampled but should be no larger than 0.75-1.5% for long samples and 0-0.5% for short samples. This lets the sample

expand laterally and is small enough for the sample to develop adhesion to the sampler for easier retrieval

- The AR should be no more than 10% for open-drive samplers (more for piston samplers)
- The OuCR should be zero
- The OCA should be no more than 10°, but 20-30° should be allowed very close to the edge to avoid damage the cutting shoe.

A numerical and analytical study by Siddique (1990) reiterated the need to limit the AR to 10%, and expanded on the above by proposing an ICR limit of 0.5% for general use, and a maximum OCA of 5°. Other studies, such as those backing the International Society for Soil Mechanics and Foundation Engineering Subcommittee on Problems and Practices of Soil Sampling (1965), suggested using a combination of AR and OCA (Table 2.7).

Table 2.7 - Combinations of Area ratio and OCA (taken from Clayton *et al*, 1995)

Area Ratio (%)	**OCA (°)**
5	15
10	12
20	9
40	5
80	4

2.3.3 Excess Soil Recovery

The aim during sampling is to collect the soil under the sampling tube, excluding that under the walls of the sampler. In many cases however, the soil under the tube's wall is not pushed fully outwards and some of it enters the tube. Significant disturbance to the sample can be caused by the recovery of excess soil and occurs predominantly when the tube thickness is high, since more soil is displaced as the tube travels through the ground and is easily pushed into the tube. It manifests itself by curved layers of soil at small excess recovery ratios, and squared layers as the ratio increases (Figure 2.6, first and second images respectively). It mostly occurs at the start of the drive, when the inside wall friction and inside pressure are small, then reduces as the pressure inside the tube builds up, and becomes more of an issue when the pressure outside the sampler is large in comparison to that inside the tube, for instance at greater depths. Soft and plastic soils are greatly affected while cohesionless soils are less so. The entrance of excess soil can be quantified by the

Recovery Ratio (Rr) which compares the length of the sample after driving (L_d) to its original length (H_o), although in practice this is hard to quantify.

$$Rr = \frac{L_d}{H_o} \qquad \text{Equation 5}$$

More representative of the sample's state is the specific recovery ratio, which examines the changes in each individual layer, and gives a more accurate picture of where the soil recovery is likely to affect the sample's properties. The use of Inside Clearance can cause a small shortening of the sample without significant disturbance, while reducing the friction between the tube and the soil. Hvorslev (1949) presented evidence of excess soil recovery in soil up to 750 mm into a clay sample (Figure 2.9), which is an obvious problem for short specimens, such as the 450mm U100 samples. Recovery Ratios between 100 and 130% were not uncommon in his extensive report, with more evidence of excess ratios in the top part of the sample.

The choice of driving method also affects excess soil recovery, with hammering producing a low ratio, and slow jacking and fast pushing a higher one. Unfortunately, the distortion effects associated with hammering outweigh the benefits of reducing excess soil recovery. To reduce the entrance of excess soil, Hvorslev (1949) recommends:

- The use of thin-walled tubes (limit the AR to 10%)
- Driving the tube at high velocities
- The use of a stationary piston sampling tube
- Increasing the length of the sample
- Using an OCA of 10° is most soils, and up to 30° immediately on the cutting edge to avoid damage: for a tube of given AR, a tube with an OCA of 20° gave a Rr of 125%, while an OCA of 14° achieved 100%
- Being aware of the risk when sampling at high depths

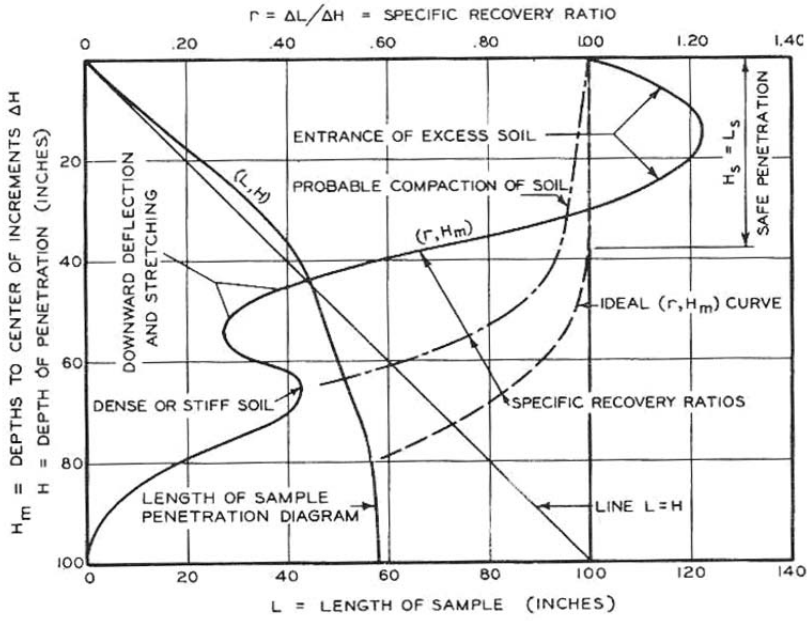

Figure 2.9 - Excess recovery in Samples: Specific Rr over Depth (from Hvorslev, 1949)

Hvorslev stated that to be considered undisturbed, a sample's specific recovery ratio should not be more than 100%, or [100 x (1 - 2xICR at cutting edge)]%, to take into account a potential shortening of the sample when inside clearance is used. This should also be monitored after sampling, by ensuring the net length and weight of the sample remain unchanged during transport, storage and handling.

2.3.4 Further sources of disturbance

Although most evidence of sampling disturbance is observed during tube driving, it also occurs at multiple occasions during the sampling process, up until testing. Some stages of this process are prone to human-error-induced distortions, such as:

- Overdriving of the tube resulting in compressed samples, or the formation of a plug of soil acting in the same manner as a piston
- Bent or worn cutting shoes changing sampler geometry
- Rusty tubes with increased friction between walls and soil sample
- Shock to the sample due to poor handling or transport
- Loss of moisture or chemical content due to poor air-tightness of sample tubes

It must be understood, however, that sampling disturbance is an unavoidable phenomenon caused first by the interaction of the sampling equipment with the soil, then by the manner in

which the sample is transported to – and stored awaiting – its final destination. Even after taking an undisturbed sample, care must be taken that it remains undisturbed until it is tested. There are four main mechanisms leading to sample disturbance:

- Mechanical deformation (see section 2.3.2)
- Changes in stress parameters
- Moisture content and void ratio changes
- Chemical changes

The following are causes of particular interest to this research project (factors which are linked to human error are not considered here). A comprehensive report on sampling procedure was produced by Hvorslev (1949) which discusses the subject in great detail.

Stress relief occurs as a result of the removal of the sample from its original anisotropic stress state within the ground. Inside the soil mass the sample will usually have been subjected to unequal horizontal and vertical stresses, which will have created elastic deformations of the soil particles, associated with the storage of a certain amount of elastic energy. Under its initial equilibrium conditions in the ground, the soil experiences a certain effective stress and no excess pore water pressures; and the strength of the soil largely depends on the water content and the bonding between particles. The extent of soil deformation and the stress response of the soil (the stress path of the sample) under a certain stress depend on the effective stresses which the soil has experienced; in other words, on the soil's stress history.

The stress path is the route (in terms of experienced stresses, total and effective), which the soil takes from its initial state to its final state. For this reason, a different stress path is expected of normally consolidated and over-consolidated clays, or for disturbed and undisturbed samples. Stress relief can induce two components: the removal of the deviatoric stress and the reduction of the mean stress in the sample to zero, which eventually happens since the sample is finally extruded from the tube and exposed to the atmospheric pressure in the laboratory (Figure 2.10a). When this occurs, capillary forces develop within the sample to respond to the sudden removal of stresses.

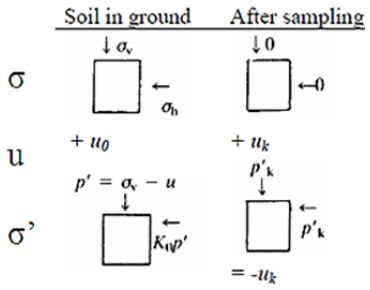

a (subscript k= after sampling)

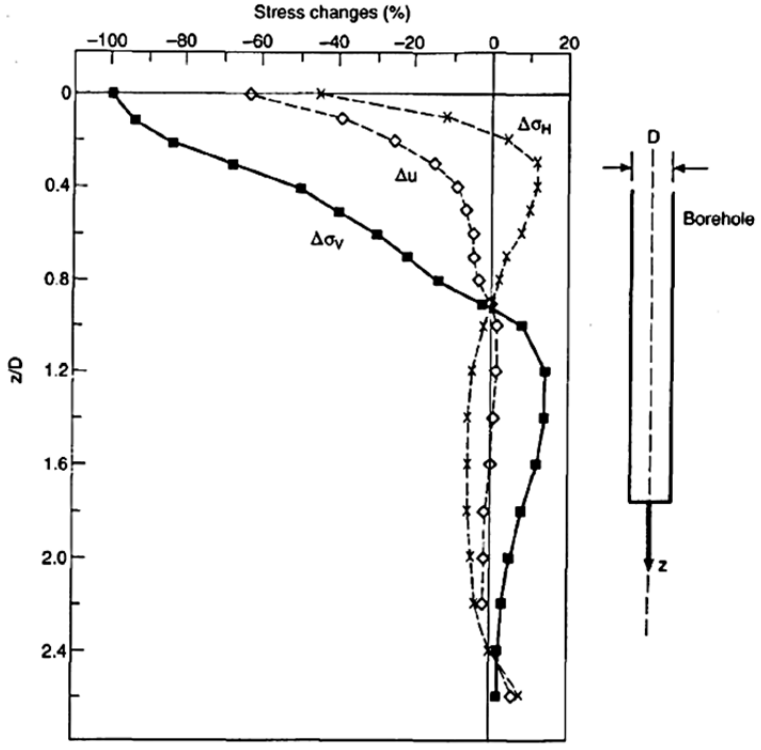

b

Figure 2.10- Stress Changes during Sampling: a) in the Sample and b) below the Borehole, cited by Clayton *et al* (1995) with a) from Skempton and Sowa (1963) and b) from Galle and Wilhoit (1962) modified by Hopper (1992)

To account for stress relief samples are reconsolidated in a triaxial cell to a proportion of the original in-situ stress prior to testing, although the effectiveness of such a technique may be reduced in the case stress relief has been sufficient to destructure the sample, such as in sensitive soils (La Rochelle et al, 1981). There are four main approaches to this issue, when conducting consolidated undrained triaxial tests:

- Isotropic reconsolidation to p', the mean in-situ stress, or that in the sample. This method is not recommended in all soils since it may yield overestimations or underestimations of shear strength and stiffness (Kirkpatrick and Khan, 1984, Siddique et al, 2000)

- The recompression technique: the sample is reconsolidated anisotropically to the in-situ horizontal and vertical stresses, which are determined mathematically using the unit weight and groundwater data from the site – this method was developed to correct for the effects of swelling rather than mechanical disturbance and is recommended in highly structured clays (Jamiokowlski, 1985).
- The SHANSEP approach (Ladd and Foott, 1974): the most recent in-situ effective stress is calculated in the manner above, and the soil's history is determined through consolidation tests on high quality samples. Samples are reconsolidated in Consolidated-Undrained tests at different OCRs, meaning that the effective stresses on the sample can be much higher than those it experienced in-situ. The relationship between the OCR and the normalised strength (C_u/effective vertical stress) is determined and applied to samples taken from the site at different depths (and hence different estimated effective vertical stresses). Its use is not recommended for heavily overconsolidated or cemented soils.
- The sample is reconsolidated along a specific stress path which encompasses its recent stress history (see 2.4.4)

The stress to which samples should be reconsolidated is a matter of some debate, and varies with type of soil. While the SHANSEP method requires the soil to become overconsolidated during reconsolidation, Raymond *et al* (1971) proposed values of 50-75% of the preconsolidation stresses for sensitive clays, while Baligh *et al* (1987) recommended 150-200% for Resedimented Boston Blue Clay. The preconsolidation pressure of a soil can be found through the study of the soil's consolidation behaviour and is generally defined as the maximum pressure experienced by the soil in its history in the ground. In reality, the value found using this empirical method can be higher than this due to aging, secondary compression and cementation. Jamiolkowski (1985) extended the definition of preconsolidation pressure to indicate a yield stress separating small-strain behaviour and larger strains which cause irrecoverable damage to the soil's structure. Lunne *et al* (2006) recommended using anisotropic reconsolidation to the in-situ stresses over the SHANSEP method from tests on Norwegian marine clay of high sensitivity. The above methods are used to minimise the effect of sampling disturbance on the properties of the sample,

although Tan *et al* (2002) suggest that this accounts more for the effects of stress relief than for the loss of structure caused by mechanical disturbance in Singapore marine clays.

Successful uses of the last three techniques are documented in the literature. Santagata and Germaine (2005) investigated both the recompression and SHANSEP method on Reconstituted Boston Blue Clay (RBBC) samples and concluded that if the strains experienced during sampling are small (<2%), the effect of sampling disturbance on the strength and stiffness could be recovered using the SHANSEP approach, while on larger strains, (>5%), the behaviour of the reconsolidated sample differed from in-situ. Samples reconsolidated using the recompression technique found their strength and stiffness partially recovered, but overestimated the soil's undrained shear strength in normally consolidated soils. Figure 2.11a and Figure 2.11b show results from Unconsolidated-Undrained triaxial tests on samples of RBBC, where a significant loss of strength and stiffness can be seen to affect the sample disturbed by strains typical of the ISA or PSA (see 2.4.3 and 2.4.4) before reconsolidation. In these, the stress-strain behaviour of the disturbed samples can be seen to be recovered somewhat using the recompression and SHANSEP methods respectively. Some discrepancies remain, especially for higher degrees of disturbance (strain cycle above ±2%).

The same conclusions were reached by Baligh *et al* (1987) on Boston Blue Clay (BBC) samples. Clayton *et al* (1992) found that in Bothkennar clays, if the strain experienced by the sample is less than 2% during sampling, reapplying the sampling stress path to reconsolidate the sample recovered the majority of its undrained shear strength.

Hajj (1990) and Hird and Hajj (1995) also reconsolidated samples of reconstituted kaolin using stress paths, with successful results for small strain behaviour only, in both normally and overconsolidated samples.

The main criticism of the SHANSEP method is the fact that it takes the samples to stresses well above the preconsolidation pressure. According to Tavenas and Leroueil (1987), this can affect the structure of the soil, and the properties measured are therefore different from an intact clay's, making this method unsuitable for some clays (for instance the Bothkennar clay, Hight *et al,* 1992). Budhu and Wu (1992) found that in their model, the undrained shear

strength of normally consolidated samples was increased by reconsolidation, while it decreased for overconsolidated soils. Unconsolidated – Undrained tests can also be conducted but their use is not often recommended.

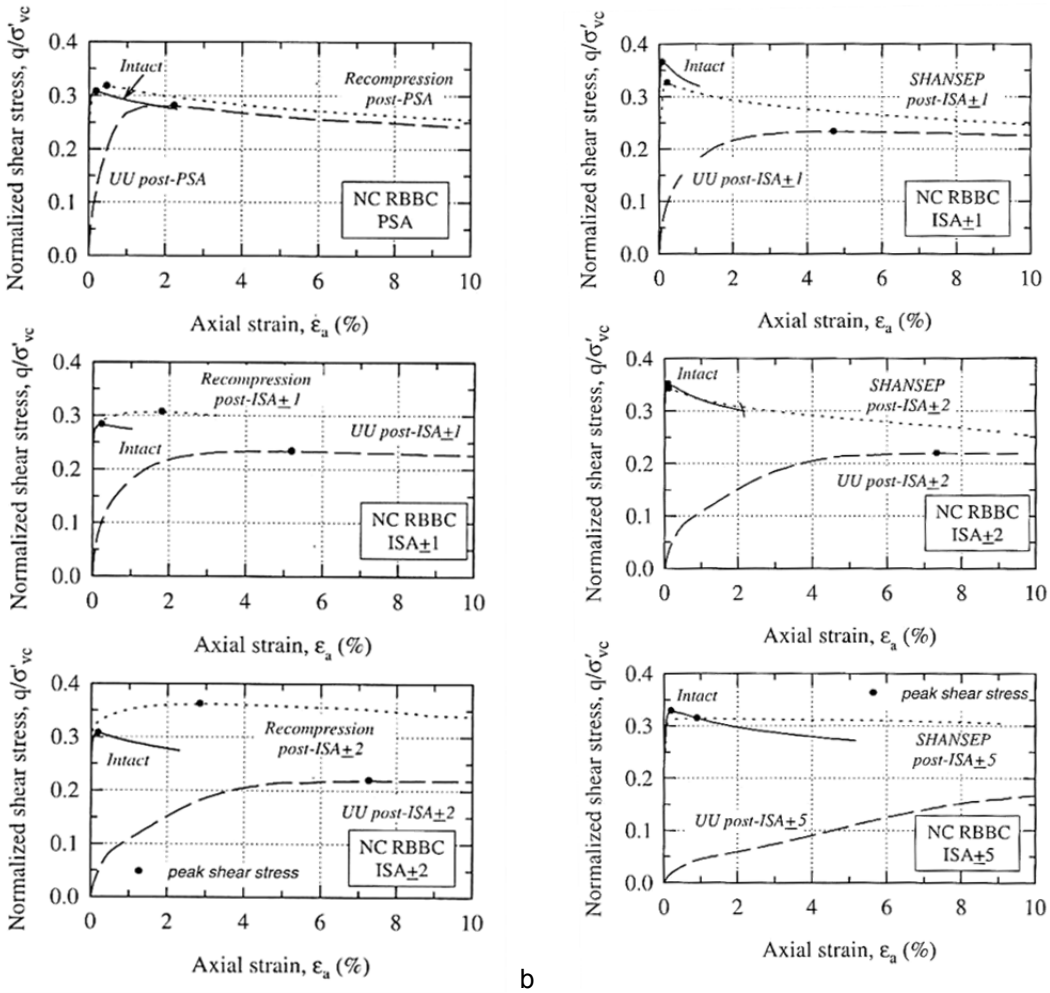

a b

Figure 2.11 - Changes in Stress-Strain Behaviour due to Sampling and Effects of Reconsolidation prior to Testing: a) with Recompression and b) with SHANSEP methods (from Santagata and Germaine, 2005)

Swelling occurs in clays for two reasons, firstly, as described above, during stress relief. Secondly, it occurs where pore pressures change significantly during sampling due to ingress of water, and is proportional to the total stress changes at the bottom of the borehole (Figure 2.10b). To reduce potentially large stress differences due to the retrieval of material, boreholes are often filled with drilling fluid (water only under groundwater level and mud above and below).

Changes in moisture content and void ratio occur during the driving of the sampler tube into the soil. Siddique et al (2009) reported that tube samples of reconstituted Dhaka clays had a void ratio higher than that of block samples.

The speed and method of sampling must be appropriate to the type of soil being recovered so as to cause as little consolidation as possible. If the speed is high enough, the process is undrained and the volume is expected to stay constant. Airtight containers are used to store the samples to ensure that no changes in water content are allowed, although water migration within the sample may still occur. Chandler *et al* (1992) found that the water content (w) in the edge of U100 samples of Chattenden Clay was up to 20% higher than at the centreline after sampling (Figure 2.12). This water migration may in some cases alter the effective stress state over time and hence yield altered test results due to the relationship of moisture content and soil strength (Clayton *et al*, 1995).

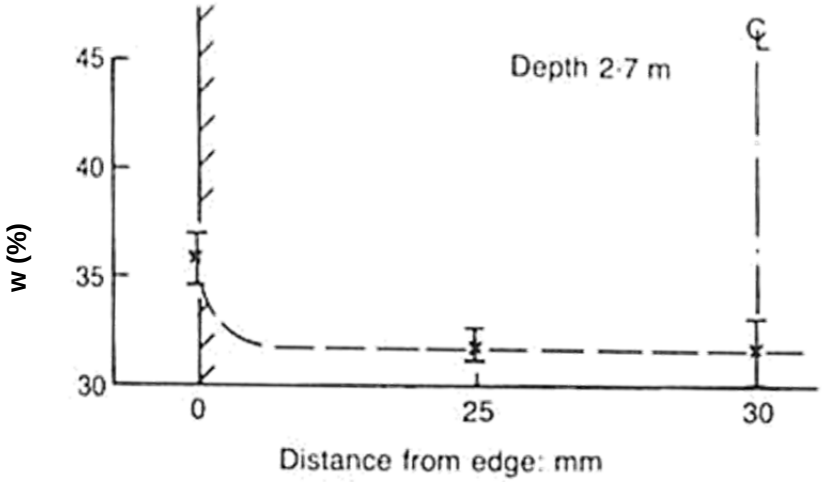

Figure 2.12 - Variation of Water Content across U100 Sample (from Chandler *et al*, 1992)

Chemical changes can affect the sample before boring if the drilling fluid is ill suited to the type of soil being extracted. Extreme temperature conditions will harm the fabric of the sample and may change the structure of the soil itself, while reactions between the tube and soil may cause the pore fluid chemistry – and hence the soil properties – to change.

These causes of disturbance can affect the sample at multiple points during the sampling process. Clayton *et al* (1995) listed the main causes of disturbance before, during and after tube driving (Table 2.8).

Table 2.8 - Sources of Disturbance, from Clayton et al (1995)

Before	During	After
Stress relief	Stress relief	Stress relief
Swelling	Remoulding	Migration of water
Compaction	Displacement	Loss of moisture
Displacement	Shattering	Freezing / overheating
Base heave	Stones at cutting shoe	Vibration
Piping	Mixing or segregation	Chemical changes
Caving	Failure to recover	Extrusion

2.4 Effects of Sampling Disturbance on Soil Properties

Past research can be divided into two typical methods of investigating the effects of sampling disturbance on the properties of soils. In the first, different samplers are used to collect samples of natural or reconstituted soils and their properties are measured to assess the impact of each sampling method on one or more of the soil parameters. In the second, the strain paths which develop within the tube sampler are studied analytically or numerically and applied to reconstituted samples. These disturbed and undisturbed reconstituted samples are subjected to laboratory tests and their behaviour compared to quantify the changes in behaviour due to the sampling process. Since these samples are prepared in the laboratory in a manner which simulates natural soil deposition and one-dimensional consolidation, the original undisturbed properties are easily obtained for comparison purposes. They are not aged and their properties can differ somewhat from natural soils, which tend to have increased strength from the aging process, including the effects of secondary consolidation, bonding, cementation and thixotropic hardening (Tavenas and Leroueil, 1987). Jamiolkowski (1985) reported that the preconsolidation pressure of RBBC increased over time. It has also been noted (Clayton *et al*, 1995) that while tests on reconstituted samples show the differences caused to a sample's stress path, they tend to underestimate the effects of sampling disturbance on the soil's undrained shear strength, since many natural soils have some extent of particle bonding and structuring. In research, a differentiation is made between the "Perfect Sampling Approach" (PSA) proposed by Ladd and Lambe (1963), which studies the disturbance caused only by the stress relief between the in-situ conditions and the atmospheric pressure at which the sample finds itself prior to laboratory testing, and the "Ideal Sampling Approach", proposed by Baligh *et al* (1987) which

studies the disturbance caused by the mechanical deformation caused by the insertion of the tube into the ground.

2.4.1 Laboratory Simulation of Sampling

A number of studies have addressed the issue of sampling disturbance with particular respect to one type of clay or set of properties being measured. The effect of sampling disturbance has been quantified in a number of situations but is highly dependent on the material being studied. Most research to date has concentrated on properties such as strength, compressibility, stiffness, and dynamic properties. Two main approaches have been used by researchers to quantify the effect of tube sampling disturbance on the properties of clays. In the first, a number of different tube samplers are used to take specimens of soil, and the stress-strain behaviour of the different samples is compared, with block samples (or samples taken with large diameter tubes such as the Laval or Sherbrooke samplers) often used as a benchmark for undisturbed behaviour. Sometimes, the vane shear test – itself considered poorly adapted to provide undisturbed data (Eden, 1971) – will also be compared to tube sampling. These approaches have the advantage of linking particular sampler parameters to a type of disturbance and to changes in physical properties. The data is verified by using multiple specimens of each type, and the studies are numerous enough to create an extensive knowledge database.

2.4.1.1 Effect on the Undrained Shear Strength

Sampling disturbance is most often linked to a reduction in the effective stresses in the sample and therefore to a reduction in its undrained shear strength (C_u), with higher disturbances creating a more significant reduction. Numerous studies on many different clays support this theory. Sampling disturbance influences the effective stress in the sample more than its cohesion and angle of friction. Milovic (1971) compared block, Shelby tube and Norwegian piston samples of Canadian clays and found a reduction in cohesion (c') of 25-30%, and a reduction in the effective angle of friction of 6-11%. These clays are sensitive and prone to severe destructuration upon sampling, therefore these values represent a worst case scenario. A summary of the studies quantifying this loss in strength is provided in Table 2.9 where the ratio of tube shear strength to undisturbed (block or Laval or

Sherbrooke) shear strength is given, since block samples are considered close to undisturbed.

Another approach was to compare several samplers with given geometry characteristics, without block or Laval samples as a benchmark – either existing samplers or tubes modified to suit the purposes of the study. These studies give an indication of the best type of sampler to use in one given soil, and identify tube characteristics which cause sampling disturbance by comparing different values of Area Ratio, Inside Clearance Ratio and Taper Angle. Results from these studies are included in Table 2.10.

Research by others also concluded a reduction in the undrained shear strength and effective stress in the sample due to the application of tube sampling by way of a strain path. In this type of study, antisymmetric or non-symmetric strain cycles predicted by the SPM were applied to undisturbed or reconstituted samples, whose behaviour was then compared to that of undisturbed samples. A summary of this research is provided in Table 2.11.

Table 2.9 - Effect of Sampling Disturbance on the Undrained Shear Strength of Samples - Comparison of Block and Tube results

Type of Clay	**Type of sampler**	**tube/ undisturbed (C_u or p')**	**Reference**
Leda clay (sensitivity = high)	Open tube, piston, block	C_u=50% on average	Eden (1971)
Champlain clays	Piston, block	C_u=50%	La Rochelle and Lefebvre (1971)
Canadian clays (sensitivity=high)	Shelby, Norwegian piston sampler, block	In CU tests, p' for Sheby was 68-72% that of block, and for Norwegian piston, 87-90% that of block	Milovic (1971)
Bothkennar Clay	ELE piston, Laval and Sherbrooke Samplers	p' in ELE samples were 50% lower than others. In Laval samples it was identical to in-situ up to 10m depth	Hight *et al* (1992)
Ariake Coastal Clay	Japanese piston (inside Ø=75mm, Icr=0%), Sherbrooke, Laval, Shelby, others	C_u: Shelby: 88%	Tanaka *et al* (2001)
Athalone laminated clay (sensitivity = 2-5, medium)	Thin wall Sherbrooke, sharp cutting edge (5° and 30°)	C_u: 128% (5°), 110% (30°)	Long (2006)

Table 2.10 - Effect of Sampling Disturbance on the Undrained Shear Strength of Samples - Comparison of different Sampling Methods

Type of Clay	**Types of tube or cutting edge**	**Extent of disturbance**	**Loss of strength if disturbed**	**Reference**
Reconstituted coastal soils (Patenga, Fakirhat, Kumira)	6 sharp samplers, OCA between 4 and 15°, AR between 10.8 and 55.2%	Blunter > sharper, thicker > thinner	YES, Increasing AR from 10.5 to 55.2% results in loss of Cu up to 47%, increasing OCA from 4 to 15° results in loss of Cu up to 51%	Siddique *et al* (2000)
Singapore Lower Marine Clay (OCR=1.3-1.45, sensitivity=3-6 (High))	Japanese thin walled piston (AR=7.5%, ICR=0%, taper angle=6°), Shelby tube (AR=11.5%, ICR=1%, OCA=20°)	Shelby> Japanese piston	YES, C_u(Japanese piston) is 30% higher than C_u(Shelby)	Tan *et al* (2002)
Boston Blue Clay	Shelby piston, sharpened Shelby piston, Sherbrooke	Shelby> Shelby piston > Sherbrooke	YES	DeGroot *et al* (2005)
Boston Blue Clay (OCR=1.1-1.2, sensitivity= Low to Medium)	Blunt / Built-in	Blunt >> Built-in	YES	Santagata *et al* (2006)
Reconstituted Dhaka clay	8 samplers with AR between 9.7 and 73.1%, OCA=5°	-	YES, 17-61% reduction in Cu when AR is increased from 16.4 to 73.1%	Siddique *et al* (2009)
Gault Clay	U100, UT100	Thick>Thin	YES, Cu at depths of over 8m was reduced by 50% for U100	Gosling and Baldwin (2010)

It can be concluded from most of the studies presented in this section that sampling disturbance causes a significant reduction in undrained shear strength for most clays, with magnitudes falling as much as 50% when compared to block samples. The water content (Tan *et al*, 2002) and void ratio (Siddique *et al*, 2009) in disturbed samples has been measured to be higher than that in less disturbed samples. In tests applying strain paths to undisturbed samples, it was shown that the PSA resulted in little change in the soil's undrained shear strength, while even small strain cycles (±1%) of ISA resulted in serious decreases (Santagata and Germaine, 2002).

Table 2.11 - Effect of Sampling Disturbance on the Undrained Shear Strength of Samples - Effect of applying a Strain Path

Type of Clay	Strain applied	sample / undisturbed (Cu or p')	Reference
Resedimented Boston Blue Clay	PSA, ISA	p': PSA: 92%, ISA: 38% C_u: ISA: 75%	Baligh *et al* (1987)
Bothkennar Clay (lightly overconsolidated)	Between ±0.5 and 2%	p': 40% for ±2% before reconsolidation, then 90% after	Clayton *et al* (1992)
Vallercia Clay (from block samples) and London Clay	±1%	p': 90% Cu: 95% after reconsolidation for Vallercia clay, unknown in London Clay	Georgiannou and Hight (1994)
Kaolin (80%) and Silty and (20%)	PSA, ISA: ±0.5 to ∞ (remoulded)	C_u:PSA: 92%, ±0.5%:88%, ±1%:87%, ±1.5%:81%, ±2%:76%, ±3%:72%, remoulded: 42% in Unconsolidated Undrained tests, ±1.5%: 115% and ±3%:118% when Ko reconsolidated	Wei *et al* (1994)
Reconstituted London Clay	ISA 0.25-2%, not symmetric	p':63-90%, 7% reduction in strength observed after reconsolidation	Siddique *et al* (1999)
RBBC (OCR=1, sensitivity=low to medium)	PSA, ISA ±1%, ±2%, ±5%	C_u: 85%, 74%, 67%, <55%	Santagata and Germaine (2002)

A notable exception to the typical reduction in shear strength is a study by Long (2001, 2003, 2006) in laminated clays, who observed densification of the sample due to partially drained tube driving, and an increase in undrained shear strength and small-strain stiffness. In the same study, small OCAs were found to decrease sample quality. The tables above show that while some tube geometry parameters must be avoided (blunt tips, thick diameters), no single best tube stands out from the others as a universal tool for avoiding sampling disturbance. The variability in soils is such that no single study can be used as a definite reference for sampling disturbance. In many cases, reconsolidation of the samples with the appropriate technique can recover most of the undrained shear strength of the sample.

2.4.1.2 Effect on the Stress-Strain Behaviour

Many of the aforementioned studies also measured the differences in the stress-strain behaviour of the clays under different strain paths or using different samplers. Three aspects were commonly observed:

- A reduction in the normalised shear stresses at a given strain (see previous section).

- A significant increase in the strain to peak strength (Kirkpatrick and Khan, 1984): +200-800% in Kaolin (Wei *et al*, 1994): +30-313% in London clay (Siddique *et al*, 1999), +100-200% in Dhaka clays (Siddique *et al*, 2009)
- A reduction in the undrained small-strain stiffness, seen by the reduction in the pre-yield rigidity, or Young's modulus, E, which represents the slope of the linear relationship on a stress-strain graph.

When tube samples were compared to block samples, the reduction in stiffness due to tube sampling could be quantified. Similarly, when different tubes were used, reductions in E were observed. Results from these studies are included in Table 2.12. When strain paths from the Strain Path Method (Baligh *et al*, 1987) were applied to undisturbed samples, a marked reduction was observed. These studies are summarised in Table 2.13.

In other studies, the stress-strain behaviour was plotted, either for Unconfined Compression tests or Consolidated-Undrained tests. Some examples are included in Figure 2.13 and Figure 2.14. In most cases, the three above aspects are observed, and many more examples of this behaviour exist in the literature (Kirkpatrick and Khan, 1984, DeGroot *et al*, 2005, Santagata *et al*, 2006, Sulkorat *et al*, 2008, and most of the references in the tables).

While some of the changes in undrained shear strength can be recovered using the appropriate reconsolidation stresses in the triaxial cell, the changes in stiffness are largely irrecoverable, making this a larger issue during sampling (Tan *et al*, 2002, Clayton *et al*, 1992). Sulkorat *et al* (2008) proposed guidelines for evaluating sample quality depending on the change in stiffness at small strains (Figure 2.15), with those experiencing reductions under -40% and strains under 2% considered very good to excellent. It is of note that the OCR influences the degree of disturbance: Kirkpatrick *et al* (1986), Hird and Hajj (1995), Siddique *et al* (1999) and Santagata and Germaine (2005) among others concluded that disturbance, and its effect on p', C_u and E, decreased with increasing OCR.

Table 2.12 - Effect of Sampling Disturbance on the Stiffness of Clay - Comparison of Block and Tube

Type of Clay	Type of tube	Changes to Stiffness (E)	Reference
Canadian clays (sensitivity=high)	Shelby, Norwegian piston sampler, block	In CU tests, E for Shelby was 45-72% that of block, and for Norwegian piston, 80-84% that of block	Milovic (1971)
Champlain clays	Piston, block	E of piston sample is 60% that of block	La Rochelle and Lefebvre (1971)
Reconstituted coastal soils (Patenga, Fakirhat, Kumira)	6 sharp samplers, OCA between 4 and 15°, AR between 10.8 and 55.2%	Increasing AR from 10.5 to 55.2% results in loss of E up to 58%, increasing OCA from 4 to 15° results in loss of E up to 62%	Siddique *et al* (2000)
Kaolin and Bay Mud	Shelby, DFSD sampler	<50% of block samples (DFSD's E is 16% higher than Shelby samples)	Safaqah and Riemer (2005)
Reconstituted Dhaka clay	8 samplers with AR between 9.7 and 73.1%, OCA=5°	7-70% reduction in Cu when AR is increased from 16.4 to 73.1%	Siddique *et al* (2009)

Table 2.13 - Effect of Sampling Disturbance on the Stiffness of Clay - Effect of applying a Strain Path

Type of Clay	Strain applied	E disturbed/ E undisturbed	Reference
Bothkennar Clay	Between ±0.5 and 2%	After reconsolidation: for ±0.5%: 132%, for ±2%: 39%	Clayton *et al* (1992)
Vallercia Clay (from block samples) and London Clay	±1%	65% in Vallercia, 75% in London clay	Georgiannou and Hight (1994)
Reconstituted London Clay	ISA 0.25-2%, not symmetric	15-36% at small strains (0.01%), 15-45% (at strain =0.1%), 19-52% (strain=0.05%)	Siddique *et al* (1999)
RBBC (OCR=1, sensitivity= low to medium)	PSA, ISA ±1%, ±2%, ±5%	100% (116% at small strains), 67%, 50%, 20%	Santagata and Germaine (2002)
RBBC (OCR=2-8, sensitivity= low to medium)	ISA ±1%, ±2%, ±8%	67%, 58%, 17%	Santagata and Germaine (2006)

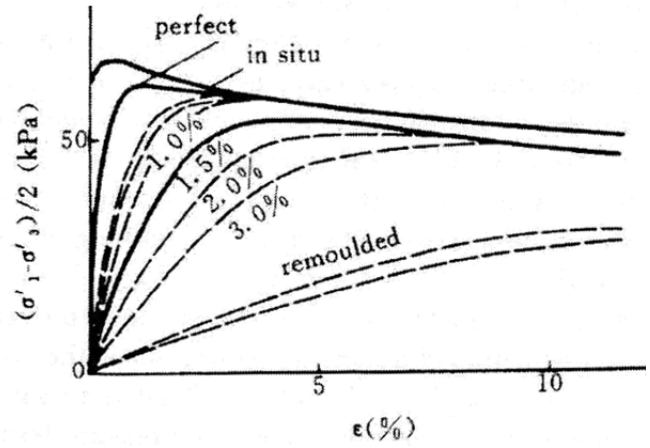

Figure 2.13 - Effect of Applying ISA Strains to Kaolin (Wei *et al,* 1994)

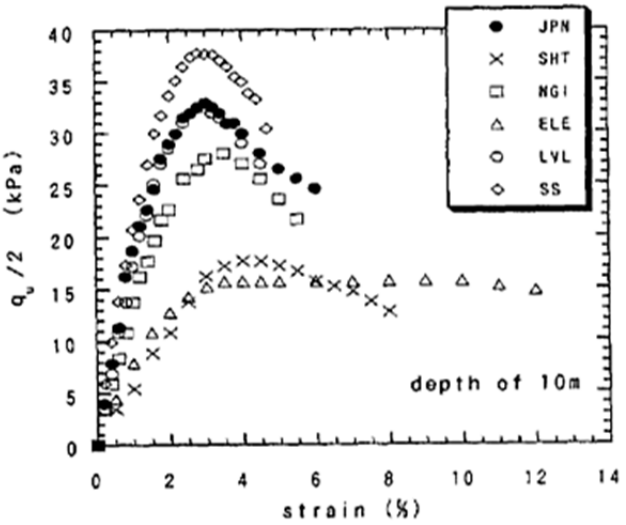

a

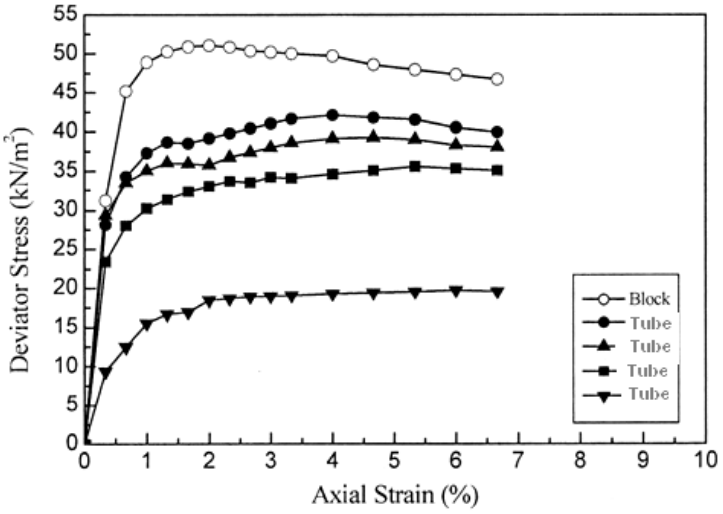

b

Figure 2.14 - Typical Stress-Strain Behaviour for Different Samplers in Same Soil: a) in Ariake Clay, Tanaka *et al* (2002) and b) in Reconstituted Dhaka clay, Siddique *et al* (2009)

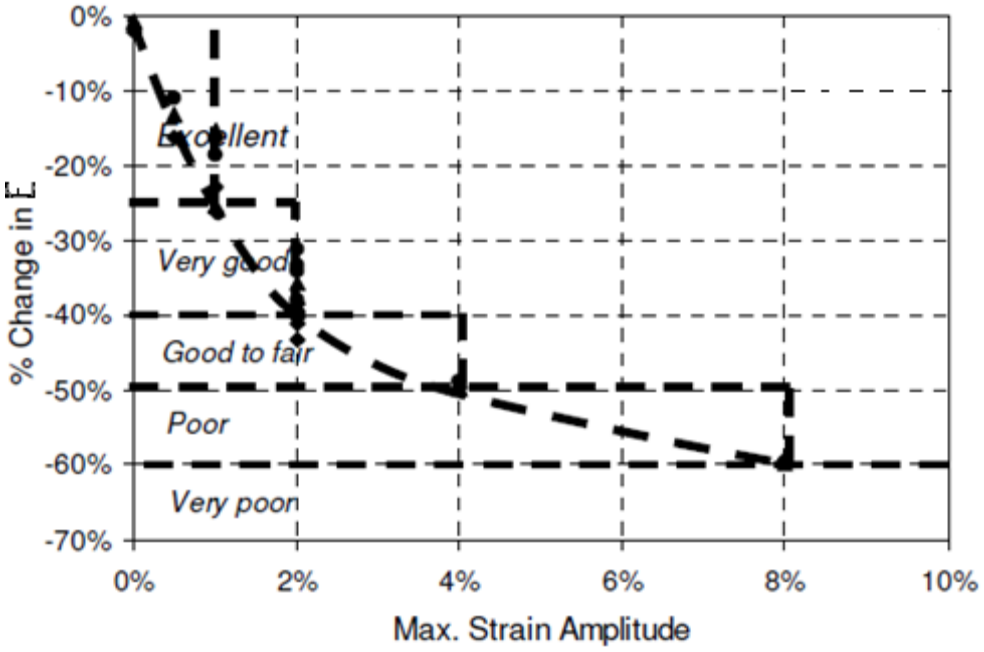

Figure 2.15 - Stiffness as a Factor for Sample Quality, from Sulkorat *et al* (2008)

2.4.1.3 Effect on the Compression Curve

A soil's response to compression is also dependent on the extent of sampling disturbance. In undisturbed clays under monotonic loading, a typical sample will experience two consolidation phases, an initial slow reduction in void ratio, followed by a rapid reduction once past a particular consolidation pressure. Nagaraj *et al* (1990) noted a difference in the consolidation behaviour of different samples, which increased with worsening sample quality (Figure 2.16a): the void ratio of disturbed samples was found to decrease faster than that of less disturbed samples at the same consolidation pressure. Prasad *et al* (2007) proposed studying the slopes of these two phases (C^*_{c1} and C^*_{c2}) in a plot of log(1+e) against consolidation pressure to quantify the amount of disturbance (Figure 2.16b). Later research by Siddique (2009) found that in reconstituted Dhaka clays, values for the compression index (C_c) for tube samples were larger than those for block samples, with more noted increases for higher sampler AR.

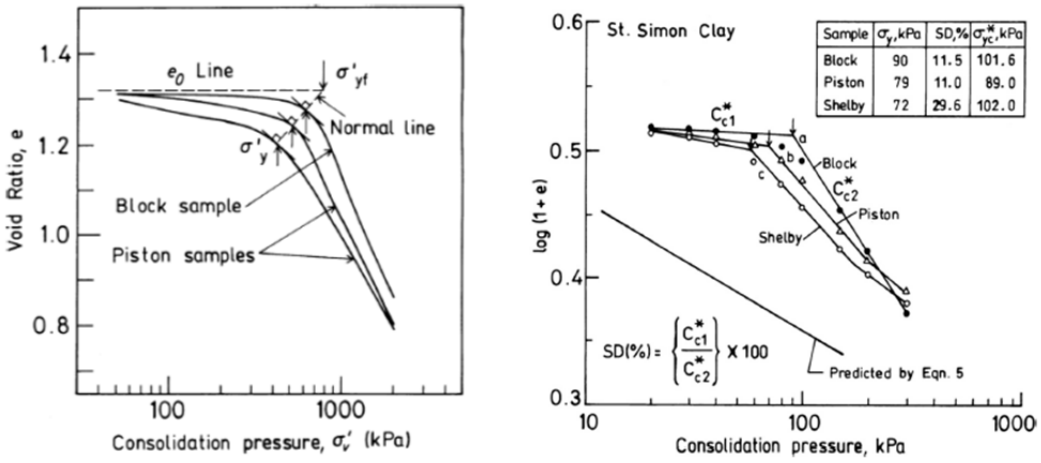

a b

Figure 2.16 - Sampling Disturbance Effects on the Soil's Compressibility: a) from Nagaraj *et al* (1990) and b) from Prasad *et al* (2007)

2.4.1.4 Sensitive Clays

Studies on sensitive clays have discovered additional disturbances specific to this type of soil. Sensitive clays are those which lose a large amount of their shear strength upon remoulding. Some onshore clays have high sensitivities, as well as most deep-sea sediment deposits (Baudet and Ho, 2004), meaning that this section is very relevant to sampling offshore. In their extreme, these are classified as quick clays, which can liquefy when subjected to increased loads and strains. These clays exhibit brittle cementation bonds which are easily disturbed during tube sampling, but not during block sampling (Eden, 1971, La Rochelle and Lefebvre, 1971, Raymond *et al*, 1971, La Rochelle *et al*, 1981). A large difference was observed from laboratory tests on block and thin-walled tube samplers: the rigidity (Young's Modulus) in piston samplers was found to be half that of block samples (La Rochelle and Lefebvre, 1971) and the undrained shear strength was also found to be halved (Eden, 1971, La Rochelle and Lefebvre, 1971). The latter study, comparing specimens of the same soil taken from block and thin-walled piston samplers in Champlain clays, found that the volume increase in the sample due to the insertion of the tube into the ground was sufficient to break the cementation bonds, and that the disturbance was uneven throughout the cross section of the sample, with vane tests in the middle of the sample revealing higher strengths and therefore less disturbance. A solution was proposed concerning the sampling of sensitive clays: to reduce the thickness and increase the diameter of the tubes used to collect samples. This would have the effect of decreasing the Area Ratio of the sampling

tube, which is in line with general recommendations for clay soils. Eden (1971) suggested that the presence of a small Inside Clearance (such as that of the Swedish foil sampler) provided enough lateral expansion to the sample to break the cementation bonds and significantly alter its structure. La Rochelle *et al* (1981) compared the undrained shear strength of soil at eight depths in the same sample taken by a piston tube and concluded that a piston should not be used in sensitive clays due to the effects of its suction upon the upper layers of the sample, which exhibited much lower strength (Figure 2.17).

Eden (1971), La Rochelle and Lefebvre (1971) and Raymond *et al* (1971) all concluded that in sensitive clays, the use of a thin-walled piston sampler - while previously considered the best design - was not appropriate for sampling, since a large proportion of the clay became remoulded and hence its properties differed significantly for the in-situ state. From a comparison of block samples, four piston samplers and one open tube sampler in Leda Clay soils, Raymond *et al* (1971) concluded that any type of tube sample resulted in severe changes in the soil's behaviour, with block samples yielding the highest strength and open tubes the lowest.

The Laval sampler was developed by La Rochelle *et al* (1981) using these guidelines. Its diameter was increased from <75mm in previous designs to 208mm, with an AR of 10% (this corresponds to a thin-walled tube) and an OCA of 5°. It is mounted with a coring tube surrounding the open sampling tube. The sampling tube is pushed into the base of the borehole, after which the corer is pushed downwards and the soil surrounding the tube is ground away and removed. Overcoring is recommended to minimise the entrance of excess soil. The sampling tube is then under less pressure and can easily be removed from the ground without excessive loss of sample. Tests on this sampling method were carried by the developers, who suggest that the quality of samples taken using this method is comparable to that of block samples, although they recognised that its use was limited to large projects due to the costs associated with the larger sampler. Later tests on clay samples by Clayton *et al* (1992) and others validated its use as well as that of the Sherbrooke sampler as an alternative for block samples – but only where the high costs could be justified.

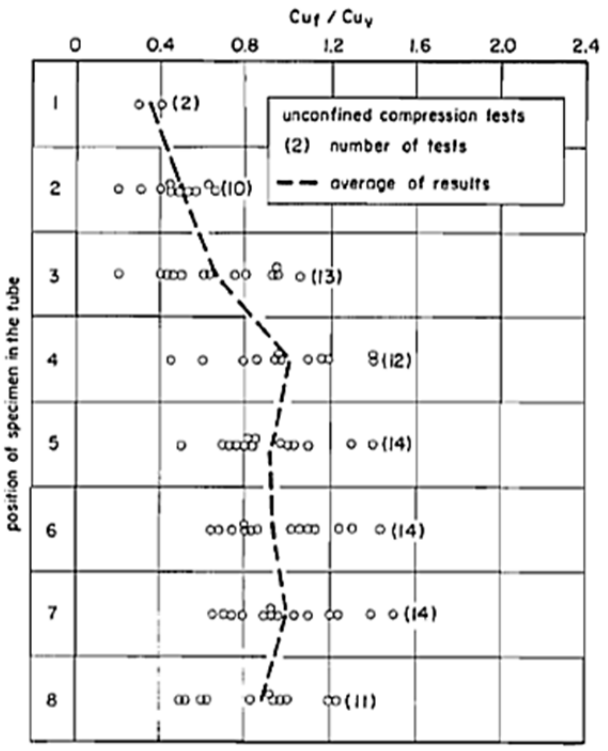

Figure 2.17 - Variation in Undrained Shear Strength in a Sample of Sensitive Clay (from La Rochelle *et al*, 1981)

2.4.1.5 Effect of Sampling Speed

The speed at which the sampling tube is driven into the ground is another source of disturbance. Hvorslev (1949) recommended the use of fast, continuous pushing as a method generating the least disturbance to the sample. Budhu and Wu (1992) compared three rates of sampling in their numerical model, 0.4, 4.0 and 40.0mm/s. Three aspects of the sample's behaviour were recorded: the change in effective stresses, the maximum displacement of an element on the sampler's centreline and the magnitude of the compressive strain ahead of the sampler. It was found that a faster speed of driving produced lower compressive strains, and significantly reduced the magnitude of the changes in stress, while lower speeds were linked to the entrance of excess soil and the development of higher wall friction – facts already observed by Hvorslev. Little difference was observed between the speeds of 4.0 and 40.0mm/s, and the authors suggested a speed of 20mm/s as an appropriate value.

2.4.1.6 Sample Storage, Extrusion and Preparation

After being retrieved from the ground, samples can be stored for a long time before testing. Hight *et al* (1992) presented a study on effective stress measurements in high quality specimens taken from Laval samples. Figure 2.18a shows that the effective stresses remain constant over time, with larger diameter specimens exhibiting the least variability. The authors also observed a 20% reduction in effective stresses in the short term, most probably due to sample transport rather than pore water redistributions within the sealed samples. Tanaka *et al* (2001) also found no variation in effective stress during 2 years storage in high quality samples of Ariake clay, while low quality samples showed a change in the short term, after which the effective stress stabilised and remained constant over the remainder of the storage time (Figure 2.18b).

Before testing, the sample is extruded from its tube. This can be done horizontally or vertically, and while the latter method causes the least disturbance, it is not always used. A study by Chung *et al* (2004) on Pusan clays compared the properties of clay samples extruded vertically out of the tube by pushing in either direction, by “normal” and “reverse” extrusion (in the direction the soil entered the tube, Figure 2.19a). Their choice of terms is interesting in that a number of sources including the current standard (EN ISO 22475-1:2006) show evidence that the recommended direction is the one in which the soil enters the tube (Messerklinger and Springman, 2009). While no recommendations are made for the extrusion of samples from open tubes and piston samplers in the standard, this applies to cores.

Figure 2.19b shows a comparison of maximum deviatoric stress (q_u) and strain at maximum deviatoric stress (ε_p). It can be seen that samples taken in the reverse method (R) show higher strain at failure and lower deviatoric stress, a typical effect of disturbance. In either case, the authors concluded that this disturbance, due to extrusion, had little influence on the sample.

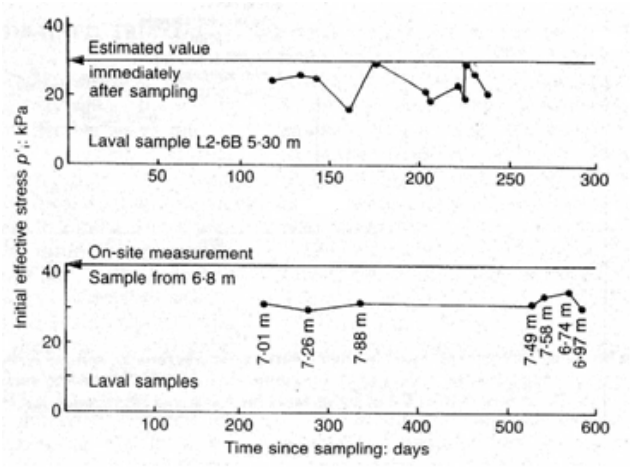

a

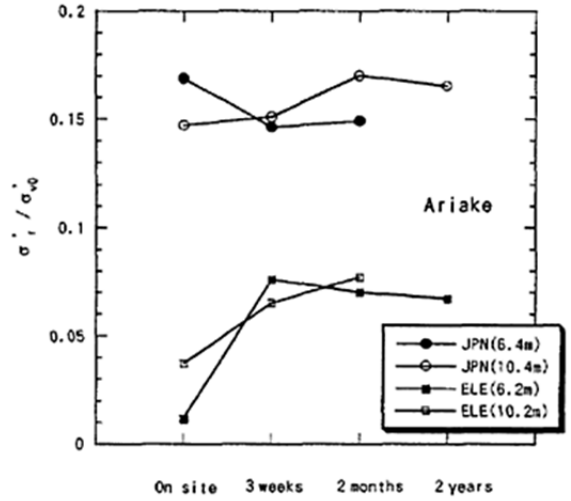

b

Figure 2.18 - Effective Stresses during Sample Storage: a) from Hight *et al* (1992) and b) from Tanaka *et al* (2002)

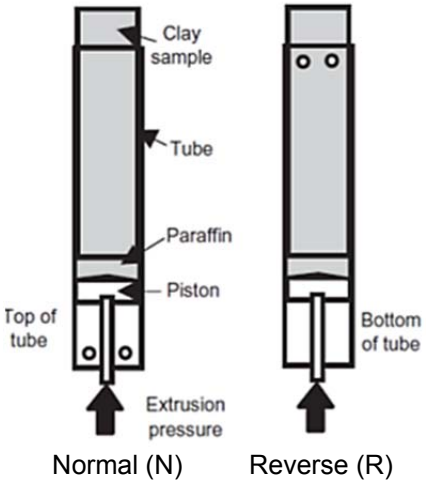

a

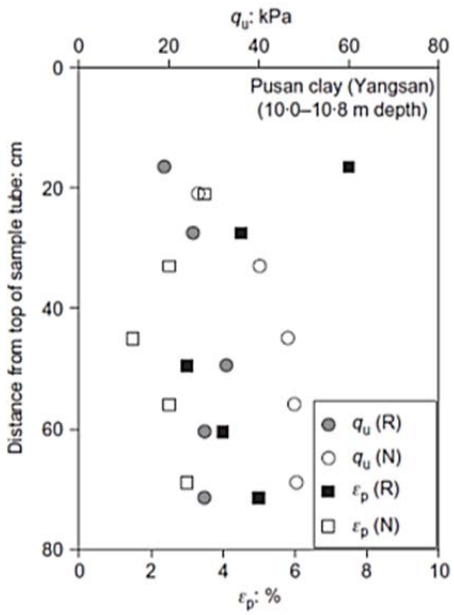

b

Figure 2.19 - Extrusion of Sample: a) Set-up and b) Effect on Properties (from Chung *et al*, 2004)

The negative pore water pressure set up during sampling varies during sample preparation. Figure 2.20 shows the dissipation of the excess pore pressure with time in Kawasaki clays (Kimura and Saitoh, 1982). Extrusion and trimming cause some difference to the pore pressure, which steadily reduces over time towards zero.

The size of the sample depends on the equipment used. Sometimes long, continuous samples are obtained, while in most cases short samples (≈450mm) are taken. Sometimes the diameter of the sample is larger than that of the specimen required for testing, in which case it is trimmed. Santagata *et al* (2006) recommended against using untrimmed specimens due to the high degree of disturbance seen in many samples. Parts of the sample are often discarded due to higher degrees of disturbance. Chung *et al* (2004) found that in 854mm samples, soil within the top 300mm and bottom 150mm of the sample is seen to be the worst affected by the whole sampling process, both in terms of void ratio (e_o) and yield stress (σ'_y). It was hypothesised that this is largely due to the high hydraulic pressures used to remove the drilling fluid at the base of the borehole, rather than to the strains caused by the penetration of the tube. The highlighted need to trim the sample agrees with Hvorslev (1949), who recommended that the first 2 to 3 tube diameters under the base of the borehole should be discarded after sampling, especially when a sample has been taken in close proximity.

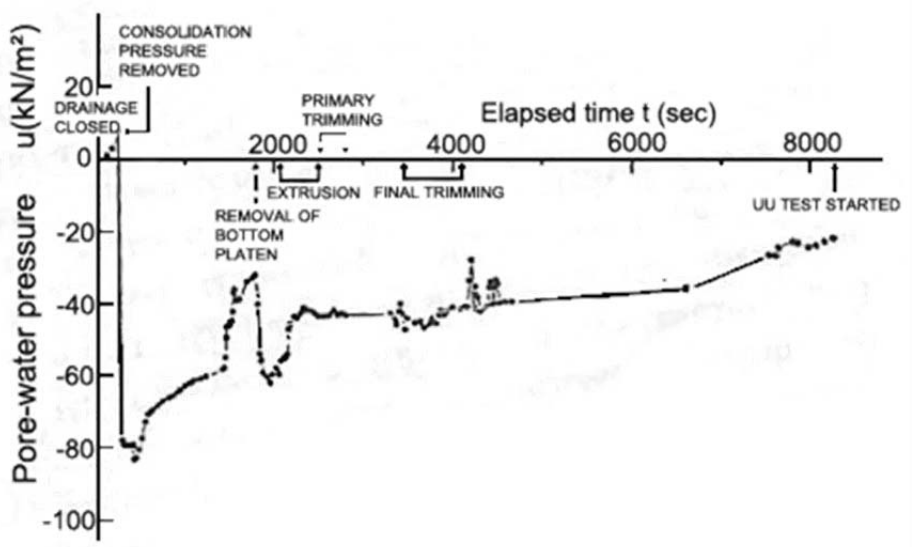

Figure 2.20 - Dissipation of Excess Pore Pressures during Sample Handling (modified from Kimura and Saitoh, 1982)

A study by La Rochelle *et al* (1981) on the effects of piston sampler in sensitive clays agreed with this, having noted that the undrained shear strength in the top layers of the sample was as low as a third of that in lower layers. Similarly, Rowe (1971) notes that the soil in the top 170mm of a 600mm long sample of organic alluvial clay was heavily disturbed, creating a softened zone with undrained shear strength as low as half that of deeper layers. Lacasse and Berre (1988) also recommended discarding the top and bottom 1.5-3 diameters unless X-ray inspection of the sample revealed no disturbance to the soil structure.

2.4.2 The Use of Stress Paths to quantify Sampling Disturbance

2.4.2.1 Soil Response to Stress

In its in-situ stress state, an element of soil in the ground will be subjected to three stress components, each acting along one direction (Figure 2.21a). In the natural deposition of soils, the stresses act primarily in the vertical direction (σ_v) and increase over time as more soil is deposited above. The horizontal stresses (σ_h) increase accordingly, following a linear relationship to the vertical stress. The coefficient of earth pressure, K_o, links these stresses following Equation 6. K_o is different for all soils and is typically less than 1 in Normally Consolidated soils. In Overconsolidated soils, K_o can be larger than 1 due to the phenomena leading to the soil becoming overconsolidated: deposition, erosion, glaciation, thawing, etc.

The behaviour of a soil can be studied by the path it takes in response to different loading conditions. In the standard triaxial cell, the pressure on and around the sample can be changed so as to replicate any combination of vertical and horizontal principal stresses (Figure 2.21b). The vertical pressure (σ_1) is controlled by the load which is applied to the sample, and the cell water provides an all-round pressure (σ_3): the two horizontal stresses are equal. For any stress state, two sets of values can be calculated: s', the mean effective stress on the sample (when one major stress is zero) and t, or q, the deviatoric stress on the sample and p', the mean effective stress (Equation 7 to Equation 10).

Each stress state experienced by the soil can be plotted on an s'-t or q-p' graph, and the curves created in this way form the stress path of the sample. Studying these paths for disturbed and undisturbed soils gives an idea of the effects of sampling disturbance.

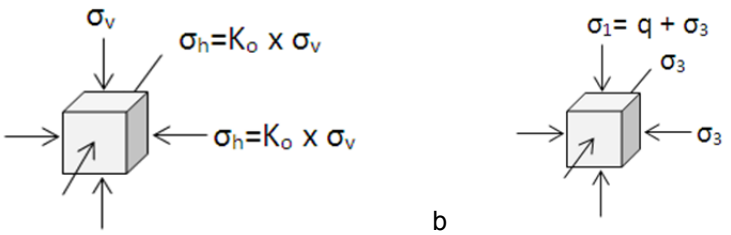

a b

Figure 2.21 - Stresses on a Soil Element: a) in the Ground and b) in the standard Triaxial Cell

$$K_o = \frac{\sigma' h}{\sigma' v}$$ Equation 6

$$s' = \frac{(\sigma'_1 + \sigma'_3)}{2}$$ Equation 7

$$t = \frac{(\sigma'_1 - \sigma'_3)}{2}$$ Equation 8

$$q = \sigma_1 - \sigma_3$$ Equation 9

$$p' = \sigma'_v \times \frac{(1 + 2K_o)}{3} = \frac{(\sigma'_1 + 2\sigma'_3)}{3}$$ Equation 10

Yielding in a soil may be defined from two laboratory tests, which determine the stress-strain behaviour of the soil and its consolidation behaviour. The yield point of a soil for each of these curves is shown in Figure 2.22a and Figure 2.22b. The response of soils to loading is the development of volumetric and shear strains, which are elastic (and therefore recoverable) before reaching the yield point, after which they become plastic and large strains occur as the structure of the soil is modified.

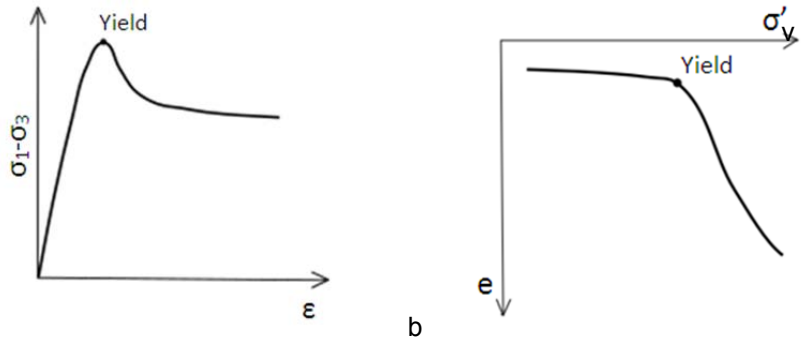

a b

Figure 2.22 - Yielding in Clays: a) in the Stress-Strain Curve and b) in the Compression Curve

Full yield curves can be created for each type of clay for a given void ratio and exist for each depth for a given deposit of soil. This has been done for a large number of existing soils: their shape depends on their plasticity and is always an elliptical curve centred on the K_o line which can be normalised by the vertical effective stress in most soils.

2.4.2.2 Constitutive Models to Describe Destructuration during Sampling

A number of constitutive models have been described to explain the link between disturbance and the irreversible destructuration of soil. In the Ylight soil model (Tavenas and Leroueil, 1977), two limit states (or yielding conditions) have been defined: that of the young (or initial) yielding of the soil and that of the aged yielding of the soil, which happens at higher pressures due to secondary consolidation of the soil which happens over time in natural soils and increases their effective stress. Tavenas and Leroueil described the behaviour of clays around these defined limit states. In particular reference to destructuration, they stated that: “the structure of the clay is destroyed when it is submitted to effective stresses in excess of its preconsolidation or, more generally, outside its limit state”.

In Figure 2.23a, soils subjected to zones 1 and 2 fail with large strains, while zones 3 and 4 undergo deformations but no failure, with zones closes to the aged limit state at risk of the largest deformations, and in zone 5 the soil undergoes no deformations or failure. In general terms, destructuration occurs when the effective stresses pass the limit state or preconsolidation pressure of the soil (since the limit state depends on the latter). Sampling disturbance is known to affect the initial yield – or bounding – surface (Tavenas and Leroueil, 1987, Hight *et al*, 1992) and may therefore cause plastic deformations within the soil specimen, changing the bonds between the soil particles and the microstructure of the sample.

Figure 2.23b and Figure 2.23c compare the stress paths of samples subjected to stress relief only (perfect samples) and sampling disturbances (from Baligh *et al*, 1987). In the case of a perfect sample of normally consolidated clay originally in the stress state at A (Figure 2.23b), the release of stress will cause no (or little) disturbance, while a sample of lightly overconsolidated clay originally at point B will touch the limit state line during stress relief,

resulting in some degree of structural disturbance. Before testing, the effective stress state lies at point C, which again, is different from that in-situ. During ideal tube sampling (Figure 2.23c), the stress path is very different and the sample can find itself subjected to the limit state, resulting in structural disturbances.

Another similar constitutive model is that of Jardine et al (1991, Figure 2.24), which defines three yield surfaces, Y1, Y2 and BS (or Y3, bounding surface, same as in the previous model). Surface Y1 is the limit of elastic behaviour, while Y2 signal the start of nonlinear elastic behaviour and the BS marks the point after which significant structural disturbance is to be expected.

Strain to Y1 is small, at around 0.001% in uncemented soil, and 0.1% in cemented soils and weak rocks (Hight, 1993), while strain to Y2 in clays is in the region of 0.04% (Jardine *et al*, 1991, Georgiannou and Hight, 1994). Bounding surface strains are higher, and are typically less than 2.5% in clays (data compiled by Hight, 1993).

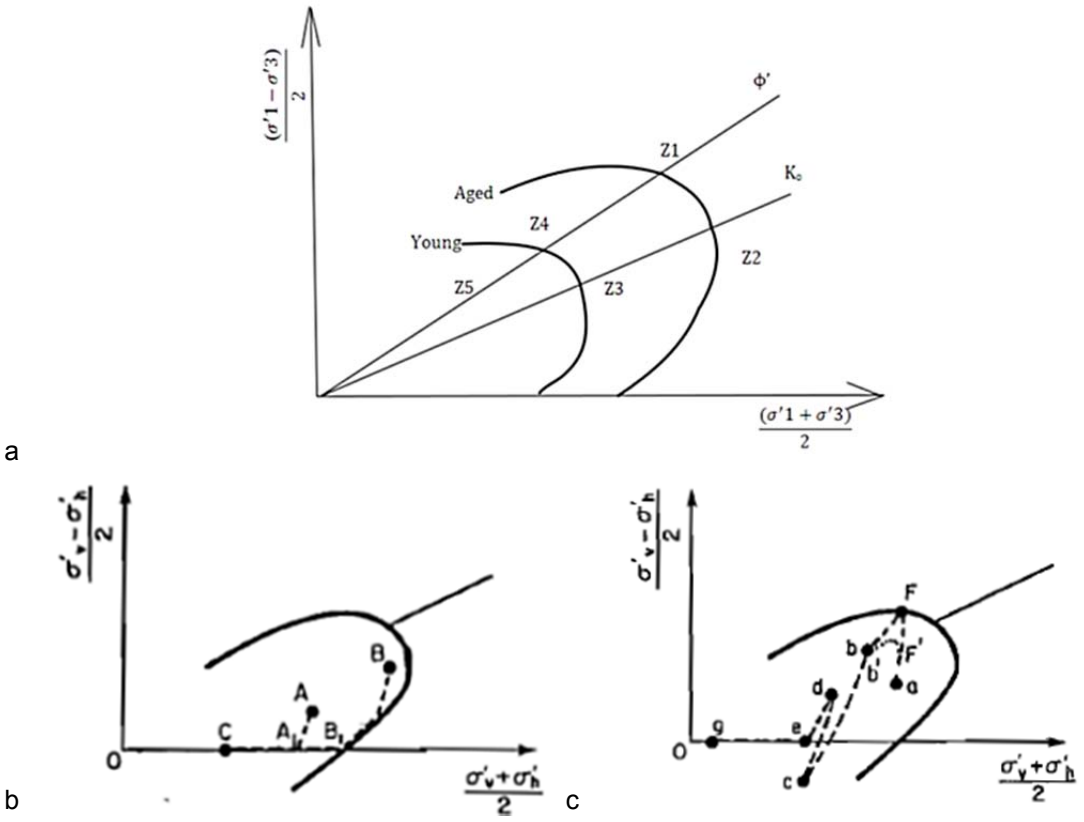

Figure 2.23 - Limit State Curves: a) defined Zones of Behaviour and b) Stress Paths for Perfect and c) Ideal Sampling (from Tavenas and Leroueil (1987))

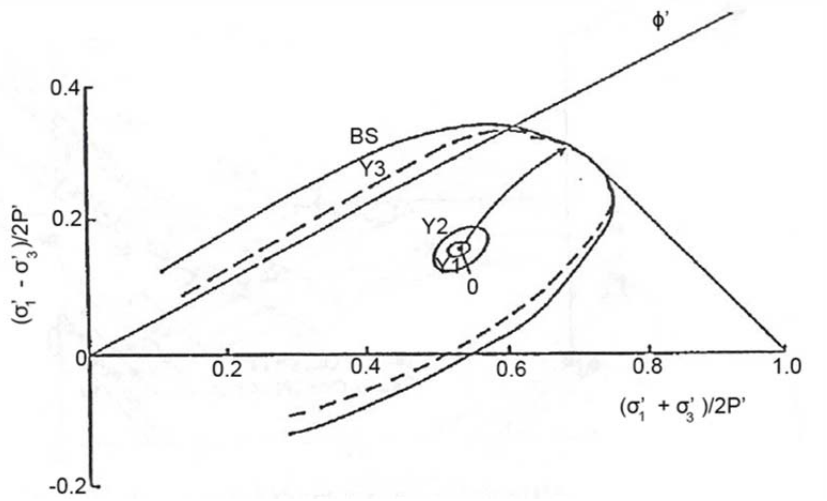

Figure 2.24 - Yield Surfaces in Undrained Soils (modified from Hight, 1993, adapted from Jardine et al, 1991)

2.4.3 The Perfect Sampling Approach

Ladd and Lambe (1963) investigated the effect of stress relief only on the behaviour of several clays. This Perfect Sampling Approach (PSA) assumes that sampling is an undrained process, and therefore that the magnitudes of the effective stresses are dependent on the negative pore pressures generated during sampling as a result of stress relief only. They proposed that the isotropic effective stress after perfect sampling, for a saturated clay with vertical stress σ_v and horizontal stress $\sigma_h = K_o \times \sigma_v$, could be calculated using Equation 11. They found that for perfect samples, the effective stress could be as low as 35% of that in-situ, up to 80% for normally consolidated clays and as high as 200% in highly overconsolidated plastic clays.

$$\sigma'_{ps} = \sigma'_v \times [K_o + A_u \times (1 - K_o)]$$

$$Where\ A_u = \frac{(\Delta u - \Delta\sigma_h)}{(\Delta\sigma_v - \Delta\sigma_h)} \qquad \text{Equation 11}$$

Skempton and Sowa (1963) also studied the phenomenon of stress relief after observing that the effective stress in samples of Avonmouth clay was 0.7 times that in the ground. By comparing five pairs of identically prepared samples of moderately sensitive Weald clay in undrained triaxial tests at different stresses, the effects of stress relief on the undrained strength of the clay could be observed. Ground conditions were simulated by a K_o consolidation of the first in each pair of samples, followed by an increase in vertical load until

failure. Stress relief was applied to the second sample in each pair by reducing the vertical load to that of the horizontal load (isotropic conditions), then testing until failure. The stress paths were different for each sample of normally consolidated soil (Figure 2.25), and similar for overconsolidated soils. In each case, the failure of samples subjected to stress relief occurred at very similar pressures. The study concluded that pure stress relief caused little change to the soil's strength: Skempton and Sowa observed no significant changes in the undrained shear strength of the disturbed samples (1-2% reduction), although it was hypothesised that more sensitive clays would be more affected.

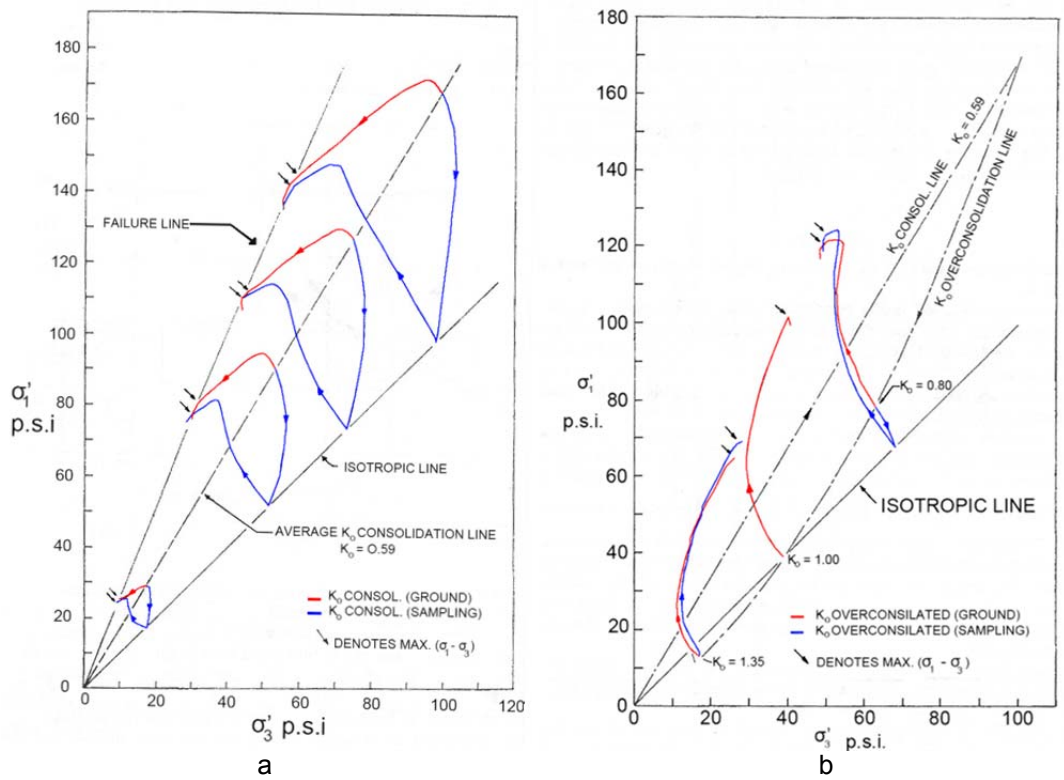

Figure 2.25 - Stress Paths for Pairs of Clay Samples subjected to "Ground" Conditions and "Sampling" Stress Relief: a) in normally consolidated soils and b) in overconsolidated soils (from Skempton and Sowa, 1963)

2.4.4 The Ideal Sampling Approach

While the PSA studies the limited effects of stress relief, another method – the Ideal Sampling Approach (ISA) – considers the effect of the sampling tube itself. Sampling disturbance has been investigated in a range of different manners. Where some researchers have attempted to quantify soil distortions and strains experimentally through soil models, others have developed computer-based software to predict the observed disturbances. The

basis of our understanding of the strains on the centreline of the sampler rests with the Strain Path Method (Baligh, 1985, Baligh *et al*, 1987). This relies on the assumption that in deeper problems, due to kinematic restraints, soil deformation is largely strain dependent since similar distortions were observed in soils with very different stress-strain behaviours. They developed a new analytical method, the Strain Path Method (SPM), to predict soil behaviour in deep geotechnical models – as a flow problem rather than using a constitutive model. The Strain Path Method is based upon an estimation of initial strains rather than stresses, which are obtained by estimating firstly the stresses present in the undisturbed ground, then the velocity field which the soil particles are subjected to during the object's penetration. The main steps of the SPM are:

- Initial stresses are estimated
- A velocity field satisfying conservation of volume is assumed for describing the velocity of soil particles moving around the sampler
- Soil deformations are obtained by integrating the velocity field along the streamlines
- The strain rates are derived by differentiating the velocities with respect to the coordinates
- The strain rates are integrated along streamlines to obtain the strain path of "soil" elements

The SPM was developed by Baligh considering the theory of Cavity Expansion, which studies the behaviour of an incompressible, isotropic and homogeneous material surrounding a spherical source which discharges a similar material at a constant rate (Figure 2.26a). The spherical source example was then adapted to model simple pile penetration by applying a uniform flow field to the original source, and the deformation around the pile was observed (Figure 2.26b). Comparisons of the predictive technique with the behaviour of experimental models found resemblance in the "basic features of actual pile penetration".

In the author's own words, the SPM is an "approximate analytical technique" used to predict strains around rigid objects being forced into the soil. The equations supporting the Cavity Expansion theory are independent of the shearing behaviour of the soil, and the material used has no shear strength. Further adaptations of the theory allowed different object

geometries to be modelled in the same fashion. Tube samplers are modelled from ring sources and specific end geometries can be created using additional superpositions of sources and velocity flows. In further research, Baligh *et al* (1987) applied the SPM to a "simple" tube sampler (illustrated by Clayton et al, 1998, in Figure 2.27). This blunt geometry is not representative of an optimised cutting shoe, and includes an element of inside clearance.

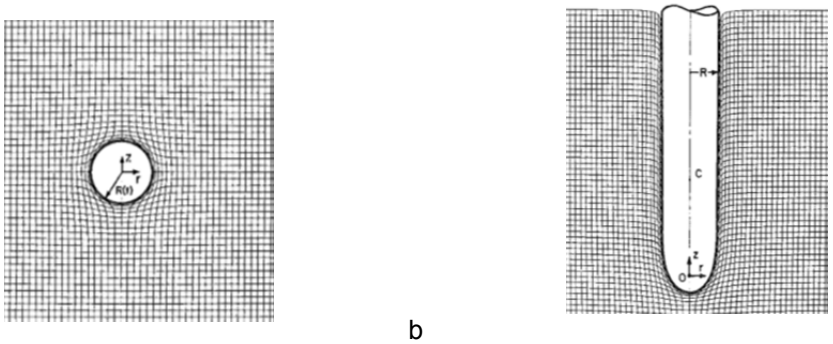

a b

Figure 2.26 - Deformation around a) a Spherical Source and b) a Model Pile using the SPM (Baligh, 1985)

The strains around the simple sampler's tip (Figure 2.28) and the strain history at the sample centreline (Figure 2.29) were thereby predicted. The ISA method completes the PSA method in that the latter considers only the retrieval and extrusions phases (the stress relief) while the former considers the driving of the sampler, during which the strains and effect on the soil's properties are found to be significantly higher than when using the PSA. The study found that the dominant strain components, when comparing radial (Figure 2.28a), tangential (Figure 2.28b), meridional (Figure 2.28c), and vertical (Figure 2.28d) at the base of the sampler, were those of vertical strains.

Deformations were observed to affect the sampler tip and the soil immediately surrounding the tube. The authors concluded that the deformations within the innermost elements within the sampler tube, within a radius of B/4 of the centreline, were small, while those in the proximity of the tube were high enough to warrant discarding the outer half of the sample during testing. The method having been developed for deep models, it is not appropriate to predict strains in soil elements close to the base of the borehole, and near the ground surface.

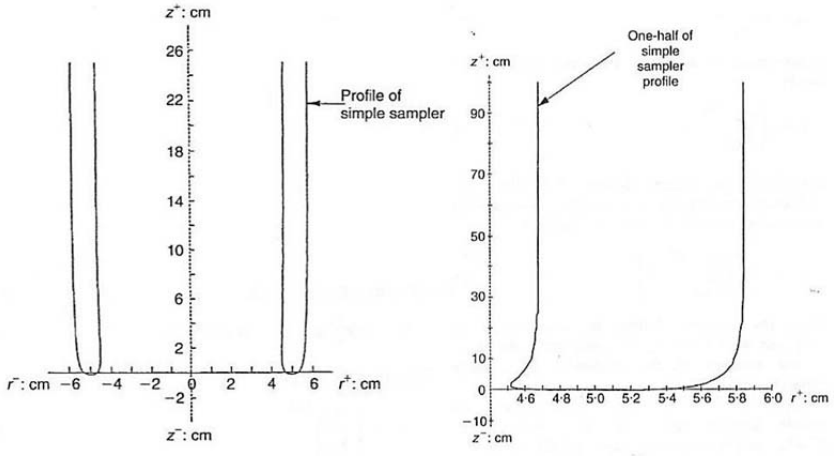

Figure 2.27 - Simple Sampler Geometry (from Clayton et al, 1998)

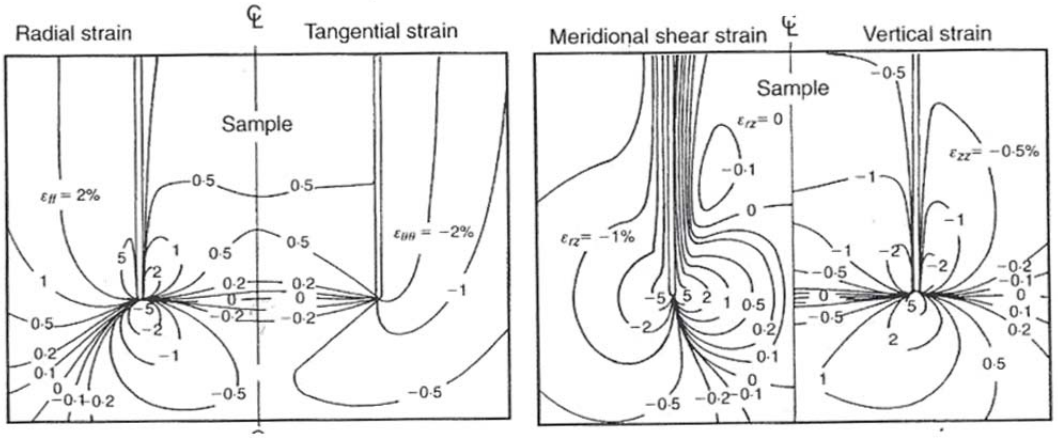

a b c d

Figure 2.28 - Strain Predictions a) at Sampler Tip b) Strain History at Centreline, modified from Baligh *et al* (1987) by Clayton *et al* (1998)

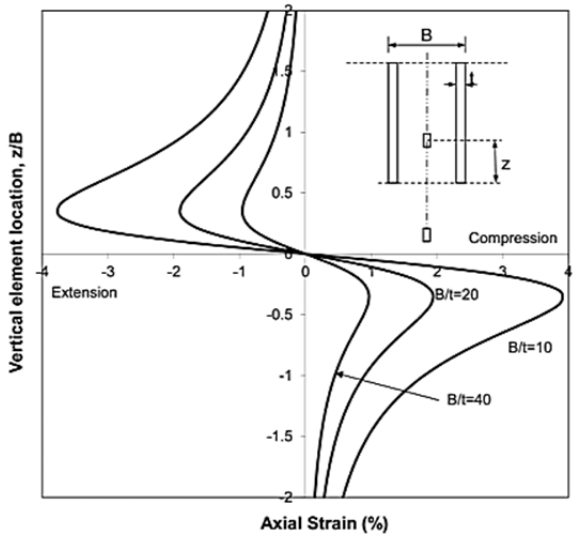

Figure 2.29 - Centreline Strain Path for a Simple Sampler, modified from Baligh et al (1987)

The study also compared the effect of the tube thickness and outer diameter on the extent of deformation at the sample centreline (Figure 2.29). By tracking a soil element's relative position to the cutting edge (z), it was discovered that on the centreline three strain phases were experienced: firstly compression ahead of the tube, followed by extension as it nears and enters the sampler and finally compression as it advances within the tube. The compression / extension / compression effects are more pronounced as the sampler diameter/thickness ratio increases, thus sampling tubes with high Area Ratios are particularly susceptible of sampling disturbance. The strain at any point is defined by Equation 12 and its peak is determined by Equation 13.

$$\varepsilon_{zz} = -ln\left(1 + \frac{2t}{B} \times \frac{\left(\frac{z}{B}\right)}{\left(1 + 4 \times \left(\frac{z}{B}\right)^2\right)^{\frac{3}{2}}}\right) \times 100 \qquad \text{Equation 12}$$

$$\varepsilon_{zz}max = 0.385 \times \frac{t}{B} \qquad \text{Equation 13}$$

With:
ε_{zz}= vertical strain (%), B= outer tube diameter (mm), t= tube thickness (mm), z= soil element position relative to cutting edge

It was suggested by the study that the strain history at the centreline of the sample provided a "reasonable estimate" of the behaviour of the soil within the central 50% of the sampling tube. The predictions were validated by triaxial tests on good quality Boston Blue Clay samples, some undisturbed and some having been subjected to either pure stress relief or mechanical deformation, which showed a reasonable fit to the predicted data. The study, however, did not entirely consider the effect of the tube geometry on the extent of disturbance, concluding that the effects of geometry affected the soil immediately surrounding the tube but not the centreline strain path. This has since been disproven by other studies, both analytical and physical (La Rochelle *et al*, 1981, Siddique, 1990, Clayton *et al*, 1998, etc).

It is of note that the idealised fluid in the study had no shear strength, no frictional properties and that the rate of tube driving was not considered – real soils which exhibit constitutive

relations and properties such as anisotropy would be expected to behave somewhat differently.

A study of the stress-strain behaviour of Boston Blue Clay (BBC) at two degrees of consolidation (OCR=1 and 4) showed that the strains predicted by the SPM for a tube with B/t=40 were sufficient to heavily impact on overconsolidated clays and cause failure of normally consolidated soils even before they entered the tube since the strain at peak strength was already exceeded (Figure 2.30). All soils behave differently, but in sensitive or structured soils, sampling disturbance is expected to cause severe changed to the sample's properties and behaviour. In other soils, the Singapore marine clay reaches peak strength at 1-2% (Tan et al, 2002), while other clays do so at strains of 0.6 to 2.3% (data compiled by Hight, 1993), which suggests that sampling disturbance will affect the properties of all but the highest quality samples.

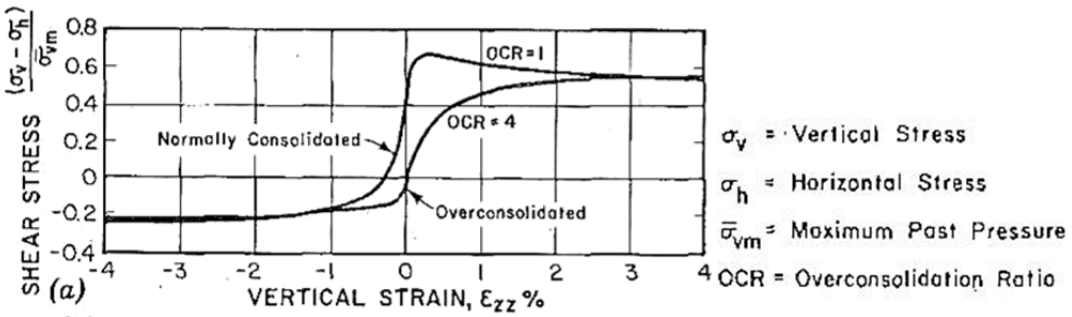

Figure 2.30 - Stress-Strain Behaviour of BBC Clay, from Baligh (1985)

2.4.5 Further Analytical and Numerical Modelling of Tube Sampling Disturbance

A number of later studies using numerical and/or analytical methods have conclusions similar to those of Baligh et al (1987). The existence of the three phases of compression-extension-compression has been corroborated by results of Budhu and Wu (1992), van Eekelen and van den Berg (1995) and Clayton *et al* (1998), while the former also concluded that the first phase of strain causes the most irreversible disturbance.

Siddique (1990) created a numerical model similar to that of Baligh *et al* (1987) to study the effect of sampler cutting edge geometry. He extended the research to include the AR, ICR and OCA to the properties already known to influence the centreline strain path, and

concluded that strains were heavily dependent on the geometry of the sampler (see also Clayton et al, 1998). It was shown that a piston sampler experienced the expected compression and extension phases in the first stages of tube driving, but that a residual extensive strain remained in the sample once in the tube (Figure 2.31). The magnitude of these strains was smaller than predicted using the SPM, and smaller than those in other samplers in the same study, such as the blunt sampler (Figure 2.32) that also experienced residual strains and no second compression phase. The often-used U100 sampler experienced a strain cycle between -1.5 and +1%, dependent on exact geometry (type 1 and 2, differ slightly in AR and ICR) and with residual extensive strains approaching – but not reaching – zero (Figure 2.33). Increasing the AR of a tube increased the peak compressive and extensive strains (Figure 2.34). Compressive strains were more affected by AR than extensive strains: strains were lowest on the centreline and increased towards the wall of the tube, with compressive strains suffering the largest increase (Figure 2.35, Figure 2.36). Increasing the ICR of a tube, however, reduced the peak compressive strain while increasing the peak extensive strain (Figure 2.37).

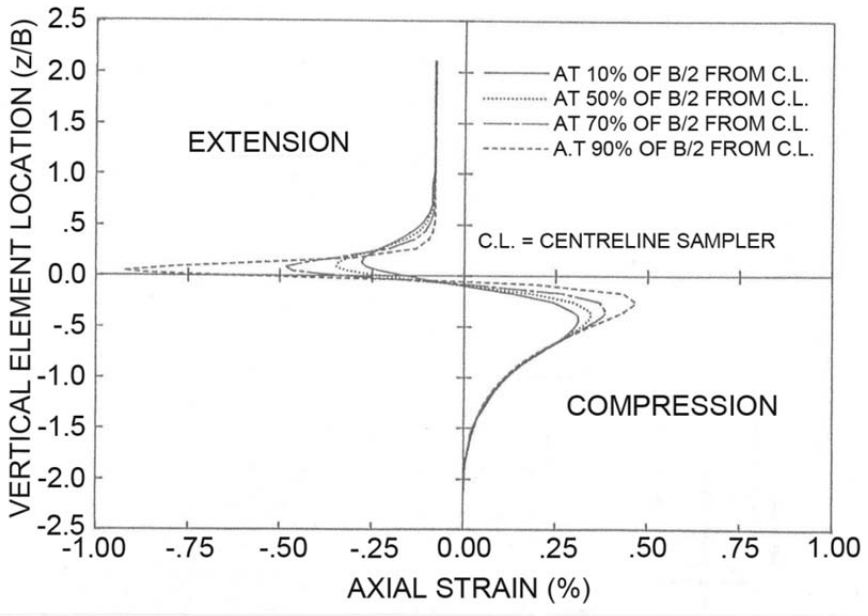

Figure 2.31 - CSP for Piston Sampler (modified from Siddique, 1990)

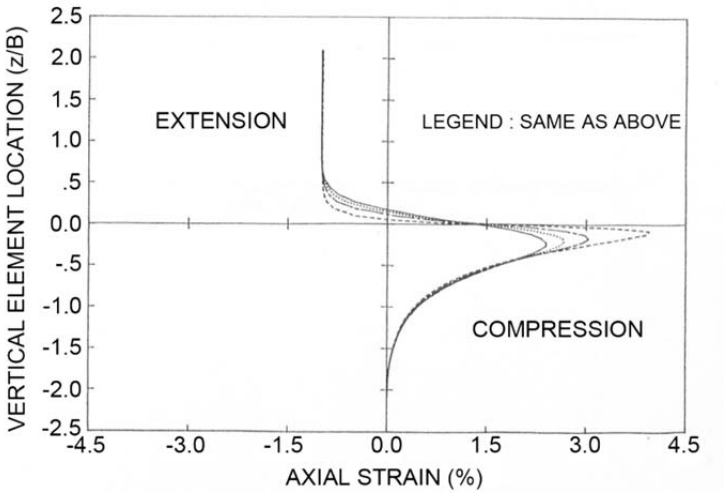

Figure 2.32 - CSP for Blunt Sampler (modified from Siddique, 1990)

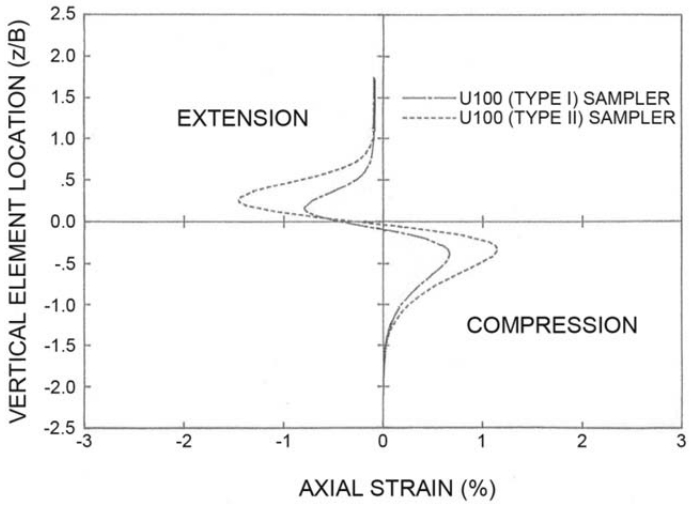

Figure 2.33 - CSP for two U100 Samplers (modified from Siddique, 1990)

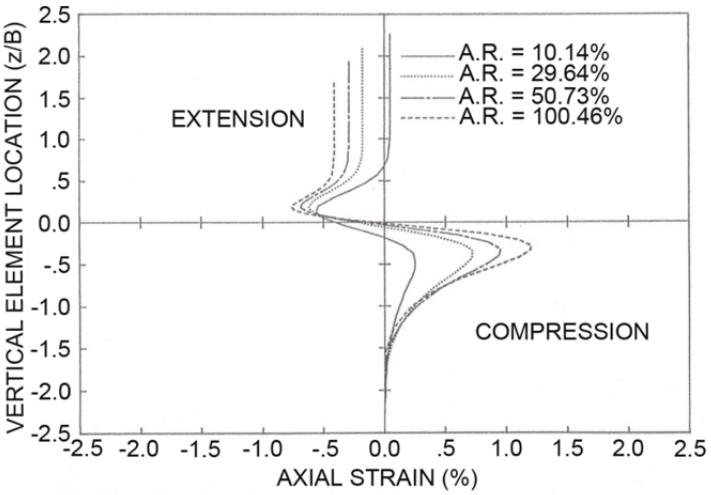

Figure 2.34 - Effect of AR on CSP (modified from Siddique, 1990)

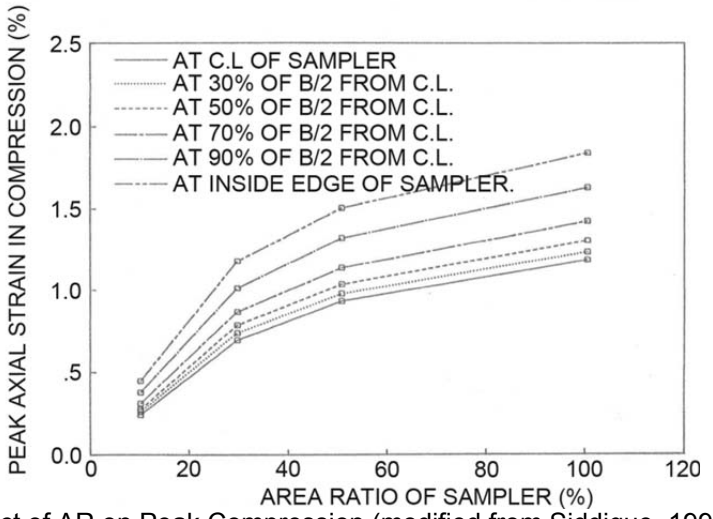

Figure 2.35 - Effect of AR on Peak Compression (modified from Siddique, 1990)

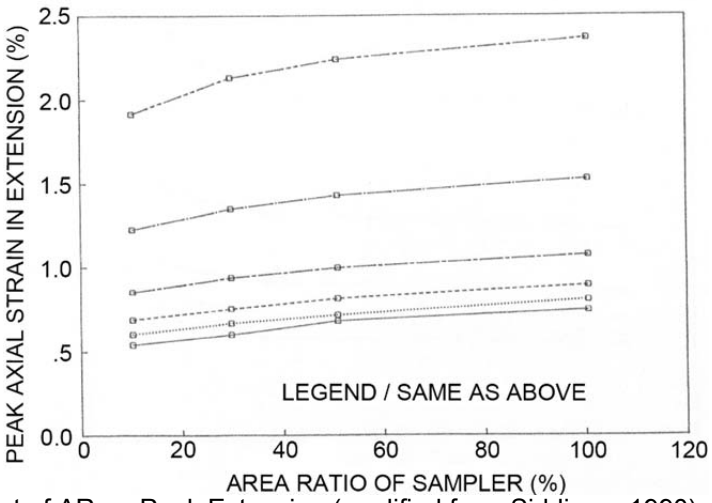

Figure 2.36 -Effect of AR on Peak Extension (modified from Siddique, 1990)

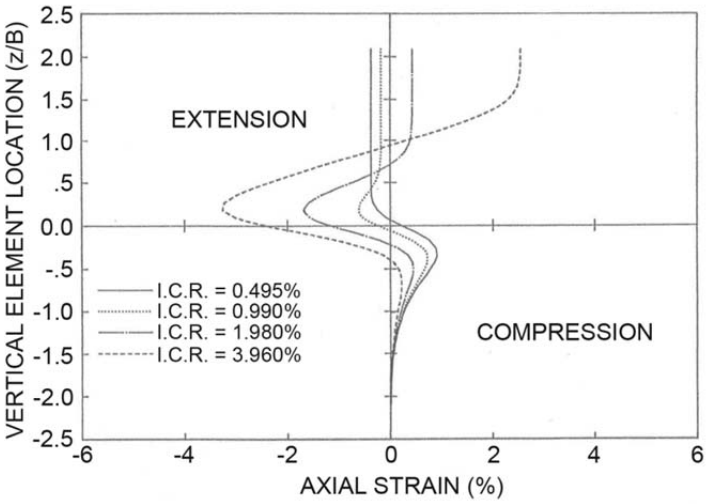

Figure 2.37 - Effect of ICR (modified from Siddique, 1990)

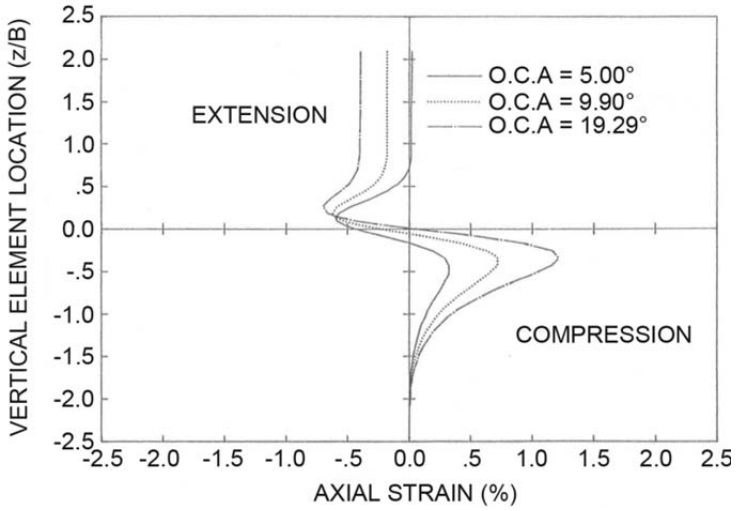

Figure 2.38 - Effect of OCA (modified from Siddique, 1990)

Residual strains, either compressive or extensive, were also found to be present in the soil within the tube. The taper angle was also found to have a large influence on the strains, with an increase in angle associated to higher peak compressive, extensive and residual strains (Figure 2.38), again with a higher impact on compressive rather than extensive strains. For the range of samplers being studied, most strains on the centreline were observed to lie within a ±2% strain cycle, and were often inferior to those predicted by the SPM. These results were validated by an analytical study by Hopper (1992). All of these discoveries go against Baligh *et al*'s (1987) conclusion that the cutting edge geometry has little influence on the Centreline Strain Path.

Budhu and Wu (1992, see also Wu, 1991) created an updated Langrangian numerical model to study ideal tube penetration in a normally consolidated modified Cam-clay model (a model considered well suited to triaxial stress states). A single cutting edge geometry was used – an in-built sharp edge with an OCA of 26.5° - although different thicknesses between 2 and 3 mm were modelled. Their study also found three strain phases of compression / extension / compression, but these were not antisymmetric as in Baligh *et al*'s SPM. Figure 2.39 shows the results for the strain path for two tests with different interface stresses, or friction: type A – present and type B – absent. The frictionless sampler's results showed a closer fit to the SPM, while the friction in the type A sampler changed the strain path considerably.

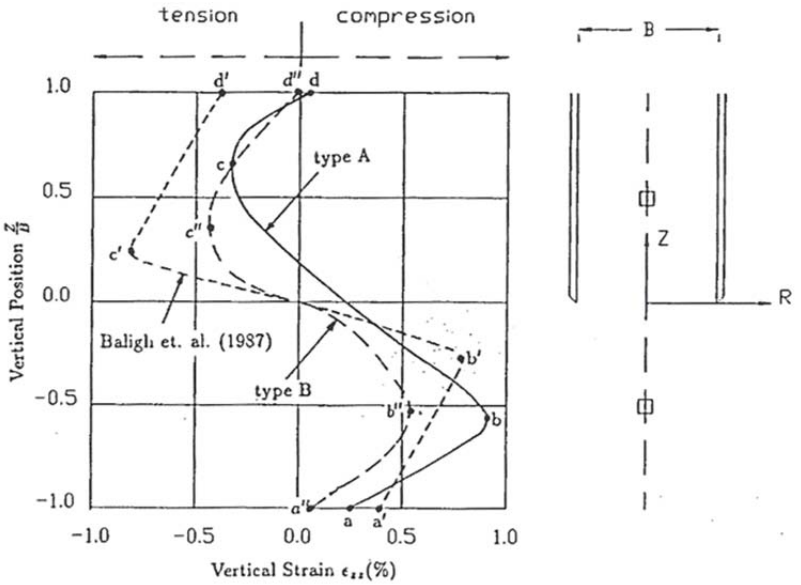

Figure 2.39 - Stress Paths for Real Sampler (A) and Frictionless Sampler (B), from Budhu and Wu (1992)

In both cases the presence of the sharp cutting edge directed more of the material away from the sample and hence the extensive strains were less significant. A study of the rate of tube penetration showed that at low speeds, the movement of soil was downwards from its initial position (Figure 2.40a, as in the SPM) but at higher speed (4mm/s and above), the movement was upwards in the tube (Figure 2.40b).

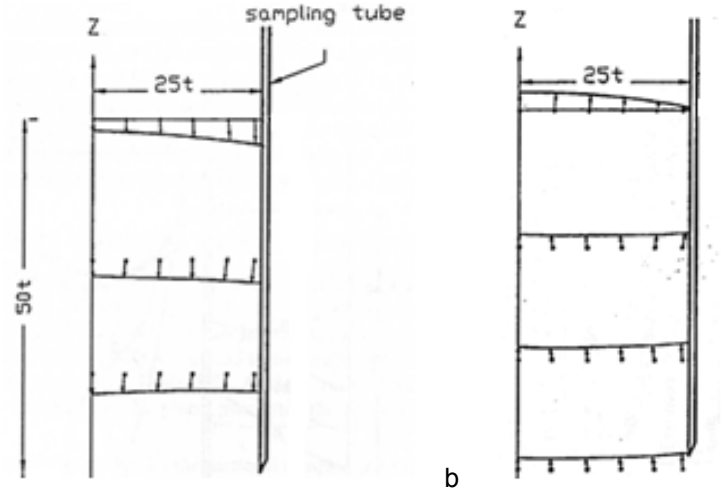

Figure 2.40 - Displacement Fields for a) slow Rate of Driving and b) rapid Rate of Driving, from Budhu and Wu (1992)

A later model by van Eekelen and van den Berg (1995) sought to improve this model by using a different numerical approach: the Arbitrary Langrangean Eulerian formulation, which varied from the approach used by Budhu and Wu in that the modelled soil could now flow through the model elements. In the previous study, soil elements in close proximity to large

deformations could distort excessively or turn inside-out, while this novel approach eliminated this risk. This new approach used a perfect-elastic-perfect-plastic von Mises model, to model the undrained behaviour of the clay.

Two piston tubes were compared: a simple piston and the Delft continuous sampler (Begemann, 1974), which had been developed to take long continuous undisturbed samples. The results of the numerical model were compared to those of a physical model using half-tubes driven into a box filled with kaolin against a viewing window. These showed a good fit, with pore pressures and deformations measured during both experiments in good agreement. Of note in this study was the tendency of the thin tube to penetrate at a small angle – rather than perfectly vertical – and the development of pore pressures, which peaked under the cutting edge and reduced inside the tube (Figure 2.41). These models are based on the assumption that the soil being sampled is at depth. This is not always the case, and to some extent, the soil below the base of a borehole cannot be considered "deep" soil.

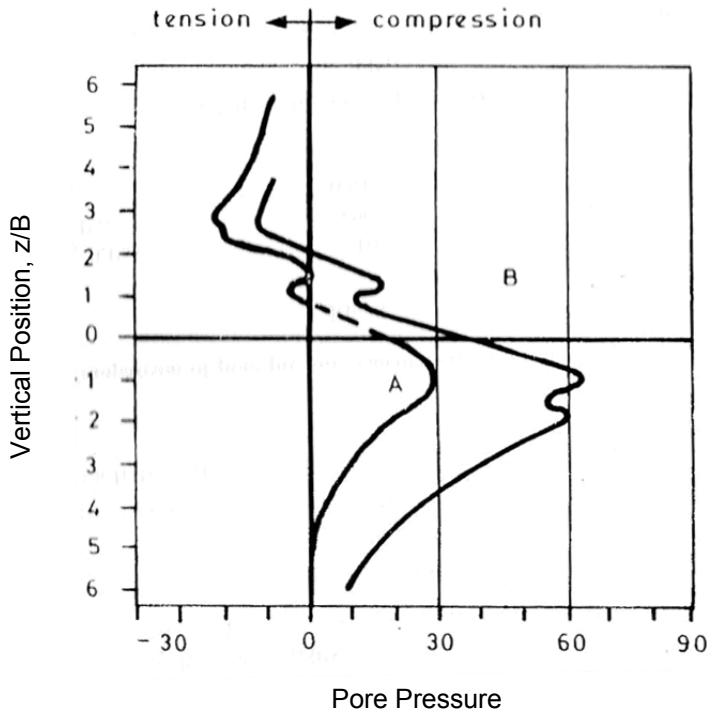

Figure 2.41 - Development of Pore Pressures (A) and Calculated Isotropic Stresses (B), from van Eekelen and van den Berg (1995)

An alternative analytical method, the Shallow Strain Path Method (SSPM) was devised by Sagaseta *et al* (1997) to model penetration in shallow soils. They based their work on observations that in some cases of object penetration into the ground, the net downwards movement of soil in and around the object predicted by the SPM did not occur. On the contrary, a heave was observed near the surface during the penetration of a round-ended tube. With tube sampling, the SSPM predicted exactly this, except for a ring of soil immediately beside the sampler wall, which would be dragged downwards with the tube (Figure 2.42a).

The SSPM differs from the SPM by the inclusion of a ground surface, modelled by image sources and sinks. This analysis assumes that the soil has some stiffness, by modelling the "soil" properties as an elastic solid or a viscous fluid and considering the model for small strain conditions. The relative displacement of the ground and the sampler is modelled – as in the SPM – by material flows, but in this case, a sink is created at a distance above the intended ground surface to absorb an equal and opposite volume to that discharged by the source.

In this solution, elements of soil at different depths under the base of the borehole experience different strains (Figure 2.42b), while in the SPM the solution was considered independent of depth. Figure 2.42b shows the different strain behaviours of elements at six initial depths (z_o) under the base of the borehole, at 15, 20, 30, 40, 60 and 80t, for a B/t ratio of 40, plotted against the embedment depth, h, divided by the thickness, t. For each curve, the soil element passes the cutting edge of the tube when its depth z_o/t and the depth of embedment h/t are equal. It can be observed that all elements undergo three phases of compression / extension / compression as in the SPM, but deeper elements ($z_o/t \geq 60$) starting out in extension.

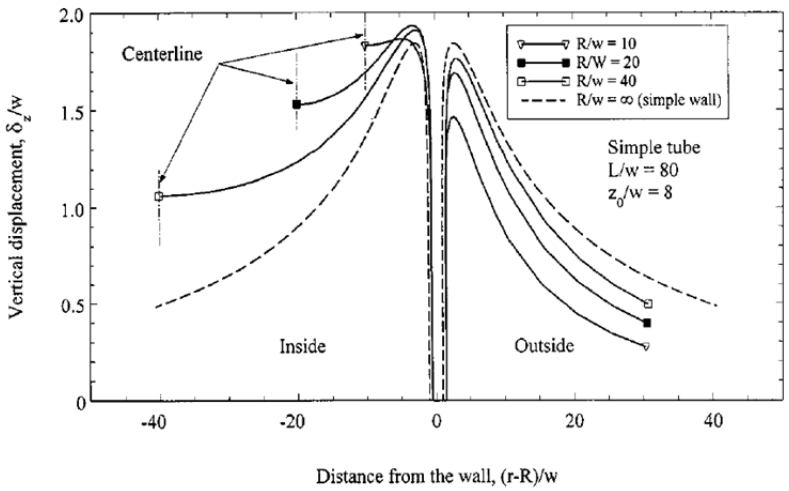

Note differences: R: Outside Diameter (B in thesis), w= thickness (t in thesis), L= length of tube

a

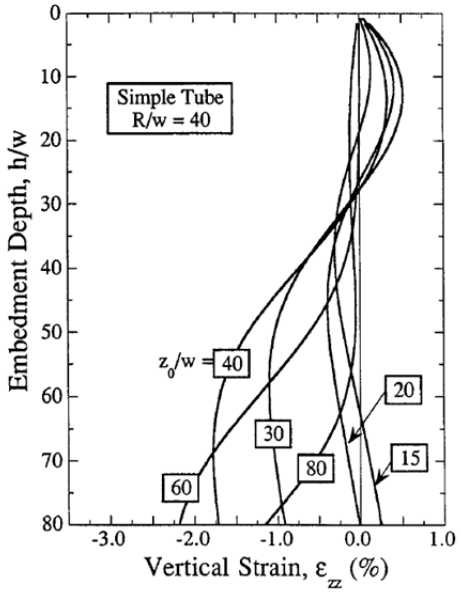

b

Figure 2.42 - Shallow Strain Path Method: a) Displacements close to the surface during Tube Sampling and b) at different Depths, from Sagaseta *et al* (1997)

2.4.6 Ground Displacements Induced by Tube Penetration

A study by Yan *et al* (2010) investigated the displacement vector fields set up by sampler penetration into the ground. Using a half-sampler driven into a kaolin model against a viewing window, displacements on the visible plane were recorded using digital photography and measured using Particle Image Velocimetry. The sampler was advanced at a slow rate of 0.71mm/s, and the model tube's diameter was 54mm. The displacement field generated in this was illustrated in Figure 2.43. Soil around the tube was pushed away from the sampler, upwards if over the cutting edge and downwards if under. All cumulative

movements were smaller than 2mm, with the largest displacements recorded inside the tube, where soil elements moved towards the least disturbed centreline. Soil originally under the sampler wall was found both inside and outside the sampling tube. Strains were not calculated, but two strain phases were identified from the displacement pattern: compression ahead of the sampler and extension close to the cutting edge. These conclusions agree with Baligh *et al* (1987), although it is of note that the viewing window may have affected results due to the friction between the soil and Perspex.

A second tube was driven into the soil within 500mm of the void left by the retrieved sample, then removed. A third tube was driven half way between the two voids. Displacements within the third sample were affected by the loss in horizontal restraining pressures, with much less soil entering the tube than in the first case. Instead, the soil surrounding the tube moved towards the unsupported holes left in the soil model. This suggests that even loosely confined soil has a tendency when disturbed to move towards zones of lower confining pressure.

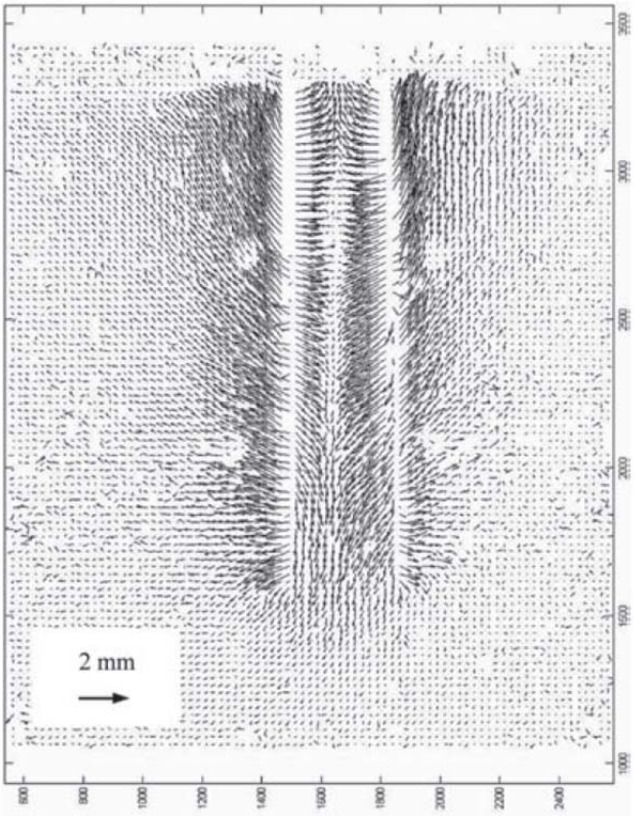

Figure 2.43 - Displacement Field after Tube Penetration, from Yan *et al* (2010)

2.4.7 Evaluating the Severity of Sampling Disturbance

Evaluating the severity of sampling disturbance is not an easy task because it is often not apparent. Disturbance can be observed or quantified:

- Visually: this is an approximate method with little reliability. Distortions are not always visible and can be obscured by the outer layer of the sample which can be severely remoulded. The top of the sample can be inspected in this manner since it is at heightened risk of swelling.
- By radiography. This technique is recommended by Jamiolkowski (1985) and Lacasse and Berre (1988) to provide more details than visual inspection
- By comparing the effective stresses in the sample (σ'_r) to those in a perfect sample (σ'_{ps}). Since the latter are not always easily obtainable and are based on theoretical values, this method is not the most reliable. However, a number of equations exist which use these parameters. Equation 14 was proposed by Ladd and Lambe (1963), although others use the same terms for different ratios.
- By studying the magnitude of the volumetric strain (ε_o) when consolidating the sample to its original in-situ stress
- By studying the yield stress of the sample (σ'_y) and comparing it to the intersection point (σ'_{yf}) obtained from the horizontal line drawn from the initial void ratio and perpendicular line from the tangent at the yield point of the compressive curve (Nagaraj *et al*, 1990, Equation 15). Again, other equations exist using similar parameters (Nagaraj *et al*, 2003).
- By using a compression curve of log(1+e) against consolidation pressure (Prasad *et al,* 2007, Equation 16). This method has the advantage of relying on easily measurable properties rather than having to assume or estimate original soil conditions.
- By comparing the change in void ratio in the sample, Δe with the sample's original void ratio e_o. The use of this method is proposed by Lunne and Long (2006) in a review of sampling disturbance, reiterated from Lunne's previous work. For marine clays, the ratio $\Delta e/e_o$ can be linked to sample quality (Table 2.14).

Table 2.14 - Use of $\Delta e/e_o$ to quantify Sampling Disturbance in Marine Clays (from Lunne and Long, 2006)

$\frac{\Delta e}{e_o}$	Very good to Excellent	Good to Fair	Poor	Very Poor
OCR = 1-2	<0.04	0.04-0.07	0.07-0.14	>0.14
OCR = 3-4	<0.03	0.03-0.05	0.05-0.10	>0.10

$$D = \frac{\sigma'_r}{\sigma'_{ps}} \quad \text{Equation 14}$$

$$D = \frac{\sigma'_{yf} - \sigma'_y}{\sigma'_{yf}} \quad \text{Equation 15}$$

$$D = \frac{C^*_{c1}}{C^*_{c2}} \quad \text{Equation 16}$$

Lacasse and Berre (1988) proposed a link between the volumetric strain during reconsolidation, ε_o, and sample quality for onshore soft sensitive clays (Table 2.15).

Table 2.15 - Relationship between Volumetric Strain and Sample Quality (Lacasse and Berre, 1988)

ε_o (%)	Quality
<1	Very good
1-2	Good
2-4	Fair
4-8	Poor
>8	Very poor

2.5 Transparent soil

2.5.1 Introduction to Transparent Soil

In the past, geotechnical research into problems at depth has been limited due to the opaque nature of soil. To study displacements within the soil body, many researchers originally used intrusive methods to quantify the behaviour of soil at given points within their experimental model. As an alternative, a number of researchers (van Eekelen and van den Berg, 1995, Yan *et al*, 2010) have used a viewing window and half-model to study the cross section of the tube during sampling. The case of tube sampling is illustrated in Figure 2.44. The major flaw in the half-model set-up is the boundary effects of the viewing window, which firstly cause a certain amount of friction and restraint to the soil, and secondly are prone to material being caught in small imperfections in the glass. In the past, one option was to

implant lead pellets into a soil model and study their movement during testing using X-ray. However, this method causes a significant amount of disturbance to the soil prior to testing, and provides a discrete rather than continuous study of the soil's behaviour. This method has since been improved by the development of the Magnetic Resonance Imaging (MRI) and X-ray Computed Tomography (CT scanning), both of which allow a detailed view onto the surface and interior of solids by creating a 3D image of the model. These techniques provide large quantities of detailed data but remain very expensive. A cheaper method for observing the behaviour of soil at depth is using transparent materials, which allow the researcher to study a plane within the soil body. The original transparent materials used to model soils were crushed glass (Allersma, 1982) and glass beads.

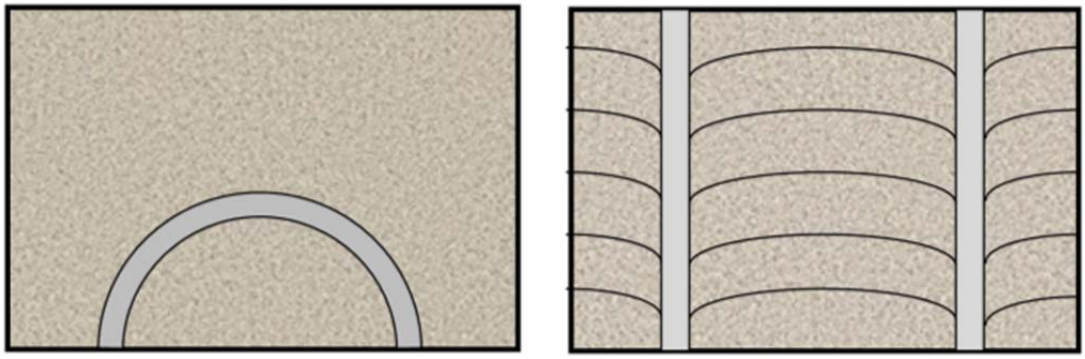

a b

Figure 2.44 - Half-Model Set-up for Tube Sampling viewed a) from above and b) through the Window

Although glass materials allow some degree of visibility into the "soil" body, they can only be used for models of limited depth due to the fact that they are optically translucent, rather than transparent. Furthermore, their ability to faithfully model the properties and behaviour of a natural soil is questionable (Mannheimer and Oswald, 1993), in particular with respect to strength, porosity, permeability and pore size. To obtain the best translucency, greater bead diameters must be used to allow light to be transmitted through the medium, which limits the modelling capability of the set-up. Where crushed glass is used, any uneven edges create an unsmooth boundary between the solid and the pore fluid, resulting in a significant amount of light refraction, which creates noise and reduces measurement accuracy.

An alternative transparent medium was developed in the early 1990s by Mannheimer and Oswald (1993) by mixing precipitated amorphous silica with a blend of two oils (mineral

white oil and a normal paraffinic solvent). Using the optimum ratio of one oil to the other, the transparency was found to be significantly greater than achieved when using glass beads. The resulting slurry, once de-aired and consolidated, was found to have porosities and permeabilities similar to those of natural soft soils. Later research by Iskander *et al* (1994) further investigated the behaviour and properties of amorphous silica slurries, using a wider range of consolidation pressures and liquid to solid ratios with the aim of developing a material to reliably model a range of clayey soils. A similar material was later developed to model sand, using silica gel as its solid component (Iskander, 2002).

2.5.2 Properties of Natural and Artificial Soils

Natural cohesive soils exhibit a range of behaviours dependent on a number of factors related to both their macroscopic and microscopic appearances. In order for an artificial material to truly model a soil, these properties need to be matched to those of a natural soil. In particular, values of strength (and associated values of internal shear resistance angle and cohesion), void ratio, permeability (or hydraulic conductivity) and consolidation and stress-strain must be closely matched. The properties of Hi-Sil T600 are summarised from works by Iskander *et al* (2002), Sadek *et al* (2002), Liu *et al* (2003) and Liu and Iskander (2010) in Table 2.16.

Table 2.16 - Properties of Transparent Clay

Particle aggregate size (μm)	Specific gravity	Permeability at 50kPa (m/s)	Initial Young's modulus, undrained (MPa)	Initial Young's modulus, drained (MPa)	c'	Φ'
1.4	2.1	1.0 x 10-8 – 5.0 x 10-7	3-19	4-15	0	36°

These have been shown to match those of soft clays and have been used in a range of studies to model different geotechnical issues, such as footings (Iskander *et al*, 2003), tunnel face stability (Ahmed and Iskander, 2011, 2012) and pile (Ni *et al*, 2010), penetrometer (Lehane and Gill, 2004), piling auger (Hird *et al*, 2010) and helical screw pile (Hird and Stanier, 2010) penetration. The stress-strain behaviour is typical of natural soils (Figure 2.45a), as are the shear strength properties (Figure 2.45b).

Amorphous silica is a non-crystalline fine white powder (particle size = 0.02μm) which when mixed to a pore fluid of same Refractive Index (RI=n=1.448 at 20°C) forms into larger porous aggregates and appears to be transparent. The transparency is due to the lack of refraction through the material, and depends on the exact match of RIs and the extent to which the mix is free from air or other entrapped impurities. Air in particular has a significant influence on the visibility through the mix, since it introduces boundaries which refract the light as it travels through the medium.

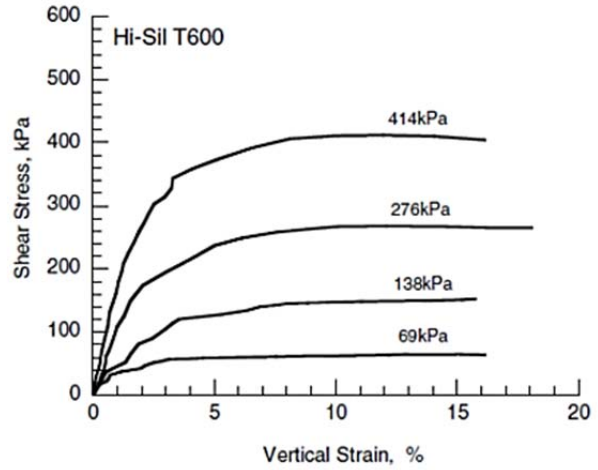

a

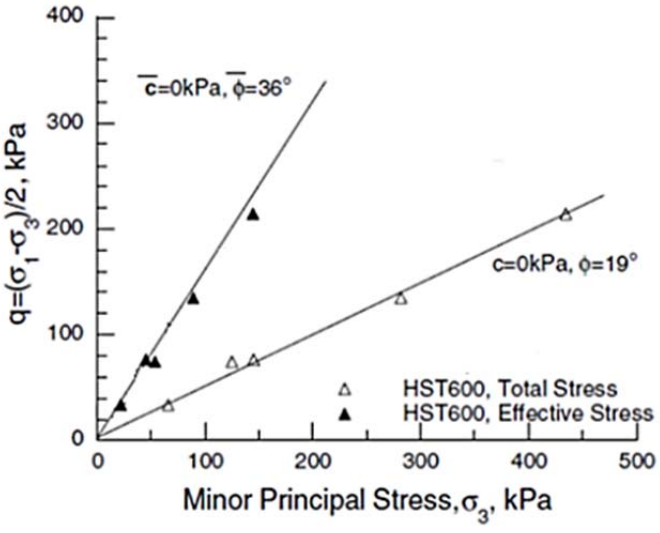

b

Figure 2.45 - Amorphous Silica (HiSilT600) Properties: a) Stress-Strain Curve and b) Shear Strength Properties (from Iskander and Liu, 2010)

Amorphous silica tends to displace air as the pore fluid is adsorbed into the particle aggregates, but excessive amounts remain due to the air entrapment during mixing due to the high viscosity of the oils. Lower viscosity alternatives were proposed by Zhao *et al* (2010), which can reduce the amount of air entrapment and reduce the high preparation

times for artificial transparent soils. Figure 2.46a illustrates the refraction of light through two mediums, M1 and M2 with properties θ, the angle of refraction, n, the refractive index and v, the velocity of the light through the medium, related through Equation 17.

$$n = \frac{\sin(\theta_1)}{\sin(\theta_2)}$$ Equation 17

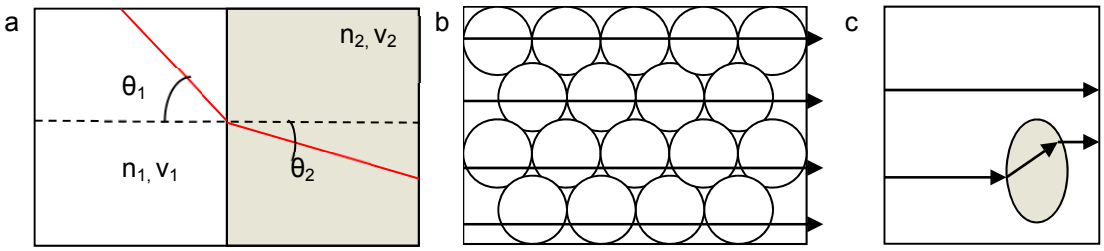

Figure 2.46 - a) Light Refraction through two Materials, b) no Refraction through matching n and c) Refraction through an Air Bubble

Since all light rays will not emerge identically, optical distortions can occur (Figure 2.46c). Where the RI is well matched between the pore oils and the powder, no refraction occurs (Figure 2.46b). Air can be removed by applying a vacuum to the slurry. For this to be effective, the solid to liquid ratio must be low, in the order of 9% by weight (Mannheimer and Oswald, 1993). At this concentration, the amorphous silica acts like a liquid and must be consolidated before it can be used to model cohesive soil. The consolidation is a slow process, due to the low permeability of the silica particles. The void ratio of consolidated amorphous silica remains high due to the presence of voids both within the aggregates formed by multiple individual particles, and the voids between the aggregates. For geotechnical purposes, only the voids between the aggregates need to be taken into account. As stated previously, for consolidated amorphous silica to reliably model soil, a number of its properties need to be similar. Iskander *et al* (1994, 2002, 2010) and others tested the following before being assured of its viability:

- Undrained shear strength: for normally consolidated samples, the behaviour of the artificial transparent soil was measured to be similar to that of natural cohesive soils. The strength was slightly higher for some of the amorphous silicas (four types were compared) and the shear modulus lower. In the case of Hi-Sil T600 (used in this project), only the modulus was found to differ from natural clays. Overconsolidated

samples showed strain softening and a rise in shear strength, consistent with the behaviour of natural soils. The shear strength parameters (φ' and c') and the residual strength were also comparable to those of natural soils.

- Consolidation behaviour. The existence of pores inside the aggregates creates a secondary, or internal, void ratio. In most natural soils, primary consolidation is dominant, followed by long term effects such as creep. Transparent soil exhibits a secondary phase of consolidation because of its internal porosity, typical of organic clay and peat soils only.
- Permeability. The permeability of the transparent soil was in the range for cohesive soils, from silt to clay.

The artificial soil created with amorphous silica can therefore be used to model soft soils. The properties of each individual model will depend on the degree of consolidation of the slurry.

2.6 Summary: Literature Review

This section presented the existing research covering sampling disturbance and its effects of some of the properties of a clayey soil. Sources spanning some 70 years of research were taken from physical modelling as well as numerical and analytical models. The main sources of disturbance were outlined, and included:

- mechanical deformations, including those due to friction and excess soil recovery
- stress relief, as the sample is retrieved from its in-situ anisotropic stress state
- chemical changes due to the presence of other materials
- moisture content and void ratio change, including those occurring during sample storage

The soil at the tube-ground interface was found to be the most influenced by shear distortions, becoming heavily remoulded by the process of tube driving, while the soil in the centreline of the tube was the least affected. Analytical and numerical models found that soil on the centreline of the sampler experienced three phases of strain during tube driving, compression ahead of the tube, then extension as it entered the tube, and finally a further

phase of compression as it travelled upwards into the sampler. The amount of disturbance to the sample was seen to be dependent on a number of tube geometry parameters, including the tube's Area Ratio (related to the tube's diameter and thickness), its Inside Clearance Ratio, and the sharpness of the cutting edge. The strain path, when applied to undisturbed reconstituted clay samples in the triaxial cell, had the effect of simulating sampling disturbance and revealed that the properties of clays were indeed heavily influenced by this process.

The main effect of these changes was to modify the bonds between the soil's particles, thus changing its internal structure and some of its properties, as revealed from a large number of studies:

- the undrained shear strength is reduced with increasing disturbance
- the Elastic Modulus, E, is reduced with increasing disturbance
- the strain at peak strength is increased

Other factors which influenced the extent of sampling disturbance are:

- higher values of OCR experience less disturbance and less significant changes in properties
- high rates of tube driving cause additional disturbance

While open-drive tube sampling not the only option available to the geotechnical engineer, it is certainly the cheapest and most common method of collecting soil specimens, and the process must therefore be well understood if laboratory tests are to be undertaken on samples retrieved using this method.

The materials used in this research were also presented, and their properties explained. Artificial transparent soils have been used since the 1990s to model a range of soils, using photography to record displacements and velocities within the ground. More details on their preparation can be found in Chapter 3, Methodology.

Most research to date on sampling disturbance has focused on two elements: the effect of applying a known strain path to undisturbed samples on the soil’s properties, and the effects

of different samplers on specimens of the same soil. While some researchers have visualised the movements on the centreline of the sampler, no studies have investigated and quantified the Centreline Strain Path through physical modelling. Even in studies observing the plane through the centreline of the tube, half-samples were pushed into natural soil models against a viewing window. Friction at the boundary window impedes the displacement in such set-ups and the true movement of soil has never been measured in this way. Current knowledge on Centreline Strain Paths comes from analytical and numerical models only, and therefore generating a realistic CSP by physical modelling would advance the current knowledge on strain paths and their effects on the properties measured in samples taken by open-tube driving. By extending this technique, changes in strain within the sample during storage and extrusion can also be studied.

Chapter 3: Methodology

3.1 Introduction

A transparent soil, white light and PIV physical model was developed to replicate tube sampling. The dimensions of the model were increased from those previously achievable by replacing the PIV laser with a white light source, and identifying the plane of interest with seeding particles. A number of approaches were considered and trialled before a final viable testing and analysis methodology was proposed (Figure 3.1). This chapter discusses the approaches used to create, test, and analyse the physical model, and comprises two main sections: the experimental approach and the analysis methodology. Details of unsuccessful attempts are included to assist future research. The tube-driving model size was twice that previously achieved with a transparent soil and laser set-up.

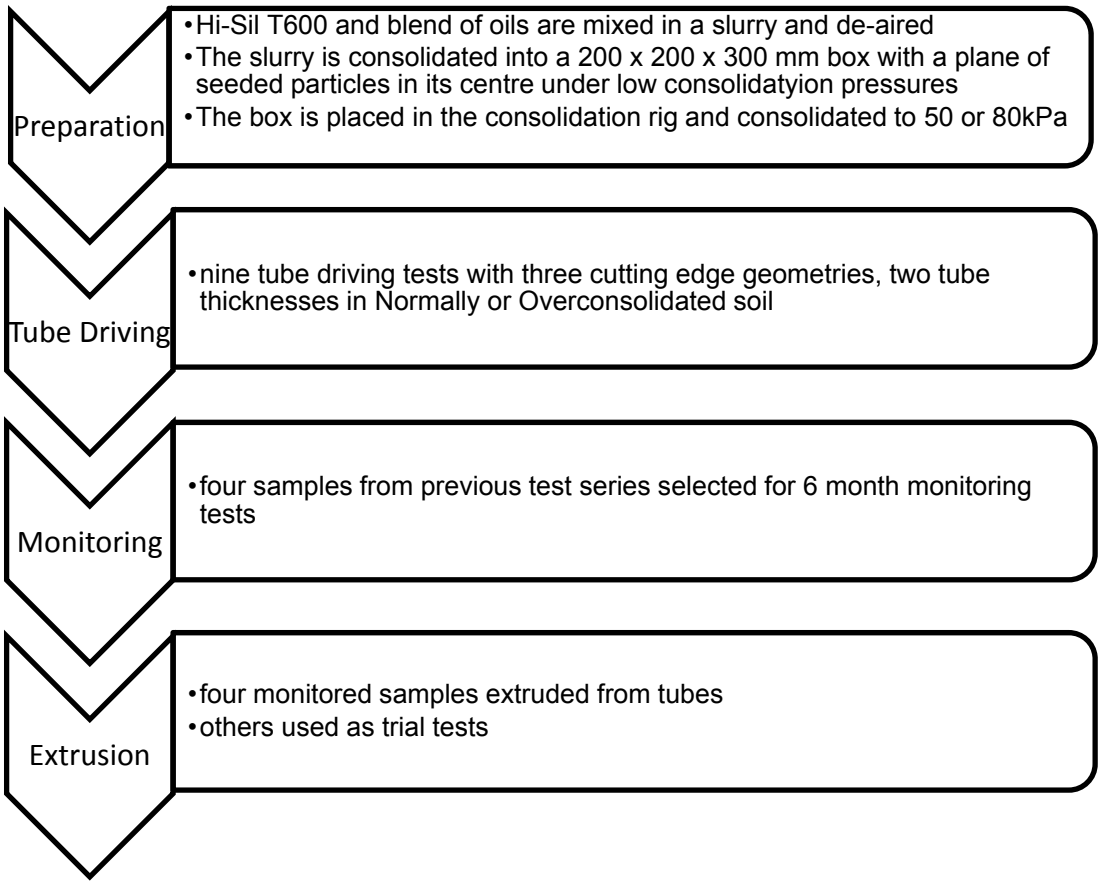

Figure 3.1 - Summary of the Experimental Methodology

3.2 Experimental Methodology

3.2.1 Introduction

The aim of this research was to develop a physical modelling system to replicate tube sampling, to study the disturbance caused to clayey soil samples during three phases of the sampling process:

- driving of the tube into the soil, when the sample is taken out of its in-situ state
- storage of the sample, before being tested in the laboratory
- extrusion of the sample, from its tube prior to laboratory testing

The main obstacle to physically studying the strains developing within the soil in and around the sampler was the inability to see through the materials, a plane running through the centreline of the sampler. In the past, solutions around this have included model half-tubes being driven into a soil model against a viewing window (Yan *et al,* 2010, van Eekelen and van den Berg, 1995) to quantify the movements in the soil using PIV or creating analytical models, but these have their own disadvantages (see Chapter 2, Literature Review). This research aimed to adapt current laser PIV techniques for use with white light, which is cheaper, removes the H&S risks associated with lasers, and provides higher intensity light, meaning that larger models can be used to study tube sampling disturbance.

While it is known that sampling disturbance can occur at other stages within the sampling process, the focus of this project has been on those where disturbance is caused even without human error. The first stage has previously been modelled numerically or analytically by a number of researchers (Baligh, 1985, Baligh *et al*, 1987, Budhu and Wu, 1992, van Eekelen and van den Berg, 1995, Clayton et al, 1998) who studied the strain path on the centreline running down the tube (or Centreline Strain Path, CSP) during the sampler's progress into the ground, but this had never been measured experimentally. The CSP can also be measured during the storage and extrusion of the soil – an aspect of disturbance that has not been measured before. Additionally, the influence of the tube's geometry parameters (such as cutting edge taper angle, Area Ratio, and Inside Clearance) on the extent of disturbance caused was studied in this research project, as well as that of the soil's

Overconsolidation Ratio. In this research, displacements and strains in a physical model are measured using Particle Image Velocimetry.

3.2.2 Particle Image Velocimetry

3.2.2.1 Basis of PIV

Particle Image Velocimetry (PIV) is a non-intrusive method which uses photography to measure displacements and derive velocities in a moving medium over a given length of time. Originally designed for studying flows in experimental fluid mechanics, its use has been adapted in recent years for a wider range of applications such as geotechnical modelling. The potential of PIV has been rapidly increasing since the eighties with the development of more sensitive and higher quality photographic equipment, making it an accurate, precise and time efficient tool for research. Both 2D and 3D PIV applications exist, but to remain within the scope of this research, only 2D PIV is investigated here. Many detailed reviews of PIV have been written, including works by Willert and Gharib (1991), Prasad (2000), Adrian (2005) and Adrian and Westerweel (2010).

Particle Image Velocimetry uses software to compare a series of recorded images of a plane within a moving fluid, separated by a known period in time, in order to obtain a velocity (or displacement). It relies on a technique called Digital Image Correlation (DIC), by which a series of elements within an image are tracked over a number of frames to determine the most probable motion of each element. To achieve this, the plane of material under consideration is converted from object-space to image-space through the process of photography by the Charge-Coupled Device (CCD) sensor within the camera. It is thereby converted to a set of data, which can be represented in analysis software (such as Matlab) as a matrix the size of the image's resolution containing the intensity (or texture, or colour value) of each pixel within the photograph (Figure 3.2).

If the material being studied is transparent and homogeneous – such as water, or the transparent soil used in this study – it exhibits a lack of texture (no variation in greyscale intensities) and displacements within the body cannot be tracked from one frame to the next. For this reason small tracer particles are added to the material. These produce a pattern which scatters the light penetrating within the body, making it possible to infer the behaviour

of the material over time. Optimising the “area-number-density” of particles (i.e. the number of tracer particles in any Interrogation Area) for a given experiment is essential to achieve a good degree of light scattering. As a general rule, larger particle diameters produce greater scattering (Melling, 1997) as does a higher ratio between the refractive indices of the particles and the surrounding material (Adrian, 1991).

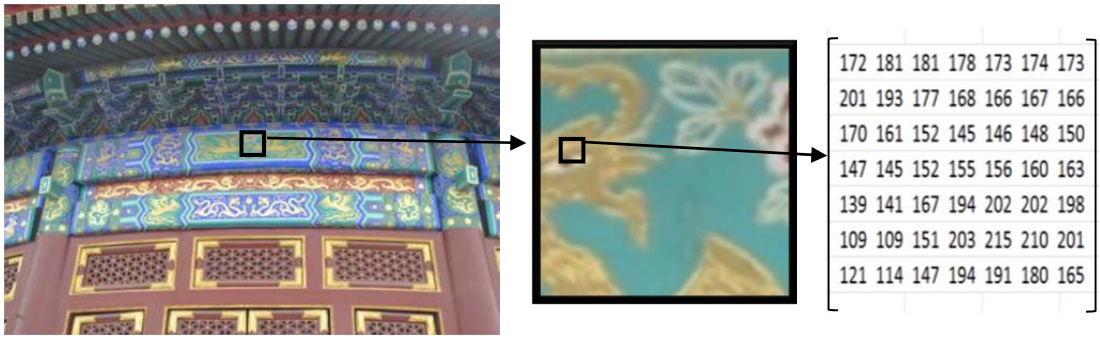

Figure 3.2 - Breakdown of a Photograph into a Matrix of Greyscale Intensities

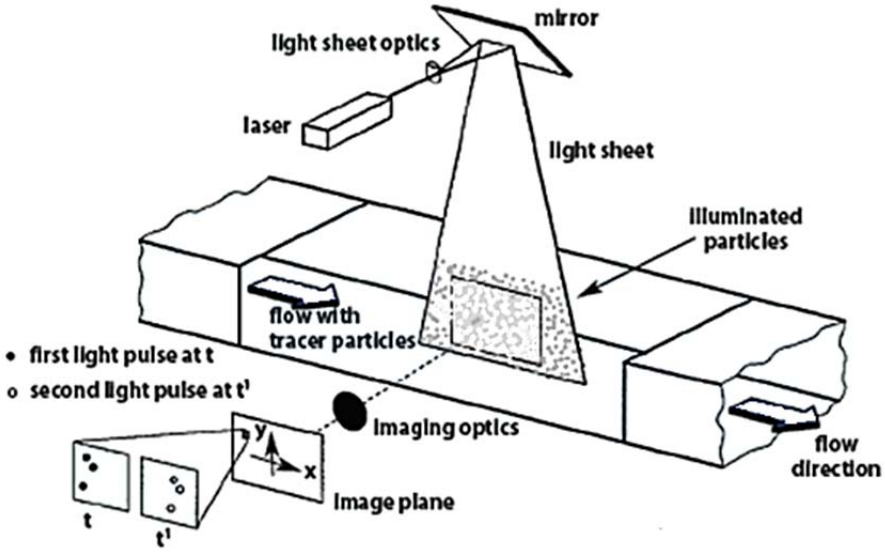

Figure 3.3 - A typical PIV Set-up for Experiments in Fluid Mechanics, from Raffel (1998)

During the experiment, the set-up is darkened and a single plane of the seeded transparent material is illuminated and studied at a time. The light source typically comes from a laser since monochromatic light reduces the risk of noise during photography and easily produces a thin light sheet, although its use is associated with high costs and health and safety issues. It is also possible to use an almost collimated white light source (Raffel, 1998), although this is more difficult than using a laser (Paul et al, 2004). Rostami et al (2007) enclosed a white light source and created a plane of white light through a slit in the enclosure. While the

"plane" expanded in thickness over distance, it was deemed a suitable replacement when the need for accuracy was not very strict. A camera is positioned orthogonally to the illuminated plane to capture images at regular time intervals. A typical set-up of a PIV system is presented in Figure 3.3.

3.2.2.2 Analysis of Images using Particle Image Velocimetry

Nowadays many choices of PIV software are available commercially and in open-source, and most have a similar function. The basis of PIV is to compare images to infer the displacements between two moments in time. To achieve this, an original image is taken as a reference. This could be:

- The first image in a series against which all photos are compared (full movement determined for each photo - appropriate for studying displacements). This produces displacement information of the form: image 1 to image 2, image 1 to image 3, image 1 to image 4, ... , image 1 to image n
- The first image in each compared pair of images (displacement or velocity over one time increment). This produces displacement information of the form: image 1 to image 2, image 2 to image 3, image 3 to image 4, ... , image (n-1) to image n

Whichever method is used, a grid or mesh of Interrogation Areas (IAs) is created over the area under consideration in the original image. Each square IA is of a given pixel size (n x n) and is recognised in the PIV software as an n x n matrix of pixel colour values (intensities). The software determines the most probable displacement of an IA between two images by finding the closest fit in the cross-correlation function (presented in detail in Raffel, 1998 and Iskander, 2010)

$$c(x,y) = \sum_{m=1}^{M}\sum_{n=1}^{N} f(m,n)g(m+x,n+y) \qquad \text{Equation 18}$$

f and g are the light intensities in image patches A and B, (x, y) represents a shift within the IA from its initial position in image A. g is larger than f such that g=f(m+δm,n+δn). f is translated strictly linearly around g to all possible locations within a pre-set search area around it. The cross-correlation function calculates the product of the light intensities f and g,

thereby finding a peak value where the intensities overlap and determining the most probable displacement of the IA. This does not account for IA rotations, although adaptations of this method have been successful in tracking these (Liu and Iskander, 2004). Each IA when compared will produce a single displacement vector. It is of note that the texture created by the tracer particles, and the size of the IAs are important elements in the PIV process. Large IAs will contain more texture and a higher number of particles for easier pattern recognition; however, the measurement precision associated with large patches is low due to the risk of distortion of the patch during testing. High tracer densities increase the possibility of overlap which causes additional problems during analysis due to the apparent change in light intensities within the material.

3.2.2.3 Digital Photography

Large quantities of photos can be generated during testing, and keeping up with the rate at which they are taken can be a challenge. Images can be either stored in an SD card or uploaded directly onto a computer via a USB link, the latter solution being used for smaller and more numerous files. If an SD card is used, it must be high speed to ensure the camera can withstand long periods of continuous shooting without buffering and slowing down or stopping altogether. Higher resolutions produce a better measurement precision but require longer processing times. It is also possible to use a digital video camera to record the experiment, then to select frames at known time intervals using image processing software such as Virtualdub (Open-source, from 2004). Its main disadvantage is its low resolution: with recent advances in digital technology, digital camcorders are appearing on the market with resolutions of up to 4MP (in recording, high resolution or definition is defined as over 1MP, and most consumer cameras offer no more than 1 to 2MP) but are still expensive compared to the same resolutions for a still camera (at approximately a 10:1 cost). Ultimately, the choice of camera type and method will depend on the required speed of frame capture (decreasing resolution with increasing frames per second required, in order to keep up with the SD card / upload to PC speed).

The main priorities during photography are sharpness of the image and contrast between the tracer particles and the surrounding medium. Sharpness requires the lens to be well

focused and a sufficient amount of light energy reaching the particles. In the case of a laser light sheet penetrating a dense medium in a parallel manner, the beam will lose energy and will produce an uneven illumination of the plane (Figure 3.4). A translucent medium will tend to blur the shape of the particles and will need more intense lighting. Contrast can be created by the colour, texture or properties of the tracer particles. Fluorescent particles will emit a particular wavelength which can easily be recognised by the software during analysis, and lend themselves particularly well to the laser set-up used in conjunction with black and white or colour photography. Alternatively, particles can be chosen for their colour or unique texture. Images are often recorded as JPEG (.jpg) files by default, but it must be noted that these are prone to lossy data compression: each time a JPEG file is opened and saved, it will suffer a small loss of detail due to the creation of compression artefacts, which result from similar and close pixels merging into one colour to save space. In small quantities, and for everyday photography, these losses are barely noticeable, but for data analysis which considers each pixel's intensity, it may be more appropriate to use lossless image files, recorded in a RAW format. Because each camera make owns its specific RAW format, these must be converted before processing into a format which can be read by the PIV analysis software. In the case of MATLAB, TIFF files can be used. These will contain more detail than the same image recorded in JPEG, and will not be prone to losses in detail, but will contain more data, which means that the files will be larger and hence will require longer processing times. There are many benefits to using high resolution images, but these can overwhelm the software if there is not sufficient memory.

3.2.2.4 Particle Image Velocimetry in Geotechnical Engineering

PIV has proven itself a reliable tool to analyse many geotechnical models (Iskander 2010), however due to the differences between fluid and soil mechanics, a number of adaptations have been made to the PIV technique and software. Geotechnical engineering will typically study much slower movements and smaller displacements than in hydraulic or aeronautical models. The need for accuracy is as great, yet the requirements in terms of lighting and image capture are less stringent for soil models where the rate of image capture is lower, resulting in more flexibility in the experimental set-up.

In soil models, the texture can be created by the soil itself provided that it is coarse and exhibits nuances in colour or brightness, and the research method uses a window to cut into the model to study the plane under consideration. This will be studied using white light instead of a laser, since the plane under consideration can only be on the surface of the model. In some cases however, it is more desirable to use a transparent material to model the properties of the studied soil, thereby increasing visibility and the possibility of conducting intrusive testing, whilst eliminating the boundary influence of the window. If using a laser it is possible to create a speckle pattern in the transparent soil for analysis (Iskander 2010), alternatively the entire volume of transparent medium (Hird et al, 2010) or the volume of soil situated on and behind the plane of interest (Ni et al, 2010) can be seeded homogeneously with tracer particles which can be tracked using the PIV method outlined previously. The area-number-density of the particles need not be as high as for fluid mechanics where the flow of pore fluid through the soil remains laminar, which encompasses the majority of geotechnical situations. It is of note that long-term monitoring PIV set-ups have the additional consideration of equipment positioning. If frames are to be captured at intervals far enough apart to warrant the removal of photographic equipment between shots, special care must be taken when replacing the camera and lighting for each image.

Specialist software has been developed for applying PIV to soil mechanics. GeoPIV (White et al, 2001, 2005, White and Take, 2002, White and Bolton, 2004) was used in this research project and has been designed to run on MATLAB. The software comprises a number of files which permit pre-processing and analysis of images which may be adapted or completed by any MATLAB-competent person. The precision of displacement measurements was found to be between 1/50 and 1/20 of a pixel for IA sizes between 16 and 50 pixels (White et al, 2001). It has been successfully used to model a range of geotechnical problems, including tunnel face stability (Ahmed et al, 2012) and pile (Ni et al, 2010), penetrometer (Lehane and Gill, 2004), and helical screw pile (Hird and Stanier, 2010) penetration.

The main limitation with using PIV and transparent soil models is one of model size. The artificial soil is not fully transparent and a laser light sheet penetrating into the model will quickly lose intensity, reducing the size physical models can reach. Figure 3.4 illustrates a light sheet created by a laser, and Figure 3.5 shows the loss of intensity at depth in the set-up by Ni et al (2010). To increase the size of the model, white light can be used since its intensity is much higher than laser light, but this means that the plane of interest must be seeded individually, rather than seeding the whole soil model. This is a challenge in itself and was the focus of this research.

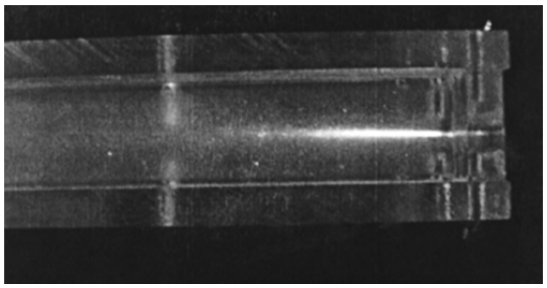

Figure 3.4 - Laser Light Sheet in a Transparent Soil Model (from Sadek et al, 2003)

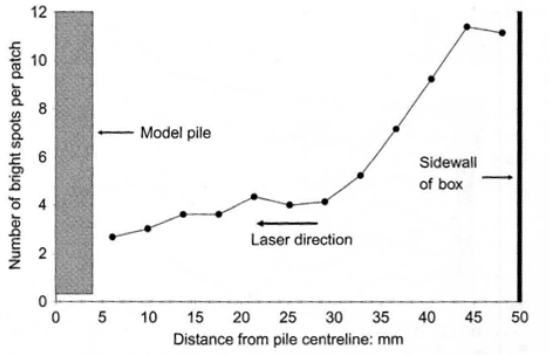

Figure 3.5 - Reduction in Visibility with Light Intensity (from Ni et al, 2010)

3.2.3 Preparing Transparent Soil to Model Clay

Synthetic soils have been developed which model the properties of clayey and sandy soils. The artificial transparent soil used in this study was made by mixing three materials:

- Amorphous Silica (HiSil T600, supplied by PPG Industries Inc.)
- Normal- Paraffin Oil C5-C20, (Banner NP 1014, supplied by Banner & Co Ltd)
- Technical White Oil (Technical White 15 supplied by Aztec Oils Ltd in early tests then replaced with Food Grade White Oil 15 supplied by Aztec Oils Ltd in later tests, with increased transparency)

Because of the Health and Safety implications associated with each of these materials, COSHH forms and a Safe System of Work were created and can be found in 0. As stated in the Literature Review, for the mix to be transparent the Refractive Index (RI) of the solid

Amorphous Silica must match that of the fluid. An oil blend with the right proportions of Normal-Paraffin (N-P) and Technical White Oil (TWO) is able to achieve this. The tolerance for the correct ratio of oils is rather narrow, since transparency is lost quite rapidly with small variations in the oil ratio (Figure 3.6a). Furthermore, the RI of each oil batch will vary somewhat since RI is not a controlled factor during its production. A transparency test must be conducted for each mix of oils, by mixing small doses of soil and varying the oil ratio, while keeping the solid to liquid ratio constant (transparency also varies with solid content). Transparency was quantified by the smallest font size readable through a known thickness of transparent soil slurry. In this case, two thicknesses were observed (40mm and 100mm), and the optimum ratio was found for each batch of material. This varied between 1.05 (TWO:N-P) to 1.2.

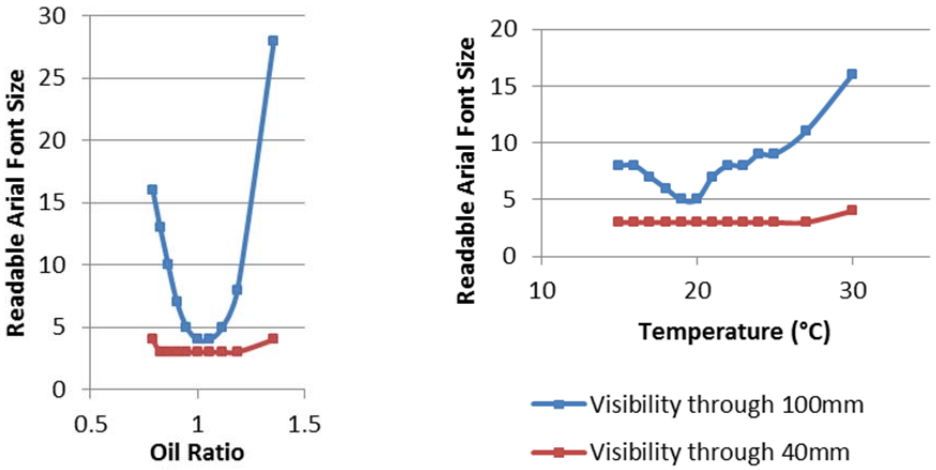

a b

Figure 3.6 - Changes in Transparency with a) Oil Ratio and b) Temperature

Another controlling factor for transparency was temperature (Figure 3.6b). Ni et al. (2010) recommended that the soil should be tested at the temperature at which it had been prepared to maintain the same degree of transparency. The temperature of the laboratory was monitored for 6 months, with automatic reading every five minutes, and although it was found to fluctuate somewhat, the room mostly remained within one degree of its average temperature. This was deemed adequate for testing without the need to further monitor temperatures during preparation or testing.

A soil slurry was originally mixed with a solid to liquid ratio of 6% by weight (11g of Hi Sil for every 200mL of oil), a value inferior to the 9% quoted in the original literature (Mannheimer

and Oswald, 1993) but found to be effective for de-airing by Ni et al. (2010). The slurry was then de-aired in a vacuum chamber until no further movement of entrapped air bubbles was noticed. The time to this stage varied with the depth of transparent soil being de-aired. Typically batches of 10L of slurry were prepared and separated into four containers with a depth of approximately 70mm. These were placed under vacuum for 5 to 6 hours, after which the tank's inlet valve was closed to maintain the vacuum overnight without additional vacuum being restored by the vacuum pump. Usually by the morning the vacuum remained at high (but not maximum) levels, and few bubbles were still entrapped within the slurry. This slurry was then consolidated to the required pressure, under which it was expected to behave like a soft or sensitive soil. During this stage, the soil reduced by approximately 50% in volume, and the oil which was forced out of the soil could be reused to prepare the next batch of slurry provided it was stored in a sealable container between uses to avoid small quantities of the oils evaporating (thus changing the oil ratio and hence the transparency achievable when the oil was mixed again with the Amorphous Silica). Also of note was the tendency of the soil to yellow over time (weeks), so batches, once prepared, were best used and tested quickly.

3.2.4 Adapting the Laser/PIV Set-up for Use with White Light

Using transparent soil and PIV it is possible to look deep into the soil and record strains in a non-intrusive manner. However, as stated previously, the transparency of the artificial soil reduces with depth, which restricts the size of the model (100mm depth is achievable, Ni et al, 2010). Two options exist to counter this problem:

- The use of a soil with increased transparency. Hird and Stanier (2010) used a fumed silica soil and achieved superior transparency, allowing doubling of previous models' dimensions. The main downsides of this method are those associated with the use of a laser and the fact that marker points for camera shake correction need to be visible in the dark. LEDs are usually used but flickering can cause their location to be poorly measured using PIV, although this may be corrected for. (Stanier et al, 2012). Fumed silica has a higher void ratio than the less transparent but more often used amorphous silica, which will have an impact on its structure and properties.

- The adaptation of the Laser/ PIV set-up for use with white light which can, for a fraction of the price, achieve greater illumination through the transparent soil and therefore higher accuracy. This second solution is the focus of this research.

The main challenge with this method is creating a single plane of texture within the soil model. In a typical PIV set-up with transparent soil and a laser, the plane of interest is located within transparent soil seeded with particles, and the visibility is enhanced by filling the front of the model with un-seeded artificial soil (Ni et al, 2010 - illustrated in Figure 3.7)

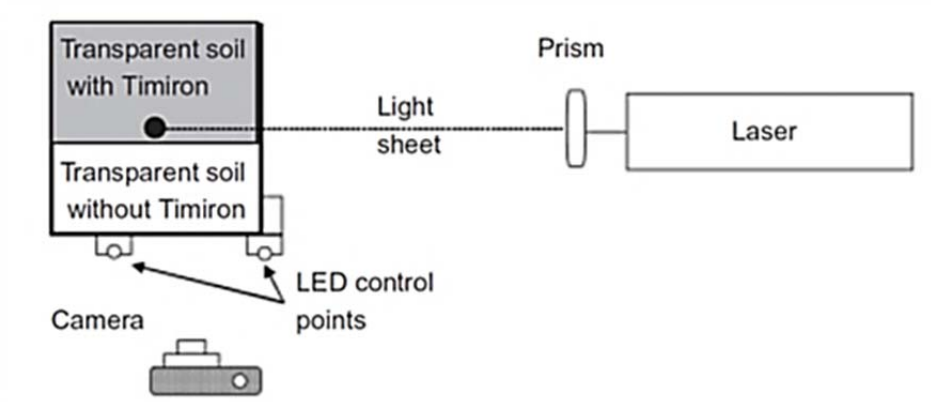

plan

Figure 3.7 - PIV and Transparent Soil Set-up from Ni et al (2010)

The aim was to create the set-up detailed in Figure 3.8, to drive a glass model sampling tube into a transparent Perspex box 200 x 200 x 300mm (L:W:H) filled with consolidated transparent soil, with the tube's centreline through a plane of seeding particles.

Three approaches were used to create the textured plane at the required depth into the soil:

- the "Z-plane" method
- the "split-sample" method
- the" horizontal consolidation" method

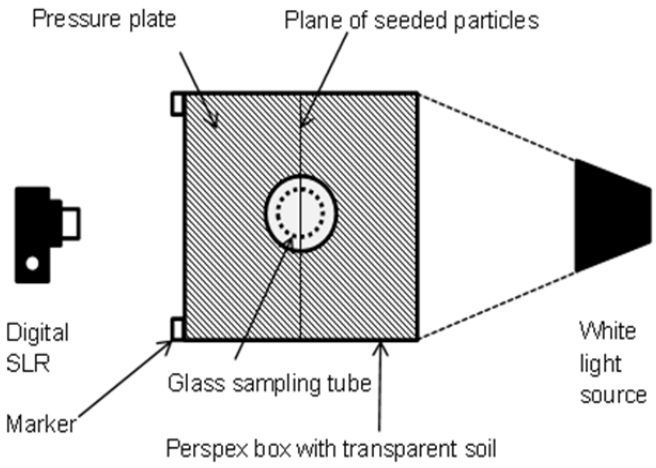

Figure 3.8 - White Light Set-Up for PIV

Requirements for the method to be considered viable included:

- The particles must be visible and appear sharp through the soil box,
- The plane must be perfectly flat and exactly at the centreline of the tube to be pushed into the box – a tolerance of 1mm either side of the centreline was deemed acceptable.
- The overall coverage: each interrogation area must contain sufficient particles
- The movement of the particles during the consolidation phase must be controllable or predictable
- The final position of the plane within the soil must be predictable

3.2.4.1 The Z-Plane Method

Originally, a Perspex box 200x200x450mm (L:W:H) with removable top (200x200x150mm (L:W:H)) was available, having been designed and manufactured for a another project. The first attempt at creating the plane was by painting a steel sheet with partly consolidated slurry and covering it with particles and inserting it into the centre of the soil box (Figure 3.9). Soil slurry was then added on either side of the plane up to the total height. After a short initial consolidation phase the sheet was slowly drawn out through the top of the box, leaving a vertical plane of particles in its place. The second phase of consolidation then took place, during which time oil was allowed to drain out of the sample by a small hole at its base. Over a period of two weeks, the height of the sample reduced by up to 40%, first under self-

weight, then under increasing pressure to 50kPa. The particles remained in the same plane during consolidation, which reduced in height along with the rest of the soil. It was observed that while the consolidation phase did not affect the seeding pattern, the earlier removal of the steel plate caused significant changes in the seeded area density (Figure 3.10), with particles “sticking” in their original location close to the bottom of the box, and many particles from the centre of the plane being dragged upwards. Upon retrieval of the steel plate, a number of particles remained attached and a number finally slid off and concentrated close to the surface.

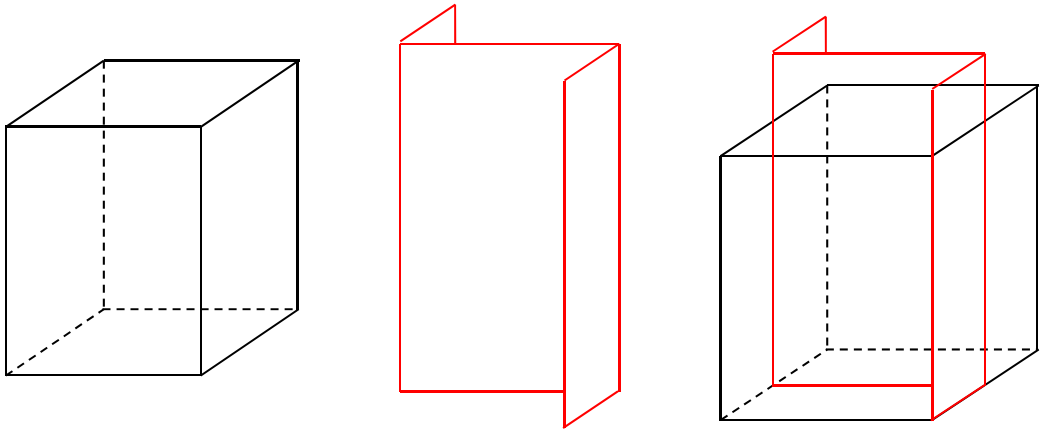

Perspex Box Z-Plane Combination

Figure 3.9 - Z-Plane Method

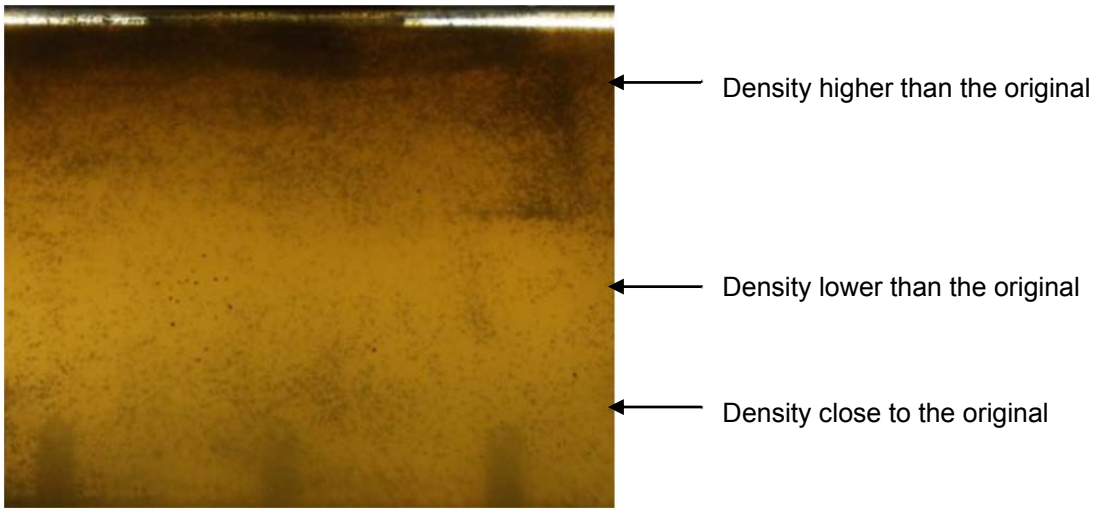

Figure 3.10 - Uneven Seeding using Z-Plane Method

Consequently none of the trial PIV analyses carried out in the upper portion of the soil yielded any usable results. The coverage was concluded to be too high for true Interrogation Area recognition, since most of the displacement coordinates were unrealistic, with

measured displacements not physically possible in the short time frame between two photographs. It was concluded that more tests could be carried out at a smaller scale to infer the effect on the disturbance of the seeding density, of the plate removal speed and the time between the pouring of the slurry and the removal of the plate. A scaled down model of the Perspex box and Z-Plane was created and initial tube driving tests were carried out to test the PIV analysis tools. It was also, however, decided to first test the viability of a new technique, the "split-sample" method.

3.2.4.2 The Split-Sample Method

The main issue with the previous method was the inability to control the position of the seeding particles. Once the desired area density was created on the steel Z-plane, it could not easily be kept undisturbed throughout the preparation stage since the removal of the steel plane introduced a significant amount of particle displacement, creating densely seeded areas (too dense for PIV) at the top and bottom of the box, and relatively empty areas near the middle. After these initial attempts, an alternative method was proposed, and used in a scale model of final dimension 80x80x180mm (L:W:H). In this new method which constructs the soil model horizontally, two Perspex boxes were used. The first, (Box A, dimensions 180x120x80mm, L:W:H) was laid horizontally on a level surface for the soil cuboid to be made up layer by layer and consolidated within it, before being removed by way of a metal trowel and slid into a second Perspex box (Box B, dimensions 80x80x180mm) – to be placed vertically – whence the tube samples are to be extracted at a later stage (Figure 3.11).

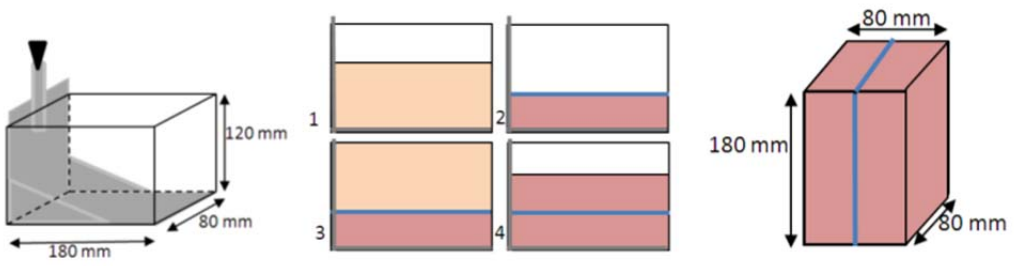

Box A and trowel

Construction sequence: light: slurry, dark: consolidated soil, blue: particle plane

Box B, filled

Figure 3.11 - Split-Sample Method

First, some transparent soil slurry was mixed, de-aired and placed within Box A, which it filled to a height of approximately 80mm (to allow for a reduction of volume of approximately half during consolidation – this was to give a half-sample of dimensions 80x40x180mm). This was left to consolidate under self-weight for 48 hours, during which time a noticeable change in volume occurred. Oil was observed to have leaked out in majority through the connections between the sides of the Perspex box, not through the top of the box, as was designed. After the initial consolidation, a pressure plate and weights were put in place on top of the sample.

After consolidation of the first half-sample, the excess oil was removed from the surface of the soil, onto which dyed sand was then sprinkled. An additional slurry layer of approximately 5mm was created on top of the seeding particles. The difficulty in this step is the tendency of the particles to move in the direction of material flow. Since the transparent soil must be placed in a manner which discourages the entrapment of air bubbles, one method was to run the fluid soil continuously down the side of the container. This worked reasonably well but did create a horizontal flow of material which significantly disturbed the seeding particles. This was also the case when the soil was carefully introduced anywhere in the box by way of a baster. When the second layer was fully settled, the box was subjected to a small amount of horizontal shaking, which equalised the seeding area density, but has the unwanted effect of lodging seeding particles in the imperfections in the sample. (This is not a very important issue as long as a good visibility of the seeding plane is maintained at different positions around the box. This effect tends to disturb the edges of the sample where visibility during preparation is important, but this would not affect the later stages of sampler driving and PIV analysis). During shaking, particles may move slightly out of plane, but the majority tend to settle back to the surface of the consolidated layer. Any particles which remain out-of-plane can be removed with a small aperture pipette without disturbing the rest of the plane. After the second layer was consolidated under self-weight, the third layer could be created with the remainder of the slurry, and consolidated in the same manner as the first layer. When consolidation was complete, the trowel was lifted with care to remove the whole sample, which was inserted into the second box where it was allowed to finish consolidating in the correct orientation (In natural soils, excluding those severely

affected by tectonic effects such as folding strata, consolidation occurs in one direction, and this affects particle orientation. To keep in line with this, the majority of the consolidation would have to be in the vertical direction, therefore any horizontal consolidation should be small when compared to vertical consolidation - here horizontal consolidation stresses were kept at 10% of vertical consolidation stresses).

The creation of the plane of seeded particles was successful and well controlled throughout the process. The area density of the particles could be chosen and put in place very accurately, and no changes were observed at any point during preparation. It was however noted that during removal of the trowel, because of a loose fit and lack of support to the soil at the edge of the trowel, the consolidated soil rippled slightly and deformed in a non-recoverable manner (Figure 3.12a). It was, however, possible to retrieve the soil as a whole with some disturbance to the edges, but with no apparent effect on the seeded plane.

a  b 
Figure 3.12 - Split-Sample Method: a) Rippling and b) Tearing

The transfer of the soil to Box B was not as successful. The sample required trimming before being placed into the second container. It was decided that as the material was extremely soft, the extra soil would be left to shear itself off as the soil entered the new box. The friction between the transparent soil and the box tore two faces of the cuboid in places, resulting in large deformations on the outside faces of the soil. During removal the soil refused to slide off the trowel, even when oiled to decrease friction. Because of the shape of the trowel, it was not possible to oil the parts of the metal which refused to yield the transparent soil. This resulted in tearing of the soil sample (Figure 3.12b). It was concluded that while the layering of the transparent soil was a viable idea (since it produced a level and predictably seeded plane), the use of the trowel was not. The main problematic issue was that of transferring the

sample from one box to the other, and doubts were cast on the scaling up of this technique. It was therefore decided to develop the horizontal consolidation method without the trowel.

3.2.4.3 The Final Approach: The Horizontal Consolidation Method

The basis of the horizontal consolidation method is the same as previously described for the split-sample method, but the model is created directly into the large Perspex testing box. The soil model is created horizontally, layer by layer, so the plane of particles can be seeded as required at the correct position. With a good understanding of the rate and extent of consolidation of the transparent soil, it is possible to predict the final position of the seeded plane within the model to approximately 1mm. For this method, an adaptation of the original box was manufactured, with two removable parts rather than one (total size: 200x200x450, L:W:H). The process is illustrated in Figure 3.13. Two layers are created with the box in a horizontal position (10L of slurry can typically be de-aired at once in the vacuum chamber so in a large model, four layers of 10cm are created one after the other), and consolidated horizontally, under a dead weight of 5kN/m^2. A plane of seeding particles is then created on the dry surface, and the box is filled layer by layer until complete. The first layer after the particles needs to be as thin as possible to avoid particles moving out of plane before the slurry consolidates enough to hold them in place. Care must be taken when creating this particular layer, since the flow of slurry will drag the particles along with it. It was found that the best method to avoid problems with this issue was to increase the oil: solid ratio for this layer only, and accept that an amount of flow would happen in the uppermost corners where the material was introduced into the box. Since this material invariably ends up being trimmed off, the lack of particles within it is not an issue. When the box is filled to the top of the bottom section with consolidated slurry, the top third of the box is detached and removed and replaced with a solid Perspex face. The box is turned 90° and is placed in the consolidation rig, which applies 50kN/m^2 or 80kN/m^2 in four of five increasing stages (Normally consolidated soil / Over-consolidated soil), by way of a pressure plate. The volume of soil continues to decrease as oil drains from it - by approx 20%. When movement appears to cease (no visible movement in 24 hours) the sample is considered ready, after which the top third of the box is removed with any soil still within it. The final dimensions of the soil model are 200x200x300 (L:W:H).

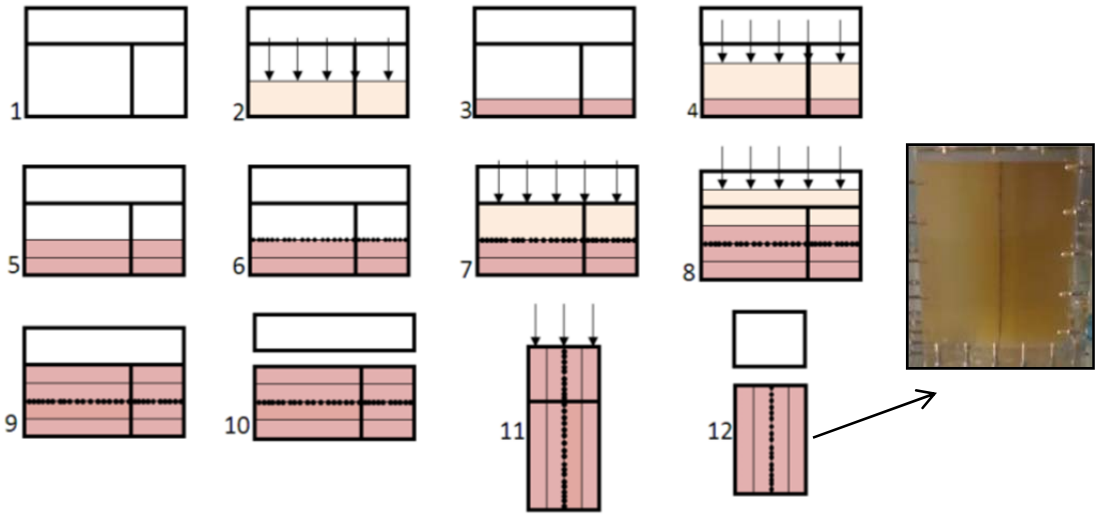

Figure 3.13 - Preparing the Soil Model using the Horizontal Consolidation Method: light=slurry, dark=consolidated

Results were good for all models prepared using this method, with most particles situated on a single plane. When care is taken to ensure the plane is parallel to the box's face, an error of less than 1mm between the top and bottom locations is easily achievable. The main challenge when working with transparent soil is the time it takes to consolidate to the texture of a soft or sensitive soil. The horizontal consolidation stages take approximately two to three weeks. The second layer of soil rarely consolidated to the exact location it was required to and therefore an additional thin layer of soil was needed to correct for this - a process which could take a few additional days. The vertical consolidation takes another two weeks. With additional time needed for installation of the heavy box into the consolidation and testing rigs, the preparation of a test can take up to 6 weeks, which restricts the amount of tests achievable in the time frame of this research project. To increase this, two boxes were created, and soil models were thus able to be created at 3 week intervals.

3.2.4.4 Selecting the Seeding Particles

The size, shape and type of tracer particles are determined such that they will not interfere with the behaviour of the experimental model, will not exhibit properties largely dissimilar to those of the material being studied, will reliably follow the motion of the fluid, and will not interact with one another (Westerweel, 1997).The type, shape and size of seeding particles are variables which were considered during the first year of the project.

The alternatives considered were:

- Spherical or irregular particles
- Fluorescent or non-fluorescent particles
- Different sizes of particles

The shape of the particle is important in PIV since the success of the analysis depends on patch recognition. Irregular particles appear to change shape and size as they rotate either in or out of plane, which can present the PIV software with two very different patches from one image to the next (Figure 3.14). This is not recommended since it increases the risk of errors and wild vectors.

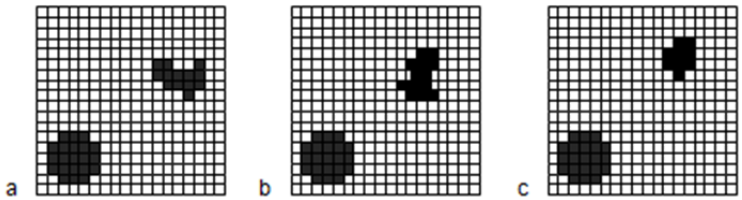

Figure 3.14 - Regular and Irregular Patch Shape Change b) in plane and c) out of plane

The size of the particles is another important factor since small particles will not be visible enough through the transparent soil under white light, but large particles will not follow the true soil movement during deformations. Due to difficulties in finding affordable small coloured particles, irregularly shaped dyed sand was used in the initial testing stages with good results. Transparent seeding particles are widely available since these are commonly used for PIV in experimental fluid dynamics, but coloured ones are not common, too large or prohibitively expensive. Attempts to colour the surface of transparent particles in permanent ink were unsuccessful since the colour did not survive the prolonged contact with the oil blend. Circular black and blue hole-less micro-beads were purchased through an online retailer and used for the main testing programme. Their diameters were 0.6-0.7mm and 1mm respectively, with the smaller ones providing the majority of the texture cover, and the larger particles providing an additional element of texture in tests where there were concerns about visibility through the transparent soil. Fluorescent particles were also considered but were rejected as a viable option due to difficulties obtaining high quality photos under UV

lighting at the required frame rate, as well as for the costs associated with obtaining the required pieces of equipment.

3.2.5 Testing

Three types of tests were carried out to study the full life cycle of the soil sample. Firstly, photographs were obtained of the model tubes being pushed into the transparent soil to retrieve a sample. Secondly, a selection of these samples were monitored for six months to assess if any strains developed within them over time, and finally, these samples were photographed being extruded from their tubes.

3.2.5.1 Test Series 1: Tube Driving

The main series of tests investigated the strains developing in the soil within and surrounding the sampling tube during its insertion into the ground. For this, a consolidated transparent soil model 200x200x300mm (L:W:H) was created in a Perspex box in the manner outlined in Section 3.2.4.3, and placed within the testing rig, which comprised a tube driving rig installed within a consolidation rig. The setting is illustrated in Figure 3.15a and b. The box was aligned with a 200x200mm pressure plate and piston attached to the consolidation rig, which fitted closely into the Perspex box and served the purpose of maintaining pressure on the soil surface (bar a hole in its centre to allow for insertion of the tube into the soil by the driving rig). To ensure that the plane of particles and the camera were orthogonal, a cylinder with markers at either end was attached to the centre of the front face of the Perspex box. Looking through the eyepiece it was possible to align the camera with the two points on either end of the cylinder (Figure 3.15c, d). Markers on the front face of the box – screws within the Perspex box (seen in Figure 3.8) – were used for the measurement of camera shake before processing. Two test settings were considered:

- Normally Consolidated soil, where the soil was loaded up to 50kN/m^2 in the preparation stage (see 3.2.4.3), unloaded to allow the installation of the pressure plate with the hole in the centre, then reloaded to 50kN/m^2, with the pressure maintained during testing (tube driving)

- Over-Consolidated soil, where the soil was loaded up to 80kN/m^2 in the preparation stage (see 3.2.4.3), unloaded to allow the installation of the pressure plate with the hole in the centre, then reloaded to 50kN/m^2, with the pressure maintained during testing (tube driving)

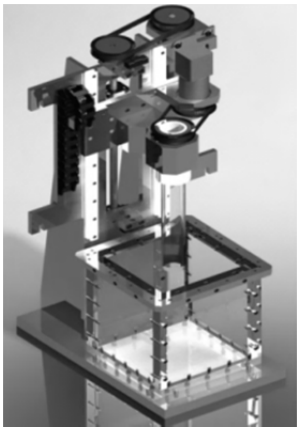

a

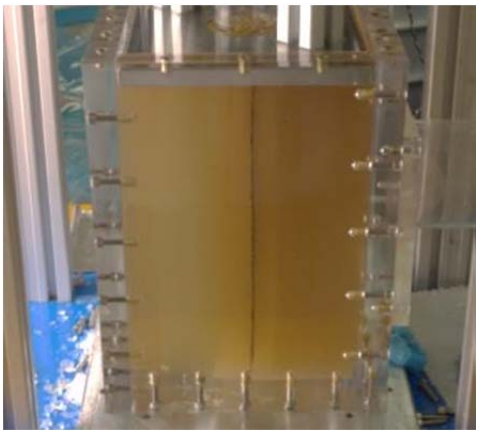

b

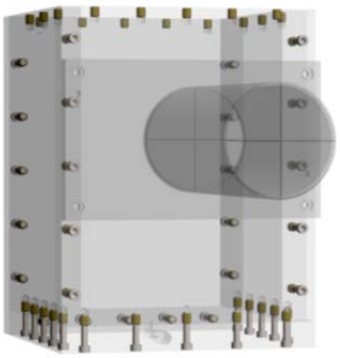

c

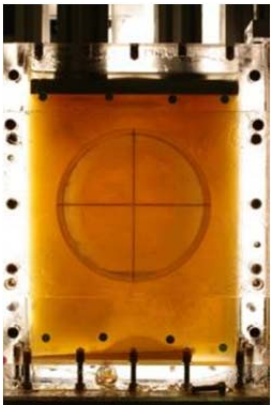

d

Figure 3.15 - Tube Driving Set-Up, a) Tube Driving Rig, b) Box set inside Consolidation Rig, c) Checking Orthogonality between Plane of Interest and Camera with the Cylinder and d) Orthogonal Set-Up

During unloading stage, if the pressure was taken off the soil too rapidly, cracks sometimes formed in the soil model due to the suction created by the pressure plate's upwards movement. These filled with air and propagated rapidly within the soil, significantly reducing the transparency. Upon reloading, these disappeared and transparency was restored. Care was taken in later tests to unload the model in small steps, over a two hour period to prevent the disturbance of the soil's structure.

This study aimed to investigate the influence of sampling tube geometry on the strains produced within the sample, and six designs of tube were tested. Table 3.1 outlines the six

tube geometries with the AR and ICR calculated from the tubes' dimensions. These cutting shoe geometries were chosen to incorporate elements of variation in the sampler design. Unfortunately, due to manufacturing and shipping constraints, it was not possible to use obtain better variations in design. The cutting edge of the geometry B tubes was fragile and chipped easily, meaning that the length over which the tapering could occur was limited (real sampling tubes have tapering lengths up to 60mm, but only 5mm were achieved in the glass tubes). It was also though that using tubes with larger sharpened cutting edge lengths would have obscured or distorted large patches of soil. It is now believed that this would not be the case. Tube diameters were also a constraint, and the manufacturers were not able to produce as thin as tubes as were ordered. This resulted in large area ratios and less variation as had been expected between the blunt and sharp tubes.

Table 3.2 describes the nine tests planned for investigating tube driving. Two models of each tube were manufactured to allow for samples to remain within the tubes for monitoring tests (see 3.2.5.2). The tubes were approximately 1:2 scaled-down models of open tube samplers, which are typically 450mm in length and 100mm outer diameter. This is approximate because of the manufacturing capabilities of the company which supplied the tubes. In each test, the model glass tube was connected to its metal holder, and held in place by a pair of O-rings. The tube was then continuously pushed through the hole in the pressure plate into the soil by the electric motor of the driving rig at a speed of 2.4mm/s.

The speed was chosen as a compromise between being rapid enough to produce undrained conditions within the soil and being slow enough that not too much movement occurred between frames taken by a high resolution camera. Excessive movements would distort the Interrogation Areas between images and reduce the software's ability to recognise them accurately.

A study by Budhu and Wu (1992) compared the pore pressure during tube driving at 0.4, 4 and 40mm/s. Slow driving speeds were observed to cause the highest disturbance, but the difference between 4 and 40mm/s was insignificant. Since the chosen speed is less than this, the process may not be fully undrained.

Table 3.1 - Model Tube Geometry Designations

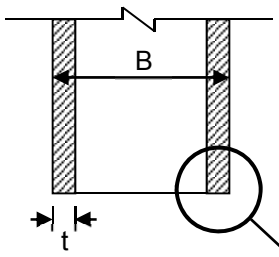	Type of Sampling Tube		
	Rounded (Blunt) Sampling Tube	Tapered Sampling Tube	Rolled and Reamed Sampling Tube
Thickness			
"Thick" (t=3.6mm)	A AR=34-35% ICR=0.4-0.8%	B AR=33-34% ICR=0.7-1.5%	C AR=37-39% ICR=1.9-2.8%
"Thin" (t=2mm)	At AR=16-17% ICR=0.1-0.2%	Bt AR=15-16% ICR=0.1-0.3%	Ct AR=19-21% ICR=1.8-3.3%

Table 3.2 - Tube-Driving Test Programme

Test	Tube	Outer Diameter (B)	Thickness (mm)	Consolidation (Over or Normal)	Over-consolidation Ratio (OCR)	Designation
1	A	52.2	3.6	NC	1	ANC
2	B	52.2	3.6	NC	1	BNC
3	C	52.2	3.6	NC	1	CNC
4	At	52.2	2	NC	1	AtNC
5	Bt	52.2	2	NC	1	BtNC
6	Ct	52.2	2	NC	1	CtNC
7	A	52.2	3.6	OC	1.6	AOC
8	B	52.2	3.6	OC	1.6	BOC
9	C	52.2	3.6	OC	1.6	COC

The tubes were driven into the centre of the soil model to reduce any boundary effects caused by the walls of the Perspex box, to a depth of 240mm (just before the tube holder

came in contact with the soil's surface). It was decided to take a single sample per model due to boundary effects and because of the results of a similar study by Yan et al (2010) who observed large soil movements in samples taken in close proximity to pre-existing boreholes in a natural clay (Kaolin) physical model. Photographs were taken by a Pentax K20D digital camera on low speed continuous shooting (this setting allowed for images to be taken continuously at a speed of up to 2 frames per second (FPS) until the SD card was full - while high speed continuous shooting was only able to take up to 40 images in a rapid burst). A remote controller was used to minimise camera shake. Photo resolution was 14.5MP in JPEG format. A typical test lasted just under two minutes and yielded some 230 images. At the end of the test, the driving rig's motor was stopped, the pressure plate was removed and the sampling tube was dug out. Typically, samples would be rotated before being removed from the ground, to shear off the base of the sample from the soil under it. The process of rotating the sample would have disturbed the embedded plane of seeding particles so it was decided to dig the sample out rather than disturb the plane, or risk not recovering the sample, since this is a possibility with soft soils. Smaller scale soil models prepared during the development of the soil consolidation investigation. Z-Plane and Split-Sample approaches were tested to gain initial results and improve the methodology. Only when the large-scale model (200x200x300mm) model was developed was the test programme started, and all nine tests listed in Table 3.2 were carried out, with a number of these repeated where something was observed not to go to plan during the test, such as the tube penetrating at an angle.

3.2.5.2 Test Series 2: Sample Monitoring

After recovery, some samples were selected for the second test series, monitoring displacements within the sample during the six months following their removal from the ground. The ends of the sample were removed and replaced with two layers of paraffin wax, making a 10mm seal. Because of the high temperature of the wax, and safety concerns about the low flash point of the oil, the first seal was made from paraffin was mixed with some vegetable oil to increase its softness at lower temperatures and protect the surface of the sample from excessive heat. This provided an adequate seal, which was then covered with a second thin layer of wax just about to lose its liquid state (the wax's temperature was

monitored with a thermometer). Due to space restrictions it was decided to choose four tubes to monitor, two normally consolidated and two over-consolidated samples. Since the Inside Clearance Ratio was thought likely to have an impact on stress redistributions within the tube, tubes A and C were selected. The plan therefore was to monitor ANC, CNC, AOC, COC. It was found out too late that the second glass tube for geometry C was too large to fit into the tube holder, and since the first C tube was already holding sample CNC in the monitoring set-up, the fourth monitoring test, COC, was changed to BOC because there was not enough time left in the project to wait for CNC's six months to finish before testing and monitoring COC for six additional months. After its tube driving test, one tube was added approximately every three weeks into a wooden rack connected to the monitoring set-up (Figure 3.16). The camera (Pentax K-r) was fixed in place so that it only needed switching on for each test, thus minimising its movement between photographs. Images were taken twice weekly over 6 months for each sample tube using a remote control to minimise camera shake. Photo resolution was 12.2MP in JPEG format. The PIV set-up was similar to that used for the first set of tests, using a white light source (in this case a light box) to backlight the soil. To avoid light reflecting off the front of the tubes, the whole set-up was contained using a blackout curtain. Before the first tube was inserted, the aforementioned cylinder was installed to ensure the camera and rack were orthogonal. Markers were stuck to the light box to later check and correct for camera shake.

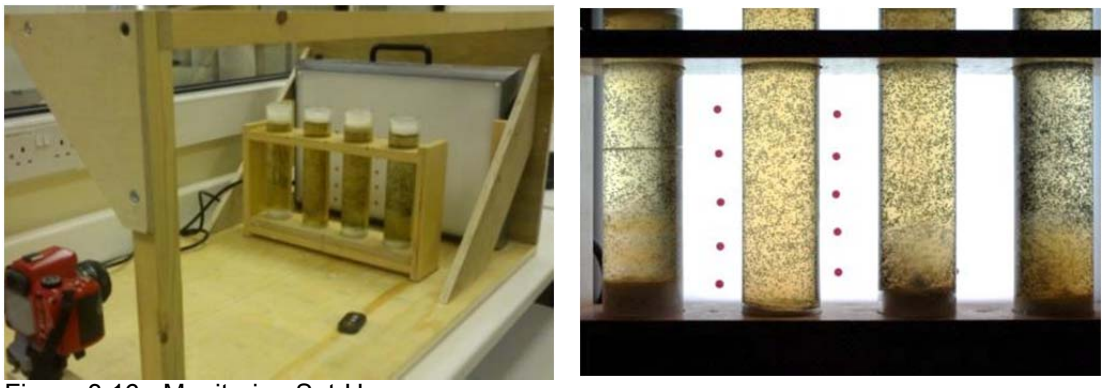

Figure 3.16 - Monitoring Set-Up

3.2.5.3 Test Series 3: Sample Extrusion

The samples chosen for monitoring tests were extruded at the end of six months. A tight-fitting piston (Figure 3.17) was attached to the tube, and was manually advanced by a

screwing mechanism so that the soil was pushed in the same direction as it entered the tube (i.e. the soil was pushed from the bottom of the tube upwards). Because the process was manually controlled rather than motorised (solution chosen for its low cost) the speed was not constant but care was taken to advance the piston as regularly as possible.

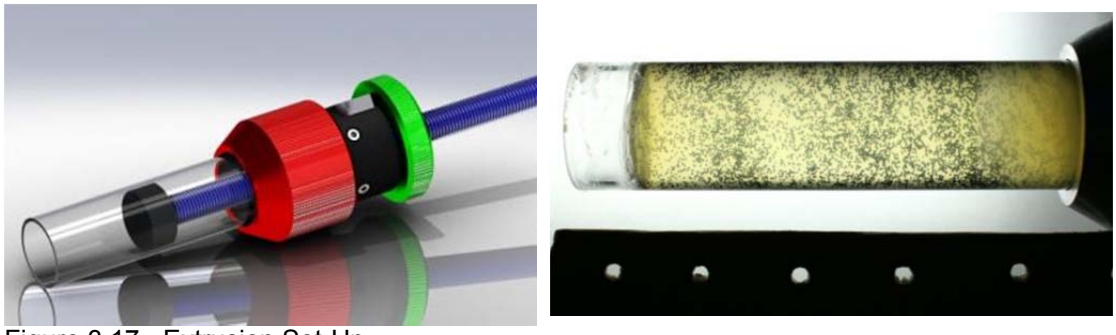

Figure 3.17 - Extrusion Set-Up

Orthogonality was checked in the same fashion as before, but since the tube had no flat surface to attach the cylinder to, it was probably not achieved to the same degree as for the other tests. The tubes were backlit as previously, and the set-up was obscured so no light illuminated the curved from surface of the tube. A piece of cardboard with holes punched through it was placed under the tube in line with the plane of particles and was used as a plate of markers for measuring camera shake before analysis. Photographs were taken using a remote controller to minimise camera shake at a rate of 3 FPS with a Canon EOS 6D and tests typically lasted for three minutes. Photo resolution was 20MP in JPEG format. Some samples not intended for monitoring were used to obtain preliminary results, and since the tests ran smoothly, their results are also included with those of the four tubes selected in 3.2.5.2.

3.3 Analysis Methodology

3.3.1 Introduction

The success of any PIV analysis relies heavily on the quality of the images used. Any displacement measured by the software will be made up of two components: the true displacement, and a certain amount of noise (Adrian and Westerweel, 2010). Ideally much of this noise should be removed before the frames are captured by using a set-up which minimises avoidable effects, but techniques for pre- and post-processing of the photographs

are commonly used. This section describes how data was obtained from each series of photographs, and how care was taken to remove noise to obtain displacement vectors which truly reflected the movements within the soil.

Noise can be caused by three components:

- Camera lens:
    - Heating of the CCD. If the CCD sensor does not have the time to cool between shots, its heat can create noise on the picture, which may be of the same order of magnitude as that of the faintest tracer particles (Raffel, 1998). The heat remaining on the CCD sensor is dependent on the ambient temperature and the rate of capture.
    - Lens Distortion: all lenses are built with inherent imperfections
- Set-up:
    - Camera shake. This can be due to random floor vibration or to the shutter mechanism. The best way of reducing this is to use a heavy or stable tripod and using remotely controlled time-lapse photography.
    - Misalignment of the camera and the observed body. The camera lens must be positioned exactly orthogonal to the plane being illuminated, and its position must be identical for every frame taken.
    - Refraction of the light through different materials. The light scattered from the particles will travel through the fluid at one velocity and refraction angle, then through any further medium at another. Before analysis of the data, calibration must be considered.
- Errors inherent to the PIV software. To quantify this, a simple test can be carried out on test photos (White *et al*, 2003,see 3.3.3.2)

Corrections for these can be performed before or after PIV analysis. All three testing stages yielded data in the form of digital photographs. The success of PIV analysis is dependent on the parameters chosen by the user and care must be taken that the results obtained are independent from the values chosen for these parameters. These were studied in detail to ensure the results found were constant regardless of choice.

3.3.2 Calibrating for Image Distortion

To separate the displacement data from the distortions caused by the setup, a calibration procedure was followed. Its aim was to compare a theoretical model for distortion with observed distortion patterns within photos taken with the camera, to either:

- Quantify the distortions and correct the data where appropriate
- Prove that some corrections are not necessary since the distortion is insignificant

This section describes the procedures used to determine the effect of distortions and explain why image magnification is partially corrected for, and why the need for lens distortion correction was deemed not necessary in the tube driving tests but essential in the extrusion tests. Similar lenses were used in the K-r and K20D so the process was only carried out once for this type of camera, on the lens most prone to distortions (35mm lens).

3.3.2.1 Camera Shake and Image Registration

Camera shake describes small apparent movements in the photograph due to external factors, such as the camera moving relative to the object being photographed between images. It is due to the shutter mechanism of the camera, and to random floor vibrations due to activity around the testing area. While it is difficult to avoid this completely, corrections can be made to the images themselves to minimise the effect. This process is called image registration, and relies on the presence within the photos of markers which are known to stay immobile during the duration of the test. These can be anything from LEDs to stickers to unique recognisable features in the vicinity of the photographed object. Ideally these should be placed on the same plane as the area under consideration in the PIV set-up, but this is not always possible. The registration software used was a code run on MATLAB which asked the user to identify the markers in the first photo in the series. It then ran a PIV analysis on the IAs containing the markers and determined their apparent movement over time. Using this displacement data, and a function built-in to MATLAB, "cp2tform", the images themselves were regenerated with the marker points at the same location in all photos.

Typical apparent movements of the markers for a continuous shooting period (Tube Driving tests or Extrusion tests) were of in the range ±2 pixels. After registration, this reduced to ±0.2 pixels in most cases, with the occasional marker displacing ±0.5 pixels. For shooting over a long period of time (monitoring tests) the apparent movements were more important because the camera was disturbed by being turned on between shots. Large (200 pixels) Interrogation Areas were used to contain the markers in all cases, and confidence in the accuracy of their displacement was high, with noise expected to be below 0.01-0.1 pixels (see 3.3.3.2). Because the movement due to camera shake was more than one pixel, this was deemed to be a necessary step in image analysis. Evidence of camera shake is plotted in Appendix C.

3.3.2.2 Lens Distortion

When a photograph is taken of a scene or object, the CCD of the camera converts the object-space coordinates of the contents of the scene to image-space coordinates within the photograph. In an ideal pinhole camera (No lens, and with a small aperture: Figure 3.18), the coordinates of each element within the scene remain in the same relative position to each other and the photographs depict exactly what the photographer expected. The addition of a lens to this ideal system, no matter how expensive, will not replicate this exactly. In most cases, the photograph will be affected by optical distortions caused by the lens which can be linear or nonlinear and can cause elements of the image to appear altered from their original state.

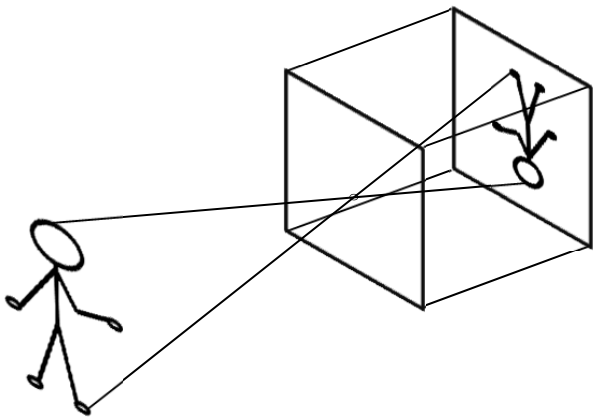

Figure 3.18 - Ideal Pinhole Camera

In PIV, understanding optical distortions is essential since even small distortions (1-2 pixels) can cause displacement vectors to be miscalculated if IAs move significantly from their original location within the photograph.

The distortion is that created by the lens itself, and can contain two elements (Adrian and Westerweel, 2010):

- Radial distortion, which is caused by lens characteristics, which can be visible as either:
    - Barrel distortion, where elements closest to the centre of the image are magnified more than those further away
    - Pincushion distortion, the opposite of barrel distortion
- Tangential distortion, which is due to a misalignment of the camera's lens and sensor

Radial distortion is illustrated in Figure 3.19. Distortion can be defined by Equation 19 as the difference between the original location (xu, yu) of and element in the photo and its distorted location (xd, yd). It is expressed either in mm or pixels relative to the element's distance (ru or rd) from the image centre (xc, yc).

Both barrel and pincushion distortions have the effect of turning straight lines curved and can be measured in photos taken by the camera, or could be calculated using a distortion model. A number of theoretical models have been documented, both in 2D and 3D (Shih et al, 1995, Heikkilä, 2000). For the purposes of this work, only 2D is considered. Brown (1965) defined a model which corrects for both radial and tangential distortions, but can be simplified for radial only (Equation 20), which itself can be simplified to a lower level (Gribbon et al, 2003 - Equation 21). The Division Distortion Model (Equation 22) is used by National Instruments (2013) and also simplifies the high degree equation to a simpler form, using one k parameter.

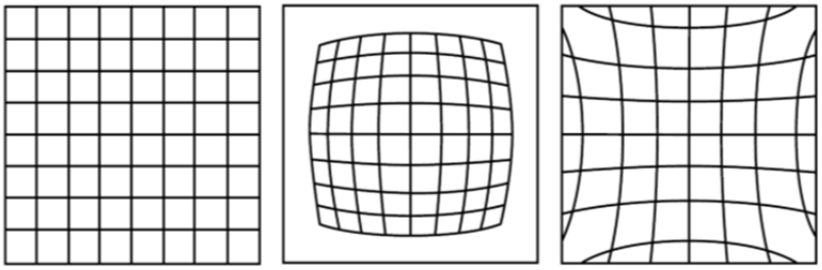

Figure 3.19 - Radial Distortion: Original Coordinates, Barrel and Pincushion Distortions (from Vass and Perlaki, 2003).

$$Distortion = ru - rd$$
$$= \sqrt{(xu - xc)^2 + (yu - yc)^2} - \sqrt{(xd - xc)^2 + (yd - yc)^2}$$

Equation 19

Much work has been done to verify, adapt and improve on these models (Gribbon et al, 2003, Vass and Perlaki, 2003, de Villiers et al, 2008, Tardif et al, 2009, Stanier et al, 2012). These equations can be applied to the distorted photographs if the lens's radial distortion coefficients K1 to Kn are known. These were not known for any of the three cameras used in this research, but could have been determined using the set-up described by Stanier et al (2012) had there been sufficient time. A typical pattern of distortion is illustrated in Figure 3.20, using the Division Distortion Model which simplifies all K coefficients to a single value k. Central patches are undistorted and far away patches are pulled into the centre of the image.

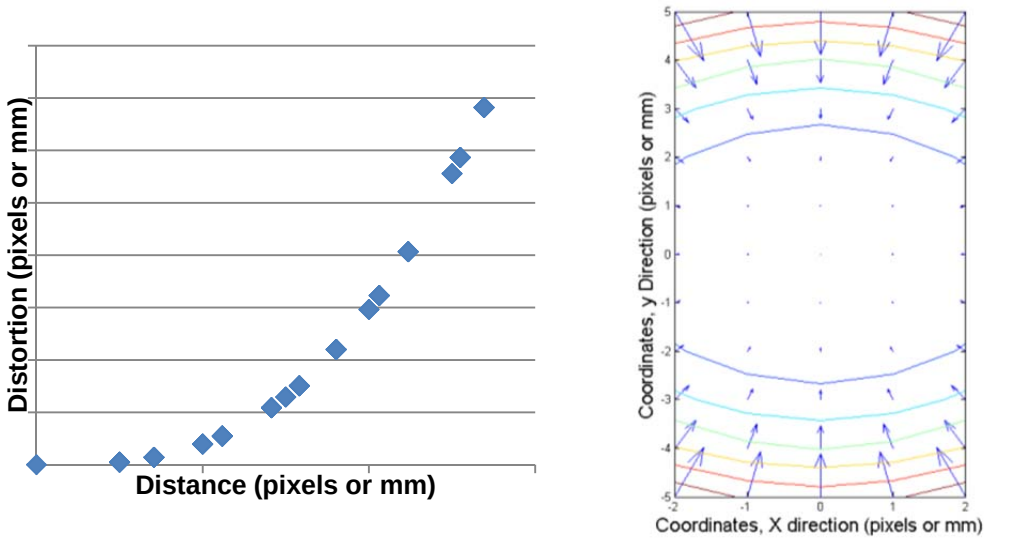

Figure 3.20 - Effects of Barrel Distortion, from the Division Distortion Model

Brown's model	$xu = xd + (xd - xc)(K1 * rd^2 + K2 * rd^4 + \cdots)$ $yu = yd + (yd - yc)(K1 * rd^2 + K2 * rd^4 + \cdots)$	Equation 20
Brown's model, simplified	$ru = rd(1 + k * rd^2)$	Equation 21
Division Distortion model	$xu = \frac{2xd}{1 + \sqrt{(1 - 4 \times k(xd^2 + yd^2))}}$ $yu = \frac{2yd}{1 + \sqrt{(1 - 4 \times k(xd^2 + yd^2))}}$	Equation 22

A method was used to quantify lens distortion in the Pentax K20D (used for the tube driving tests). It is explained in Appendix D and it was concluded from the results of this study that correcting for lens distortion in this case was not necessary.

3.3.2.3 Light Distortion

Light refraction through the various transparent materials used is the single most important source of distortion: photographing a plane behind materials of different Refractive Indices (RI) will yield photos on which the plane has been magnified by the light bending as it meets each boundary between materials. Using an ideal pinhole camera, Figure 3.21 illustrates the path a ray of light travels from its position on the plane of seeded particles to the camera, and where the camera sees it to originate from. Refraction (the angle change the light experiences at it crosses the boundary between two materials) occurs up to four times in the set-up for the tube driving tests and causes the plane of particles to appear magnified since it moves the apparent location of the particles outwards from the centre of the image.

Using the same calibration plate as described in Appendix D, and the photograph taken through all materials (photo B), the effects of lens distortion and material refraction were studied. The average spacing in the centre of the photograph was found to be 87.99 pixels and was used to recreate the original coordinates of the undistorted marker points, and the distortion for each point is presented in Figure 3.22. The image was, in this case, distorted by the effects of both lens distortion (equal to that presented previously) and refraction. The distortion that is visible in Figure 3.22 is created by the lens and agrees with the behaviour seen in the previous section.

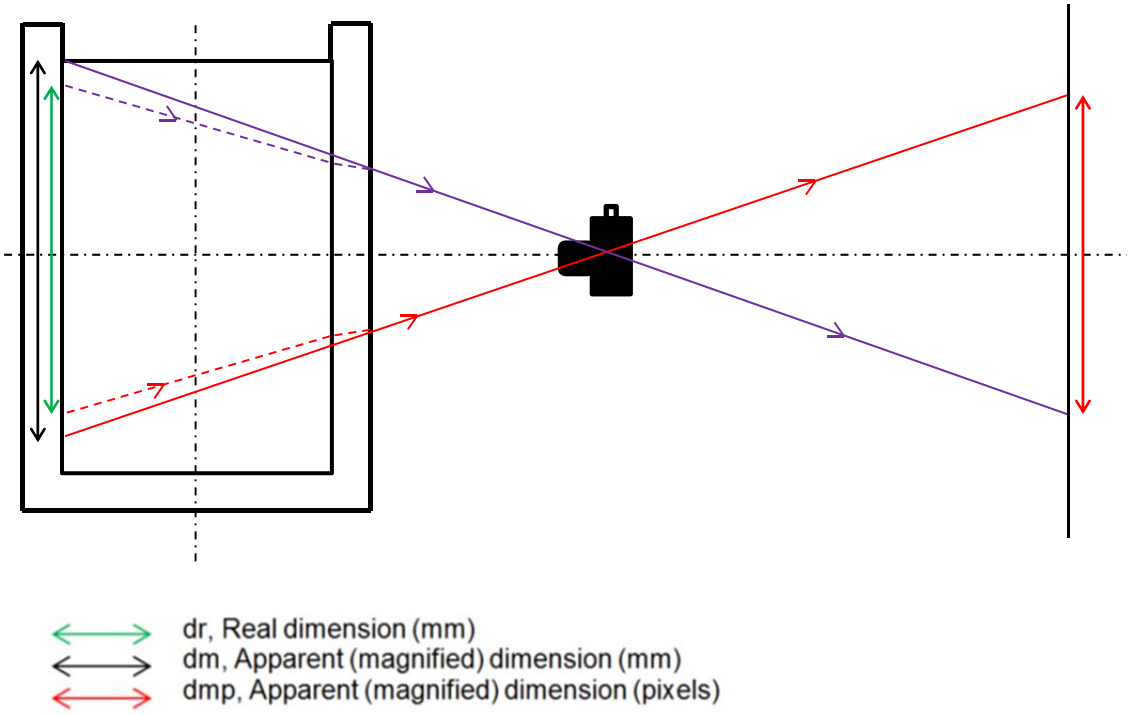

Figure 3.21 - Effects of Refraction

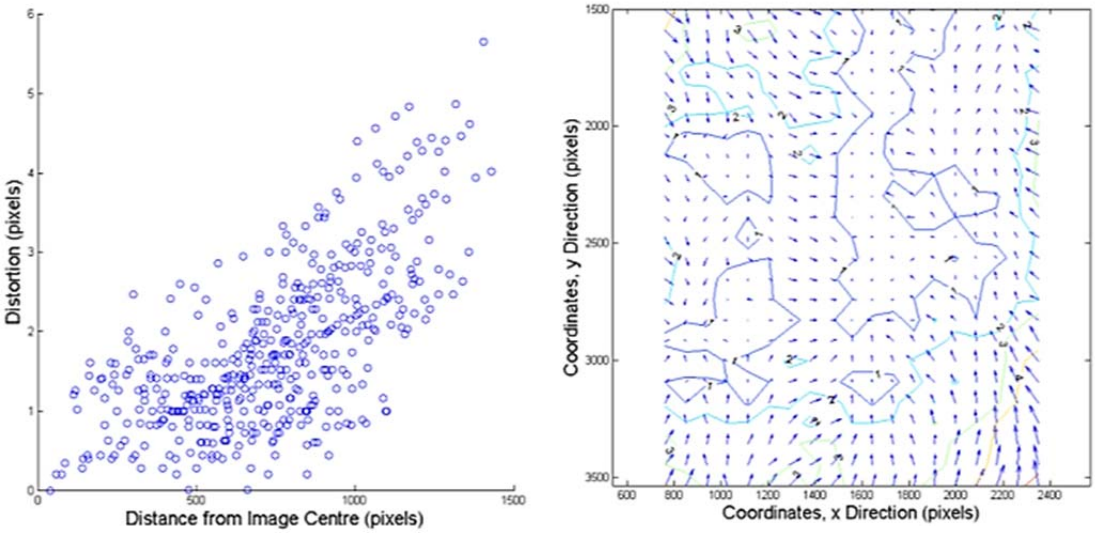

Figure 3.22 - Evidence of Barrel Distortion in Photo B from Calibration Plate

Since the distortion in Figure 3.22 is similar to that in Figure D. 1 (lens only distortion), this suggests that the distortion created by refraction increases linearly with distance from the image centre, and is hence pure magnification. In magnification, the coordinates of each point, each displacement and each dimension are scaled up by the same factor, meaning that the spacing used to recreate the undistorted coordinates of all marker points is the same spacing as that between all marker points in the image – this explains why it does not

register as distortion and is absent in Figure 3.22. We know that magnification does not occur in the case of lens-only distortion by studying lens distortion models and their behaviour. On the basis of this linear relationship, the sole data correction required for magnification is that of a Linear Scale Factor (LSF) to convert pixels to mm. Since the governing element in the image distortion is magnification, this can be obtained by measuring (in pixels) the dimensions of an object within the photograph of known size (in mm), and dividing the two values. Repeating this for more than one dimension increases the confidence in the LSF. Values for each test are included in Chapter 4.

Furthermore, the data from the two photographs can be compared by taking the ratio between the central marker spacings, to reveal the magnification caused by the materials.

$$Magnification\ caused\ by\ the\ materials = \frac{Spacing\ in\ Photo\ B}{Spacing\ in\ Photo\ A} = \frac{87.99}{83.5} = 1.05$$

3.3.2.4 Partial Light Distortion

The two previous steps were used to determine which elements of distortion had to be taken into account when processing the PIV data. It was decided that while corrections could have improved the accuracy of measurements, corrections were not necessary and a LSF could be measured from any test photo.

In reality, some corrections need to be applied to the data, since the most likely source of distortion from one frame to the next is because of the glass tube. While all other sources of distortion affect each patch of soil similarly during the test, the progress of the tube will subject the soil within it to an additional distortion. Using the calibration plate technique would have been difficult inside the tube so it was decided to investigate whether the effect of the tube could be added mathematically. To quantify this, a Matlab script was written which could calculate the magnification caused by the refraction of the light through the materials in the test set-up. Since the effects of the tube on its own cannot be calculated, it was decided to create a first model without the tube and a second one with the tube (which could be adapted to include different tube thicknesses), and subtract the effects of both models to determine the tube's contribution to distortion. This was done using known dimensions of material layers, and Refractive Indices (RI) for each material: Air (1.00028),

Perspex (1.495) and Transparent Soil (1.448 – Mannheimer and Oswald, 1993), yielding a correction equation applicable to any soil element of known (magnified / apparent) distance to the centre of the image. This relationship is linear (Figure 3.23), and this agrees with the study of Photograph B, although its effects are small, with elements at the edge of the soil (centre + 100mm) distorted by an additional 0.015mm for a thick tube and 0.008mm for a thin tube. The magnification factor is calculated from the gradient (a) of the line plotted in Figure 3.23, using Equation 23.

$$Magnification\ factor = \frac{1}{(1-a)} \qquad \text{Equation 23}$$

The gradients are included in Table 3.3. The limitation of relying on a theoretical model was that even small (1%) variations in RI can cause significant variation to the studied relationship (Figure 3.23), so data from the real set-up had to be obtained. Using Equation 23, the magnification factor was found to be 1.05, which agrees with that found by comparing photos A and B. This validates the theoretical model and allows the refraction caused by the tube to be corrected mathematically.

Table 3.3 - Gradients of Magnification Lines

	Model	Gradient
(a_1)	No tube	0.047743
(a_2)	Tube – 3.6mm thick	0.047895
(a_3)	Tube – 2mm thick	0.047827
(a_4)	Effect of Thick Tube: (a_2)-(a_1)	0.000152
(a_5)	Effect of Thin Tube: (a_3)-(a_1)	0.000084

The distortions caused to the object being photograph are summarised in Table 3.4. An additional optical distortion is caused by the geometry of the cutting edge since this is uneven in thickness and curvature, and this may have additional effects of the measured patch positions.

a

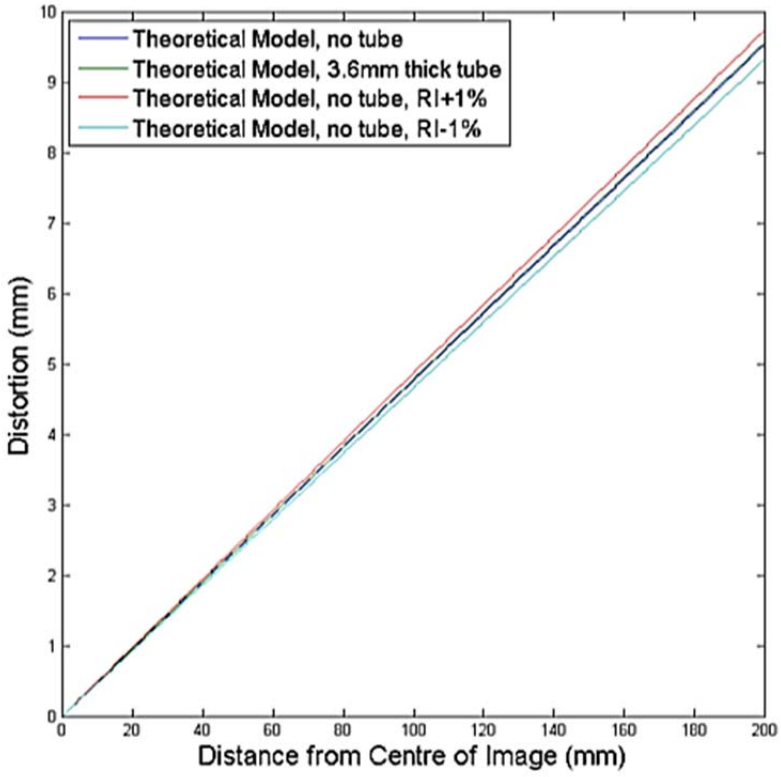

b

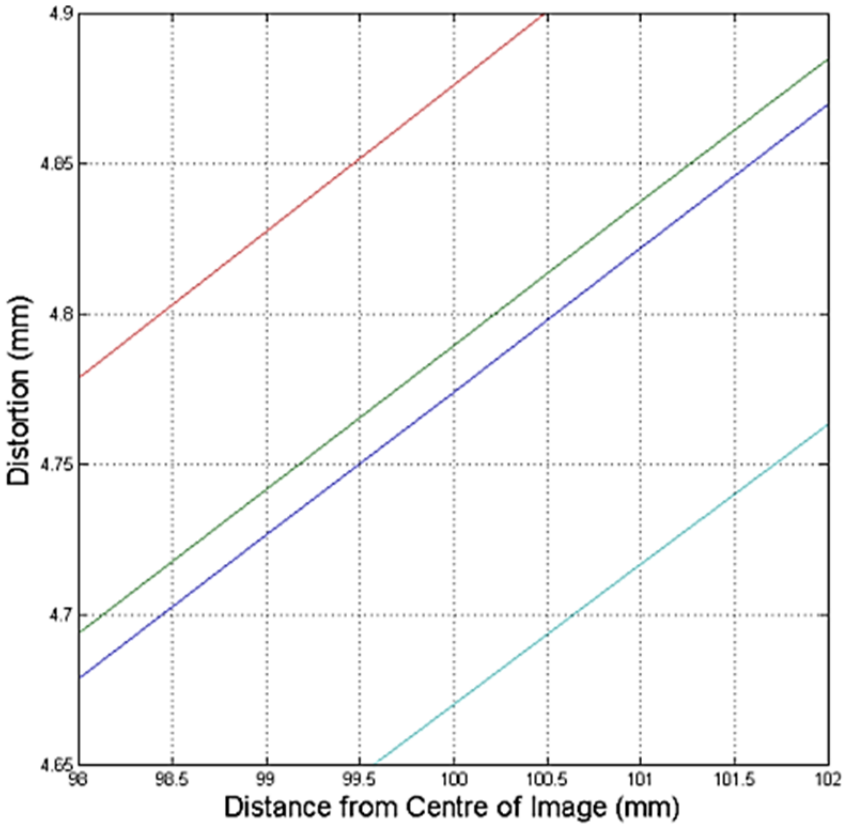

Figure 3.23 - Refraction Model Comparisons: a) Full Model and b) Zoom at Model Edge

Table 3.4 - Summary of Optical Distortions

1	2	3
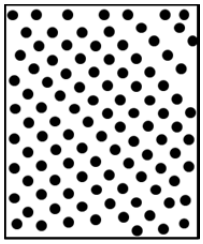	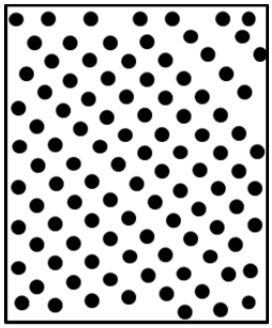	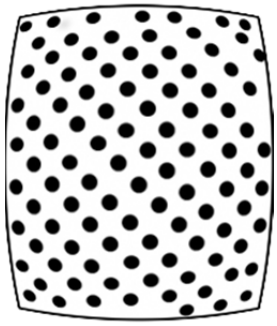
The plane of particles	The plane seen through the soil and Perspex	The photograph of the plane seen through the soil and Perspex
Marker points at constant spacing x1	Marker points at constant spacings, x1+δx	Marker points at varying spacings, x1+δx-[M], with [M] a matrix of nonlinear distortions found from Figure 3.25 below
NO CHANGE	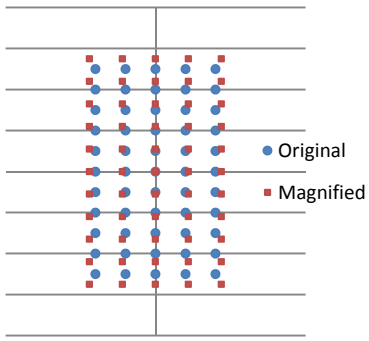	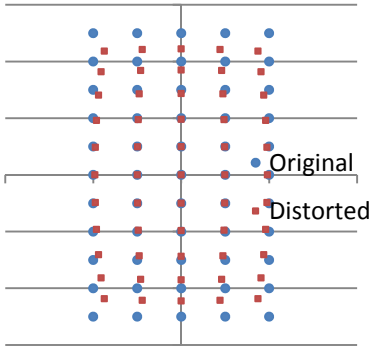
	Figure 3.24 - Change in Coordinates due to Magnification Only	Figure 3.25 - Change in Coordinates due to Radial Distortion Only
No Magnification, No Distortion	Linear Magnification caused by (2)	Linear Magnification caused by (2) + Nonlinear distortion caused by (3)

The process was repeated for the Canon EOS 6D fitted with its 50mm lens, since during extrusion, soil elements were displaced by hundreds of pixels and were therefore prone to different degrees of lens distortion throughout the series of photographs. Barrel distortion for this camera is quantified in Figure 3.26, and was found to be similar to that of the K20D in terms of real space displacement (in mm rather than in pixels). All displacements measured in the extrusion tests were corrected for this. Figure 3.27a plots a strain path uncorrected for lens distortion and Figure 3.27b plots the same strain path corrected using the data in Figure 3.26. In Figure 3.27a, the soil which was originally furthest from the top of the tube appeared to extend before being compressed. In reality this is due to the soil element passing close to

the centre of the photograph and experiencing higher magnification at the centre of the lens. After removal, the true strain becomes visible, although small errors still remain due to the scatter of data in Figure 3.26.

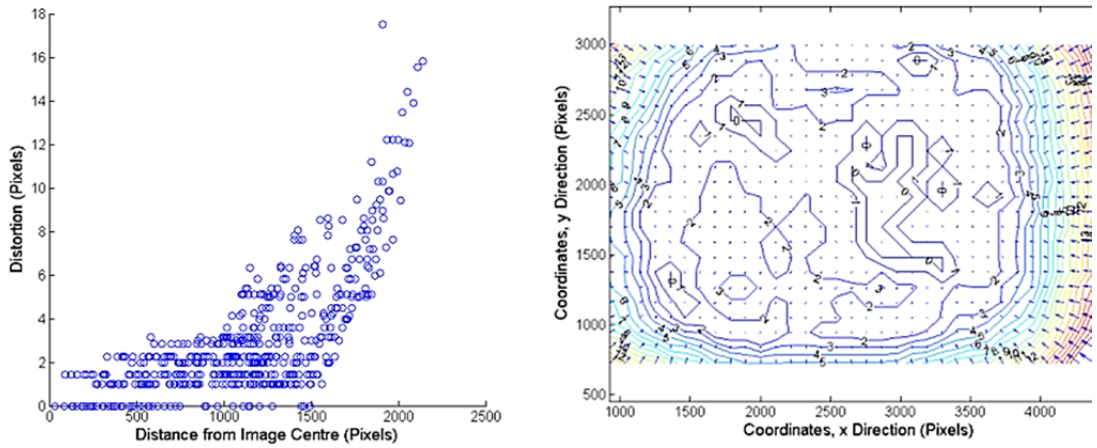

Figure 3.26 - Evidence of Barrel Distortion in Canon EOS 6D

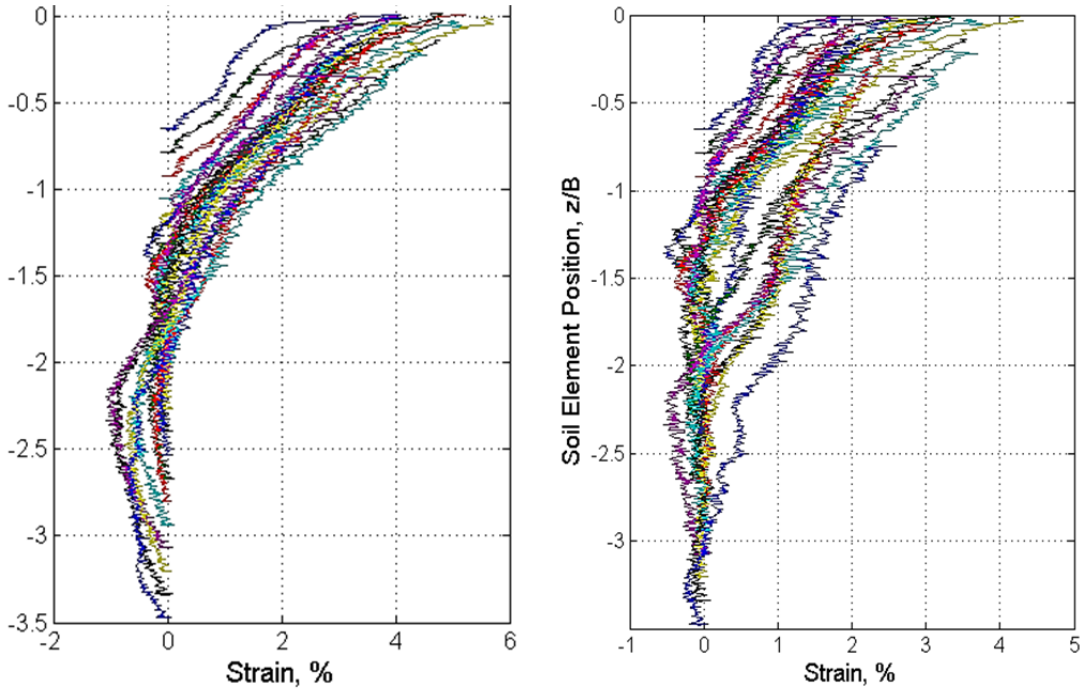

a b

Figure 3.27 - Centreline Strain Paths for Extrusion: a) uncorrected and b) corrected for lens distortion

3.3.3 Choice of PIV Analysis Parameters

A successful PIV analysis depends on the user's skill and experience with the software. Analysis parameters must be chosen such that they will not influence the displacement vectors which are to be determined. Different PIV runs on the same series of photographs

may yield different displacement vectors, and a thorough analysis programme is required to obtain reliable data. A review of these parameters and their effect on the data follows.

3.3.3.1 Effect of Leapfrog Value

The PIV software relies on the user to choose the analysis parameters. The first of these is the Leapfrog value (White and Take, 2002) which represents the photo interval at which each Interrogation Area's texture contents and position are updated. A Leapfrog value of one means that the contents of the patch are updated before each photograph with those found for the previous photograph and the software compares Image 1 to 2, Image 2 to 3, Image 3 to 4, ... , Image (n-1) to n, while a Leapfrog value of 3 compares Image 1 to 2, Image 1 to 3, Image 1 to 4, 4 to 5, Image 4 to 6, Image 4 to 7,... , Image (n-3) to n. In either case, the data can be collated to obtain all image data in the form Image 1 to Current Image, by calculating total displacement over time. The advantage of using low leapfrog values is that because the IA is updated regularly, it reflects the changes which happen within the IA itself, so IA recognition is easier for the software and is therefore more accurate. It does however have two main disadvantages:

- Any analysis error or inaccuracy which affects the displacement data at the time of the IA update becomes part of the cumulative displacement data. Increasing the number of updates increases the inaccuracies added onto the data.
- A pixel can only contain one colour (since it is converted from RGB to greyscale during processing), so if a displacement of the IA of coordinates (100, 200) in Image 1 is calculated as being say 12.3 pixels downward in Image 2, its new coordinates are (100, 212.3). When the software considers this new updated IA, it cannot consider the correct patch, so some rounding must occur. This will happen each time the patch is updated.

Leapfrog can also be set to a number higher than the total number of images in the series, in which case all images are compared to the first (“Full Leapfrog”). This is the ideal setting since this reduces random error and IA location rounding. Setting the leapfrog too high can cause the software to cease recognising the IA after it undergoes excessive deformation. In the Tube Driving tests, the soil deforms rapidly as it enters the tube (and undergoes optical

distortion due to the tube's cutting edge geometry) - recognition being paramount to accurate measurements, choosing the right Leapfrog was essential. In the early stages of the tube driving tests, fifteen different Leapfrog values were used and the measured displacements were compared. An example of the final IA positions (Test1 ANC) is given in Figure 3.28 for soil elements at different initial depths between 0.5 and 3B under the base of the borehole. The high number of wild vectors seen in the two IAs closest to the surface is due to the soil moving up into the tube and therefore not being visible in the photograph. Those IAs are replaced with the closest match and thereafter provide erroneous vectors.

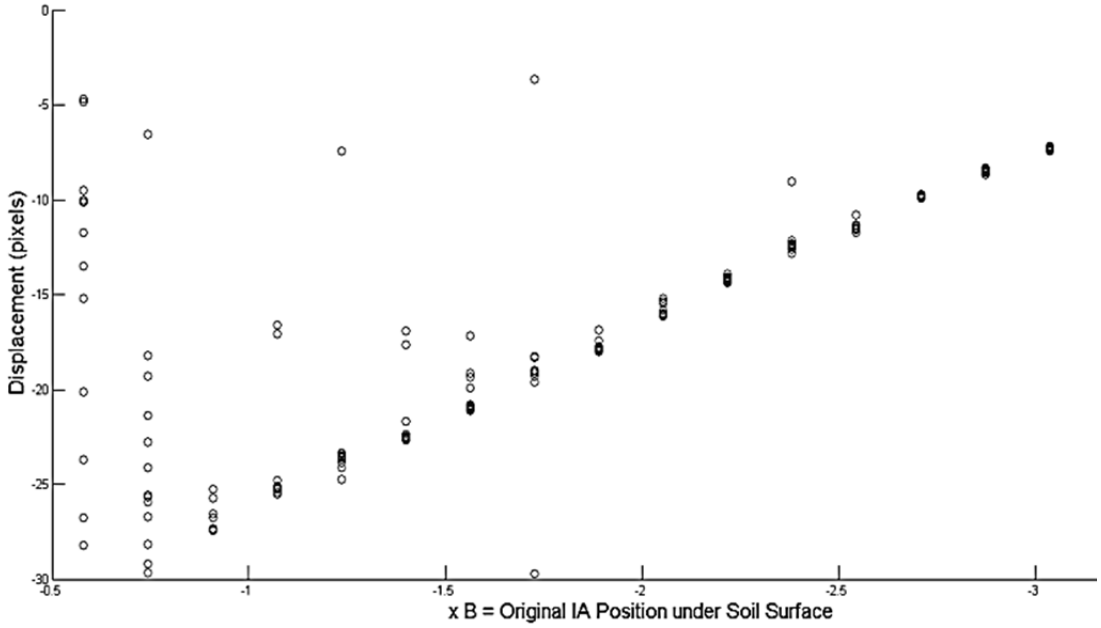

Figure 3.28 - Example of final IA Positions - with Wild Vectors

This method, although lengthy due to the need to run the analysis fifteen times, had the advantage of providing sufficient data points to be able to prove a wild vector was indeed a wild vector rather than the soil behaviour. It also provided sufficient data to produce a trendline for the final patch positions, and to quantify random errors. It also identified the leapfrog values which were not appropriate for the test (because this varied between tests, it was impossible to choose a constant Leapfrog value to run all tests with). Wild vectors were defined mathematically as lying outside two standard deviations away from the median of the fifteen results. The median rather than mean was chosen because wild vectors can be one or two orders of magnitude out of the typical measurement, and this would affect the

mean significantly. It is, however, not assumed that the measurements necessarily follow a Gaussian distribution.

3.3.3.2 Effect of Interrogation Area Size

The size of the IA controls the software's ability to recognise it. A larger patch will contain more pixels and therefore more texture than a smaller one, which lowers the chances of two patches being very similar and being mistaken for each other. The PIV software's ability to recognise patches from a particular series of photos can be studied as follows (after White *et al*, 2003):

- A photo from each test is taken and its left side is cropped 36 pixels
- A PIV analysis is run between the original and the cropped photos using an mesh with at least 1000 IAs
- The PIV run is repeated for various patch sizes: 48, 72, 96, 120, 144
- The apparent movement of patches is compared to the 36 pixels they have actually moved, and the number of displacement vectors within each error bracket is counted to determine the error bracket within which 99% and 100% of vectors fall

The accuracy and precision for PIV runs on a typical transparent soil model in tube driving lighting conditions is presented in Table 3.5. All tests yielded different results, but the trend was identical: larger IA sizes yield smaller errors. However, the gain in accuracy came at a high cost in measurement density: the number of vectors reduces ninefold between IA size 144 and 48 pixels, and yields a fourfold gain in accuracy, meaning that at high IA sizes, the vector field will be heavily space-averaged. The results for all tests are included in Table 3.6. These PIV runs were performed after the Tube Driving analysis was complete, meaning that these photos had been used in similar ways, except for tests 1 and 4, on which many preliminary tests had been run (high photo usage), and tests 8, 10 and 12, for which the current analysis was carried out on photos which had not been part of the original PIV runs (low photo usage). From these results and trial runs using the PIV software, an IA size of 72 was deemed acceptable for yielding displacement fields and an increased size of 96 was chosen for measurements used to calculate strains.

Table 3.5 - Errors in PIV analysis of Displacement Vectors

Error bracket : 36 pixels ± (pixels)	0.01	0.02	0.03	0.04	0.05	0.06	0.07	0.08	0.09	0.1	0.11	0.12	0.13
IA size (pixels)	48	48	48	48	48	48	48	48	48	48	48	48	48
% of vectors in error bracket	44.5	62.0	78.4	89.1	93.5	95.2	97.2	98.2	98.4	98.7	99.0	99.3	99.4
IA size (pixels)	72	72	72	72	72	72	72	72	72	72	72	72	72
% of vectors	59.7	77.3	90.9	96.4	98.1	98.9	99.4	99.8	99.9	99.9	99.9	99.9	100.0
IA size (pixels)	96	96	96	96	96	96	96	96	96	96	96	96	96
% of vectors	70.4	87.1	96.1	98.3	99.3	99.6	99.9	100.0	100.0	100.0	100.0	100.0	100.0
IA size (pixels)	120	120	120	120	120	120	120	120	120	120	120	120	120
% of vectors	78.6	91.8	97.8	99.2	99.8	99.9	100.0	100.0	100.0	100.0	100.0	100.0	100.0
IA size (pixels)	144	144	144	144	144	144	144	144	144	144	144	144	144
% of vectors	85.6	95.3	99.4	100.0	100.0	100.0	100.0	100.0	100.0	100.0	100.0	100.0	100.0

Table 3.6 - PIV accuracy in all Tube-Driving Tests

				IA size				
Test	**Photo Usage**	**Transparency**	**NC/OC Soil**	**48**	**72**	**96**	**120**	**144**
				Error encompassing 99% of vectors (pixels)				
Test 1	high	low	NC	>0.18	0.16	0.13	0.11	0.11
Test 2	medium	low	NC	>0.18	0.17	0.13	0.11	0.1
Test 3	medium	medium	NC	0.17	0.11	0.08	0.08	0.07
Test 4	high	low	NC	>0.18	>0.18	>0.18	0.16	0.15
Test 5	medium	high	NC	0.15	0.11	0.08	0.07	0.05
Test 6	medium	high	NC	0.09	0.05	0.04	0.04	0.03
Test 7	medium	high	NC	0.11	0.07	0.05	0.04	0.03
Test 8	low	low	OC	0.04	0.03	0.02	0.02	0.01
Test 9	medium	low	OC	>0.18	0.18	0.14	0.11	0.11
Test 10	low	high	OC	0.07	0.05	0.04	0.04	0.03
Test 11	medium	low	OC	>0.18	0.13	0.1	0.09	0.08
Test 12	low	high	OC	0.13	0.08	0.07	0.05	0.04

The above study revealed that:

- Accuracy depends on the texture and lighting in each photo, not just on the software
- Increased transparency (later tests using the second type of mineral oil) yields smaller errors
- Photos which have been used in a larger number of analyses have higher errors. This suggests that jpegs lose information when handled.
- IA size 72 yields acceptable results but wild vectors decrease for size 96 without losing too much detail

This agrees with the conclusions of a study by White *et al* (2003) that found that PIV performed better for larger photo resolution, and larger IA size (Figure 3.29).

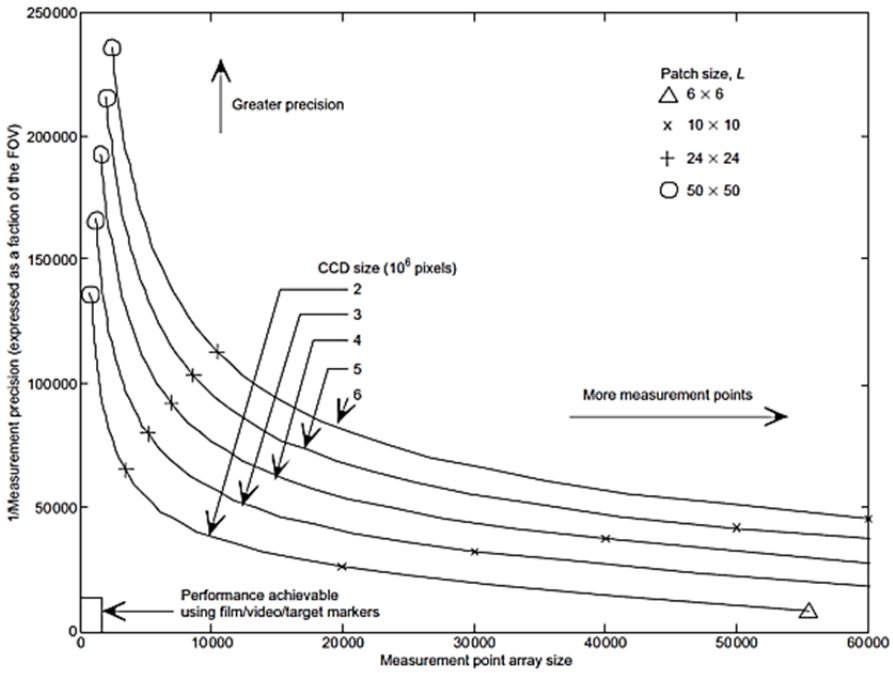

Figure 3.29 - Performance of PIV for different Camera Resolutions and IA Sizes (from White *et al*, 2003)

Since strains are to be calculated from displacements, and will therefore be space-averaged, it was decided to study the effect of using different IA sizes to calculate the strain. The strains used to calculate the CSP using the SPM (Baligh *et al*, 1987) were used to find their corresponding displacements, using soil elements of size 0.58 pixels (or 0.05mm). There is no unique solution: although the difference between the displacement at the two depths of z/B=2 and z/B=0 remains constant in all cases, their values are determined by the starting

displacement (double-headed arrow in Figure 3.30). The strain curve was then recreated using elements spaced at 24, 48, 72, 96, and 144 pixels. Peak strains could be underestimated by up to 15% using a spacing as small as 24 pixels, while non-peak strains were usually well represented by all spacings, with strain values in larger spacings 99-101% those predicted by Baligh using minute (0.58 pixel) spacings. Spacings 24-96 predicted similar peak strains, although the peak was missed by the larger spacing, 144 pixels. This concluded that using an IA size of 96 pixels would not significantly affect the strain data.

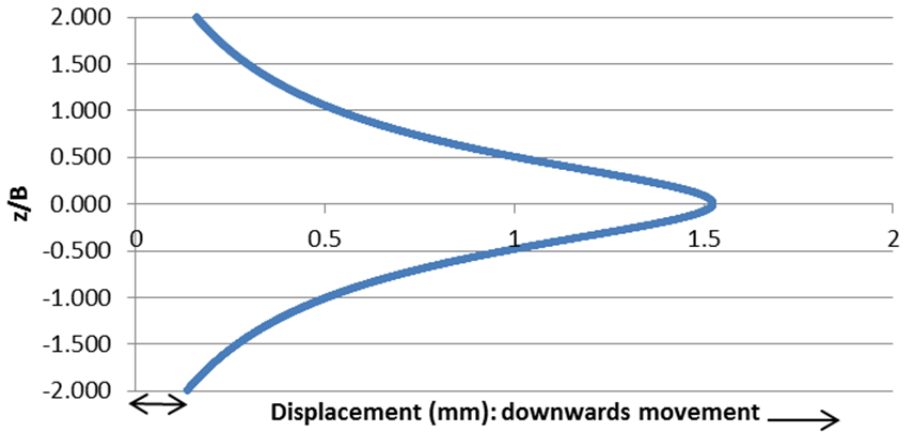

Figure 3.30 – Predicted Displacements from the SPM (Baligh et al, 1987)

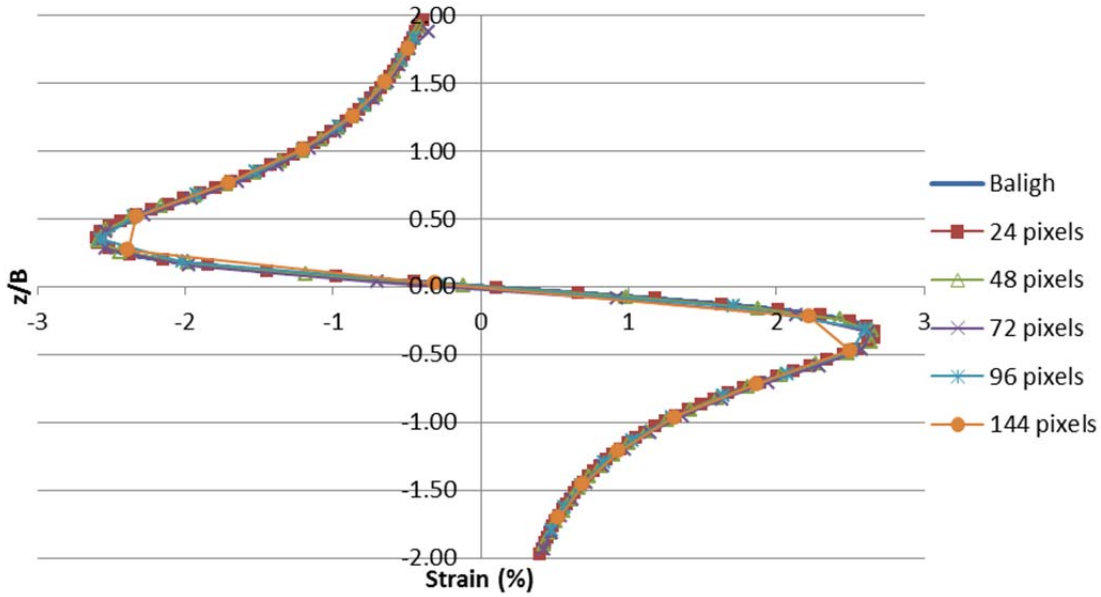

Figure 3.31 - Centreline Strain path recreated from Displacement Data using different Spacings

3.3.3.3 Effect of other Parameters

Two additional parameters need to be taken into consideration: the search zone and the frame rate. The former describes a value set by the user to choose a search zone around the IA's initial position. One too large will considerably slow the analysis down, while one smaller than the real movement being measured will produce a wild vector since the IA's new location will not be found within the search zone. The latter is the number of photos the camera takes per second, and is dependent on the camera's inbuilt ability, the type of SD card used (high speed is required, 95Mbps or above), the lighting conditions, the corrections being applied to the photo (such as lens distortion correction and many other options which the user can choose to enable or disable) and the battery charge. The frame rate is also connected to the image resolution, since this determines the size of the image file and hence the speed at which it is stored on the card. There is therefore a balance to be struck between frame rate (as high as possible), image resolution (as high as possible) and the speed at which movements occur within the physical model (must be set to replicate field conditions as faithfully as possible). Limitations in the frame rate of the available cameras, and the need to maximise data resolution, since small movements are to be accurately measured, the compromise was to set the tube's driving speed at 2.3mm/s.

3.3.4 Centreline Strain Path

Strain can be calculated from displacement vectors by considering the elongation between two points due to their displacements. Strain is defined by Equation 24, itself equal to Equation 25 in a coordinate system. This, calculated for any two IAs over time, gives its Centreline Strain Path (CSP). The CSP requires two sets of data: displacement vectors for a given soil depth over time and the position of the cutting edge in each photo. The latter was determined by drawing two 5mm dots on the tube's cutting edge before the test and tracking their position over the series of photographs using geoPIV. Since strain depends on two displacement vectors, the error in both of these must be small if the correct strain is to be measured. Initial attempts to recreate the CSP was unsuccessful, with strain values for a given soil element varying significantly with each different Leapfrog value.

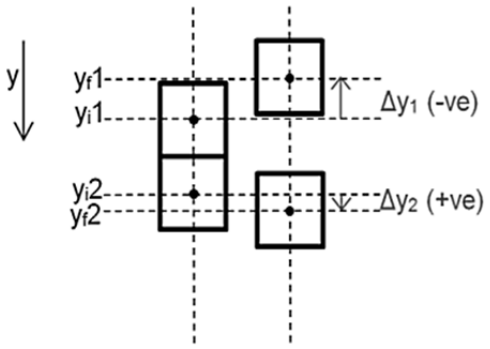

$$\varepsilon = \frac{l_o - l_f}{l_o}$$

l_o=original length
l_f=final length

Equation 24

$$\varepsilon(\%) = 100 \times \frac{(y_f 2 - y_i 2) - (y_f 1 - y_i 1)}{(y_i 2 - y_i 1)} = 100 \times \frac{\Delta y_2 - \Delta y_1}{original\ spacing}$$

Equation 25

Figure 3.32 shows a plot of the strain history (or CSP) of a single soil element during the tube driving test, calculated from 15 PIV analyses using Leapfrog value between 4 (IA updated often) and 72 (IA updated rarely): strains for the same soil element at the same point in time varied by 36% between calculations, meaning that data from one single analysis could not be used with confidence. Furthermore, soil elements at different depths showed significant variations with no correlation between strain and depth once the soil had entered the tube. However, strains before entering the tube appeared to show a behaviour that changed in line with the soil element's depth (Figure 3.34) and all data runs at different Leapfrogs yielded very similar results before entering the tube at z/B=0. Figure 3.34 plots the CSP of soil elements at different initial depths (before tube driving) – while it is clear that overall, deeper elements experience lower residual extensive stress, the CSPs are not "in order".

It was obvious that poor patch recognition due to the soil entering the sampling tube and the errors due to leapfrog values were to blame:

- Using a full leapfrog (each image compared to first in series) yielded good results for displacements and strains before the soil entered the tube. Recognition thereafter was poor, with most IAs showing wild vectors.
- Other leapfrog values showed measured values for displacement for any given point within ± 5 pixels (0.5mm) – this small error was significant enough to miscalculate strains.

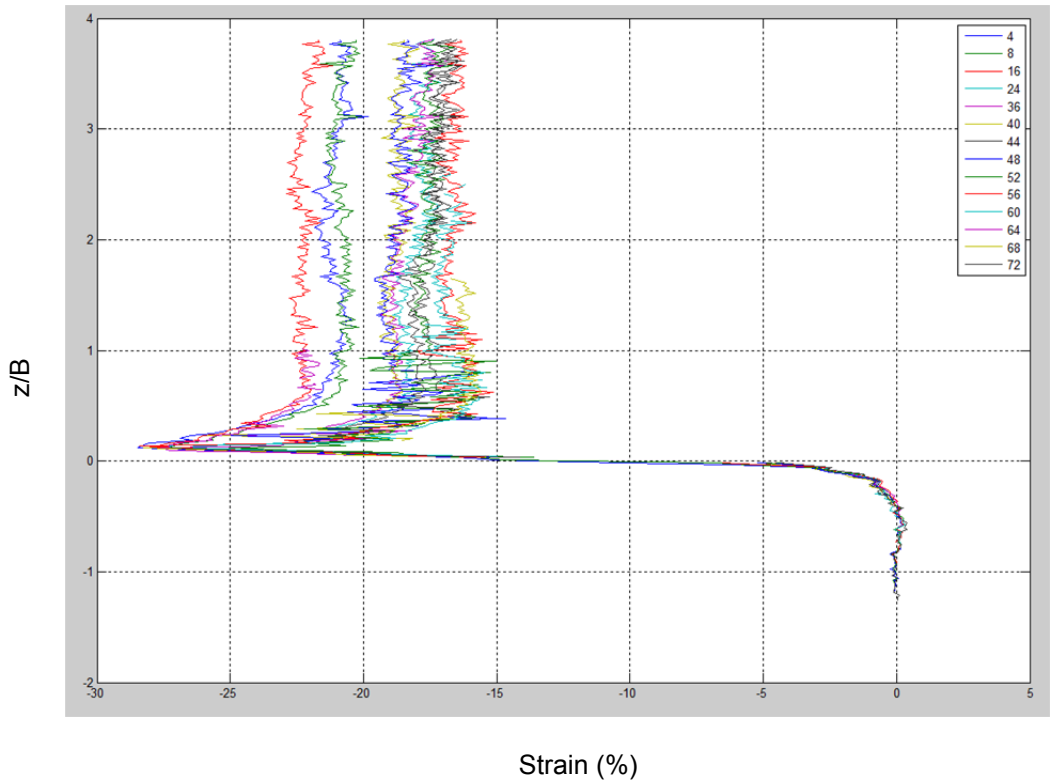

Figure 3.32 - Variation of Strain Calculation for a Single Soil Element using Different Leapfrog Values Between 4 and 72

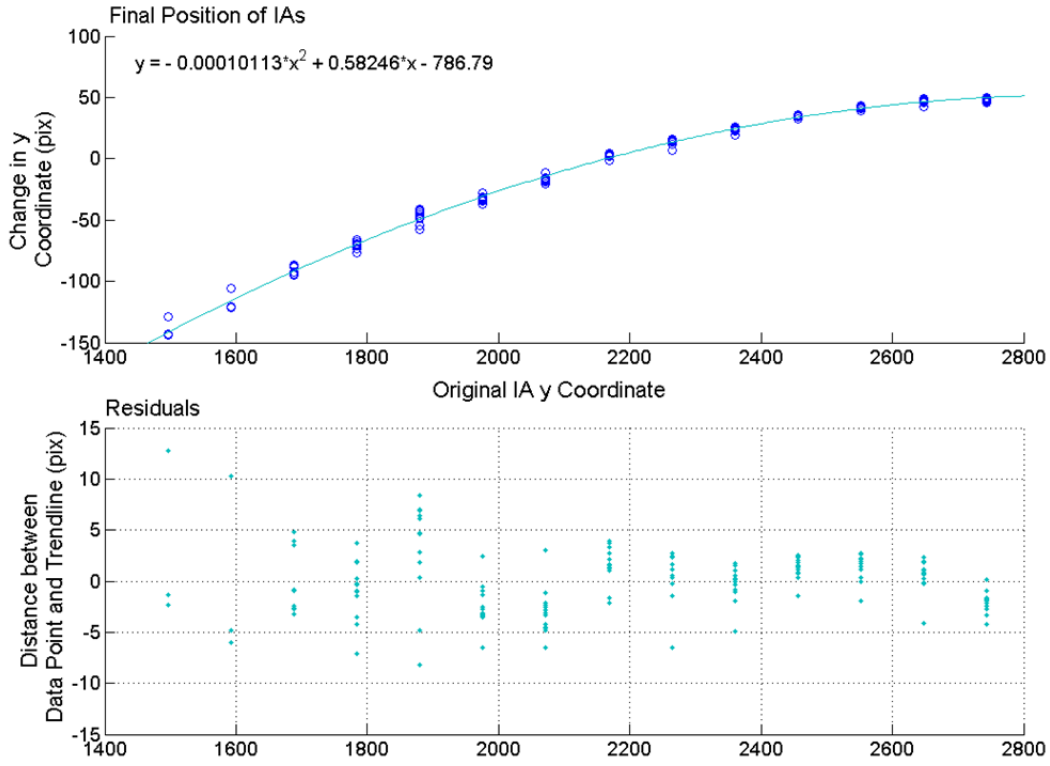

Figure 3.33 - Use of a Quadratic Trendline to Correct IA Final Locations

Ideally, a Leapfrog value should be set to its maximum, so the results of the full leapfrog before the soil enters the tube can be taken as accurate. Figure 3.28 shows the IA positions when the tube is fully driven to a depth of 4B under the soil surface. After removing wild vectors in the manner outlined previously, the data can be fitted to a quadratic curve which will give a reasonable estimate of each IA's final position on the y axis after tube driving (Figure 3.33). These y coordinates can be used to recreate a mesh of IAs, which can be used to run the PIV analysis backwards (from the final photo to the initial photo) with a full Leapfrog value, thus creating the top half of the CSP with minimal distortion from either the tube's distorting effects or from the errors associated with using a lower leapfrog value. To verify this method, fifteen different leapfrog values were used on the backwards analysis to determine via a quadratic fit curve the position of the original IAs. The difference between the original, user-specified y coordinates and those determined using this technique never exceeded 0.4 pixels (0.04mm), which was considered adequate. Following this, the two halves of the CSP were spliced together, with the optically distorted portion in the middle missing where excessive distortion had taken place (Figure 3.35). When corrected, the data clear behaviour trends, which could easily be compared with those in other tests.

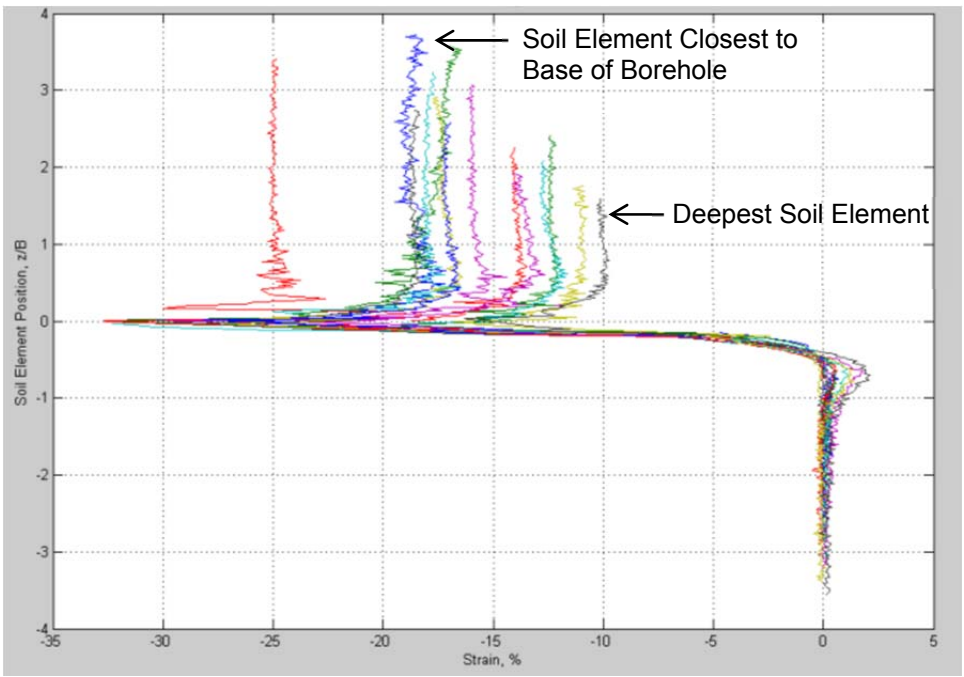

z/B

Strain (%)

Figure 3.34 - CSP with no Correction

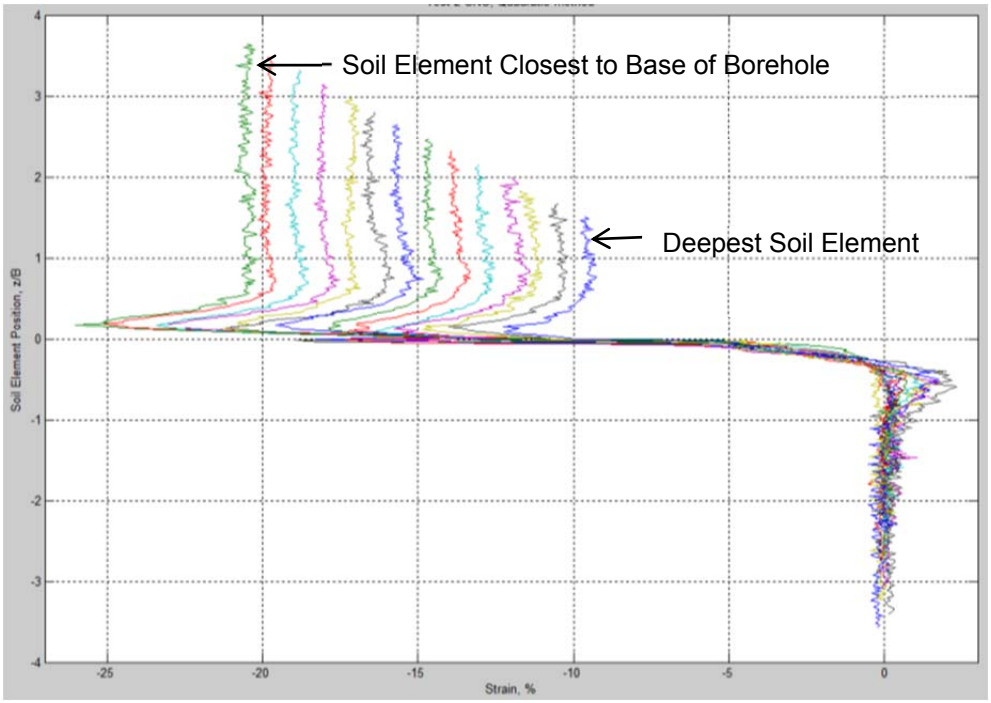

Figure 3.35 - CSP corrected with Quadratic Method and Splicing

3.3.5 Summary – Analysis Methodology

This chapter presented the methodology which was developed to study tube sampling disturbance. Adapting a novel approach resulted in a lengthy process and required many checks to be carried out to ensure the system's accuracy and viability.

Three types of tests were described, one to model each part of the sampling process:

- Tube driving (main focus of the research)
- Tube storage
- Sample extrusion

A reminder of the preparation and testing procedure is included in Figure 3.1. The equipment was chosen so that a PIV and white light set-up could be used. This is an adaptation of a typical PIV and laser light set-up, which is commonly used to study displacements in transparent media. For this to be usable, a plane of particles needed to be seeded into a transparent soil model, which was a difficult and painstaking process, but when achieved yielded many benefits. The tube-driving model size was twice that previously achieved with a transparent soil and laser set-up.

Developing this testing procedure included:

- the design and manufacture of a number of unique parts (Appendix A)
- trial tests on scaled-down models for the tube driving tests
- adapting the equipment for a larger model than previously used in similar tests
- the testing of options for which materials and seeding particles were to be used

The viability of these testing procedures was assessed using photos taken of the set-up. Steps were taken to ensure that data gathered from the tests was representative of the real soil movements, and not affected by the software's ability to process the images using PIV.

Steps were taken to ensure that the displacements and strains calculated by the PIV software truly reflected the movement of soil during testing. It was found that the tube-driving set-up could be used to measure displacements on the tube's centreline to a good degree of accuracy. A rigorous analysis methodology – which involved running the analysis multiple times at different settings – was followed to remove the effects of small errors in the software's ability to recognise patches of texture. Failure to remove these would have resulted in erroneous strain calculations which make the data impossible to interpret.

- The effect of lens distortion was measured and found to be small – with distortions having only affected areas far from the main field of interest – it was therefore decided not to correct for these.
- The refraction of light through the tube was another small source of errors in the software's estimation of IA location. This was quantified and corrected for using a theoretical model for light refraction through each of the materials.
- The use of a more transparent medium to model soil in later tests removed most of the small errors in patch recognition and hence the need to manipulate the data prior to strain calculations.

The Centreline Strain Path was sensitive to these errors, and a method was devised to remove these to obtain an accurate representation of the strain history on the sampler's centreline. This involved:

- Running 15 PIV analyses at different Leapfrog values (including Full leapfrog) to determine an average measurement of final IA locations at the end of the test
- Fitting a quadratic trendline to the data of these 15 runs and calculating from the equation of the trendline the final position of the IAs (Appendix F)
- Creating a mesh with these coordinates and running the analysis from the final photo to the first photo at full Leapfrog
- Creating the CSP for the backward and forward analyses at full Leapfrog, with data corrected for optical distortions due to tube
- Splicing these together to obtain the full strain path

Analysis for the monitoring and extrusion tests was more straightforward due to a good visibility though the soil and to the lack of optical distortions to be taken into account.

Chapter 4: Physical Modelling of Sampling Disturbance during Tube Driving

4.1 Introduction

Sampling disturbance occurs primarily as the tube is driven into the ground and the soil experiences changes in stress conditions as well as mechanical deformation caused by contact with the tube itself. The deformation is known to depend on the type of sampling method used, and the tube's cutting edge geometry and Area Ratio are closely linked to the disturbance caused to the sample. A physical model was developed to combine white-light Particle Image Velocimetry (PIV) and transparent soil to allow a clear view into the depth of the soil body, on the plane through which the sampler is driven. The process of tube driving was modelled using a glass tube which was pushed into the artificial soil model at a constant rate of 2.3 mm/s, while photographs were taken at a rate of approximately 2 frames per second so that movements within the soil body due to tube penetration could be recorded and tracked over time. This chapter presents the main body of the experimental work carried out during this research, and includes:

- Frictional properties of the materials used
- Physical Modelling of the Centreline Strain Path set-up from Baligh *et al*. (1987)
- Displacements in and around the tube sampler during tube driving
- Strains on the centreline of the sampler during tube driving
- Soil layer profiles during tube driving

A discussion is also included on:

- The effect of Overconsolidation Ratio (OCR) on tube sampling disturbance
- The effect of tube cutting edge geometry on extent of disturbance
- The effect of Area Ratio on extent of disturbance
- The effect of drive angle on the soil displacement inside and out of the tube

4.2 Friction between Tube and Soil

One concern during testing was that the friction between a natural soil and a steel sampling tube might not be modelled adequately in a set-up using transparent soil and a glass modelling tube. Since the issue of sampling disturbance is known to be related to the friction generated in the proximity of the tube wall as it is pushed into the soil, it was decided to investigate the frictional properties of both combinations of materials through shear box testing. Most commonly, shear box tests are used to determine the angle of friction of a material, by shearing a 60x60x50mm (L:W:H) sample of said material at a slow and constant rate (Figure 4.1). The shear box apparatus can also be used to shear two different materials along a predefined plane. For this study, blocks of glass and steel of dimensions 60x60x25mm (L:W:H) were manufactured to exactly fit the bottom half of the shear box mould, with their surface exactly at the predefined shear plane. The top half of the mould was filled with either undisturbed transparent soil taken from the sides of the Perspex box after a tube driving test (previously consolidated to 50 kPa –Figure 4.1), or with Kaolin clay.

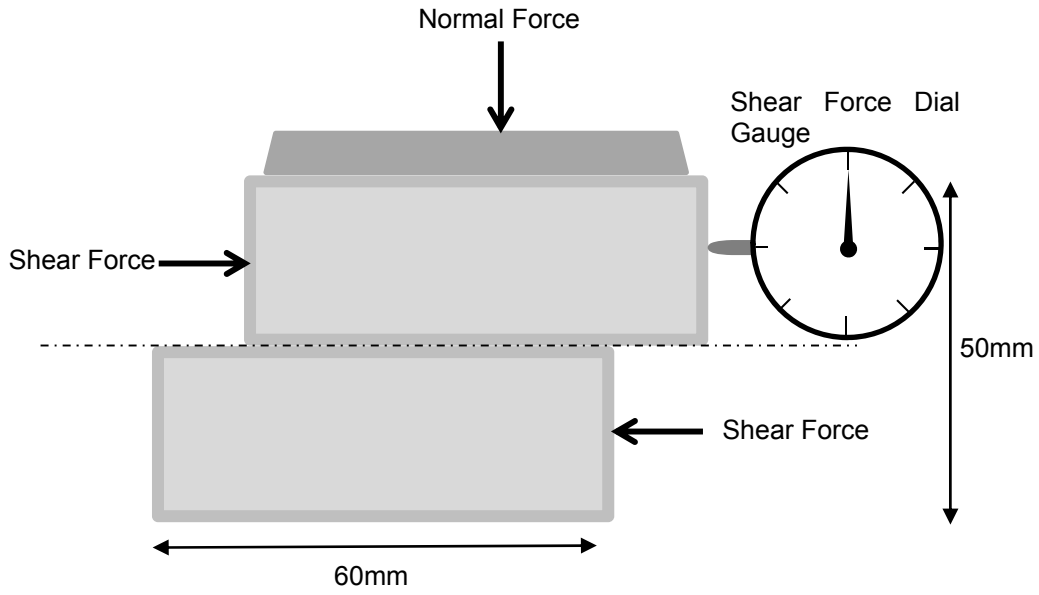

Figure 4.1 - Shear Box Apparatus

The clay samples were made by mixing the dry clay with water and compacting it with a Proctor hammer in a larger mould, then taking square samples with the mould cutter itself. The half-samples were then placed on top of the block of corresponding material within the

shear box apparatus, covered with their corresponding pore fluid (water for Kaolin and a blend of Technical White Oil and Normal-Paraffin for the Transparent Soil) and loaded with weights. Samples of Transparent Soil and Kaolin are illustrated in Figure 4.2.

Figure 4.2 - Preparation of Shear Box Half-Samples: Transparent Soil and Kaolin

Six three-minute tests were carried out on kaolin + steel samples, at three normal stresses: 37, 62 and 111kN/m^2. The samples were allowed to consolidate under the normal load before shearing, until no settlement was recorded over 30 minutes. The rate of shear was set to the maximum achievable on the shear box apparatus, 2 mm/minute, to reflect as close as possible the tube driving speed during testing. Measurements were taken every 5 seconds over the first 30 seconds, then every 10 seconds for an additional two and a half minutes. The shear stresses are plotted over time in Figure 4.3. It is of note that this rate is unusually high for a shear box test, so the area being sheared reduced rapidly.

Six shear box tests were carried out on Transparent Soil / Glass samples as previously. The shear stresses are plotted over time in Figure 4.4. The data in Figure 4.3 and Figure 4.4 can be used to determine two friction attributes for the pair of materials:

- The peak friction angle, by plotting the line between three peak shear stress points at different normal stresses
- The constant volume friction angle, by plotting the final steady state values of shear stress for three different normal stresses

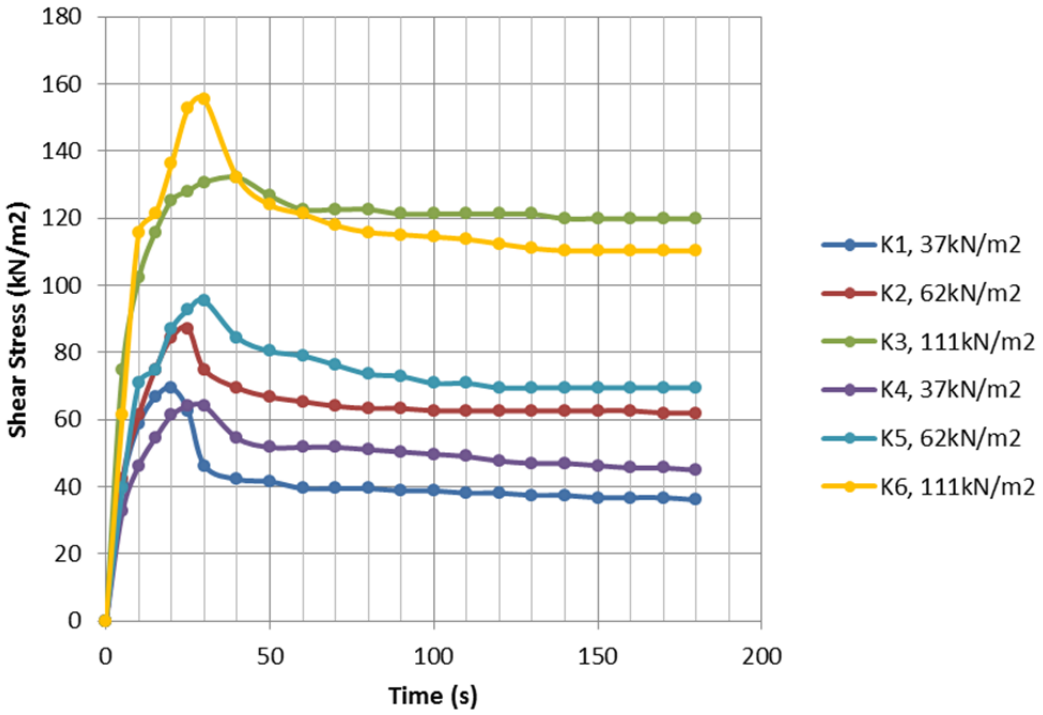

Figure 4.3 - Shear Box Data for Kaolin Samples K1-6

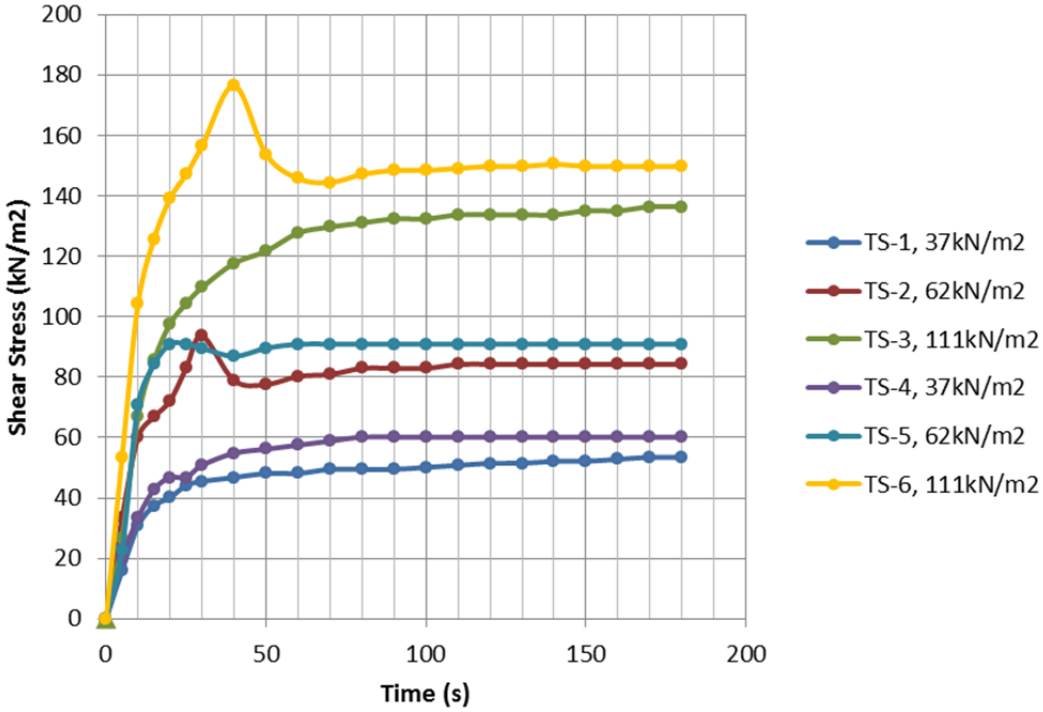

Figure 4.4 - Shear Box Data for Transparent Soil Samples TS1-6

The angle between the plotted line (Figure 4.5) and the horizontal gives the above angles. The Kaolin / Steel tests yielded both a peak and constant volume stress value but only two

out of the six Transparent Soil / Glass tests showed a peak stress distinct from the final (constant volume) value, making it difficult to obtain a peak friction angle since each line requires at least three points to negate the effects of any variations in data. As is apparent from the equation of the line through the peak values for Transparent Soil / Glass (Figure 4.5, y=0.4658x -2.8806), the behaviour seems to indicate negative cohesion between the materials, which is unlikely, if not impossible. This indicates that the data points are not sufficient to determine a peak angle of friction, since one or both of the points is non-representative of the typical behaviour. This is most probably due to differences in the set-up between tests, or because of the rapidly changing shear force measured from the dial on the apparatus making it likely that a peak value may have been missed while a previous value was recorded. The focus therefore remains on a comparison between constant volume angles of friction.

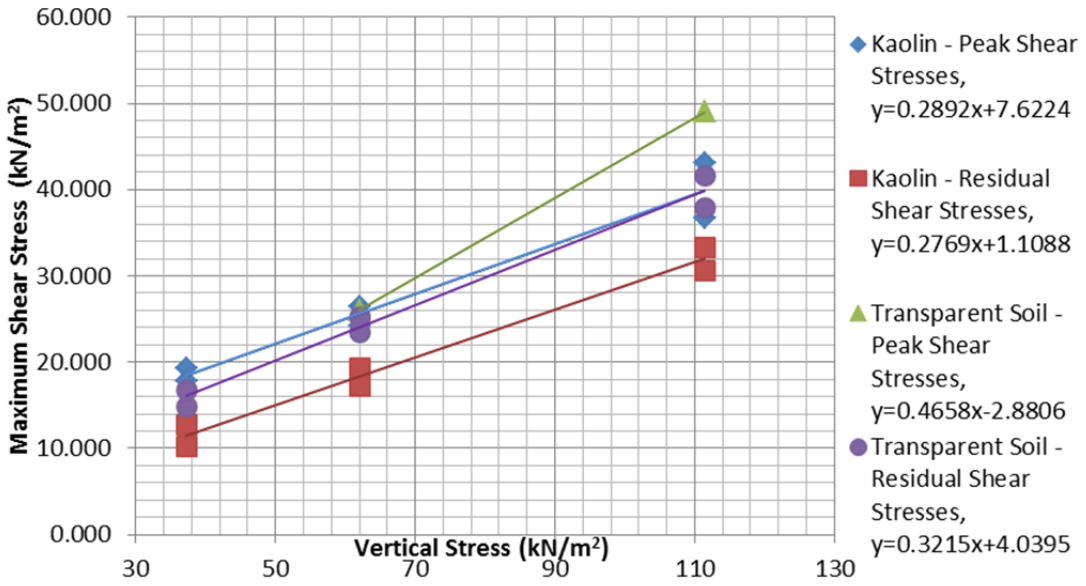

Figure 4.5 – Peak and Constant volume Strength Results

The angle of each line was calculated from its gradient. These are included in Table 4.1.

Table 4.1 - Angles of Friction

Material	Kaolin / Steel		Transparent Soil / Glass	
Strength	Peak	Constant volume	Peak	Constant volume
Angle of Friction	16.1°	15.5°	25.0°	17.8°
Note	Valid	Valid	Not Valid	Valid

The results suggest that the constant volume friction between Kaolin and Steel (15.5°) is similar than that between Transparent Soil and Glass (17.8°), although their constant volume cohesions differ (1.1 and 4.0 kN/m^2 respectively). This difference is likely due to the nature of the soil particles, which are plated in the case of kaolin and rounded in the case of silica. The peak angle of friction and cohesion for Kaolin were found to be higher than its constant volume values, as would be expected.

In reality, steel sampling tubes are unlikely to be totally smooth, and may exhibit different frictional properties due to rust or soil residue from previous uses. The effects of steel roughness on clay-steel frictional properties were studied by Tan *et al* (2008), who conducted shear box tests on half samples of Kaolin clay with steel half samples of varying surface roughness, from completely smooth to rusty. No difference was made between peak and constant volume stresses since no peaks were observed during testing. The research concluded that angles of friction varied from 18.57° for smooth to 28.44° for rusty steel (although cohesion was similar, between 1.2 and 2 kN/m^2). Combined with the results of this study, this places the measured friction angle for Transparent Soil / Glass at the lower end of the scale, but still within the friction expected during tube driving. This suggests that the shear stresses at the material interface should be comparable in the model and in real sampling; this supports the use of transparent soil and glass tubes to model steel tubes sampling clayey soils.

4.3 Trial Test: Physical Modelling of the Centreline Strain Path from the Strain Path Method

The Strain Path Method (SPM), the analytical solution created by Baligh *et al* (1987), modelled a round-ended (blunt) tube sampler penetrating a soil body modelled by a homogeneous, incompressible and inviscid fluid. It was based on observations that at depth, geotechnical problems are strain rather than stress related. The controlling factors for the extent of deformation to the soil elements were the tube's outer diameter (B) and thickness (t). In the following sections, the behaviour of soil elements in a physical test was studied as their relative position to the tube's cutting edge – z/B – varied. In many of the following graphs and illustrations, some conventions were used:

- Negative strains are those in extension, positive strains are those in compression
- Negative displacements are those towards the top or left side of the photo, positive displacements are those to the bottom or right.
- Individual patches of soil, called soil elements, were identified by their initial location, z_o (Figure 4.6a)
- Graphs following the displacement of these individual soil patches did so using their position relative to the cutting edge. Sign conventions are illustrated in Figure 4.6b.

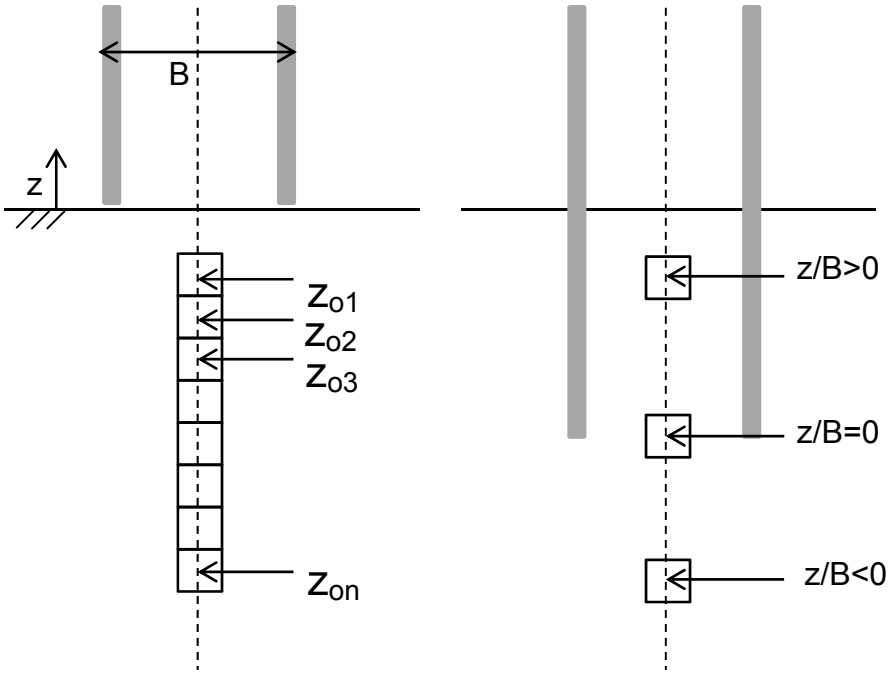

a b

Figure 4.6 - Sign Conventions for Centreline Strain Paths

In this study, one test was set up specifically during the early stage to resemble the SPM case: a 200x200x300mm (L:W:H) transparent soil model was prepared and consolidated to 50kPa inside a Perspex box, after which the pressure on the surface of the soil was released and a glass tube (B=51mm, t=2.8mm) was driven into the soil. 112 photos were taken at a rate of 0.9 frames per second (fps). Figure 4.7a to Figure 4.7c show a detail of test photos taken at three points during tube driving. The colours and brightness have been modified in these sample photos only, to increase the contrast between the soil and the glass beads. As the tube progressed downwards, the soil in and around the sampler moved away from its initial position, and the glass beads embedded in the soil reflected this displacement, which would otherwise be difficult to quantify. In these photos, some notable glass bead

arrangements can be identified, and their position can be seen to vary slightly across the series of photographs – in this test, many particle arrangements can be observed moving downwards with the tube. These displacements can be tracked using Particle Image Velocimetry software.

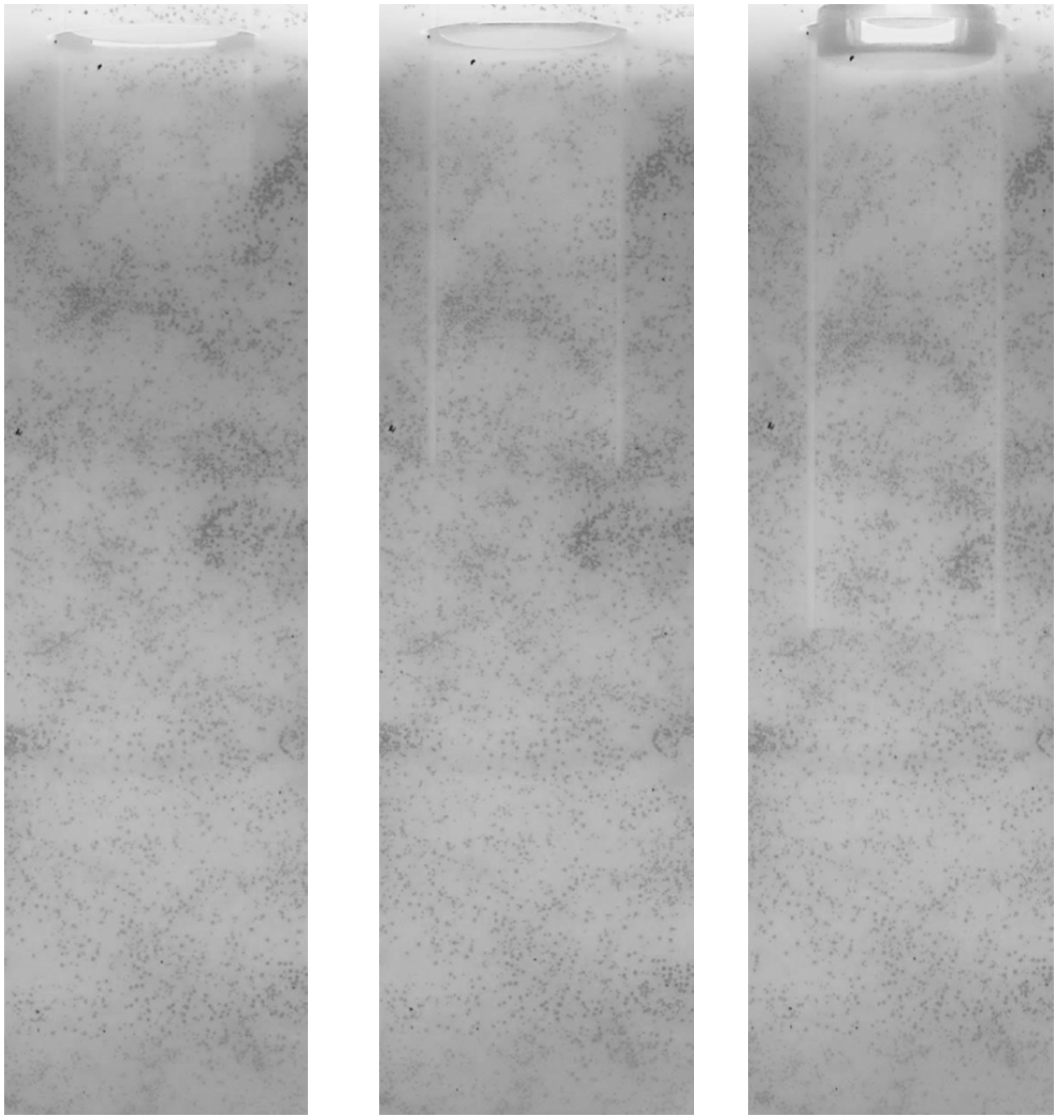

a b c

Figure 4.7 - Progression of Sampler in Tube Driving Tests

After pre-processing of the photos in the manner outlined in Chapter 3, a rapid PIV analysis was run on 2 intermediate photos using GeoPIV to produce the displacement vectors at different points in time. The general behaviour of the soil in and surrounding the tube during tube driving is illustrated in Figure 4.8. The displacement vectors were created from 48 pixel Interrogation Areas (IA) around the tube and 72 inside it. Soil immediately in the sampler wall's path was not included in the analysis since it distorted excessively and produced wild

vectors. While IAs of size 48 pixels are prone to errors, their small size maximises the detail by increasing the number of vectors per area. For illustrating general behaviour this is adequate, but strain calculations will require better accuracy and therefore bigger patch sizes. This explains the high number of wild vectors visible in Figure 4.8 (evidence of wild vectors can be an unlikely value or a blank, which is evidence of wild vector removal. In Figure 4.8, less than 1% of vectors were removed manually to improve the clarity of the images, since the results vectors were scaled up 5 and 3 times respectively, and wild vectors disturbed the view of the data). The tube and the ground surface's locations are included as dotted and full lines in the image.

The soil inside the sampler showed a downwards movement ahead of the tube, consistent with the initial compressive phase in Baligh's (1987) Strain Path Method. Significant displacement vectors appeared at a depth of 1.25-1.5 tube diameters under the cutting edge, identifying a zone of major influence for sampling disturbance, although in reality the zone of influence extends far further, with evidence that small movements occur in depths over 3-3.5B under the cutting edge. In Figure 4.9, patch displacement is plotted for soil elements on the centreline of the tube at various depths in relation to the cutting edge for two moments in time during the test, at half and full sampler penetration. In both cases, disturbance is present at depths over 1.5B under the cutting edge, which is most evident at half drive when sufficient soil remains under the sampler in which to measure displacements. The disturbance at depth highlights the need to avoid using soil elements too close to the model's base, to avoid boundary effects. For the tube in question, 3-3.5B represents 153 to 179 mm under the cutting edge of the tube. This depth of soil should ideally not be driven into during the test since it would be overly compressed due to the boundary effects by the bottom of the Perspex Box. In the current test, a depth of 143 mm of soil was left between the base of the model and the cutting edge of the tube at full penetration. In future tests, caution should be exercised in two respects:

- The strain path of elements too deep within the model will be affected by an element of compression or outward movement due to the soil's downwards movement being restricted

- The strains measured for other soil elements once the maximum recommended driving depth is reached may also be affected by boundary effects

The soil around the sampler was pushed outwards and upwards in the case of soil above the cutting edge, and outwards and downwards in the case of soil under the cutting edge of the tube. Soil immediately outside the sampler was pushed downwards. The height of the soil model was measured before and after the test and was found to have heaved a minimum of 1.75 mm upwards over the whole model, which compensates for at least 97% of the volume of the tube inserted into it. The remaining volume may have been expelled from the model by way of oil consolidating out of the soil, casting doubts that the process was fully undrained.

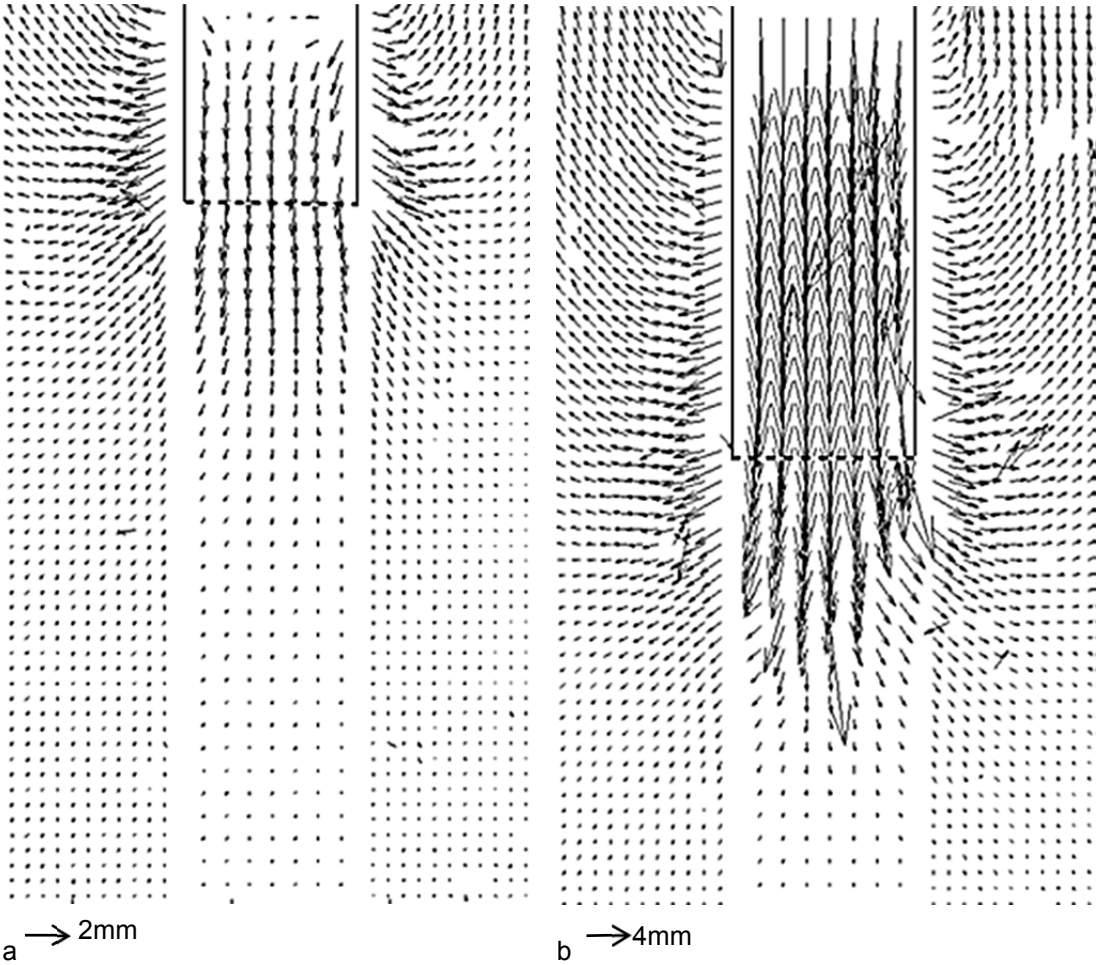

Figure 4.8 - Displacement Vectors in Soil (no Overburden pressure) - a) at half drive (1.6 tube diameters) and b) at the end of tube driving (3.2 tube diameters)

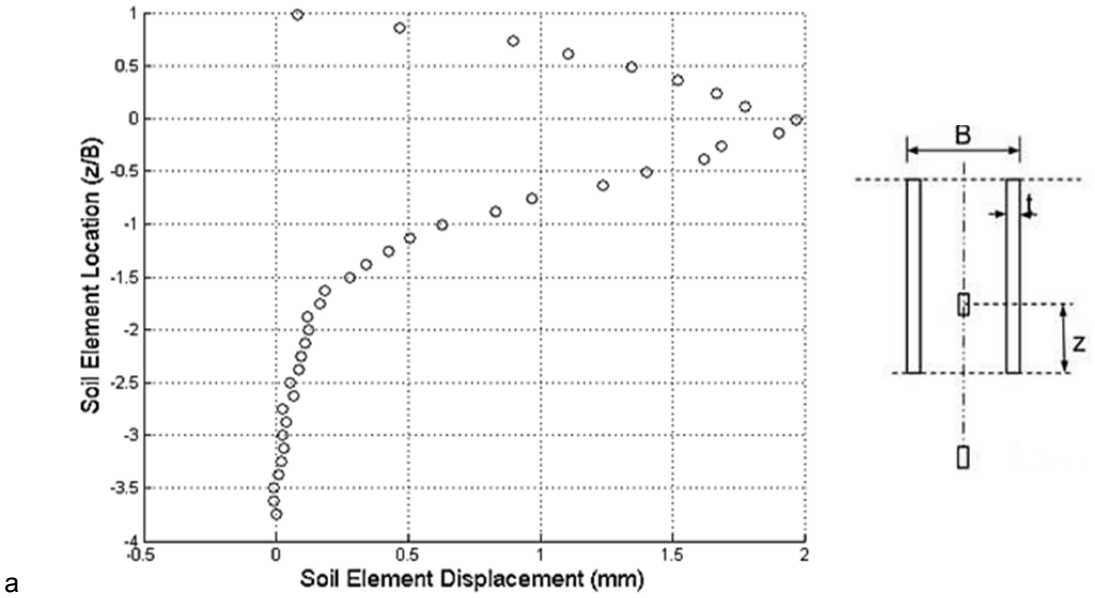

a

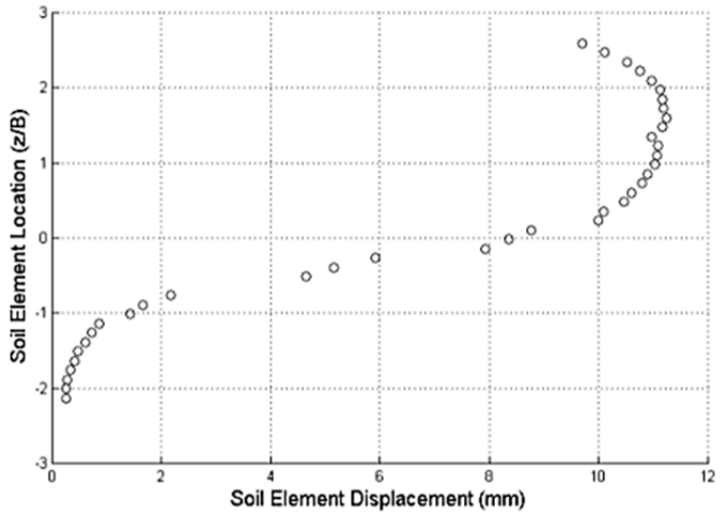

b

Figure 4.9 – Accumulated Soil Element Displacements for Unconfined Test at a) half-drive and b) full drive

The effect of tube driving on the layers of soil is illustrated in Figure 4.10and Figure 4.11, where movement vectors are plotted from the soil elements' original position. In all cases, soil layers within the sampler end up deeper than their original position and experience a drag-down effect from the sides of the tube, with soil in close proximity of the wall most affected. Soil under the sampler is more significantly deflected on the centreline than under the sampler's wall. Results are presented for penetration depths of 1.6 and 3.2B, and for soil layers at 1B and 2B above and below the cutting edge, as well as on it. The general behaviour is illustrated in Figure 4.12. This type of deformation in clay layers within a sample was observed by Hvorslev (1949 – Figure 2.6).

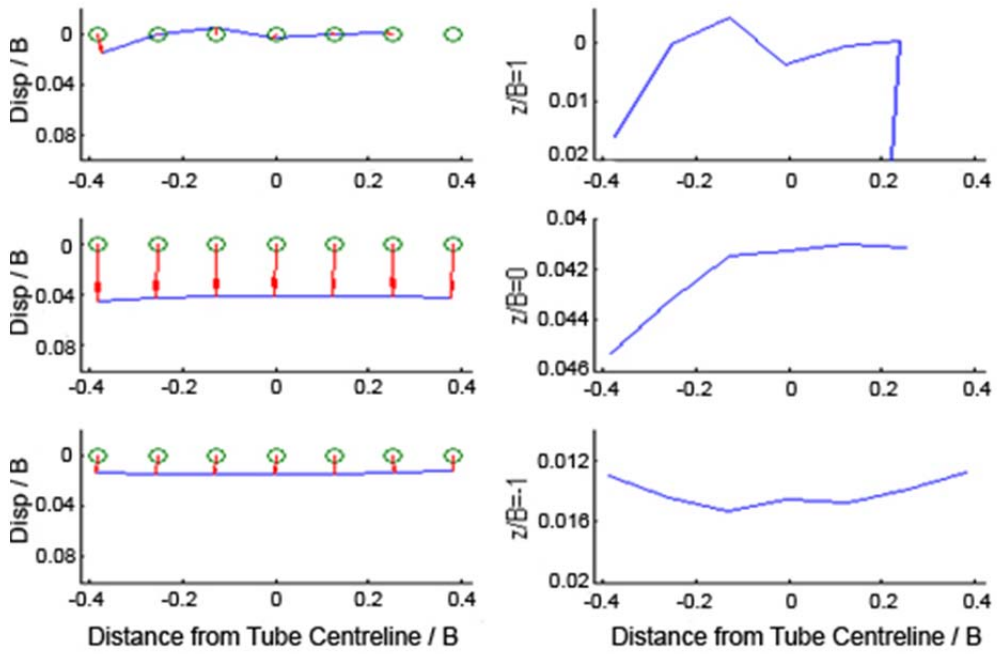

Figure 4.10 - Soil Layer Deformation within the Tube at Half Penetration Depth

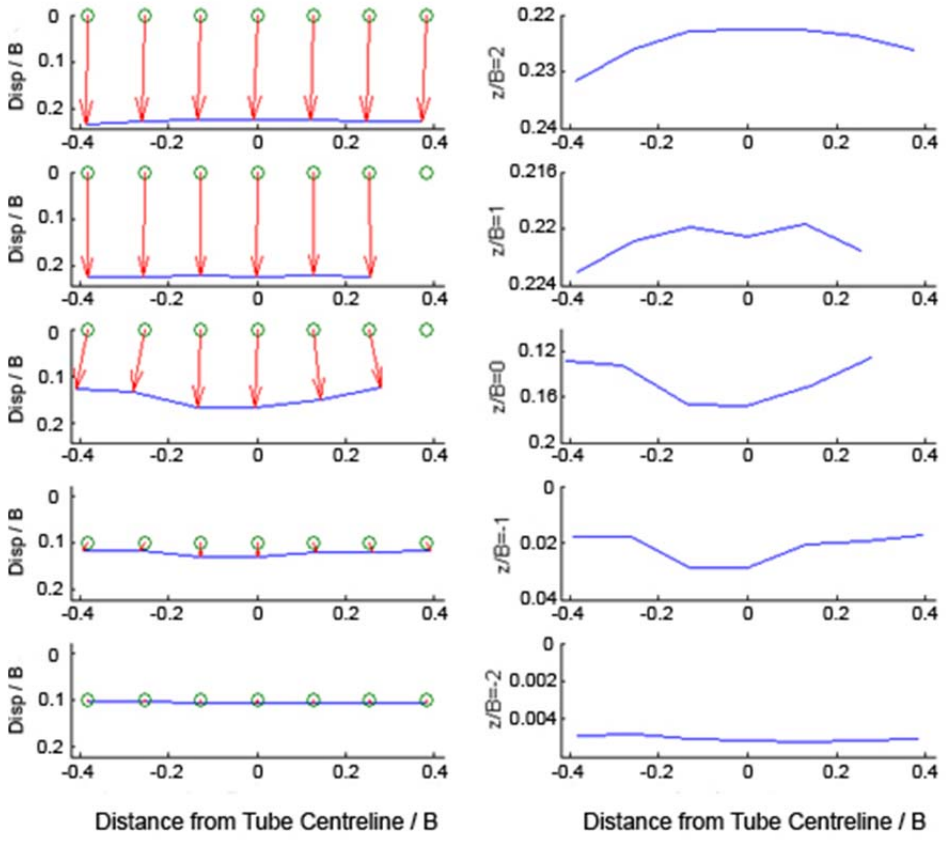

Figure 4.11 - Soil Deformation within the Tube at Full Penetration Depth

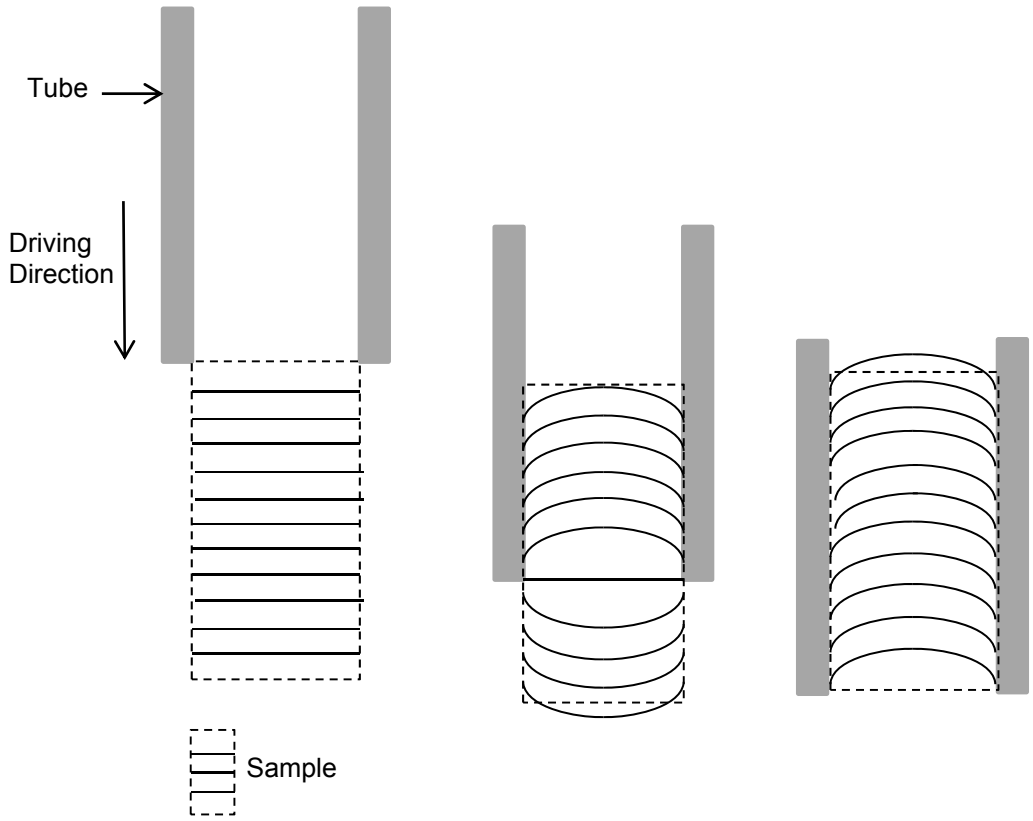

Figure 4.12 - Behaviour of Soil Layers during Tube Penetration

The strain path for soil elements on the sampler's centreline was calculated for different depths using Equation 25 and compared to the Strain Path Method (Baligh *et al*. 1987). It was observed that the Centreline Strain Path was not constant with the depth of the element, but that soil was affected in relation to its depth under the base of the borehole (Figure 4.13). Three distinct strain phases were observed:

- A compressive phase in soil ahead of the sampler's cutting edge
- An extension phase as the soil element entered the tube
- A final compressive phase as the soil is driven upwards in the tube

The general behaviour agreed with the SPM, although the behaviour was not antisymmetrical and the peak strains were different to those predicted by the analytical solution for a tube of same outer diameter (B) and thickness (t). Residual extension strains in the soil after sampling were also evident in the soil elements close to the surface while

residual compression was present in deeper elements. The effects of tube sampling disturbance decreased with depth, with soil elements close to the surface experiencing larger peak-to-peak strains, and larger recompression one inside the tube.

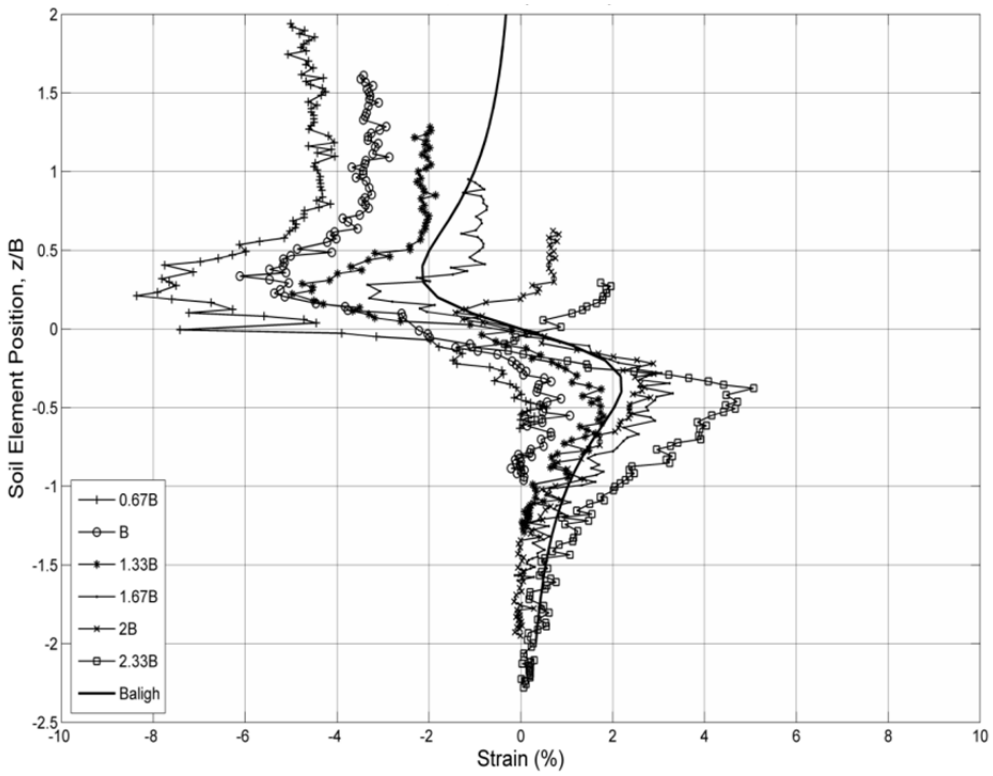

Figure 4.13 - CSP for Unconfined Soil, Tube A

A similar study by Yan et al (2010) modelled tube sampling by driving a half-tube piston sampler (B=56mm, t=1mm) into a Kaolin physical model against a viewing window. Using PIV techniques they captured and measured the resulting displacement fields inside and outside the sampler. Ground heaving was observed on the ground surface, caused by an upwards movement of the soil in a zone extending to 1.5 tube diameters away from the sampler wall. A smaller zone of influence was observed under the sampler, at approximately 1B away from the cutting edge. The soil within the tube was most heavily affected in its soft upper layers where a significant upwards movement was observed, as well as an inwards movement of approximately 1mm, while the soil on the centreline was relatively unaffected except in soil close to and under the cutting edge, where 0.5 to 1mm downwards displacement vectors were recorded. Allowing for differences in the tube's geometry (and hence the expected strains), the tests are compared in Table 4.2.

Table 4.2 - Comparison of Present study with Yan *et al* (2010)

	Current study	**Yan *et al*.**	**Discussion**
Size of model (L:W:H)	200 x 200 x 300 mm	950 x 500 x 1250 mm	The relatively small size of the physical model puts it at risk of boundary effects. The model cannot be as large as desired since visibility through transparent soil reduced at depth.
Influence zone outside / under sampling tube visible to the eye	>1B / 1.25B	1-1.5B / 1B	The zones of influence are similar, which increases the confidence in using a smaller model with higher boundary effects.
Influence zone outside / under sampling tube	Movements recorded at 3-3.5B	Not in study	Boundary effects are more important than at first glance – care must be taken in future tests. Baligh *et al* (1987) predicted significant strains (implying displacements) still existed at 1.5-2B. Further extending their model to 4B reveals soil movements thereafter are small but do exist. It is of note that the model converges towards zero movement at depth, but never reaches 0.
Vector density	1 vector per 6.35mm^2	1 vector per 3.85mm^2	A better coverage was achieved by Yan *et al* due to better visibility of the plane being studied. This has allowed more detail to be obtained.
Movement of soil elements by the sampler wall	Not studied and difficult to observe in current model	Move towards the sampler's centreline	
Movement of soil elements on the centreline	Most movement in top layers of soil (up to 11mm).	Little movement in top layers of soil. Up to 1mm in lower half of sampler	Both studies agree qualitatively with the SPM but lack of details in Yan *et al* and use of different tube geometries does not allow for a direct comparison.
Evidence of three phases of strain	Calculated using patches on the centreline	Interpreted from zones of vectors	
Behaviour of soil surface	Evidence of heaving – 1.75mm, accounts for volume of tube	Evidence of heaving – not quantified	Comparable

It should be noted that although Yan *et al* achieved a higher vector coverage due to better visibility of the plane of interest, the boundary conditions due to the increased friction between the kaolin and the viewing window might heavily influence the soil's movement during tube driving. Using transparent soil, despite the added difficulties visualising the plane of interest, would better quantify the real soil movements inside the soil body.

The results of this study, which acted as a trial test for the main testing programme, confirmed it was possible to model tube driving using the methodology presented in Chapter 3, and that the CSP could be obtained. It was apparent, however, that due to poor transparency at depth in consolidated soil, larger patch sizes were required for the PIV analysis, reducing the vector area density, and hence the amount of detail in the vector fields. Since the main focus of this study was the CSP rather than the full displacement fields, it was decided to increase patch size for the centreline analysis, and hence obtain more accurate results, with fewer data points. Although this meant that the strain was being calculated over larger areas, it was demonstrated that this had little effect on the recorded strain values (see Chapter 3).

4.4 Soil Movement in and around the Sampler during Tube Driving

4.4.1 Test Programme

After a successful trial test in unconfined soil, a series of tests was carried out on soil models where the surface was confined by a pressure plate allowing the soil to be maintained under an overburden of 50kPa to simulate the presence of soil around the side of the borehole. Twelve tube-driving tests with nine different combinations of soil consolidation and sampler geometry were run over a period of 12 months, each lasting approximately 1.5 to 2 minutes and generating some 200-250 photographs for analysis. The geometries in question were:

- A: blunt sampler
- B: sharp sampler, tapered at an angle of 30° over 3mm for thick tubes and over 1.5mm for thin tubes
- C: blunt sampler with an inside clearance ratio

All tubes' outer diameter (B) was 52.20 ±0.06mm. Thick (t=3.60 ±0.08mm) and thin (t=2.00 ±0.08mm) tubes were manufactured for each cutting edge geometry. Details of all tubes were given in Chapter 3. Tests were run in soil models prepared at different overburden pressures, which determined the Overconsolidation Ratio of the artificial soil: normally consolidated (NC, OCR=1) or lightly overconsolidated (OC, OCR=1.6).

Three of the nine tests were repeated at a later date due a problem with the set-up, either because of a poor placement of the seeded particle plane during the model's preparation, poor soil transparency, or because of sampling tube penetrating the soil at an angle due to the poor performance of the connection between the glass tube and its metal holder.

This section presents the movement of soil in and around the sampler during tube driving for all tests. A number of dimensions were measured using image viewing software (Microsoft Office Image Viewer) which allowed for a to-the-pixel manual measurement of the coordinates of elements within the image, such as tube centreline location, tube dimensions, location of the tube cutting edge for any given photograph, etc. These are included in Table 4.3. The tubes' centreline coordinates and conversion factors (pixels per mm) reveal small differences in the position of the camera in each set-up. Small differences in camera speed were also observed and are due to a number of factors including lighting intensity and battery charge. The dates of the tests are also included since later tests benefitted from increased transparency due to a change in oil supplier, and therefore yielded fewer wild vectors and less noise (see Chapter 3).

The photographs were pre-processed prior to the PIV analysis in the manner outlined in Chapter 3. They were then rotated according to the tube's driving angle so that the tube and its centreline appeared vertical in the image. This had the effect of changing the centreline of the photo (the exact location of the original centre of the photo is important for image calibration purposes). A test photograph was copied and marked with a yellow dot before rotation and its new coordinates measured for future calibration purposes. Rotating the photographs allowed a PIV mesh to be created over the centreline of the tube.

Table 4.3 - Tube-Driving Tests, Set-up Parameters

Geometry / soil	Test Date	X Coordinates: tube centreline / rotated image (pixels)	Plane of particles within ± 2mm of centre of tube?	Drive speed (mm/s)	Drive angle from vertical (final)	Frames per second	Pixels / mm at tube edge	Initial Observations
A-Unconfined	03/2012	1631/3264	YES	1.06	0	1.92	11.33	Satisfactory
ANC	14/09/12	1578/3153	YES	2.36	+0.6	2.09	11.22	Satisfactory
BNC-1	30/08/12	1522/3104	YES	2.46	0	2.14	11.20	Satisfactory but poor soil transparency
BNC-2	11/01/13	1550/3145	YES	2.36	-0.5	2.19	11.01	Satisfactory
CNC	03/08/12	1572/3145	YES	2.30	-0.5	2.11	11.28	Satisfactory
AtNC	25/02/13	1622/3225	YES	2.43	+1.5	2.18	11.03	Excessive Drive Angle
BtNC	26/03/13	1576/3153	YES	2.43	+0.5	1.95	11.00	Satisfactory
CtNC	20/05/13	1535/3145	YES	2.36	-0.5	2.18	11.00	Satisfactory
AOC-1	24/07/12	1526/3186	NO	2.35	-1.0	2.08	9.27	Off-Centreline, different camera position, Excessive Drive Angle
AOC-2	10/10/12	1731/3297	YES	2.40	+2.4	2.20	11.24	Excessive Drive Angle
AOC-3	05/07/13	1536/3137	YES	2.36	+0.4	1.68	11.11	Satisfactory
BOC	18/10/12	1544/3145	YES	2.43	+0.5	2.13	11.22	Satisfactory
COC	29/04/13	1592/3225	YES	2.43	+1.5	2.25	10.91	Excessive Drive Angle

As previously, the main focus points of the tests were:

- To generate a vector field of soil movement in and around the sampling tube, at three points during the tube penetration
- To calculate the strains on the centreline of the sample (CSP) and compare these to those predicted by the SPM and other analytical studies
- To compare the CSP for:
    - Different B/t ratios
    - Different cutting edge taper angles
    - Different OCRs

To be aware of the zone of influence of the sampler in the soil around it, so that analysis can take this into account. The success of a number of tests was affected by the set-up. In four tests, the tube penetrated at an excessive angle: by studying the movement of soil elements on the centreline it was found that where the drive angle equalled or was inferior to 0.6°, the elements remained on the vertical centreline, while at angles exceeding this, a horizontal component was observed as the tube did not slide straight down along an angled centreline but also had a purely vertical component. Unfortunately, due to time restraints, not all these tests were repeated.

4.4.2 Zone of Influence under the Tube's Cutting Edge

In the trial test, where the soil's surface was unconfined, the main zone of influence of the sampler had been measured to be 1 to 1.5 B under the tube's cutting edge, with smaller disturbances (in the order of 0.5mm) recorded in deeper soil. For all remaining tests, a pressure plate was added to the set-up to model the confining effects of soil layers around the base of the borehole. New tubes were manufactured to model different cutting edge geometries, and since these were longer than the original tube, their depth of penetration was greater, meaning that at full penetration they were well within 3B of the box's base. Since the presence of the pressure plate restricted the upwards flow of soil around the sampling tube, it was decided to check if the zone of influence of the sampler was increased, thereby reducing the amount of soil which could be considered unaffected by boundary effects.

A grid of IAs was created over the centreline of the sampler for all tests, and the boundary effects were determined in the manner outlined for the previous test. The findings agreed with those from the unconfined test, with a major zone of influence extending until 1 to 1.5B under the cutting edge, and smaller soil movements (close to zero) under that. While an identical soil behaviour was not observed in all tests, a typical curve is illustrated in Figure 4.14, where the location of each IA is represented by a single dot. At half-drive, soil under the sampler's cutting edge (z/B<0) has moved downwards slightly, by less than 1mm, while soil inside the tube (z/B>0) has moved upwards from the IA's original location by up to 10 mm. The spacing between these individual IAs has lengthened, suggesting that strains have developed between each set of points. At full drive, when the soil is fully within the sampling tube, the spacings have all increased, which implies that an extensive strain has been set up and remains within the sample well after the individual soil elements have passed the cutting edge. This behaviour is different to that observed in the unconfined test, and in Baligh *et al*'s analytical solution where the spacing between IAs inside the tube reduces again in the region of its original value (Figure 4.9a and b).

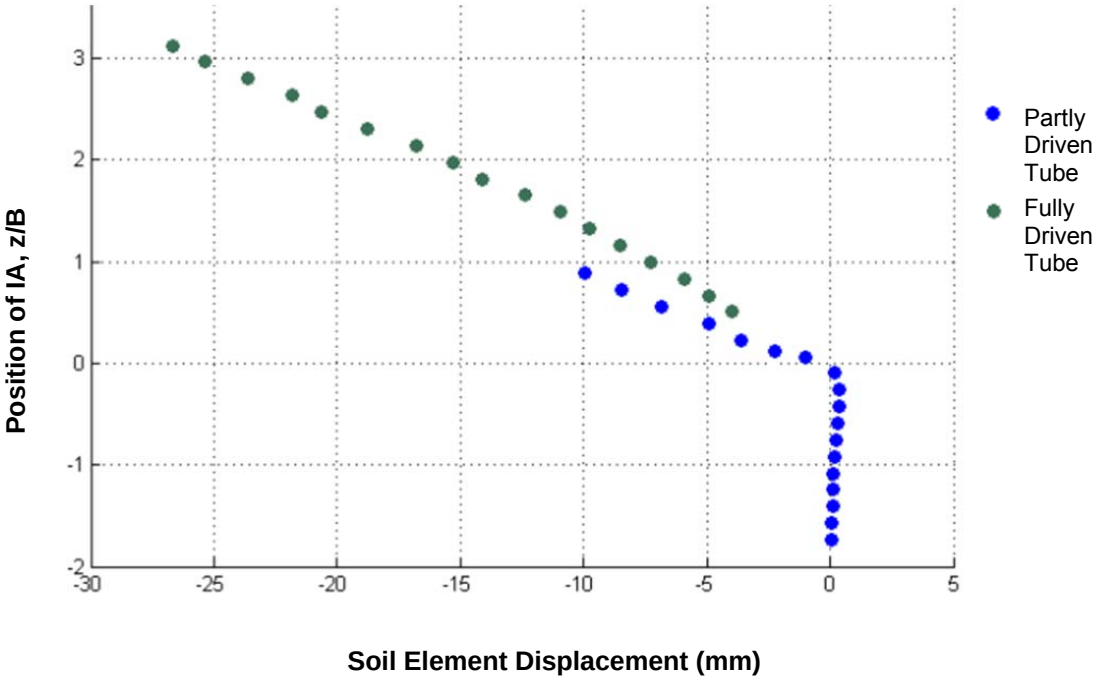

Figure 4.14 - Soil Displacement for a typical Confined Test

4.4.3 Movements in and around the Tube

Meshes of IAs were created over the original photo of each test, inside and around the tube to obtain displacement fields in the soil at different stages in tube penetration, at eight depths of penetration into the soil between 0.5 and 4B (by using these photos only this is the equivalent to using a leapfrog value of approximately 36). The variation in texture quality between tests is visible in the results by the number of wild vectors created during the PIV analysis. To increase accuracy while still keeping an acceptable vector coverage, the dimensions of the IAs was varied in each test:

- For low quality textures, IA size was set to 72 pixels and the mesh was made of three sub-meshes, one in the tube and one on either side, meaning that soil under the tube's wall was not monitored
- For medium quality textures, a full mesh covering the whole soil area was used, with patch size = 72 pixels
- For high quality textures, a full mesh covering the whole soil area was used, with patch size = 48 pixels

The variation in texture quality is illustrated in Figure 4.15 for tests BNC-1 (low quality texture), ANC (medium quality texture) and CtNC (high quality texture). The improved transparency in some tests was caused in large part by using a different Technical White Oil, better mastery of contrast in digital photography under difficult lighting conditions and in set-ups with transparent soil with a smaller OCR.

In most cases, the data for soil in the upper 1B of soil is not included since it ends up in the tube holder and is therefore no longer visible in later stages of the tests, creating wild vectors. The results in this section are presented as vector fields plotted for each test at depth of penetration 2, 3 and 4B (Appendix E - Figure E. 1 to Figure E. 12, with an example in Figure 4.16), with vectors scaled up by a factor of 3. The soil's surface is immediately above the first row of vectors, and the tube's cutting edge is indicated by a dashed line. For the data of a single test to be included on one page for easy comparison, vectors are only plotted to a distance up to 1B away from the tube wall. The full-field soil behaviour has been analysed and gives a more complete picture of the tube's influence zone, which is seen to

extend to and probably over 1.5B away from the sampler's wall. In all tests, the soil surrounding the sampler was pushed outwards and upwards if over the cutting edge and outwards and downwards if under. Soil inside the tube underwent more significant displacements than that outside the sampler, with elements on the centreline moving up to 35mm, while those in the surrounding soil moved between 0 and 3mm. Soil directly under the sampler's wall formed wild vectors and the final location cannot be found using this method. In most cases, the soil's reaction to tube driving is similar to that in the unconfined test, albeit with larger displacements inside the tube: soil layers inside the sampler show a downwards curve, while soil under the cutting edge shows an upwards curve, as was illustrated in Figure 4.12 for the trial test.

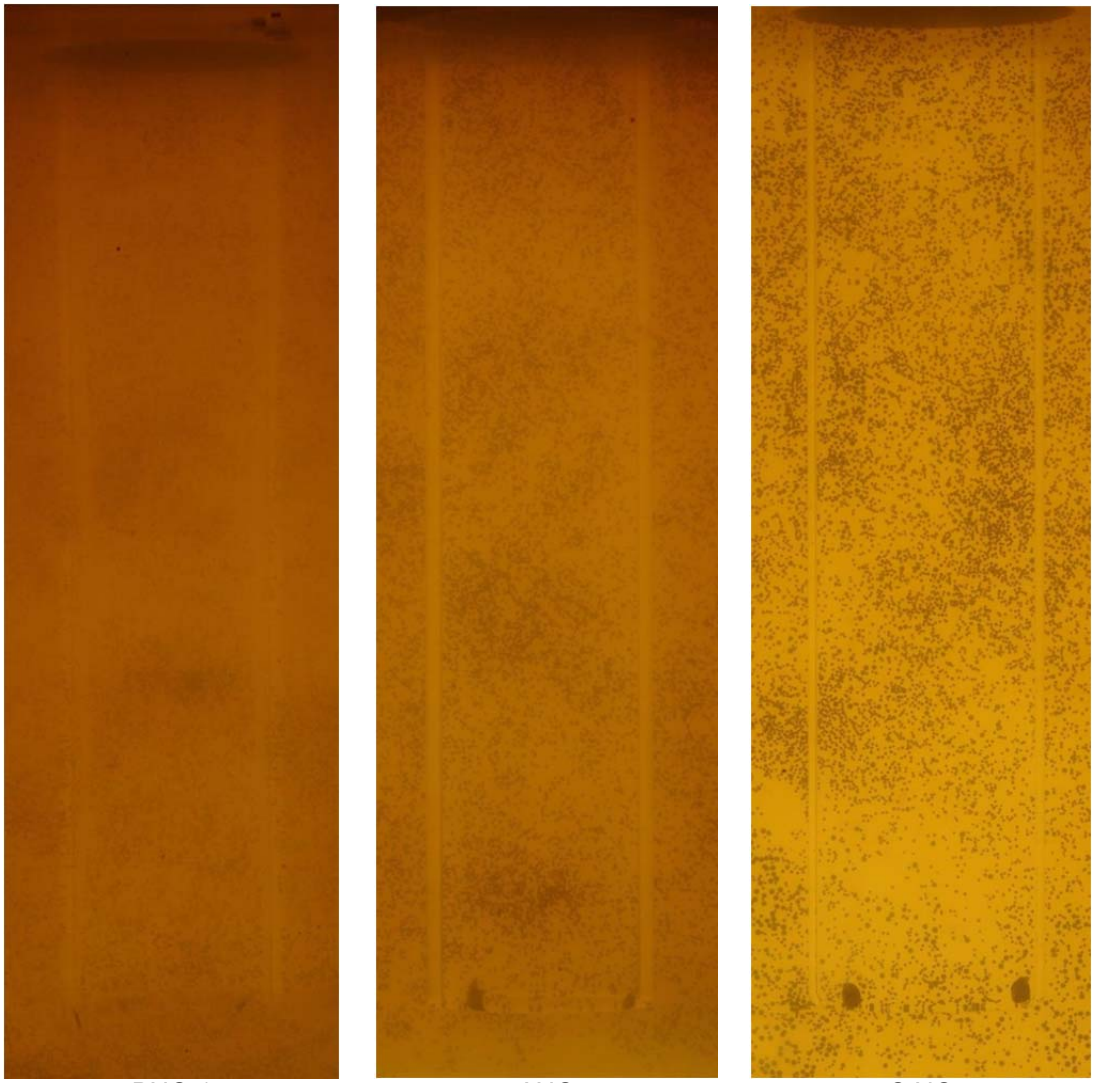

BNC-1 ANC CtNC

Figure 4.15 - Texture in Test Photographs: BNC-1, ANC and CtNC

Test 1: ANC	Scale = x3
4B	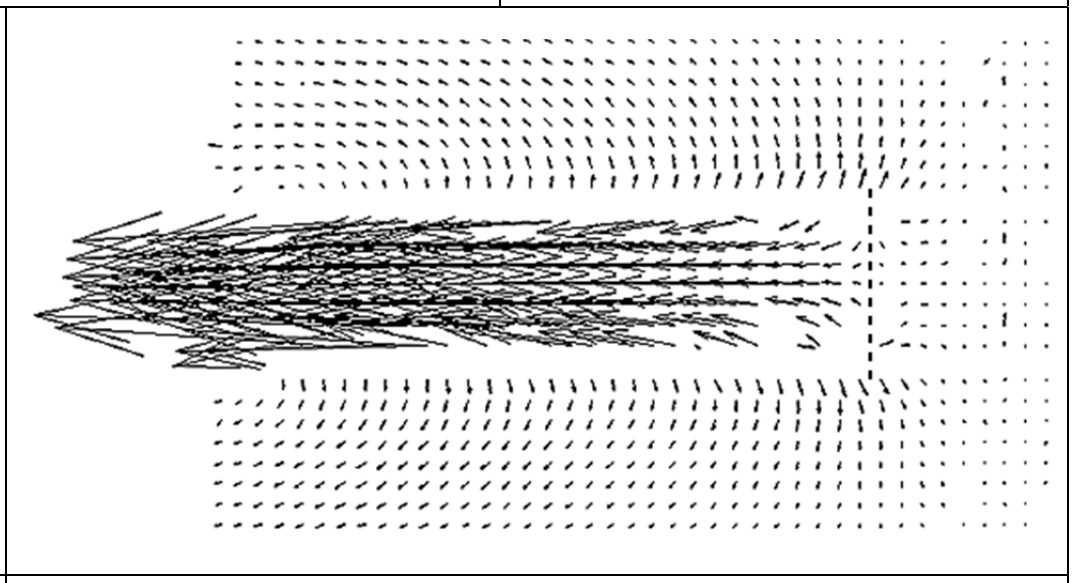
3B	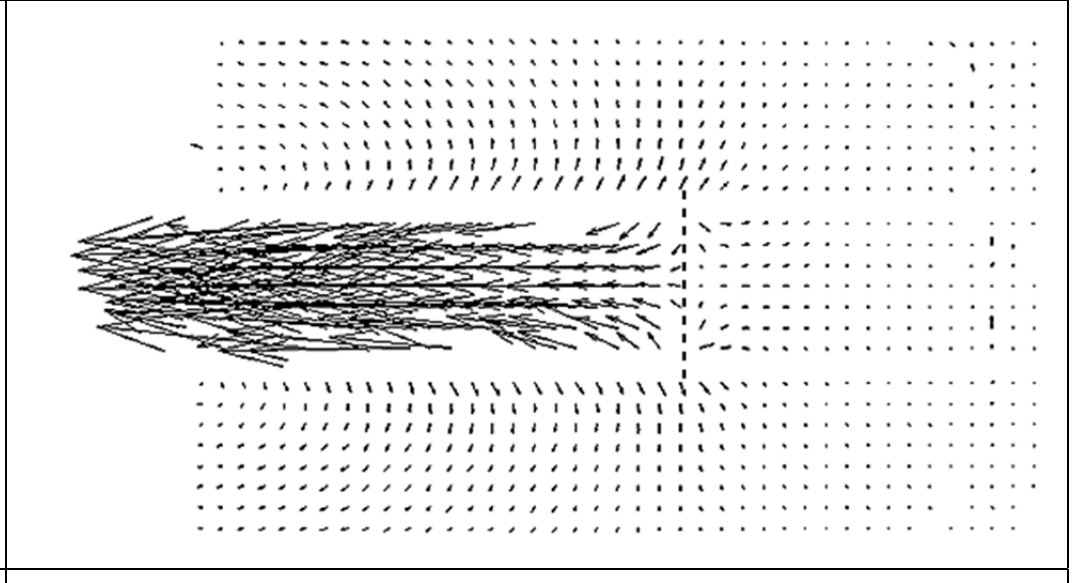
2B	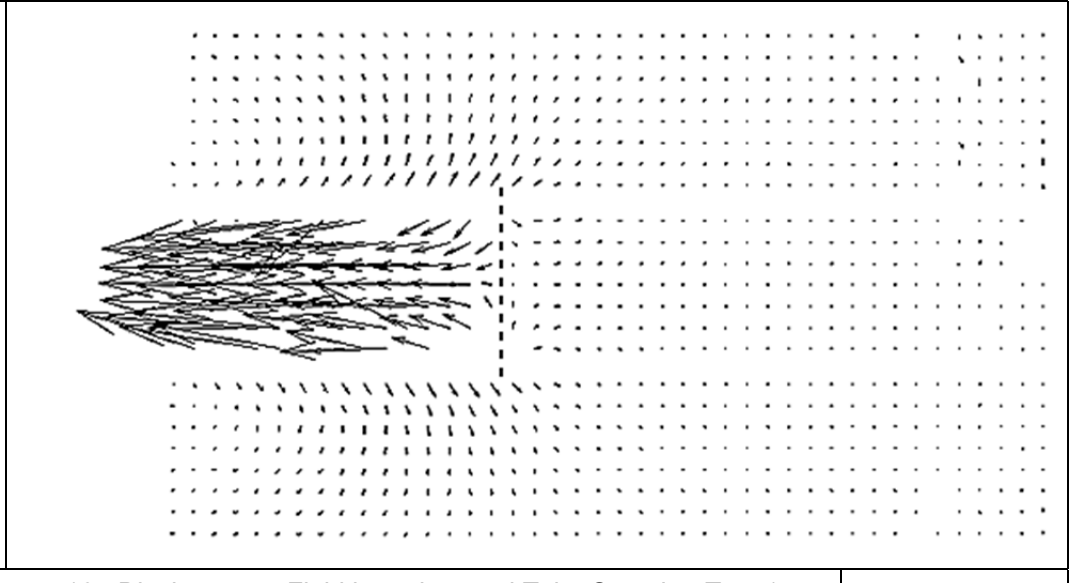

Figure 4.16 - Displacement Field in and around Tube Sampler, Test 1 (ANC)

→ 4mm

While these vector fields are useful to describe the general movement of soil, they do not consider the full behaviour over time. Figure G. 1 to Figure G. 12 are included in Appendix G and illustrate the movement of soil elements on the sampler's centreline, in both x and y directions. A number of IAs situated on the sampler's centreline were tracked over the full photo sequence, and their cumulative displacements are presented. Soil elements closest to the base of the borehole (initial depth=-4/6B) are highest in the graph, while deeper elements (initial position up to -19/6B) are the lower data series. An example of this behaviour is illustrated in Figure 4.17.

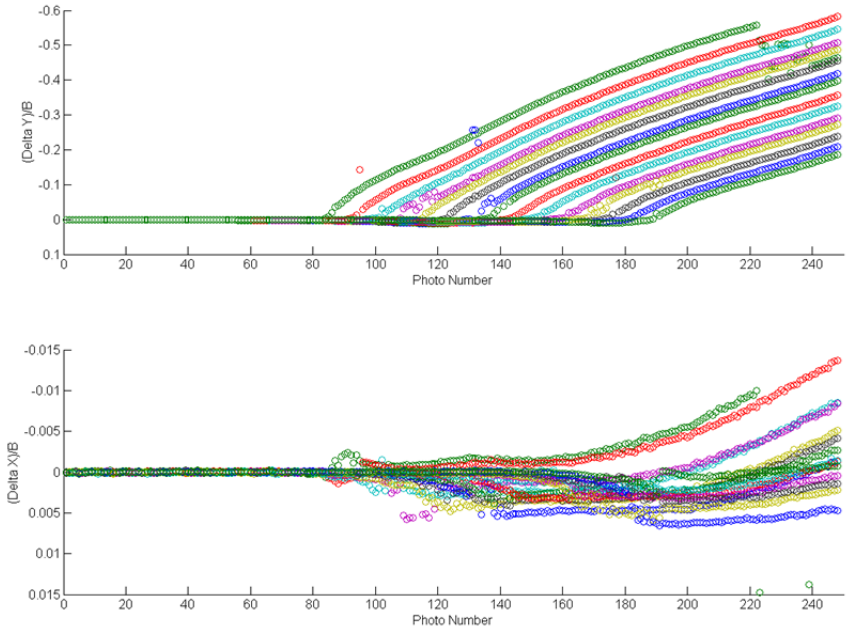

Figure 4.17 - Sampling induced Displacements in test ANC

Initially, in a typical tests, soil under the cutting edge undergoes a downwards movement (y direction) between 1 and 5mm. During this phase, according to analytical models, the soil experiences compressive strains. This is followed by a movement upwards inside the tube, where – in the most extreme case – soil elements were seen to rise up to 40mm above their initial location. In most tests, this almost linear rise continues until full tube penetration. However, in a number of cases, the movement of soil over time is more complex. In Tests AOC-2 and BtNC, the soil moves upwards only for a short amount of time before being pushed downwards into the soil. Tests AOC-1, AtNC and COC also show evidence of phases of downwards movement. Since there is no pressure on the top of the sample, this

downwards movement can be explained by the interaction of the tube walls and the soil. It is hypothesised that “plugging” occurs, by the formation of a plug of soil inside the tube, which is driven down with the sampler.

This phenomenon is a known issue in tube driving, and has been documented by Hvorslev (1949). Research by Miller and Lutteneger (1997) showed that plugging in open-ended piles depended on the method of driving, the internal diameter and the soil’s OCR: driving caused the least plugging, as did piles with the largest internal diameters and soils with the lowest OCR. Interestingly, four of the five tests showing evidence of plugging are those where the tube penetrated at an angle superior or equal to 1° from the vertical. Horizontal movements (x direction) were much smaller than those in the vertical direction, typically under 0.2mm, with soil elements originally on the centreline remaining so during tube penetration. In some cases, due to an excessive drive angle, soil elements were pushed away from the centreline of the tube, and horizontal movements up to 1.5 mm were observed in the most extreme case of plugging. From the vector fields and displacements of interrogation areas on the centreline over time it becomes apparent that not all tests are comparable. Table 4.4 summarises the issues with each test and highlights the elements which may cause difficulties in comparing the data. It is obvious that plugging will affect the strains within the sample since extensive strains are impeded and compressive strains are created as the plug moves down into the soil – since this affects two tests fully and three intermittently, some comparisons cannot be made.

Table 4.4 - Issues affecting Tube Penetration Tests

Test	Plugging	Excessive Drive angle	Transparency
ANC	NO	NO	Medium
BNC-1	NO	NO	Poor
BNC-2	NO	NO	Medium
CNC	NO	NO	Medium
AtNC	intermittent	YES	Good
BtNC	YES	NO	Good
CtNC	NO	NO	Good
AOC-1	intermittent	YES	Poor
AOC-2	YES	YES	Poor
AOC-3	NO	NO	Good
BOC	NO	NO	Poor
COC	intermittent	YES	Medium

4.4.4 Comparison with the SPM – Displacement Data

Displacement curves for a partly driven tube (Geometry A, thick-walled) in both confined and unconfined normally consolidated soil are presented in Figure 4.18. The soil's displacement at a depth of 2B under the cutting edge was measured and using Equation 25, the displacement data was extracted from the SPM and also plotted for comparative purposes, starting for each test at the measured value for the deepest element. While neither curve fits the analytical solution, the unconfined soil's behaviour is closest and exhibits the expected downwards movement of soil and symmetry about the tube's cutting edge (z/B=0). The pressure plate used in all other tests produces a resistance to the aforementioned surface heave, forcing the soil within the model into the easiest path: into the sampling tube, thus creating significant upwards flows of material in 10 out of the 12 confined soil tests. This significant change highlights the need to consider boundary conditions when modelling tube driving, both physically and analytically. Hvorslev (1949) stated that with the risk of excess soil recovery increased with depth of sampling, a risk which becomes obvious from the difference in soil behaviour between both types of test – confined and unconfined.

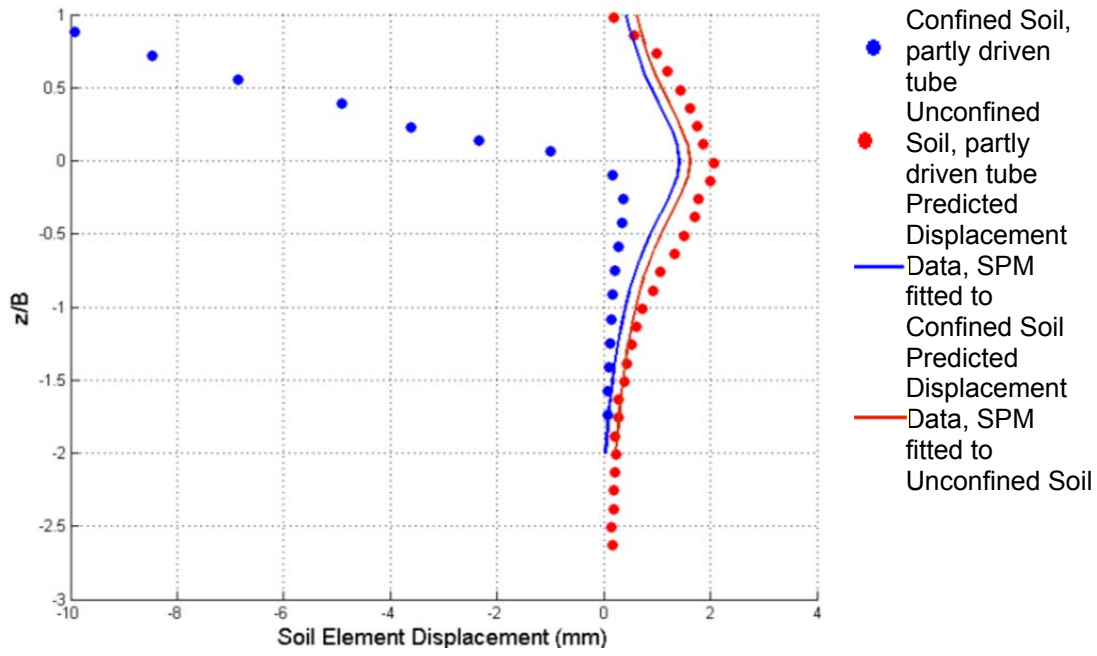

Figure 4.18 - Displacement for Tube Geometry A for Confined and Unconfined Soil

It was decided to investigate whether the excess soil recovered within the tube was soil which would have moved downwards and away from the sampler had the soil model been

deeper. Figure 4.14 shows a typical displacement curve for soil elements on the centreline of the sampler at a low amount of tube penetration and at full penetration. At this low amount of sampler penetration the tube is at 3B from the base of the Perspex box, so the displacement curve should be relatively unaffected by boundary effects. Figure 4.14 shows that at this stage, excess soil recovery is already evident within the tube, and that shallower layers also appear to be affected. This is also evident in the curve for the fully driven tube, which suggests a gradual increase in soil volume within the tube rather than a step increase due to boundary effects. The incremental displacement field for Test AOC-3 also illustrates this phenomenon at a tube depth of 2B (Figure 4.19). The displacement vectors do not show the overall movement since the start of tube penetration, but the displacement of soil over 10 photos, or 5 seconds. The tube and cutting edge's locations are obvious from the vector field, scaled up 10 times. Most of the vectors indicate that the soil under the tube is pushed away from the sample, while a limited number in the close vicinity of the cutting edge are pulled inwards and upwards. These few vectors are responsible for the excess recovery ratio, the lengthening of the sample, and the residual strains remaining in the specimen after removal from the ground. The results of excess soil recovery are illustrated in Figure 4.20, where soil under the sampler's wall is collected, and as a result, the tube no longer contains exclusively the desired specimen, but a distorted sample with increased dimensions.

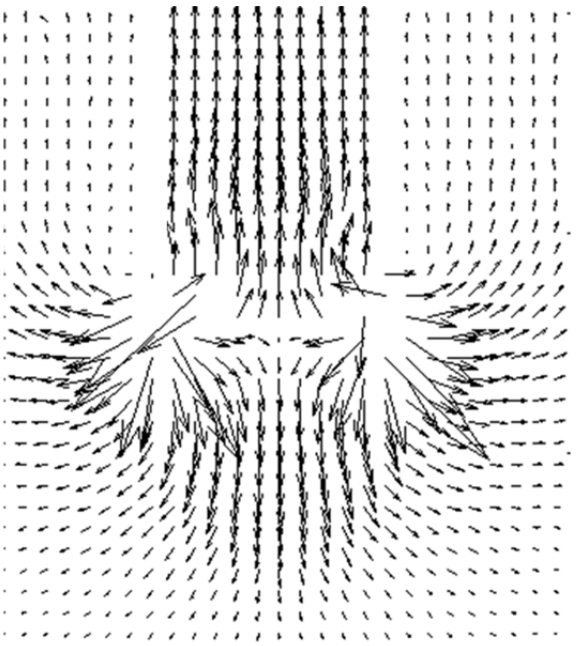

Figure 4.19 - Soil Displacements around Cutting Edge over 5 seconds, Test AOC-3

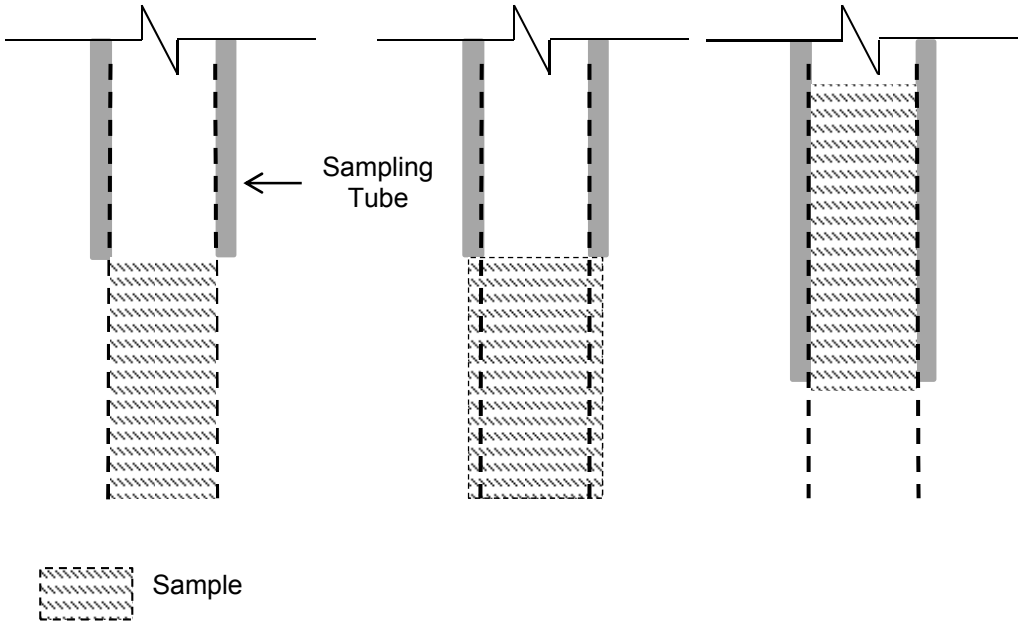

Figure 4.20 - Excess Soil Recovery in Open-Tube Driving

4.5 Centreline Strain Paths

The Centreline Strain Path was plotted for all tube driving tests, using data generated with a PIV analysis using an Interrogation Area of 96 pixels, or approximately 8.7mm. This IA size was shown to be large enough to provide adequate accuracy while being small enough to provide a sufficient vector density in the area under consideration. 16 IAs were created in a mesh comprising one column along the centreline of the tube, in the zone between the base of the borehole (or surface) and a depth of 3 tube diameter under the surface, considered unaffected by boundary effects at the base of the box. It is worth reminding that using a full Leapfrog value during PIV analysis yields the fewest random errors and is therefore advisable. However, the optical distortion through the tube makes this impossible for the software to recognise the IA when using a full Leapfrog and therefore 15 PIV runs were carried out to get an average final IA location, by applying a quadratic trendline to the displacement data in the photo capturing the moment the tube had been driven to a depth of 4B under the base of the borehole. In most tests, this photo marks the point where the zone of influence under the tube just touches the base of the box, and using data from photographs after this one could lead to distorted data being generated. The equation of the

trendline was used to find the final (residual) strains in soil elements at different depths in the borehole. Plotting the CSP was done in two parts: a forwards PIV analysis at full Leapfrog from photo 1 to photo at depth 4B using the original mesh of IAs gave the highest possible accuracy, then a backwards analysis using full leapfrog from photo at depth 4B to photo 1 using the mesh with updated patch locations to correct for the errors of using a low leapfrog value. This methodology is described in Chapter 3. The final IA location graphs are included in Appendix F, where wild vectors have been removed and a quadratic trendline applied.

These final location curves allow the overall strain in the still visible part of the sample to be measured. Most samples exhibit high excess recovery ratios, and therefore the upper part of the samples can be hidden from view inside the tube holder. Although the hidden volume of soil is different in all tests, a comparison can be done for soil at a given depth. Coordinates of soil elements originally at depths under the ground surface of -2/3B and -3B were compared at sampler penetration depths of 2B and 4B under the ground surface and the overall strain between each pair of points is presented in Table 4.5. Since neither of these depths experiences peak compressive or extensive strains at these points in time, the strain between these can be taken as a more permanent elongation of the sample. Negative strains are those in extension.

Table 4.5 - Overall Strains in All Samples at Penetration depths 2B and 4B

	Overall Strain (%)					
Depth of tube penetration	**2B**			**4B**		
Tube Geometry	**A Rounded sampler**	**B Sharp sampler**	**C Inside clearance**	**A**	**B**	**C**
Thick walled tube, Normally consolidated soil	-12.6	(-11.0) -11.7	-11.5	-18.3	(-16.3) -17.5	-15.5
Thin walled tube, Normally consolidated soil	-4.3	-4.3	-3.0	-6.6	-6.1	-5.0
Thick walled tube, Overconsolidated soil	(-9.7) (-6.9) -9.7	-11.1	-7.1	(-16.2) (-8.2) -12.7	-17.3	-9.0

Values in brackets are those for tests which were required to be repeated due to problems with the test set-up, usually an excessive driving angle. Looking at the other tests, initial observations seem to indicate that:

- The magnitudes of overall centreline strains in thick-walled samplers in NC soils are similar for all cutting edge geometries, pointing to similar excess recovery ratios. The same is true for thin-walled samplers in NC soil
- Geometry C yields smaller overall centreline strains in all soils than tubes without inside clearance. This is due to the sample being allowed to expand outwards inside the tube as well as upwards.
- OC soils experience lower overall centreline strains than NC soils
- Excess soil recovery amounts for most of the overall strain, with thin-walled samplers being less affected than thick-walled samplers
- The measured overall strains are larger than would be required to cause failure in clay samples (see 2.4.4)

The influence of the excess recovery of soil – the entrance of soil under the tube's walls into the tube rather than it being pushed into the surrounding ground – is significantly higher than the tube's cutting edge geometry.

The CSPs generated from the data from the confined tests showed a number of variations. Due to increased transparency of the soil, models created later in the test programme had fewer wild vectors and formed a complete CSP rather than have many wild vectors close to z/B=0, which had to be deleted from the graph. The major differences were:

- The maximum Compressive strain ahead of the tube
- The maximum Extensive strain inside the tube
- The Residual strain as the sample moved upwards into the tube
- The rate at which the Extensive strains reduced with depth
- The magnitude of the peak extensive to residual strain

The surface heave was also measured manually between the first and last photos in each test, and was seen in all cases to rise. Figure 4.22 to Figure 4.33 present the centreline strain paths for each test. For clarity, some of the 15 strain paths per test have been removed and data is plotted for soil elements at original depths of 1 to 3B under the base of the borehole, every 0.5 B. The CSPs generally resembled those predicted by Baligh *et al* (1987), with three distinct strain phases: compression ahead of the sampler, followed by a

rapid extension phase as the tube approaches the soil element, and finally a last compressive phase inside the sampler. The two main differences were the variation of strain with initial depth of the soil element, and the magnitude of the extensive strains. All strain paths are plotted alongside those predicted by Baligh *et al* for a sampler with the same B/t ratio. While the SPM is an approximate analytical method, the centreline strain path is mathematically defined and provides a general solution applicable to any sampler dimensions. Other numerical and analytical solutions cannot be so readily compared with the geometries used in this study.

The results are divided into three categories: Thick Tube, Normally Consolidated (NC) soil, Thin Tube, Normally Consolidated soil, Thick Tube, OverConsolidated (OC) soil.

In the following CSP graphs, a number of strains were considered. These are the peak extensive and compressive strains, the recompression inside the sampling tube, the peak-to-peak strain and the residual strain. These are illustrated in Figure 4.21.

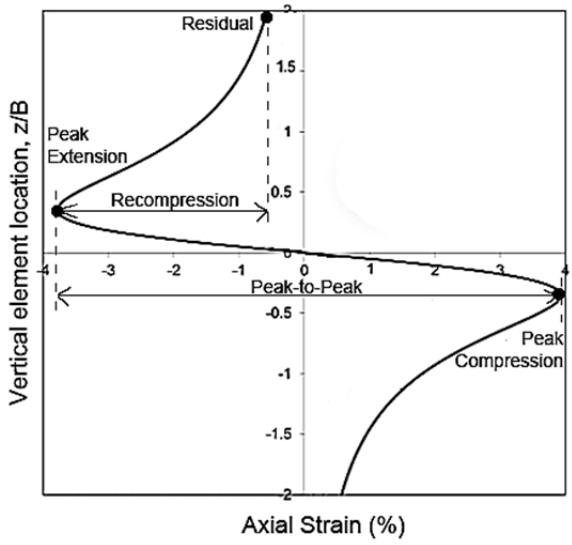

Figure 4.21 - Strains in a Centreline Strain Path

4.5.1 Category 1: Thick Sampler, Normally Consolidated Soil

Category 1 comprises ANC, BNC-1, BNC-2 and CNC. This set of tests was particularly successful despite the reduced transparency of the soil. Adequate CSPs were obtained for ANC (Figure 4.22), BNC-2 (Figure 4.24) and CNC (Figure 4.25). BNC-1 (Figure 4.23) has an

incomplete CSP, with data for the peak extensive strain missing. This is due to poor IA texture and poor visibility through the soil model.

Soil elements located between the surface and a depth of 2B can be considered heavily disturbed and ideally are not used in laboratory testing. Data at 2 and 3B is worth studying since it should be acceptable for testing. Data from these tests is summarised in Table 4.6. Initial observations in all four tests show an obvious difference between the data measured in the physical tests and that predicted by Baligh *et al* (1987). Extensive strains are up to ten times those predicted close to the surface and 5 to 8 times at a depth of 3B. Compressive strains are up to half those predicted. Consequently, the peak-to-peak strain experienced by these samples is 2.7 to 4.4 times higher than predicted. The low values of surface heave indicate that the volume of soil displaced by the tube was not fully pushed into the soil surrounding the sampler. In fact, comparing the theoretical volume of the tube inserted into the soil and the volume rise in surface shows that the surface heave accounts for between 25 and 75% of the tube volume in the whole series of tests, which suggests that the high extensive strains are due at least in part to the recovery of excess soil from under the walls of the sampler. The difference between the peak extensive strain and the residual strain (i.e. the strain which remains more or less constant within the tube) is a better direct comparison since it represents the recompression inside the tube. This value is closer to that predicted, but is still 10-50% higher, for soil elements at a depth of 3B.

Legend for Figure 4.22 to Figure 4.33:	
	Initial depth of soil element= 1B under base of borehole
	1.5B
	2B
	2.5B
	3B
	CSP from Baligh *et al* (1987), constant over depth

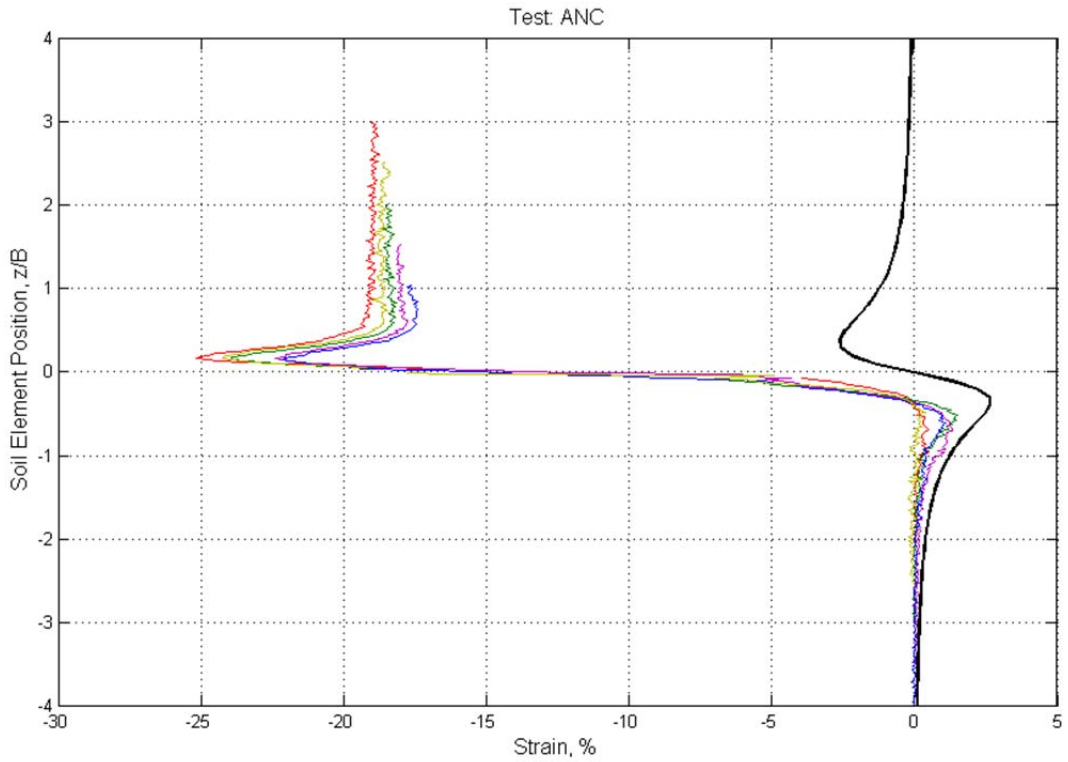

Figure 4.22 - Centreline Strain Path: ANC

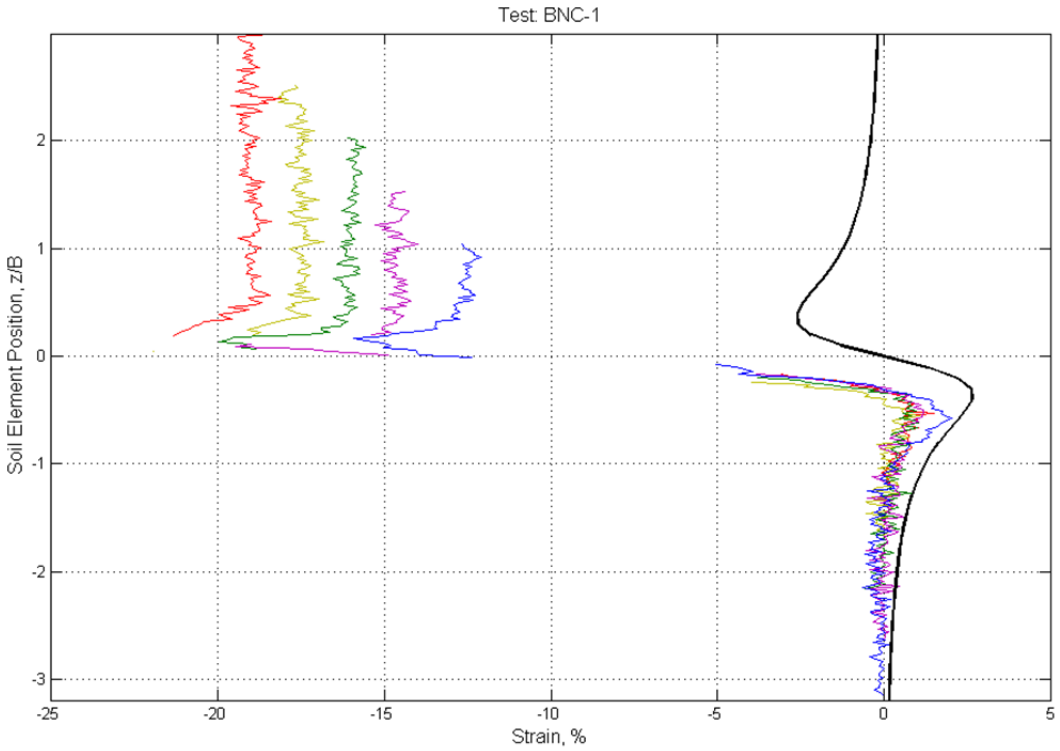

Figure 4.23 – Incomplete Centreline Strain Path: BNC-1

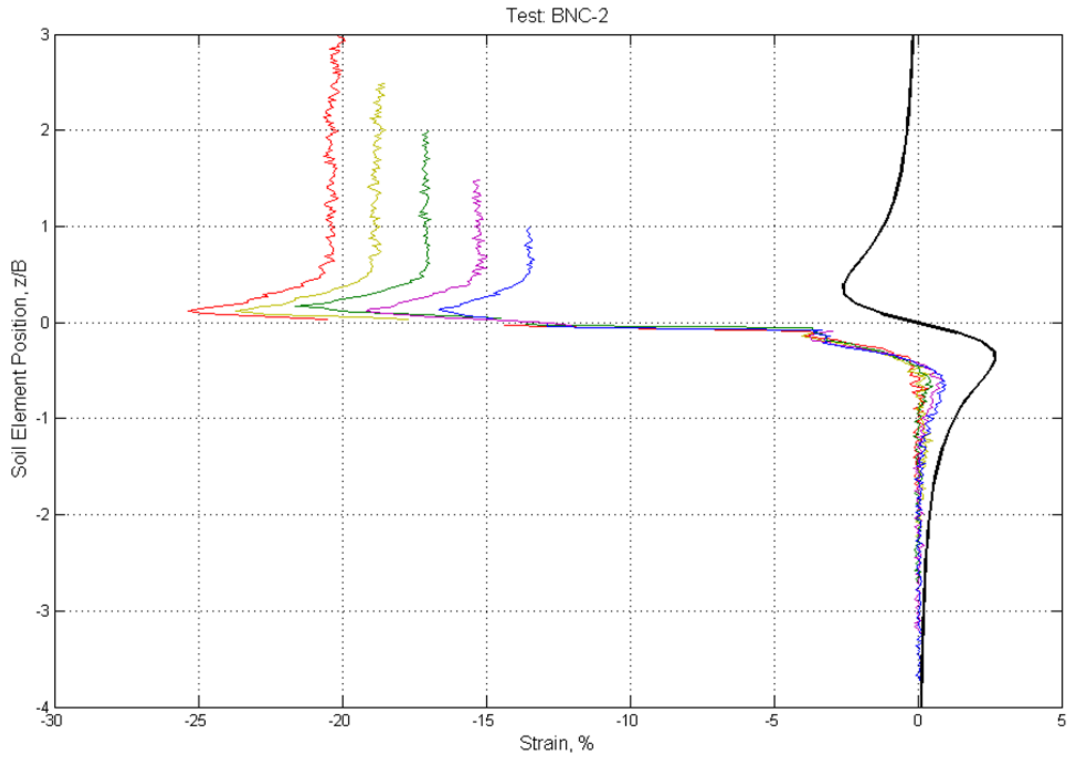

Figure 4.24 - Centreline Strain Path: BNC-2

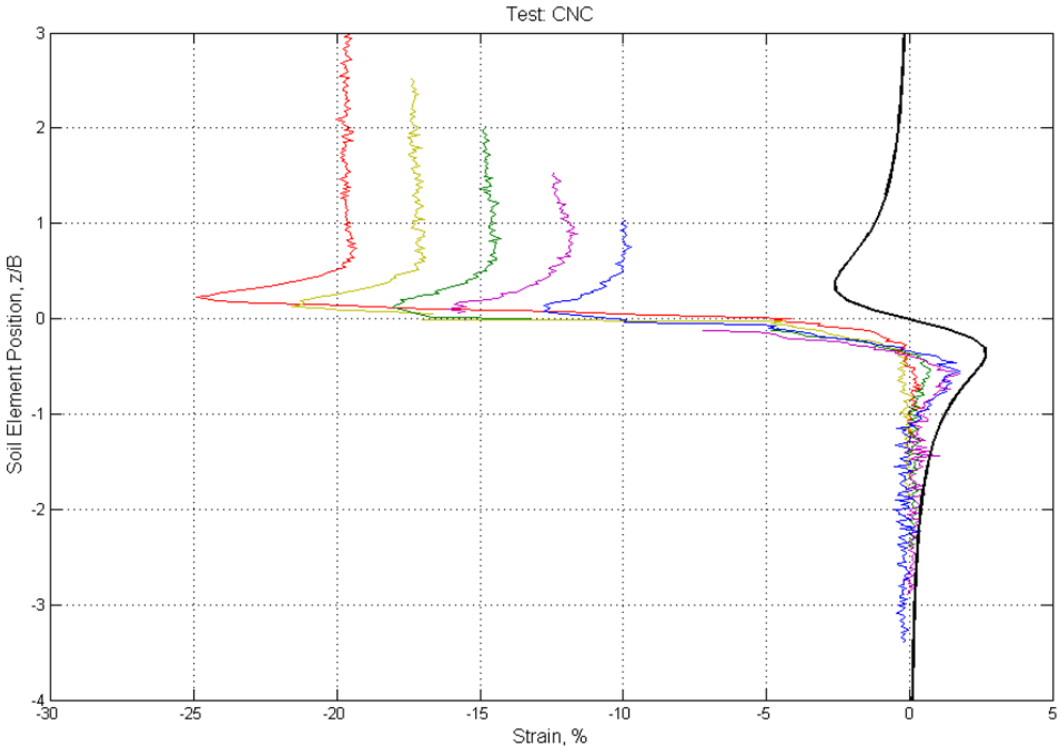

Figure 4.25 - Centreline Strain Path: CNC

Table 4.6 - Results of Tube Driving Tests in Normally Consolidated Soil, Thick Tubes

Test	Soil at Depth	Peak Compressive Strain (C), %	Peak Extensive Strain (E), %	Residual Strain (R), %	Δ(R) each 0.5 B, %	Peak E – R, %	Peak C – Peak E, %	Surface heave (mm)
ANC	B	0.4	-25.2	-19.1	0.3	6.1	25.6	0.8
	2B	1.5	-23.9	-18.4		5.5	25.4	
	3B	1.1	-22.2	-17.7		4.5	23.3	
BNC-1	B	1.0	-	-19.0	1.7	-	-	1.0
	2B	1.0	-20.0	-15.9		4.1	21.0	
	3B	1.7	-15.9	-12.7		3.2	17.6	
BNC-2	B	0.1	-25.4	-20.2	1.7	5.2	25.5	1.0
	2B	0.4	-21.6	-17.0		4.6	22.0	
	3B	0.9	-16.7	-13.5		3.2	17.6	
CNC-1	B	0.5	-25.0	-19.7	2.4	5.3	25.5	1.0
	2B	0.7	-18.0	-14.9		3.1	18.7	
	3B	1.7	-12.8	-9.9		2.9	14.5	
ISA, B/t=14.5	n/a	2.7	-2.6	<0.5	n/a	<2.6	5.3	n/a

4.5.2 Category 2: Thin Sampler, Normally Consolidated Soil

Category 2 comprises AtNC, BtNC and CtNC. The CSPs behaved similarly to those of thick tubes, with large extensive strains and compressive strains typically of the same order of magnitude as those predicted by Baligh *et al*. It is of note that the tube in AtNC penetrated at an angle of 1.5°, and tube BtNC experienced a significant downwards movement, both of which may influence results. Extensive sampling strains were approximately half those of thick-walled tubes, which supports the hypothesis that excess soil recovery is the main cause of the significant extension of the sample. Centreline Strain Paths are illustrated in Figure 4.26 to Figure 4.28, and data is summarised in Table 4.7.

Table 4.7 - Results of Tube Driving Tests in Normally Consolidated Soil, Thin Tubes

Test	Soil at Depth	Peak Compressive Strain (C), %	Peak Extensive Strain (E), %	Residual Strain (R), %	Δ(R) each 0.5 B, %	Peak E – R, %	Peak C – Peak E, %	Surface heave (mm)
AtNC	B	0.2	-9.1	-7.8	0.7	1.3	9.3	0.7
	2B	0.4	-7.5	-6.5		1.0	7.9	
	3B	1.4	-6.0	-5.2		0.8	7.4	
BtNC	B	0.2	-10.4	-8.6	1.3	1.8	10.6	0.7
	2B	0.4	-6.3	-5.5		0.8	6.7	
	3B	4.9	-4.6	-3.5		1.1	9.5	
CtNC	B	0.3	-6.4	-4.0	0.6	2.4	6.7	0.4
	2B	0.2	-8.4	-5.3		3.1	8.6	
	3B	0.1	-9.3	-6.5		2.8	9.4	
ISA, B/t=26.1	n/a	1.5	-1.4	<0.5	n/a	<1.4	2.9	n/a

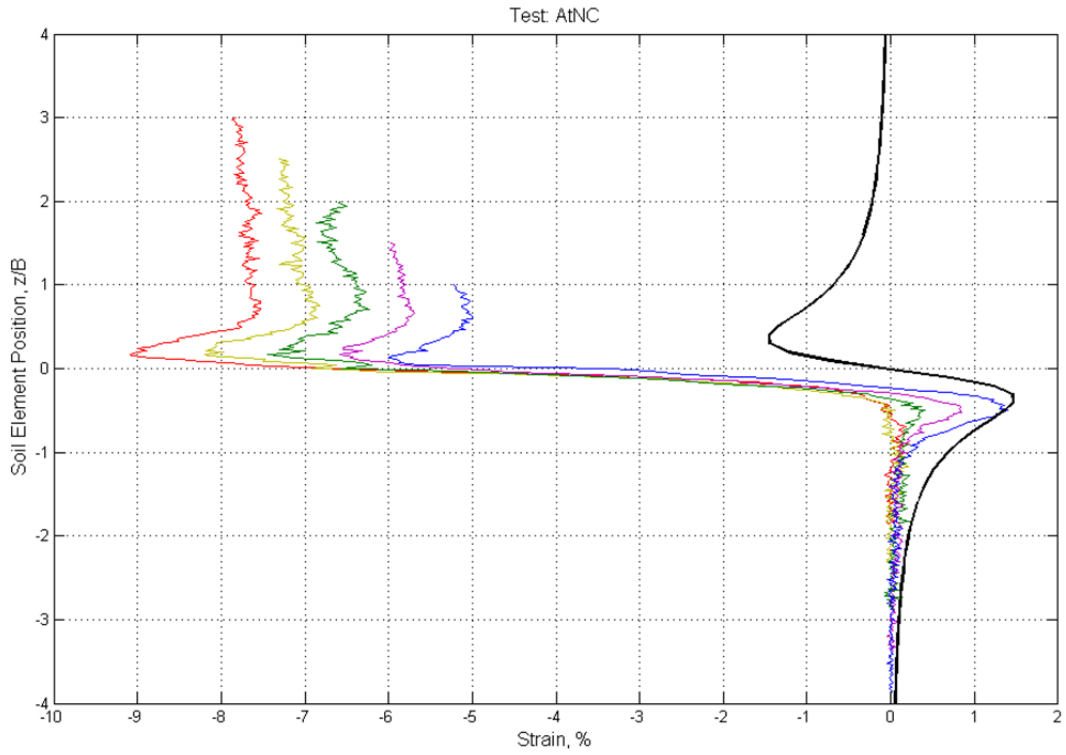

Figure 4.26 - Centreline Strain Path: AtNC

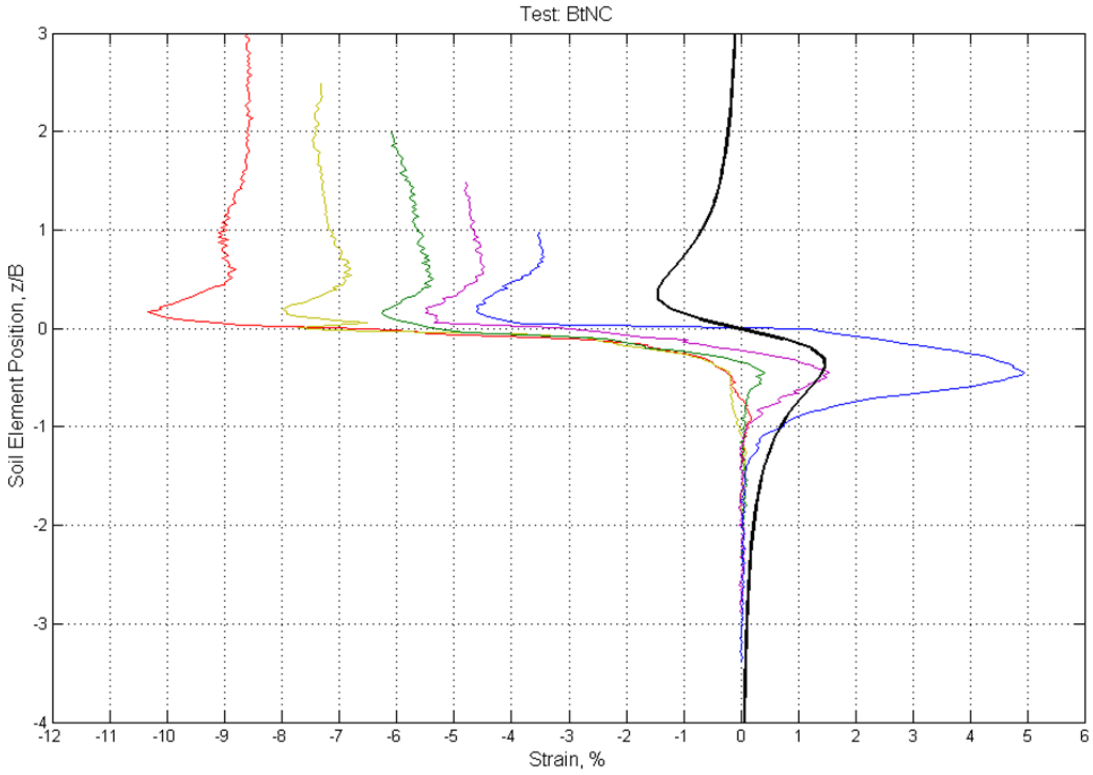

Figure 4.27 - Centreline Strain Path: BtNC

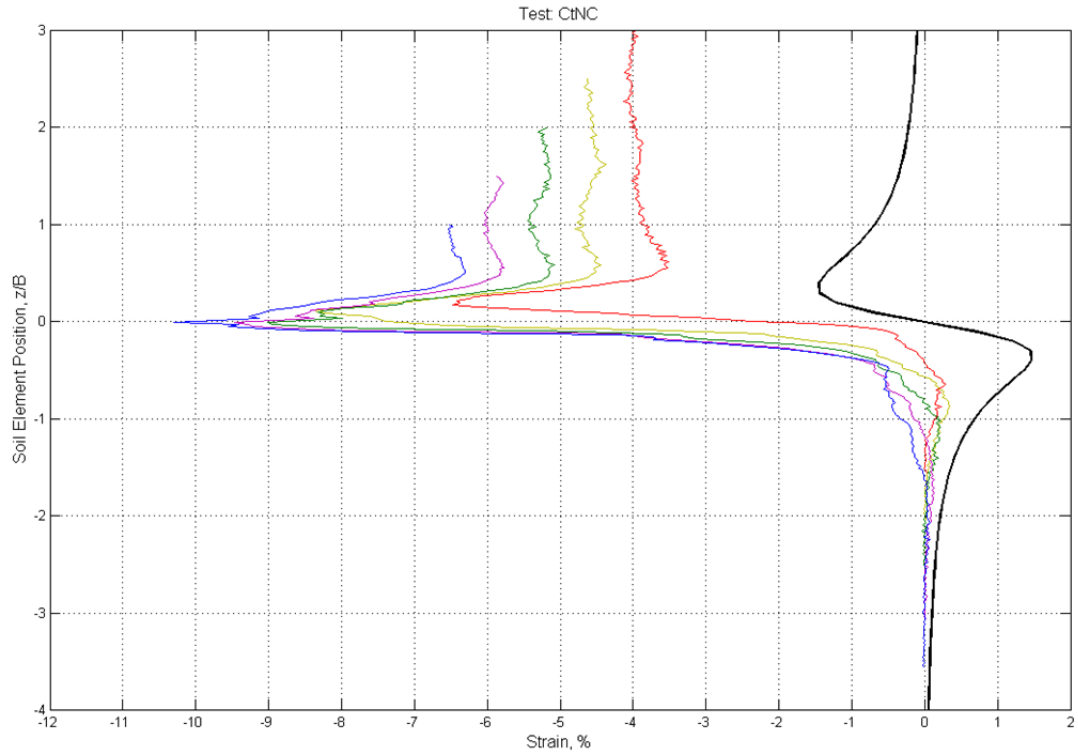

Figure 4.28 - Centreline Strain Path: CtNC

4.5.3 Category 3: Thick Sampler, Lightly Overconsolidated Soil

Category 3 comprises five tests in lightly overconsolidated soil (OCR=1.6): AOC-1, AOC-2, AOC-3, BOC and COC. AOC-1, AOC-2 and COC experienced some degree of downwards movement in the later stages of testing. Test BOC suffered from poor soil transparency due to a long model preparation time and because overconsolidated artificial soil is prone to losing transparency. Data close to the tube's cutting edge yielded wild vectors, making the CSP incomplete around z/B=0. Tests AOC-1 and AOC-2 were repeated because the tube was driven at an angle superior to 0.6°, causing plugging. Data from the CSPs is included in Table 4.8.

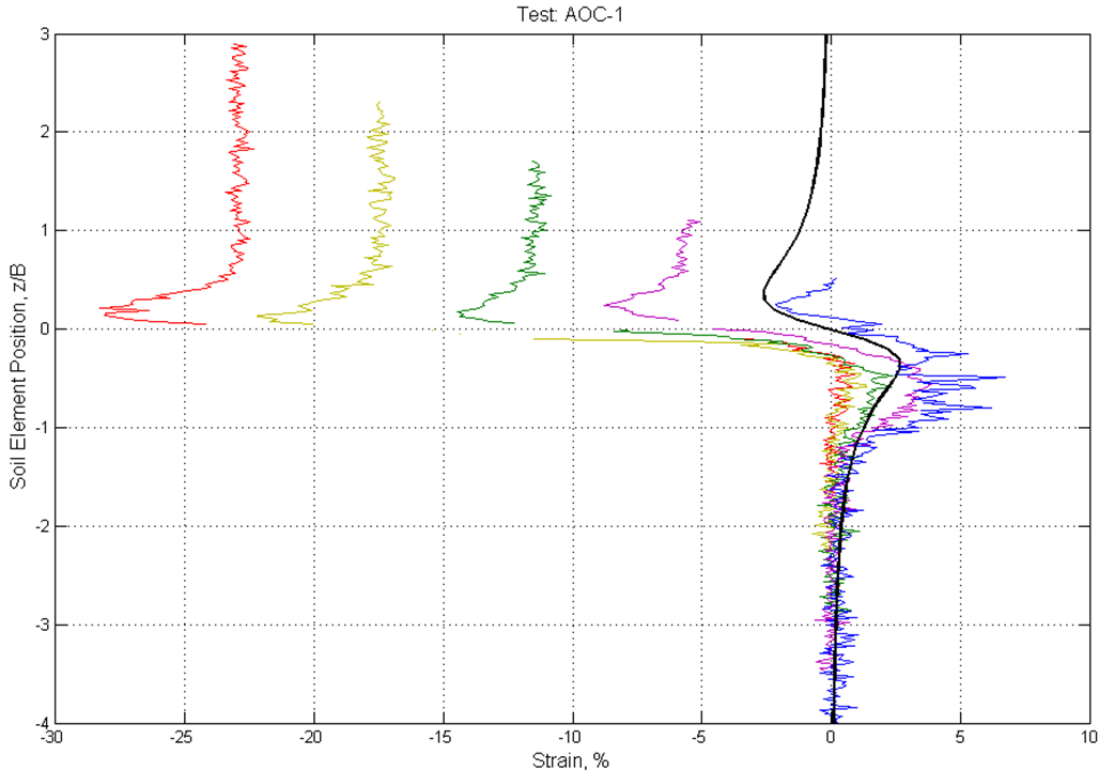

Figure 4.29 - Centreline Strain Path: AOC-1

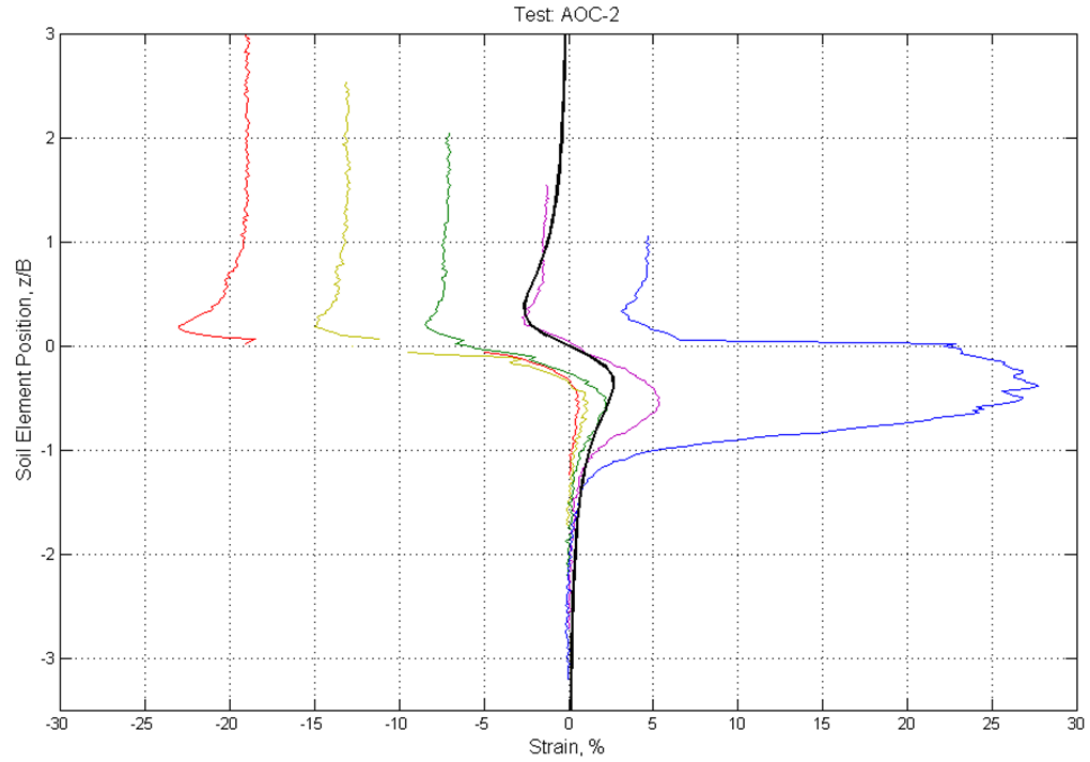

Figure 4.30 - Centreline Strain Path: AOC-2

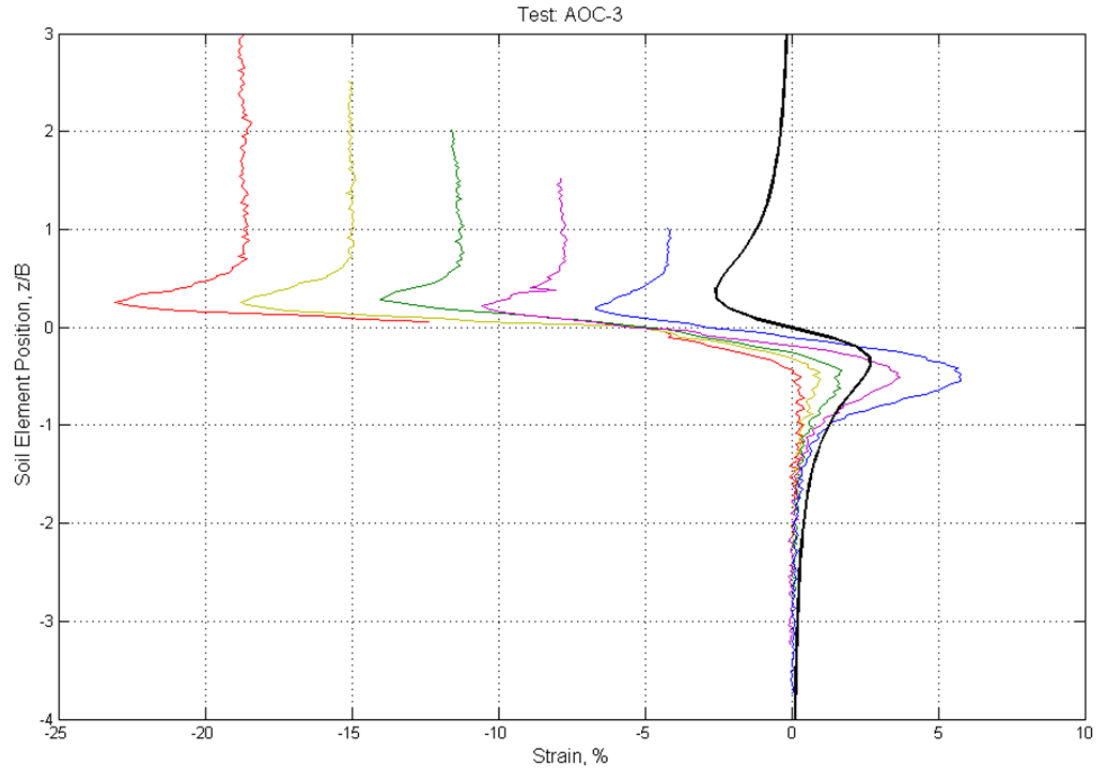

Figure 4.31 - Centreline Strain Path: AOC-3

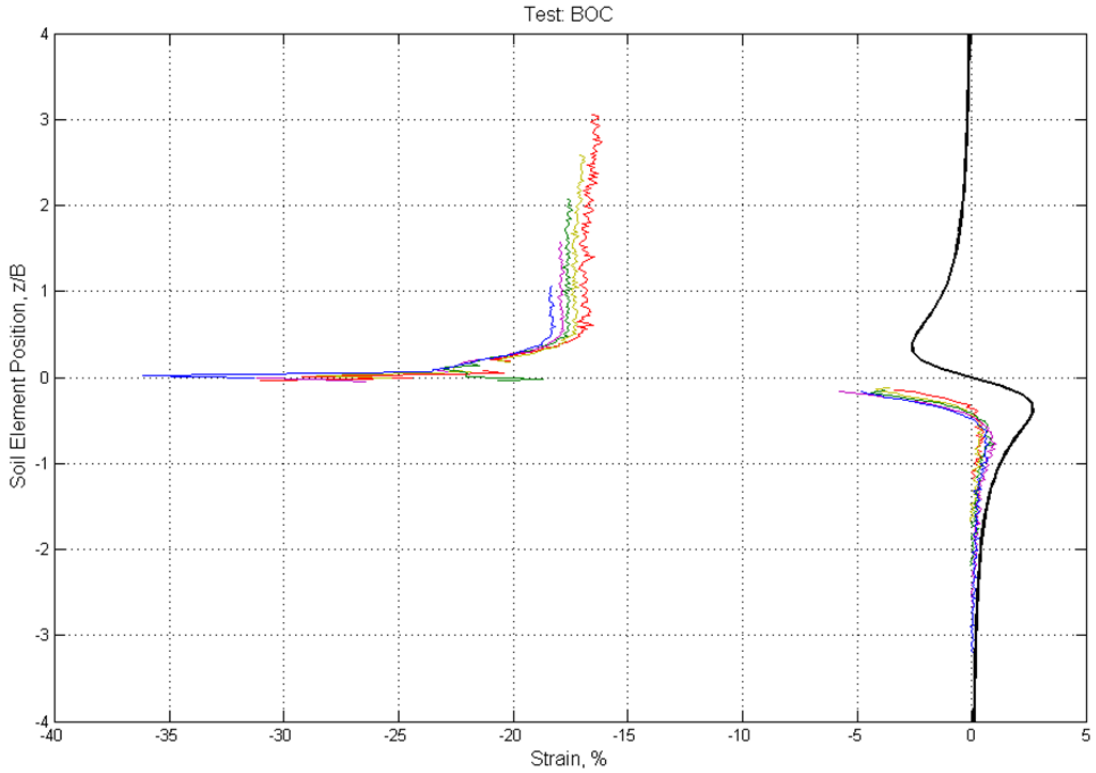

Figure 4.32 - Centreline Strain Path: BOC

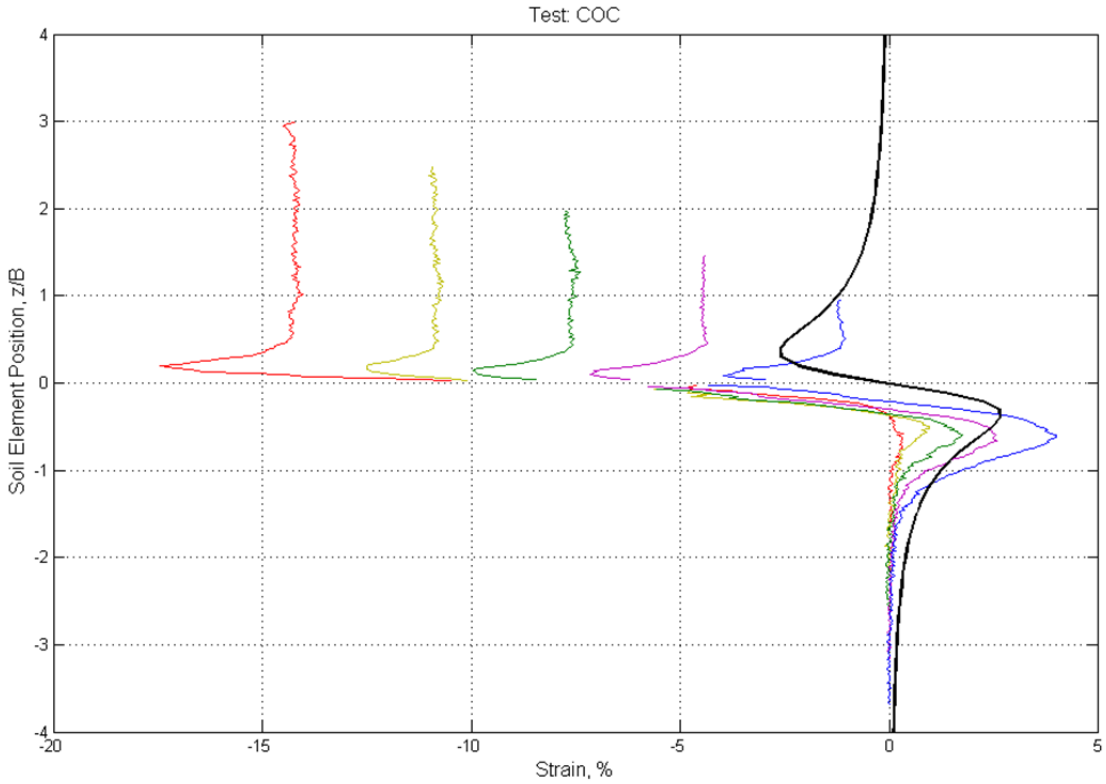

Figure 4.33 - Centreline Strain Path: COC

Table 4.8 - Results of Tube Driving Tests in Overconsolidated Soil, Thick Tubes

Test	Soil at Depth	Peak Compressive Strain (C), %	Peak Extensive Strain (E), %	Residual Strain (R), %	Δ(R) each 0.5 B, %	Peak E – R, %	Peak C – Peak E, %	Surface heave (mm)
AOC-1	B	0.9	-28.2	-23.0	5.8	5.2	29.1	0.9
	2B	2.2	-14.4	-11.5		2.9	16.6	
	3B	6.6	-2.1	-		-	8.7	
AOC-2	B	0.5	-23.0	-19.0	5.9	4.0	23.5	2.1
	2B	2.2	-8.5	-7.2		1.3	10.7	
	3B	27.8	+3.2	+4.7		1.5	24.6	
AOC-3	B	0.4	-23.0	-18.5	3.6	4.5	23.4	1.3
	2B	1.6	-14.0	-11.4		2.6	15.6	
	3B	5.7	-6.7	-4.2		2.5	12.4	
BOC	B	0.0	-29.1	-17.1	0.5	12.0	29.1	0.6
	2B	0.0	-23.0	-17.7		5.3	23.0	
	3B	0.0	-36.1	-18.4		17.7	36.1	
COC	B	0.4	-17.5	-14.2	3.2	3.3	17.9	1.1
	2B	1.7	-10.0	-7.7		2.3	11.7	
	3B	4.0	-4.0	-1.2		2.8	8.0	
ISA, B/t=14.5	n/a	2.7	-2.6	<0.5	n/a	<2.6	5.3	n/a

4.5.4 Initial Observations

All but two tests showed similar behaviour, soil elements close to the surface experienced larger extensive and residual strains and smaller compressive strains than soil elements at higher initial depths. The two exceptions were tests CtNC and BOC, which experienced an opposite trend: strains amplified with depth. While the causes of this anomaly are not clear, both these test are associated with an atypical surface heave. Each test category appears to have a typical rise, 1mm for thick tubes in NC soil, 0.7mm for thin tubes in NC soil, and uncertain for thick tubes in OC soil, but most probably superior to 1mm. Values for the CtNC and BOC tests are inferior to these, 0.4mm and 0.6mm respectively. Other tests which were required to be repeated (AOC-1, AOC- 5) also exhibit atypical heaves. This could be due to an issue with the consolidation rig which exerts pressure on the surface of the soil model. While it was identically set in all tests, failure of the pressure system may have occurred, either as a drop in pressure, which may explain relatively high surface rises, or if the pressure lever jammed during the test, which would hold the pressure plate in place against the surface of the soil, making it difficult for the soil to move upwards. It is of note that in the unconfined test, the soil heaved by 1.75mm when the thick-walled tube was inserted, which represents a significantly higher volume of soil pushed outwards into the soil than in the confined tests.

Test BNC-1 was repeated due to poor transparency. The results from both tests are similar, most strain measurements in the repeated test being only 5-8% higher than in the original, which shows that the test set-up is capable of obtaining repeatable results.

A comparison of the plotted CSPs with those predicted by the Strain Path Method reveals that the compressive strains are in fact overestimated by Baligh *et al* (1987). This was also observed by Siddique (1990), in an analytical study. Measured extensive and residual strains are an order of magnitude higher than those predicted by the SPM and by Siddique, and the behaviour is not antisymmetric, with much higher extensive strains than compressive strains. The residual strains decrease over depth, which suggests that the recovery ratio also decrerased with depth, or with the length of the sample. This agrees with Hvorslev (1949), who observed that the recovery ratio was over 100% in soil close to the

base of the borehole (i.e. the top of the sample), and reduced to under 100% at the lower end of the specimen (Figure 2.9).

4.6 Effect of Plugging

Only one comparison can be made to infer the effect of plugging on the strains experienced by the sample. Three tests were run with the same set-up: AOC-1, -2, and -3, with some evidence of plugging in the first, full plugging in the second and none in the third. The strains experienced during these tests are summarised in Table 4.9, where they have been normalised by the values for AOC-3. Because of the dimensions of the physical model, any plugging rapidly moves the soil into the zone close to the base of the model, which is rigid and therefore causes the soil to be compressed. The effect of plugging seen here refers to that in the test rather than that in real samples. Studying this sheds some light on the magnitudes of the values found in the tests where intermittent or full plugging is observed, and therefore assists in the task of comparing values between tests where some plugging is seen. This effect was more severe in test AOC-2, where the drive angle was 2.4° from the vertical, than in test AOC-1, where the drive angle was only 1.0°. The main effect of plugging is to increase the peak compressive strain, particularly in soil elements at depth, which are pushed into close proximity to the base of the box, where boundary effects are more pronounced. Comparing AOC-2 and AOC-3 gives a direct contrast between no plugging and full plugging, while AOC-1 is only partially affected – this is evident by the difference in compressive strains experienced in AOC-1 and AOC-2. The peak extensive strain and residual strain are also affected, and reduce with increased plugging. Again, the effects in AOC-2 are more pronounced than in AOC-1, where no effect is seen in upper layers (around a depth of 2B under the base of the borehole) on peak extensive and residual strains. Plugging is also associated with the movement of soil elements off of the centreline of the tube, which is apparent in the X portion of Figure G. 1 to Figure G. 12 as displacements of up to 15 mm in the direction perpendicular to the sometimes rotated centreline. Many of these changes are due to the movement of the sampling tube, which is more complex than if the angle of drive was 0°. Rather than comprise of a movement downwards along the rotated centreline of the tube (y vector), the sampler also experiences a purely vertical

movement (vector v, Figure 4.34). Soil was moved away from the centreline towards the lower side of the rotated sampler.

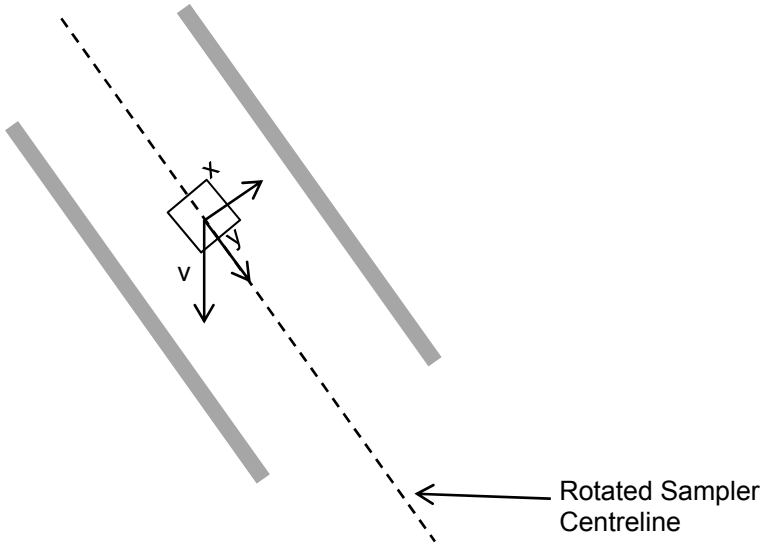

Figure 4.34 - Displacements caused by Rotated Centreline

Table 4.9 - Effect of Plugging on Strains Experienced by AOC

	at Initial Depth	AOC-1	AOC-2	AOC-3
Peak C Strain	2B	1.38	1.38	1.00
	3B	1.16	4.88	1.00
Peak E Strain	2B	1.03	0.61	1.00
	3B	0.31	-	1.00
Residual Strain	2B	1.01	0.63	1.00
	3B	-	-	1.00

4.7 Effect of Cutting Edge Geometry

The aim of this research was to obtain three sets of data, one for each category, so that the effects of tube geometry and soil overconsolidation ratio could be compared. Unfortunately, due to plugging in five tests and possible equipment malfunction in two tests, this was not fully possible. To study the effect of cutting edge geometry on the extent of tube sampling disturbance, the following comparisons are made:

- Category 1: ANC, BNC-1, BNC-2, CNC – no reported issues
- Category 2: AtNC, BtNC – caution in analysis due to significant plugging in BtNC, and possible effects in AtNC due to small plugging phase at the end of the test: it is expected that compressive strains may be overestimated and extensive and residual strains may be underestimated.

- Category 3: AOC-3, COC– caution in analysis due to small plugging phase at the end of test COC – here again, compressive strains may be overestimated and extensive and residual strains may be underestimated.

Table 4.10 presents the peak compressive and extensive strain results from Table 4.6 to Table 4.8, normalised by the strains generated by tube geometry A for each depth in each category. Blunt tubes (Geometry A) produce higher peak extensive strains than both sharp tubes, and those with inside clearance. Tapering even a short length of the tube's cutting edge (1.5mm in thin tubes and 3mm in thick tubes) can reduce the peak extensive strains by 23 and 25% at a depth of 3B into the sample, for thin and thick-walled tubes respectively. Increasing the Inside Clearance from 0.4% to 3.3% in thick-walled tubes reduces the peak extensive strain by 40-42% in both lightly OC and NC soils. Peak compressive strains are over an order of magnitude smaller than extensive strains, and the effect of tube geometry on these in uncertain. It appears that small variations in the running of the test can influence the peak compressive strains more significantly than any given cutting edge geometry. It can be tentatively suggested that increasing Inside Clearance may increase peak compressive strains. Data from test BtNC is affected by plugging, and hence the downward movement of the soil brings the sample into close proximity of the base of the box, where it can experience higher compression between the plug and the rigid base, which could explain the high value of peak compression. In the final successful run of test BNC, the peak compressive strains are smaller than those generated when using a blunt tube.

Table 4.10 - Effect of Cutting Edge Geometry on Peak Strains

	Peak Extensive Strain			Peak Compressive Strain		
Category 1: ANC, BNC-1, BNC-2, CNC						
Depth	Geometry A	Geometry B	Geometry C	Geometry A	Geometry B	Geometry C
B	1.00	- / 1.01	0.99	1.00	2.50 / 0.25	1.25
2B	1.00	0.84 / 0.90	0.75	1.00	0.67 / 0.27	0.47
3B	1.00	0.72 / 0.75	0.58	1.00	1.82 / 0.82	1.55
Category 2: AtNC, BtNC						
B	1.00	1.14	-	1.00	1.00	-
2B	1.00	0.84	-	1.00	1.00	-
3B	1.00	0.77	-	1.00	3.50	-
Category 3: AOC-3, COC						
B	1.00	-	0.76	1.00	-	1.00
2B	1.00	-	0.71	1.00	-	1.06
3B	1.00	-	0.60	1.00	-	0.70

Residual strains indicate the degree of disturbance to the soil structure which remains inside the tube. In many analytical models, this eventually approaches zero, but can be affected by the cutting edge geometry (Clayton *et al,* 1998). In all twelve tests, significant amounts of residual strains were observed. This is in large part due to the recovery of excess soil, but varies with cutting edge geometry and tube thickness. The residual strains are significant in soil elements originally close to the base of the borehole, but reduce with depth.

Table 4.11 - Effect of Cutting Edge Geometry on Residual Strains

	Residual Strain		
Category 1: ANC, BNC-1, BNC-2, CNC			
Depth	Geometry A	Geometry B	Geometry C
B	1.00	0.99 / 1.06	1.03
2B	1.00	0.86 / 0.92	0.81
3B	1.00	0.72 / 0.76	0.56
Category 2: AtNC, BtNC			
B	1.00	1.10	-
2B	1.00	0.85	-
3B	1.00	0.67	-
Category 3: AOC-3, COC			
B	1.00	-	0.77
2B	1.00	-	0.68
3B	1.00	-	0.29

Again, sharpening the cutting edge reduces strain significantly, by 24% in thick tubes and by 33% in thin tubes at a depth 3B, while increasing the ICR reduces residual strain by 44 and 71% in NC and lightly OC soils respectively (Table 4.11).

Peak to peak strains have also been included in the analysis since the variations in peak compressive strain were not successfully linked to tube geometry. These quantify the full strain cycle experienced by the specimen. Recompression is defined as the difference between the peak extensive and residual strains, and gives a measure of the soil's behaviour inside the tube. High residual strains indicate a large permanent alteration to the soil's structure. Similar to previously, using a thick-walled sampler, the peak to peak strain was highest in blunt tubes, with strains in sharp tubes 23-24% lower in NC soils and 35% lower in OC soils. Using an ICR also reduced the peak to peak strain by 38% in NC soils (Table 4.12). In thin samplers, the peak to peak and recompression strains appear larger in tubes with a sharp cutting edge, but as previously, these are exaggerated by the plugging effects in BtNC.

Table 4.12 - Effect of Cutting Edge Geometry on Peak to Peak and Recompression Strains

	Peak to Peak Strain			Recompression		
Category 1: ANC, BNC-1, BNC-2, CNC						
Depth	Geometry A	Geometry B	Geometry C	Geometry A	Geometry B	Geometry C
B	1.00	- / 1.00	1.00	1.00	- / 0.85	0.87
2B	1.00	0.83 / 0.87	0.74	1.00	0.75 / 0.84	0.56
3B	1.00	0.77 / 0.76	0.62	1.00	0.71 / 0.71	0.64
Category 2: AtNC, BtNC						
B	1.00	1.14	-	1.00	1.38	-
2B	1.00	0.85	-	1.00	0.80	-
3B	1.00	1.28	-	1.00	1.38	-
Category 3: AOC-3, COC						
B	1.00	-	0.76	1.00	-	0.73
2B	1.00	-	0.75	1.00	-	0.88
3B	1.00	-	0.65	1.00	-	1.12

The above data can be compared with that published by Siddique (1990), who used an analytical model to simulate tube sampling disturbance in specimens taken with a range of cutting edge geometries. Table 4.13 shows that both studies agree on the effects of taper angle on the strains generated within the sample in all points but one: in his study, Siddique found that increasing the taper angle from 5 to 19.3° reduced the amount of recompression experienced by the sample. In this study, however, recompression increases with bluntness.

The studies on the effects of ICR disagreed on most points, most significantly on the behaviour in extension. Siddique predicted increased peak extensive strains in tubes with larger inside clearances. In this study, 2D vertical strain is considered. It is possible that a horizontal strain component due to the lateral expansion of the sample as it enters the tube plays a part in the increase seen in the analytical model. Consequently, the peak to peak and recompression strains are affected.

Table 4.13 - Comparison of Results with Siddique (1990)

		This study	Siddique (1990)
Effect of increasing ICR on …	Peak C Strain	possibly increased	reduced
	Peak E Strain	reduced	increased
	Residual Strain	reduced	reduced
	Peak to Peak Strain	reduced	increased
	Recompression	reduced	increased
Effect of increasing Taper Angle on ...	Peak C Strain	increased	increased
	Peak E Strain	increased	increased
	Residual Strain	increased	increased
	Peak to Peak Strain	increased	increased
	Recompression	increased	reduced

4.8 Effect of Area Ratio

In this section, results are normalised by the strains generated during tube penetration of a thick-walled sampler. Table 4.14 compares the peak strains in thick and thin-walled tubes. The effect of Area Ratio is more pronounced than sampler cutting edge geometry, since it governs the volume of soil displaced by the sampler compared to that of the sample itself. Unsurprisingly, extensive strains caused by the recovery of excess soil are 59-73% lower in thin-walled tubes. This agrees with results from studies by Siddique *et al* (2000, 2009), Gosling and Baldwin (2010) and others on natural clays. The effect on compressive strains is less pronounced, but it is reminded that BtNC is affected by plugging, and hence the downward movement of the soil brings the sample into close proximity of the base of the box, where it can experience higher compression between the plug and the rigid base. Similarly, in test AtNC, deeper elements will be more affected by the small phase of plugging at the end of the test, which could explain the high value of peak compression. In soil less affected by plugging, increasing the AR increases the peak compressive strain.

Table 4.15 compares the residual strains in thick and thin-walled tubes. Similarly to extensive strains, those in thin-walled samplers are less affected, with strains at depth as low as a quarter of those in thick-walled tubes. The thin-walled tubes in this study are at the borderline of being classified as thick according to Eurocode 7, meaning that real thin-walled tube samplers will be even less affected by excess soil recovery and large extensive and residual strains.

Table 4.14 - Effect of AR on Peak Strains

	Peak Extensive Strain		Peak Compressive Strain	
Geometry A: ANC, AtNC				
	Thick-walled tube	Thin-walled tube	Thick-walled tube	Thin-walled tube
AR	34-35%	16-17%	33-34%	15-16%
Depth: B	1.00	0.36	1.00	0.50
2B	1.00	0.31	1.00	0.27
3B	1.00	0.27	1.00	1.27
Geometry B: BNC-2, BtNC				
B	1.00	0.41	1.00	2.00
2B	1.00	0.29	1.00	1.00
3B	1.00	0.28	1.00	5.44

Table 4.15 - Effect of AR on Residual Strains

	Residual Strain	
Geometry A: ANC, AtNC		
	Thick-walled tube	Thin-walled tube
AR	34-35%	16-17%
Depth: B	1.00	0.41
2B	1.00	0.35
3B	1.00	0.29
Geometry B: BNC-2, BtNC		
B	1.00	0.43
2B	1.00	0.32
3B	1.00	0.26

Table 4.16 presents the effects of AR on peak-to-peak strain and recompression. The overall strain cycle in tubes with a lower Area Ratio is 46-68% smaller than that in thicker tubes, despite an increase in compressive strains due to plugging. Samples taken in thinner tubes are also subjected to 64-82% less recompression inside the sampler.

Table 4.16 - Effect of AR on Peak to Peak Strain and Recompression

	Peak to Peak Strain		Recompression	
Geometry A: ANC, AtNC				
	Thick-walled tube	Thin-walled tube	Thick-walled tube	Thin-walled tube
AR	34-35%	16-17%	33-34%	15-16%
Depth: B	1.00	0.36	1.00	0.21
2B	1.00	0.31	1.00	0.18
3B	1.00	0.32	1.00	0.18
Geometry B: BNC-2, BtNC				
B	1.00	0.42	1.00	0.35
2B	1.00	0.30	1.00	0.17
3B	1.00	0.54	1.00	0.34

Table 4.17 compares the results of this study with those of Siddique (1990) on the influence of AR on the extent of sampling disturbance. Both studies agree on most points, with one notable exception. Increasing the Area Ratio of a tube is seen to increase the amount of recompression experienced by the sample in this study, while it is predicted to reduce by Siddique.

Table 4.17 - Effect of AR: Comparison with Siddique (1990)

		This study	Siddique (1990)
Effect of increasing AR on …	Peak C Strain	increased	increased
	Peak E Strain	increased	increased
	Residual Strain	increased	increased
	Peak to Peak Strain	increased	increased
	Recompression	increased	decreased

4.9 Effect of Overconsolidation Ratio

The effects of OCR on the extent of sampling disturbance are more clear-cut. Results in Table 4.18 have been normalised at each depth by values for NC soil. Similarly to the comparisons made previously, observed effects are amplified with depth. Peak Extensive strains are 69-70% lower at depth in lightly OC soils than they are in NC soils, while peak Compressive strains are significantly higher in OC soils. Residual Strains are also reduced in OC soils, by up to 88% in samplers designed with inside clearance. Table 4.19 presents the residual strains normalised at each depth by those in NC soil.

Table 4.18 - Effect of OCR on Peak Strains

	Peak Extensive Strain		Peak Compressive Strain	
	NC	OC	NC	OC
Geometry A: ANC, AOC-3				
Depth: B	1.00	0.91	1.00	1.00
2B	1.00	0.59	1.00	1.07
3B	1.00	0.30	1.00	5.18
Geometry C: CNC, COC				
B	1.00	0.70	1.00	0.80
2B	1.00	0.56	1.00	2.43
3B	1.00	0.31	1.00	2.35

Table 4.19 - Effect of OCR on Residual Strains

	Residual Strain	
	NC	OC
Geometry A: ANC, AOC-3		
Depth: B	1.00	0.97
2B	1.00	0.62
3B	1.00	0.24
Geometry C: CNC, COC		
B	1.00	0.72
2B	1.00	0.52
3B	1.00	0.12

Table 4.20 presents the data for peak-to-peak strain and recompression, both of which are reduced in OC soils, by 45 and 47% for blunt tubes and 38 and 44% for tubes with an inside clearance.

These findings agree with work by Santagata and Germaine (2005) on Resedimented Boston Blue Clay (RBBC), who observed a significant reduction in the effects of sampling disturbance in soils with increasing OCR.

Table 4.20 - Effect of OCR on Peak-to-Peak and Recompression Strains

	Peak to Peak Strain		Recompression	
	NC	OC	NC	OC
Geometry A: ANC, AOC-3				
Depth: B	1.00	0.91	1.00	0.74
2B	1.00	0.61	1.00	0.47
3B	1.00	0.53	1.00	0.56
Geometry C: CNC, COC				
B	1.00	0.70	1.00	0.62
2B	1.00	0.63	1.00	0.74
3B	1.00	0.55	1.00	0.97

4.10 Discussion

In these last sections, the influence of Inside Clearance Ratio, Outer Cutting edge Angle, Area Ratio and Overconsolidation Ratio on the extent of sampling disturbance were investigated. The results of tests on a physical model were used to study the displacement in and around the sampling tube over time, and to calculate the strains on the centreline of the sampler over time, which defined the Centreline Strain Paths for each tube geometry / soil OCR combination. The following points could be compared with existing analytical studies:

- The shape of the Centreline Strain Path
- The magnitude of the strains in the CSP
- The effect of ICR, AR, OCR on peak extensive strains, peak compressive strains, residual strains, peak-to-peak strains and recompression.

It is of note that while the analytical studies do not suffer from close boundary effects due to the walls of the model, or small variations in set-up, they depend on user-defined geometry and material parameters, which may or may not reflect the actual behaviour of soil during tube driving.

In open-drive tubes, it appears that the area ratio defines the degree of disturbance, since much of this is due to excess soil recovery. In past analytical models, the predicted extensive strains on the sample's centreline were an order of magnitude lower than those measured in the tube-driving tests. These large extensions are due to excess soil recovery in tests where a pressure plate is applied to the surface of the soil model to simulate the effects of an overburden pressure around the base of the borehole. In the test without the

pressure plate, large extensive strains do not develop, and the behaviour is comparable to that predicted by Baligh *et al* (1987). In both cases, and using all tube geometry and soil OCR combinations, three phases of strains were identified: compression ahead of the sampler, extension as the soil element approaches and enters the tube, and finally another phase of compression as the sample travels upwards into the sampler. The presence of these three phases has been predicted and observed by a number of researchers (Baligh *et al*, 1987, Siddique, 1990, Budhu and Wu, 1992, van Eekelen and van den Berg, 1995, Clayton *et al*, 1998, and to some extent by Yan *et al*, 2010). In these studies, the strain cycle in the Centreline Strain Path – when quantified – was an order of magnitude lower than those found in this study using the pressure plate. In the original research by Baligh *et al*, the CSP was found to be antisymmetric about the point at which the soil entered the sampler, and depended neither on the soil element's depth, nor the sampling tube's geometry. Further research by others disproved the latter hypothesis by investigating the strain paths created by different samplers in analytical models. It was found that varying AR, ICR, and OCA modified the peak compressive and extensive strains experienced by the sample, and that the strain path was not antisymmetric, with – depending on the tube's geometry – either more significant peak compressive or extensive strains. In the analytical and numerical models, excess soil recovery was not considered, yet in the physical model in this study, this behaviour dominated the extensive strains developing within the sample. In two tests, a plug appeared to form inside the sampling tube from the start of driving, while in three others, plugging was experienced at one stage during the tube's penetration into the ground, often near the end of the drive.

It has been assumed in existing analytical models that the CSP was the same for any given soil element on the centreline of the sampler. In all tests – confined and unconfined – this was found not to be true. Elements closest to the base of the borehole are the worst affected, with lower peak compressive strains and higher peak extensive strains.

Sampler cutting edge geometry and OCR of the soil affect the magnitudes of the strains experienced by the specimen.

The extent of disturbance increases with:

- Decreasing OCR
- Increasing AR
- Increasing OCA
- Decreasing ICR

The results of this study generally agree with the existing literature on this subject, although some new elements have been found to have a more severe impact than previously thought. In particular, excess soil recovery is a little studied phenomenon which was seen to affect all open-tube driving experiments in this study, whereas it is not considered in the analytical solutions. This has important implications for the use of thick walled open drive tubes in site investigation, since these can produce severely distorted samples. A comparison of an unconfined test – where no pressure was applied to the surface of the model during tube driving – with data from Baligh *et al*'s (1987) analytical solution, the Strain Path Method, revealed differences in soil behaviour. In the numerical and analytical studies reviewed in Chapter 2, the solution is identical at any given depth. It is apparent from the shallow strain path method by Sagaseta et al (1997) that any soil deposit close to being unconfined will have a behaviour different from deeper deposits, for which the Strain Path Method was devised. In real cases of sampling, soil at different depths in the borehole will tend towards following the general solution for either deep or shallow soil elements. In any case, when modelling tube penetration, overburden conditions must reflect those in the ground: while sampling is indeed a "deep" penetration problem, many samples which are taken are short, in the order of 450mm, and in the case of open-tube sampling, are taken straight from the base of the borehole, meaning that most samples taken with open ended tubes will indeed undergo some lengthening, especially in the top part of the specimen. Even when a slurry or fluid is used to support the borehole, the stress upon the base of the borehole will not equal that in the soil around it, and excess soil recovery may occur.

Clay samples having experienced strains over ±5% are irreversibly distorted, their shear strength and stiffness reduced. Even using appropriate techniques of recompression or reconsolidation in the triaxial cell, these samples will no longer reflect their in-situ behaviour

(Clayton *et al,* 1992, Santagata and Germaine, 2005). The strains experienced in this study are larger than this in the top three tube diameters of the sample, and often below this as well, especially in the case of thick-walled tubes.

Plugging was also observed, and affected samplers where the drive angle was superior to 1° from the vertical. The tolerance for a straight, unaffected sample is therefore relatively small, especially in soils where rigid objects are present which can deflect the tube off its original orientation.

All of these elements combine to produce samples with a severely distorted internal structure in the top of the specimen, with disturbance reducing over depth. It is likely that the strains due to excess soil recovery even in thinner tubes are sufficient to produce irrecoverable changes in strength and stiffness in the upper portion of the sample. Deeper soil will be less affected by excess soil recovery, which is encouraging for longer continuous samples, although short samples taken with open ended tubes (e.g. 450mm U100) may contain only a small proportion of usable soil for laboratory testing.

Chapter 5: Physical Modelling of Tube Storage and Sample Extrusion

5.1 Introduction

Sampling disturbance does not exclusively occur during tube driving. During storage, negative pore pressures and variations in moisture content across the sample set up during tube driving can redistribute, causing some change to the soil's structure. During extrusion, the forces on the sample inside the tube can be comparable to those during tube driving, and the friction at the tube edge may cause some amount of disturbance. Two sets of tests are presented in this section. In the first, four samples were kept inside their tubes, sealed with paraffin wax after being removed from the model during tube sampling tests, and monitored over six months to determine whether any pore water movement or redistribution during storage would create strains inside the sample. In the second, six samples were extruded from their tubes after storage and the strain paths on the centreline and at the edge were measured to determine the extent of disturbance experienced by the sample during extrusion.

5.2 Sample Storage

Four tubes with different cutting edge geometries and soil conditions (normally and overconsolidated) were kept upright in a rack, and photographed twice weekly over six months using a Pentax K-r. These were:

- ANC: geometry A (blunt, thick tube), normally consolidated
- CNC: geometry C (rolled cutting edge with inside clearance, thick tube), normally consolidated
- AOC: geometry A (blunt, thick tube), overconsolidated
- BOC: geometry B (sharp, thick tube), overconsolidated

Tube BOC replaced the original choice of tube COC due to logistical problems. It had been planned to investigate the differences between tubes with and without inside clearance.

The set-up was darkened using a blackout curtain and backlit using a light box. Circular stickers were placed on the light box to study the apparent movement of the background due to camera shake. From data taken from 15 such markers, it became apparent that camera shake was significant and not easy to correct for. Apparent movements of these immobile points between frames were typical of a slight rotation, up to the magnitude of 0.2°, with vectors up to 40 pixels, or 4mm. This type of movement is not easily removed using image registration since the PIV analysis treats all displacements at pure translations in x and y directions rather than rotations. Strains would have remained the same regardless of camera rotation, provided that the distance between the tubes and camera remained the same, while displacements would be greatly affected. Figure 5.1a and Figure 5.1b represent apparent movements in tube CNC at three and six months storage time. Displacement vectors have been scaled up 20 times.

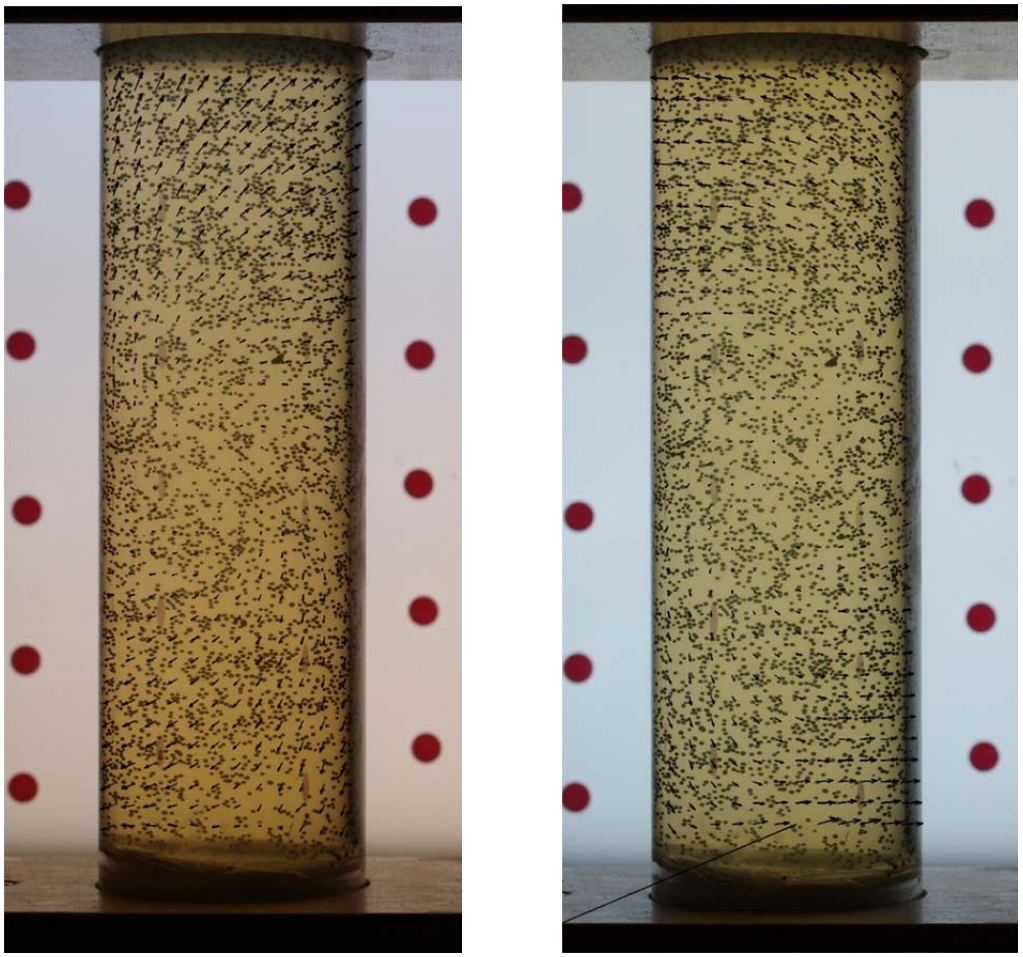

a b

Figure 5.1 - Apparent Movement due to Camera Shake (Monitoring Tests) at a) 3 Months and b) Six Months Storage Time

The reversal of direction of the vectors points to a random movement of the camera rather than to a real soil movement. Similar behaviour was observed in other photographs, where movements appeared to develop and disappear over time.

It was decided to study volumetric strains in the whole sample. A grid of Interrogation Areas was created over the inside of the tube in the first photograph and a Matlab script was written to calculate strains between each set of four IAs, as illustrated in Figure 5.2. The area enclosed by the four centroids was compared to its original area, and the area strain, or volumetric strain (ε_v) was expressed in percentage change (Equation 26). This is true assuming that the strain conditions are axis-symmetric. For comparative purposes, four parts of the sample were considered, from the top quarter to the lowest quarter, each divided into 96 Interrogation Areas (Figure 5.3).

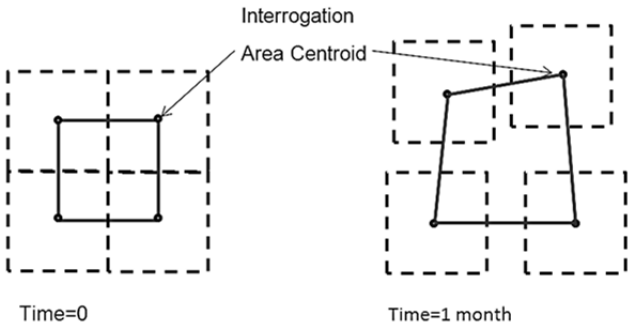

Figure 5.2 - Change in Area Enclosed by Four Interrogation Areas

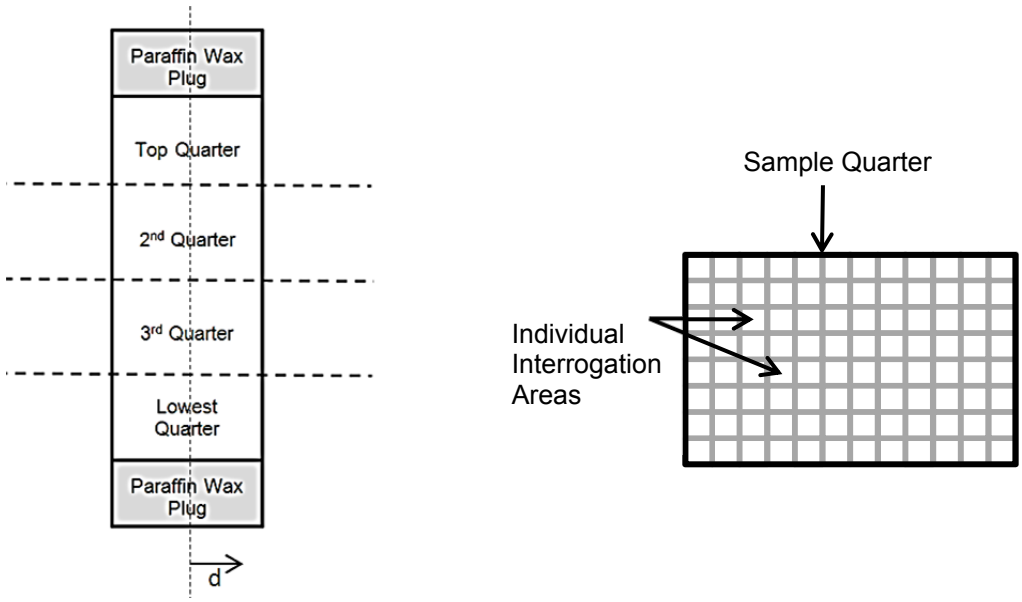

Figure 5.3 - Division of Sample for Analysis

$$\varepsilon_v = 100 \times \frac{(\sqrt{A})^3 - (\sqrt{A_o})^3}{(\sqrt{A_o})^3}$$ Equation 26

With A_o= Original Area between 4 IA centroids, A= Area between 4 IA centroids at any time.

Data for each of the four tubes is presented for 1, 3 and 6 months storage time in Appendix H, and the behaviour observed in test ANC is illustrated in Figure 5.5. In all cases, the soil closest to the centreline experienced a rise in volume, or swelling, while the soil close to the walls shrank. Volumetric strains were small, mostly in the range ±1.5%. These strains suggest a migration of pore fluid from the side of the sample, towards the centreline. This behaviour agrees with results from a study by Chandler et al (1992), who reported an increased water content in the outer soil layers in recently retrieved samples. Maximum and minimum limits containing 95% of the data in Figure H. 1 to Figure H. 12 are presented in Table 5.1, to the nearest 0.05%. It is seen that this fluid migration is typically more severe in soil in either extremity of the specimen than in the centre, and that the bottom quarter of the sample is often the worst affected. This behaviour increases over time, with strains typically rising by 50-150% between 1 and 6 months storage time. Differences between tubes do not appear to be linked to tube geometry or soil Overconsolidation Ratio, but rather depend on the integrity of the paraffin seal. A loss of moisture over the lower part of the sample is visible in all samples at different storage times, with the formation of an air pocket adjacent to the seal (Figure 5.4). This is usually present in multiple photos, and can remain for a number of weeks.

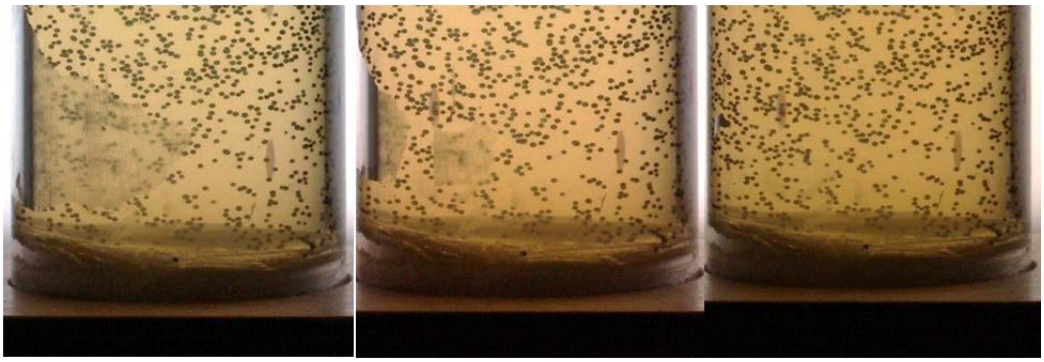

Storage Time (days):	137	140	155

Figure 5.4 – Air Pocket in Test CNC

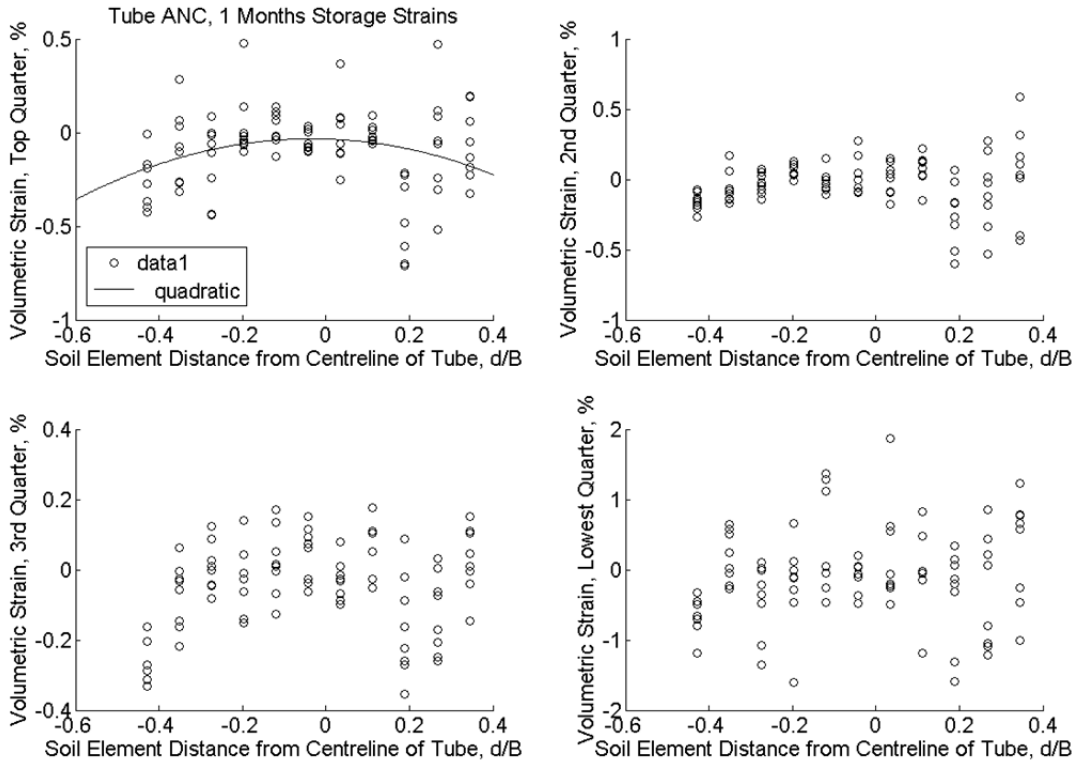

Figure 5.5 - Volumetric Strains measured in test ANC, after 1 Month Storage

Table 5.1 - Volumetric Strains in Monitoring Tests

		Volumetric Strain (max/min, %) at:		
Test	Sample Quarter	1 month	3 months	6 months
ANC	1	+0.25/-0.45	+0.40/-0.80	+0.15/-0.75
	2	+0.30/-0.40	+0.90/-1.60	0.00/-1.20
	3	+0.25/-0.30	+0.55/-0.75	+0.30/-1.00
	4	+1.00/-1.40	+1.30/-1.50	+0.90/-1.80
CNC	1	+1.20/+0.30	+1.45/-0.45	+1.50/-1.20
	2	+1.20/0.00	+1.35/-0.60	+1.45/-1.20
	3	+0.90/+0.25	+1.20/-0.60	+1.50/-1.20
	4	+0.85/-0.40	+1.35/-0.75	+1.60/-1.20
AOC	1	+0.40/-0.75	+1.05/-1.30	+0.85/-2.25
	2	+0.75/-0.75	+1.50/-1.50	+1.50/-1.80
	3	+0.75/-0.75	+1.50/-1.50	+1.00/-2.05
	4	+1.20/-1.50	+1.00/-1.50	+0.75/-2.30
BOC	1	+0.70/-0.45	+1.20/-1.05	+2.10/-2.05
	2	+0.55/-0.30	+0.85/-1.00	+1.15/-2.05
	3	+0.55/-0.40	+0.85/-0.85	+1.45/-1.80
	4	+0.75/-0.75	+1.00/-1.40	+1.58/-1.95

It is known that during storage, the effective stresses within the sample experience changes soon after sampling in the case of low quality samples, and stay constant in high quality specimens. In the long term, all samples reach a constant effective stress state (Tanaka *et al*, 2002). Disturbance during sampling causes a change in pore pressures, which over an initial period, causes these changes in effective stresses. During dissipation of the excess pore pressures, a migration of water through the sample's soil structure takes place, from the exterior of the sample where moisture content in the highest (Chandler *et al*, 1992), to the drier centre of the specimen. This behaviour was observed here, creating strains of ±2.30%. The water content of the transparent soil samples could not be measured either before or after storage, so the overall change over time cannot be known. The paraffin caps were adequate since most of the moisture was retained, although the development of air pockets suggested that no perfect seal was formed. It is recognised that this is partly due to the oily materials used in this study, which will have prevented full adhesion between the melted wax and the glass tube.

5.3 Sample Extrusion

Six samples were horizontally extruded from their tubes, in the direction of the original flow of material into the sampler (from the bottom of the tube to the top). This was done by attaching the model sampling tube to a holder and manually working a piston to drive the soil out of the tube. The images were corrected for camera shake and PIV analysis was used to determine displacements and strains on the sample's centreline and close to the sidewall of the tube. The tube geometries in question were the four used to study sample storage (ANC, CNC, AOC, BOC) and two used as trials, which also yielded results, BNC and BtNC.

Strains were calculated in the manner described in Chapter 2, and strain paths were created for each sampler. The data presented in this section has been corrected for lens distortion, since the displacement of Interrogation Areas is such that the spacing between two IAs is expected to appear to change as it crosses different distortion gradients. With barrel distortion, the magnification is greatest close to the centre of the image, and decreases at the edges. When two soil elements cross the image from right to left as in the extrusion set-up, the spacing between them appears to expand as it approaches the centre of the image,

and then contract as it once more travels to the side of the image. This will create its own apparent strain path.

Once corrected for lens distortion, the strain paths were created and are presented in Figure 5.8 to Figure 5.20, for soil elements on the centreline and immediately adjacent to the tube's wall. Figure 5.6a shows a photo during the experiment and the original position of a centreline grid of Interrogation Areas. Soil inside the tube has a high transparency and visibility is ideal for PIV analysis. Once the soil is pushed out of the tube, air enters the sample and visibility is immediately degraded such that the original IAs are no longer recognisable to the PIV software and wild vectors are produced (Figure 5.6b – 3 wild vectors are visible as arrows not following the general movement of the sample). Figure 5.8 shows the strain path through the series of photographs. It is evident that after soil elements reach the edge of the tube and come in contact with the air, the IAs are no longer recognised and wild vectors are produced. The graphs thereafter contain data only until this point, and therefore represent half-CSPs. A legend for the strain paths is given in Figure 5.7a and b.

a

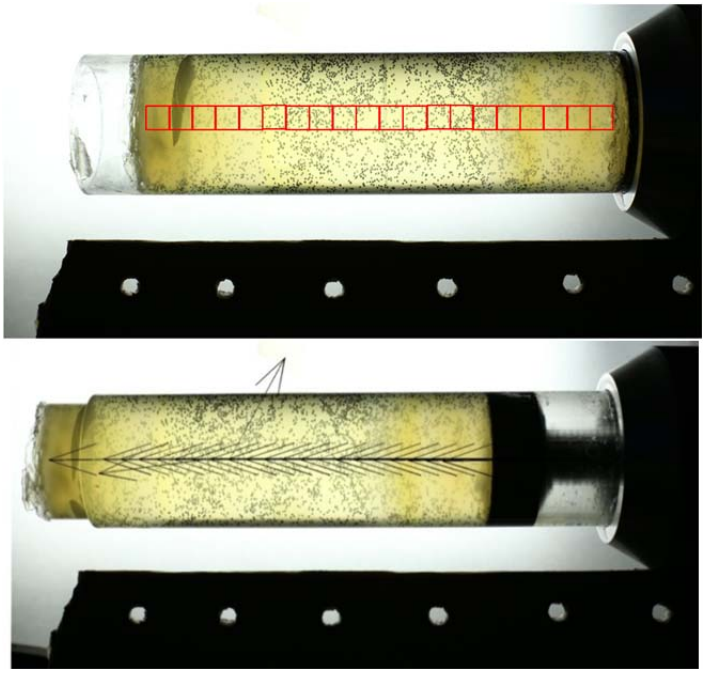

b

Figure 5.6 - Sample Photo During Extrusion Test ANC: a) original photo with IAs and b) with displacement vectors

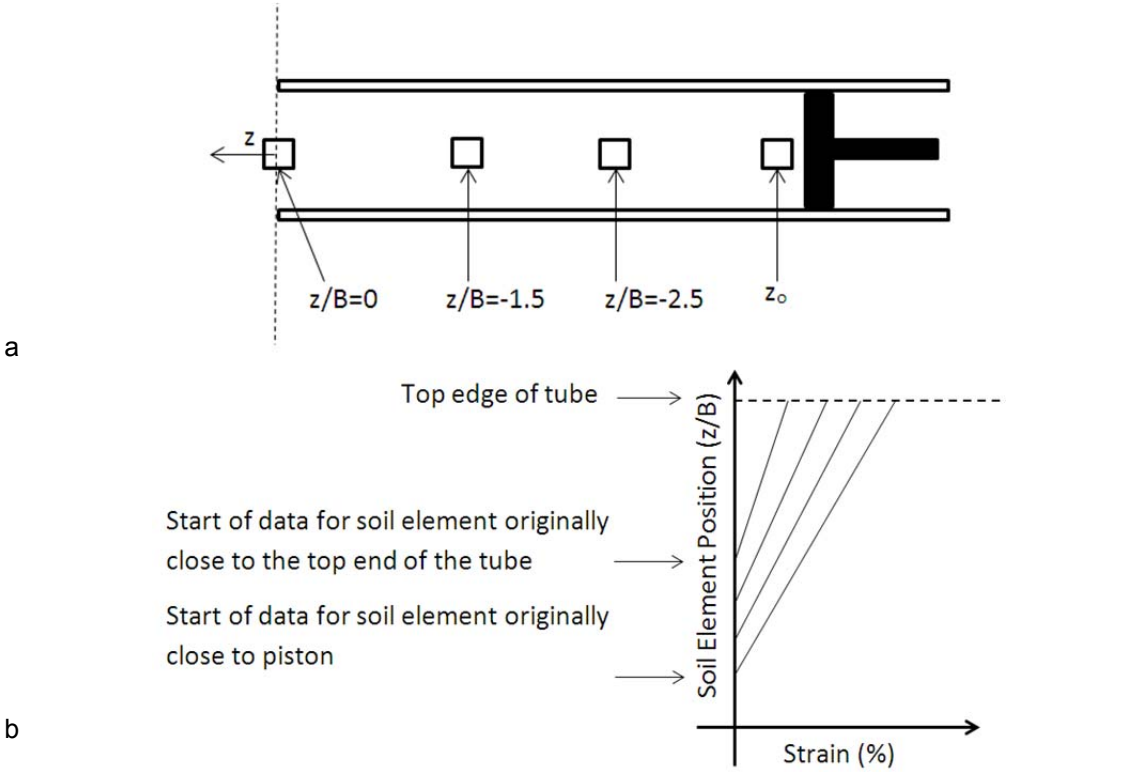

Figure 5.7 - Legend for Extrusion Test Graphs: a) Position of soil Element and b) Data Series

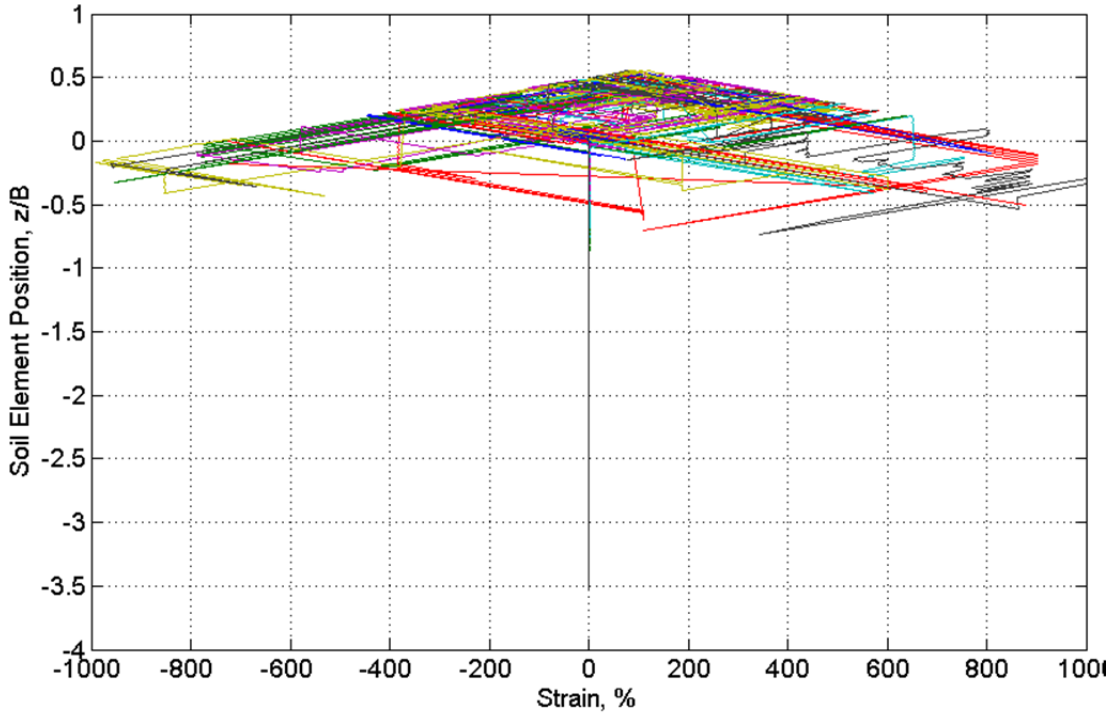

Figure 5.8 - Strain Path: BNC, Original Data

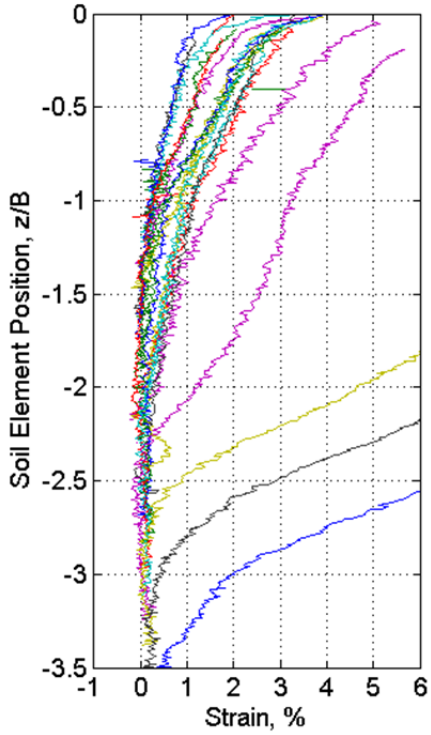

Figure 5.9 - Strain Path: ANC, Centreline

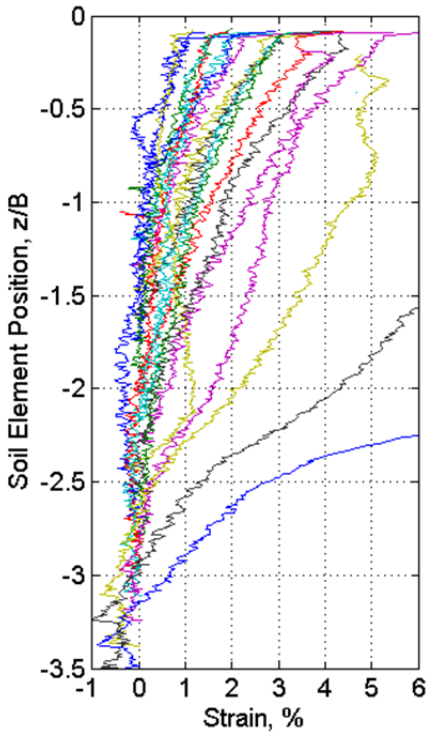

Figure 5.10 - Strain Path: ANC, Sidewall

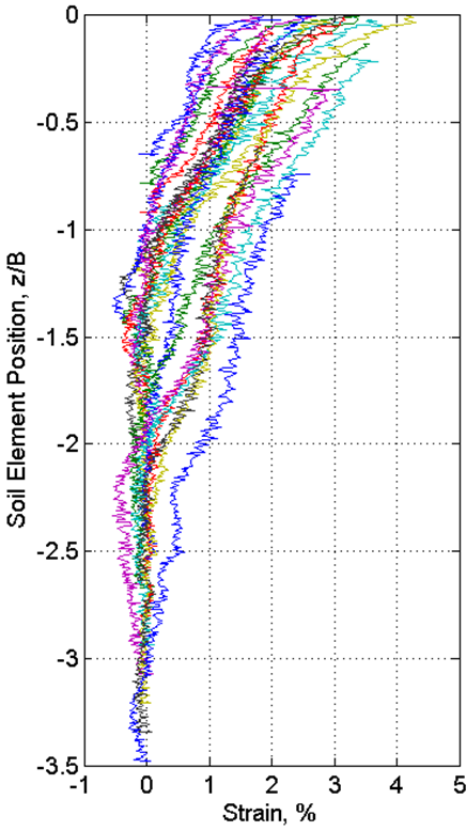

Figure 5.11 - Strain Path: CNC, Centreline

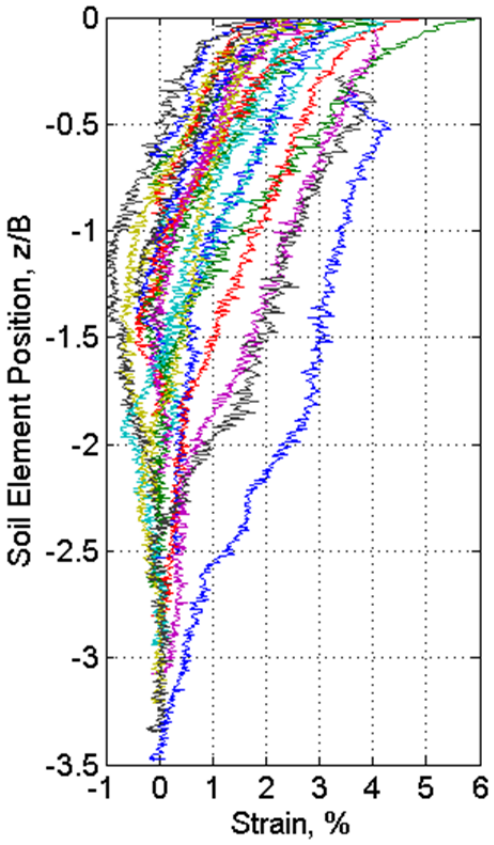

Figure 5.12 - Strain Path: CNC, Sidewall

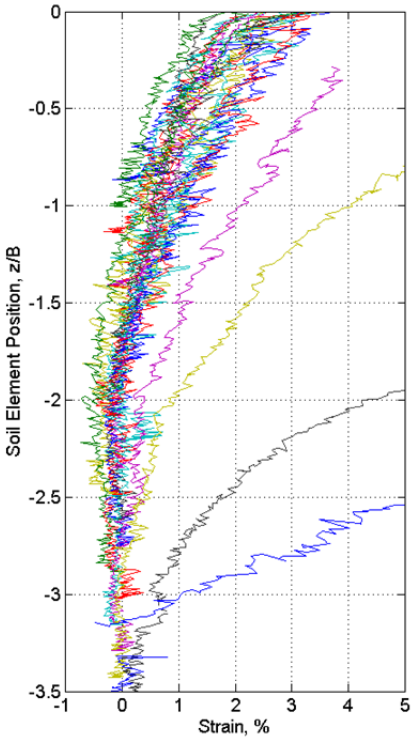

Figure 5.13 - Strain Path: AOC, Centreline

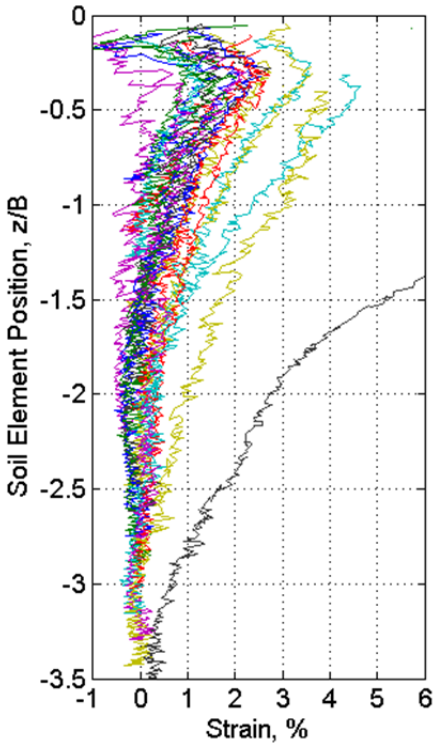

Figure 5.14 - Strain Path: AOC, Sidewall

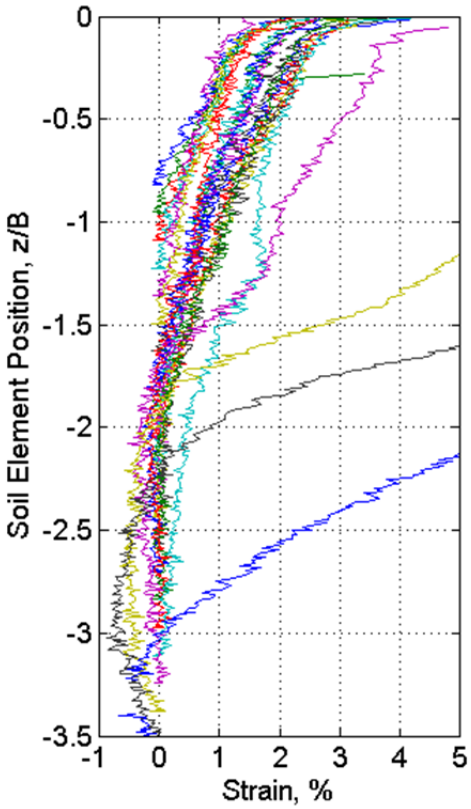

Figure 5.15 - Strain Path: BOC, Centreline

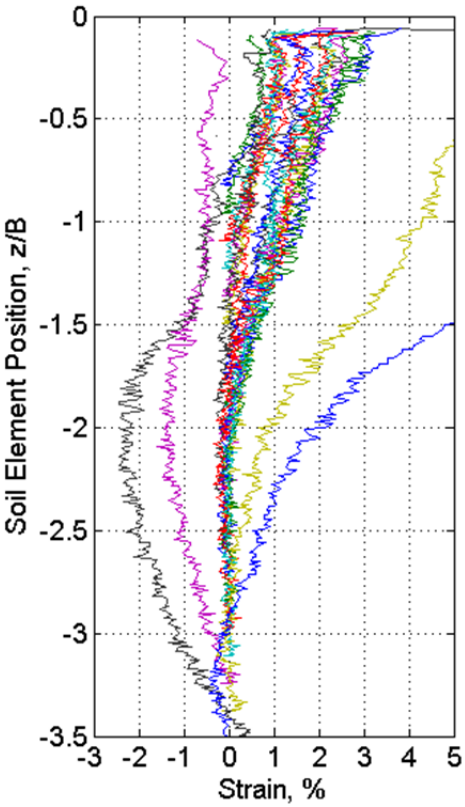

Figure 5.16 - Strain Path: BOC, Sidewall

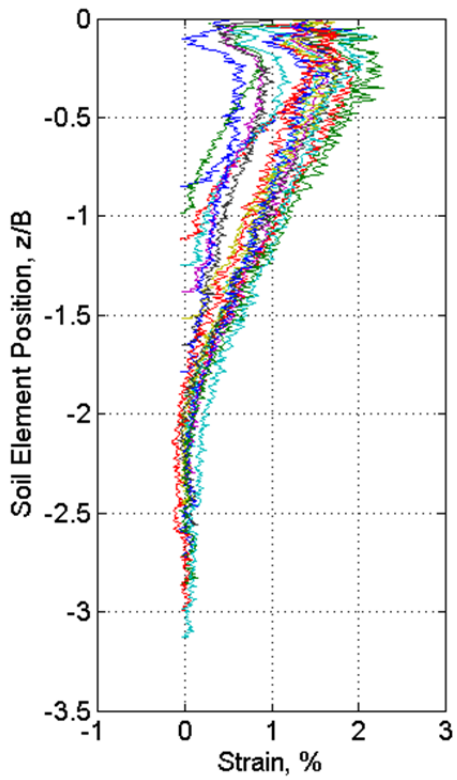

Figure 5.17 - Strain Path: BNC, Centreline

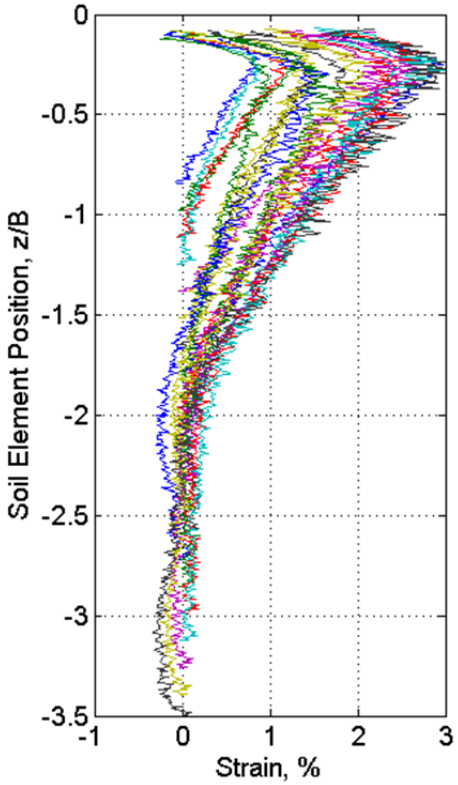

Figure 5.18 - Strain Path: BNC, Sidewall

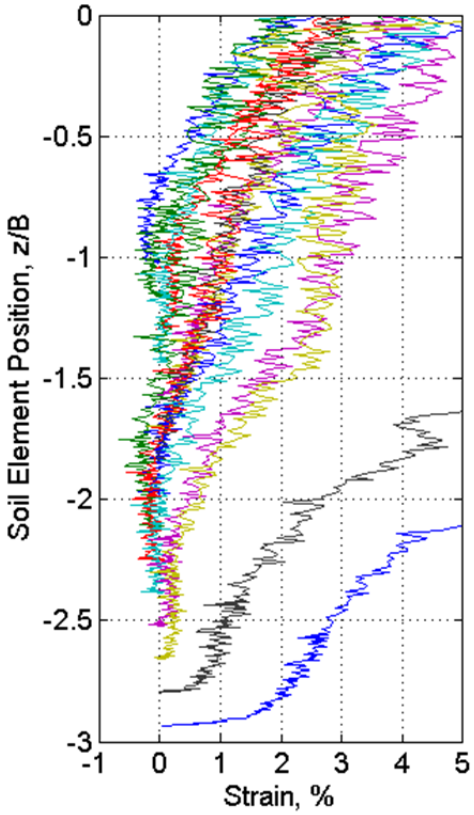

Figure 5.19 - Strain Path: BtNC, Centreline

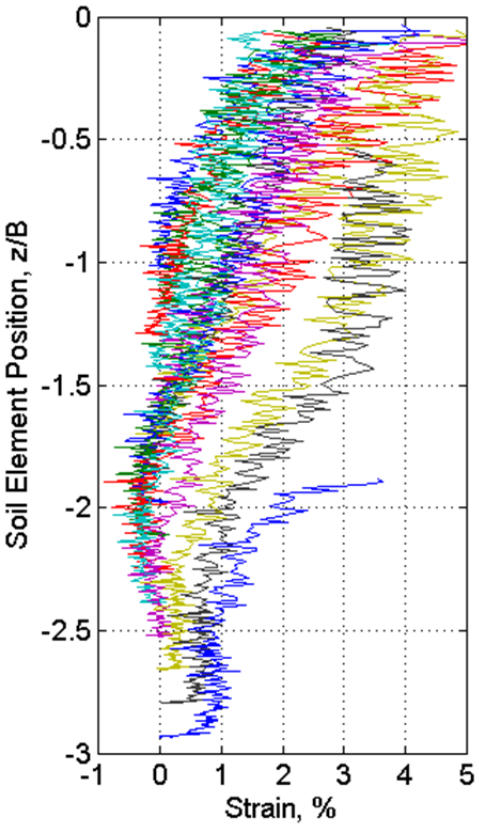

Figure 5.20 - Strain Path: BtNC, Sidewall

In these graphs, the strains experienced by the soil element between its original depth and the tube top are plotted, and show a similar behaviour in all settings. As in the CSPs during tube driving, the magnitude of strains was found to be dependent on the original position of the soil element. When inside the tube, the action of the extruder creates compressive strains in the specimen, which are larger in soil close to the piston and small in soil close to the top of the tube.

No correction such as that used for the tube driving tests was applied to this data, and as a result, the real strains may differ by small amounts (strain ±0.5%) to those plotted – using a full leapfrog was not possible in this case since the material being studied experienced large movements, from one end of the tube to the other, and setting such a large search zone during PIV analysis would have required very powerful computers with a lot of memory. Nevertheless, a leapfrog value of 64 allowed for a reasonable compromise between accuracy and processing time. The data curves are not smooth; some show variations in strain between subsequent photos. An extreme example of this can be seen in Figure 5.19 and Figure 5.20. This is most probably due to flickering of the LED panel used to light the set-up. This would cause fluctuations in light intensity and may change the texture recognised by the PIV software.

The magnitude of the peak compressive strains experienced inside the tube was in the order of 0-5% for most of the soil elements in the tube, rising with depth to over 20% in deep elements closest to the piston. In all cases, deeper elements were more significantly disturbed than those close to the tube's top edge. Extrusion is therefore expected to cause significant damage to the part of the sample closest to the piston, which should not be used in laboratory testing. A recommended distance of the piston can be set at 1 tube diameter, according to data in the six tests.

These deep elements highlight the difference in behaviour between soil elements close to the sampler wall and on its centreline, with higher compressive strains on the centreline than beside the sampler wall. This is not immediately apparent from the curves for the shallower elements, since their strains are similar and uncorrected for inaccuracies due to low leapfrog. A comparison of two elements of same distance from the top of the tube (Table

5.2) and from the piston (Table 5.3) in each test reveals that this is indeed the case in many but not all tests, with peak compressive strains at the centreline up to 23% higher than beside the tube sidewall, although the difference in the parts of the sample which are to be used in laboratory testing (i.e. not the soil at both ends of the sample) is small, and contained within the margin of error for inaccuracies due to using a low leapfrog value.

Some differences were observed between different cutting edge geometries, although these can be explained by differences in sample length, making some of the soil elements further from the piston or tube top than others. High values in test BtNC suggest that tube geometry might not be the most significant element having an impact on strains, which are more affected by small differences in set-up (extrusion speed, length of sample). In any case, the presence of an inside clearance in test CNC appears to have no effect on the strains during extrusion, as their magnitude is at neither extreme of the data spread. No strong link was made between storage time and peak strains. When comparing samples with similar storage times (ANC, CNC, AOC, BOC: 6-9 months), lightly OC samples experienced lower strains than NC samples.

Table 5.2 - Peak Strains at 1.5 and 2.5B Initial Depth into the Sample, on Centreline and beside Tube's Wall

Test	ANC	CNC	AOC	BOC	BtNC	BNC
Peak Strain for Soil Element at Original Depth = 1.5B from top of tube (%) On Centreline	3.64	2.53	2.18	1.39	4.32	0.91
Peak Strain for Soil Element at Original Depth = 2.5B from top of tube (%) On Centreline	3.70	3.53	3.49	2.48	4.60	1.58
Peak Strain for Soil Element at Original Depth = 1.5B from top of tube (%) At Sidewall	2.93	2.43	1.77	1.28	4.08	2.56
Peak Strain for Soil Element at Original Depth = 2.5B from top of tube (%) At Sidewall	3.01	3.07	3.53	2.20	4.60	2.45

Table 5.3- Peak Strains at 1.5 and 2.5B Initial Distance from the Piston, on Centreline and beside Tube's Wall

Test	ANC	CNC	AOC	BOC	BtNC	BNC
Peak Strain for Soil Element at Original Depth = 1.5B from piston (%) On Centreline	3.38	3.55	3.22	2.62	2.21	1.98
Peak Strain for Soil Element at Original Depth = 2.5B from piston (%) On Centreline	3.30	2.14	2.47	2.53	3.69	1.77
Peak Strain for Soil Element at Original Depth = 1.5B from piston (%) At Sidewall	4.28	4.12	3.16	2.80	2.08	1.84
Peak Strain for Soil Element at Original Depth = 2.5B from piston (%) At Sidewall	3.75	2.65	2.09	2.45	3.63	1.50

It is unrealistic to aim to discard all parts of the sample experiencing strains causing irrecoverable damage, since these should be limited to a point lying between 2 and 5% (Clayton *et al*, 1992), and this could include over ¾ of the sample. By discarding the lower 1B of the sample, the remaining specimen will have experienced a maximum compressive strain of 5%, which is in itself sufficient to cause irreversible damage to the sample's structure, which may not be recovered even using an appropriate reconsolidation method. Since friction governs the behaviour of the specimen inside the tube, long samples may experience larger strains during extrusion.

Chung *et al* (2004) compared samples extruded in the direction of the original flow of the soil into the sample ("Reverse direction") with those extruded from the top of the tube ("Normal direction") and concluded that the Reverse direction caused more significant disturbance. If this is indeed the case, extruding using the normal direction is beneficial to the sample in that it will experience less disturbance during extrusion, but also in that the most disturbed part of the sample after tube driving (the top 2-3 tube diameters) will be in contact with the piston during extrusion, meaning that less of the sample will have to be discarded.

Disturbances occurring during storage and extrusion are not as well researched as those caused by tube penetration. Few studies have addressed these issues, probably because there is little opportunity to improve on these processes in the laboratory. Split samplers do

exist, which remove the need for extrusion by allowing the tube to be opened lengthways after retrieval from the ground, but these have a high Area Ratio and therefore usually produce distorted samples (Barnes, 2000). The use of a gel-push sampler could also reduce strains during extrusion since it benefits from reduced friction between the polymer liner and the wall of the tube.

5.4 Summary: Storage and Extrusion Strains

Four samples were stored for a period of 6 months and photographed twice a week to record movements in the soil due to pore fluid redistribution. Soil close to the sampler's wall reduced in volume by up to -1.5%, while soil close to the centre swelled by up to 1.5%. Soil elements close to the ends of the tubes were particularly prone to such changes. Variations in moisture content can also be attributed to a partial failure of the paraffin seal, which can degrade over time. This was evident by the occasional presence of air pockets close to the base of the sample, which would disappear over time as the void would fill with moisture from inside the sample. These effects increased over time, with strains after 6 months 50 to 100% higher than after 1 month.

The four stored samples were later photographed being extruded from their tubes, to measure movements due to this process. Two additional specimens were taken from recent tube driving tests to trial the system. Strain paths were plotted for soil elements along the sampler, both on the centreline and immediately adjacent to the tube's sidewall. Samples were found to be compressed while still inside the tube, up to 5% in soil elements further than 1 tube diameter away from the piston. Soil closest to the piston was heavily compressed and it was recommended it be discarded as it would be unsuitable for laboratory testing. Tube geometry appeared to have little discernible effect on strains experienced by the sample during extrusion, while soil with higher OCRs was less affected than NC soil. The strains experienced during extrusion were deemed sufficient to produce irrecoverable changes to the soil's properties, even provided a suitable method of reconsolidation was used. Strains outside the sampler were not quantified due to a loss in transparency of the transparent soil outside of the glass tube.

Chapter 6: Conclusions and Recommendations for Further Work

6.1 Tube-Driving Tests

6.1.1 Concluding Remarks

A white light PIV set-up was developed to model tube driving. Twelve model glass tubes were photographed being driven into an artificial transparent soil model confined by a pressure plate on the surface of the soil to model an overburden pressure. PIV software was used to measure the displacements within the soil body on a plane running through the centreline of the sampler. Full-field vector plots were obtained, which showed the movement at three tube penetration depths, of the soil inside and outside the sampling tube. The soil on the centreline was further studied, with strains derived from displacements and plotted over time to generate Centreline Strain Paths for each of the twelve tests. The method developed in this study has, for the first time, allowed strains within the sample to be measured physically, and could be further used to measure the effects of shear developing on the sampler wall.

In an unconfined trial test, displacements and strains were similar in magnitude to those predicted by the SPM, while those in confined tests behaved differently. Generally, it was seen that soil in the sample experienced a downwards movement of a few millimetres from its original location before being raised inside the sampling tube by as much as a few centimetres. The soil around the sampler moved outwards and upwards in the case of soil above the level of the tube's cutting edge, and outwards and downwards in soil under the level of the cutting edge. The exact final location of the soil under the sampler's wall was not identified using PIV because of excessive distortion developed in these Interrogation Areas during tube penetration. However, a rise in the level of the soil surface outside the sampler and inside the tube revealed that typically, the soil originally under the sampler's walls was partially pushed outwards into the soil and partially inwards into the sample. The risk of this soil entering the tube increased with overburden pressure, and samples taken in the set-up with the pressure plate were visibly longer than in the test without it. It was found that in

open-drive tube samplers in unsupported boreholes, the main cause of structural disturbance to the specimen is caused by excess recovery of soil. For tubes with an AR around 16-17%, this was measured at 105-107% while for thicker tubes with an AR of 34-39%, the same section of the sample showed excess soil recovery of 116-118%. This recovery of soil from under the tube's walls increased the volume of the sample, thus causing irreversible damage to its structure.

Soil plugging was also observed: it affected 5 out of the 12 tests. Two were severely affected while three showed limited evidence of the formation of a plug. This manifested itself as a downward movement within the tube, as the plugged soil was dragged deeper by the friction between the sampler's wall and the plug. It was seen in most tests in Overconsolidated Soil, but was also present in Normally Consolidated soil and could not be linked to any element of the tube's geometry.

The effect of open tube sampling was compared in tubes with different cutting edge geometries: round-ended, sharp, and blunt with an inside clearance. Two tube thicknesses were compared, and while both tubes were considered "thick" by Eurocode 7, the thinner of the two was at the borderline of the Area Ratio acceptable for thin tubes. Tests were carried out in Normally Consolidated soil for all tube geometries, and in Lightly Overconsolidated soil (OCR=1.6) with the thicker set of tubes. The CSPs were compared to investigate the effect of each geometry or soil parameter on the extent of sampling disturbance.

The CSPs displayed the expected pattern of three phases of strain: compression ahead of the cutting edge, then a rapid phase of extension as the soil approached and entered the tube, and finally a second compression phase as the soil moved upwards in the tube. These CSPs were depth-dependent and non-antisymmetric, contrary to early work by Baligh *et al* (1987). Elements close to the base of the borehole were more heavily disturbed than those at depth, with higher extensive, peak-to-peak and residual strains, indicating that some of the sample would not be fit for testing. No cut-off point was identified within a depth of three tube diameters into the specimen, which is worrying for short samples taken in the field. In all cases, the peak extensive strain and residual strain were larger than the peak compressive strain.

In all following comparisons, data used is that for a soil element at a depth of 3B under the base of the borehole:

- It was found that sampling disturbance had a greater effect on specimens taken in normally consolidated soil, than those in overconsolidated soil, with peak-to-peak strains reduced by 43-45% using blunt tubes and tubes with an inside clearance respectively. Peak extensive strains reduced by 69-70% in OC soils, while peak compressive strains increased two- to five-fold. Recompression within the sampler was also reduced in OC soils.
- As noted previously, the thickness of the tube governs the amount of soil displaced, and therefore tubes with greater wall thicknesses are more prone to the recovery of soil originally situated under the walls of the sampler. This excess recovery increases the peak extensive, compressive and residual strains experienced by the sample, as well as the peak-to-peak strain. Samples taken by thick open-tubes are therefore expected to be heavily disturbed. If the tube is sharpened over a sufficient length, however, or if the geometry is not conducive to excess soil recovery, the strains may be reduced.
- Increasing the tube sharpness from blunt to an angle of 30° from the vertical reduced the peak extensive and compressive strains by 25 and 17% respectively in thick walled tubes in NC soil. Peak extensive strains were similarly reduced by 23% in the thinner tubes. Residual strains were reduced up to 33%, and peak-to-peak and recompression strains were similarly reduced. Considering that 30° is not very sharp, strains could be reduced even further by designing or using tubes with smaller taper angles, which would more closely resemble real sampling tubes, where taper lengths of 60mm and angles of 5-30° are not uncommon. .
- Comparing blunt tubes with a 0.4-0.8% and 1.9-2.8% Inside Clearance Ratio, samples with a higher ICR experience higher peak compressive strains and lower peak extensive strains. Residual strains are 44% lower in NC soils and 71% lower in OC soils. Some of this reduction is due to the fact that samples are allowed to expand laterally as well as upwards inside the sampling tube, and hence a shortening of the sample would be expected.

Tests by Clayton *et al* (1992) and Santagata and Germaine (2005) on samples of reconstituted clay concluded that applying strains of ±5% to specimens resulted in irrecoverable reductions in strength and stiffness, while samples having experienced a ±2% strain cycle could recover most of their properties through an appropriate reconsolidation technique. The strains measured in the present study were in the order of +0-2% in compression and up to -25% and -10% in extension in thick and thin tubes respectively. Samples taken using an open-drive tube sampler in an empty borehole are severely disturbed by the recovery of excess soil, and may not be suitable for laboratory testing. That being said, the excess soil recovery and associated strains rapidly decrease with depth into the sample, and longer continuous samples may experience smaller strain cycles, provided that the friction between the sampler and the soil is not excessive. In all cases it is recommended that at least the upper 3 tube diameters of soil be discarded for thin walled samplers, and more than this for thick-walled samplers, to keep the strain cycle well below 5%.

6.1.2 Test Limitations

The main limitation of the test series was the lack of variation in geometry. The effect of tube geometry was dominated by the effects of Area Ratio, since only small variations in the cutting edge geometry of the manufactured glass sampling tubes were achieved. More realistic taper angles would result in thinner tubes over the extent of the cutting shoe, and as such would result in less disturbed samples, where the effect of cutting edge geometry would be more noticeable. The tests have highlighted the detrimental effect of high AR but this has dominated the strain behaviour in the samples. It is however known that high quality samples have been obtained with real tube samplers with a high Area Ratio (the Swedish piston sampler with AR=44%, Clayton *et al*, 1995). Since the AR dictates the amount of soil displaced by the tube, it is the cutting edge geometry which is responsible for directing the displaced soil, and a well-designed sampler will direct this excess soil away from the inside of the sampler. Using more realistic sampler geometries would provide a better insight into the role of cutting edge in the redirection of the soil displacements.

The set-up for the tube driving tests has two main limitations. The first is the small number of tests which were carried out. Each test taking up to 6 weeks to prepare and run, even by duplicating the testing equipment, it was not possible to run more than 12 tests. The second is the small portion of soil within the model which could be considered unaffected by boundary conditions imposed by the walls of the Perspex box. Displacement measurements were taken in soil up to a depth of three tube diameters under the base of the borehole, with the top two tube diameters expected to be heavily disturbed. Elements deeper than this were found to experience higher levels of compression close to the base of the Perspex box and were therefore considered to be affected by boundary conditions.

With regard to the first issue, it would have been beneficial to repeat some of the tests to ensure that the results were comparable. Test BNC was re-run due to poor visibility through the soil model in the first instance, which meant that peak extensive strains were not obtainable because of wild vectors. Results between both BNC tests were within 5-8% of each other, which shows that small variations occurred between set-ups, but that overall, data between runs was consistent.

It had not been expected that plugging may occur, and this phenomenon did not become apparent until late in the testing stage. The original aim had been to compare three sets of data:

- Geometries A, B and C, thick tubes in Normally Consolidated Soil (ANC, BNC, CNC)
- Geometries A, B and C, thin tubes in Normally Consolidated Soil (AtNC, BtNC, CtNC)
- Geometries A, B and C, thick tubes in Overconsolidated Soil (AOC, BOC, COC)

Unfortunately, due to plugging, poor visibility and suspected poor performance of the pressure plate, only one of these series, ANC, BNC, CNC, yielded data unaffected by these issues. Other tests were used to confirm result seen in this first test series, once effects of plugging had been studied.

This limitation is common to this type of physical modelling in geotechnical engineering. Similar studies (van Eekelen and van den Berg, 1995, Yan et al, 2010) using kaolin clay models only presented data from a limited number of tests: in the former case, only two tests were carried out using different tube geometries in separate clay models, in the latter, a same tube was driven into the same soil model three times at small spacings. While this not ideal, experimental results must be obtained, and so this labour intensive process must be followed.

While the hypotheses concerning the effect of tube geometry (ICR) on the extent of sampling disturbance presented in this study are backed by limited test data, other elements have more substantive evidence to back them up: the effect of OCR and AR on sampling disturbance, the high risk of excess soil recovery, the shape of the CSP, and others.

6.2 Storage Tests

6.2.1 Concluding Remarks

At the end of the tube driving tests, four tubes (ANC, CNC, AOC, BOC) were selected to be stored for a period of 6 months, during which time photographs were taken of the static tubes at a rate of 2 per week. PIV was used to measure displacements on the seeded centreline within the glass samplers and volumetric strains were calculated from these. Small strains were observed, with soil elements on the centreline swelling by up to 1.5% while those close to the tube's wall shrank by up to 1.5% after six months, suggesting that increased pore pressures set-up during sampling in the periphery of the sample redistributed by means of a pore fluid migration. This swelling and shrinkage increased over time, by 50-100% between 1 and 6 months.

Soil at either end of the sample was more affected than soil at the centre, with soil at the base more so. The paraffin wax plugs appeared to have provided adequate protection against moisture loss since the outside of the sample remained unaffected by significant losses in transparency. Some localised air pockets filled with pore fluid over a period of a few days to a few weeks, suggesting that some moisture was lost.

No link was made between the magnitude of the strains and the cutting edge geometry, nor was there an apparent difference between normally consolidated and lightly overconsolidated samples.

6.2.2 Test Limitations

This series of tests ran smoothly, but encountered one problem: turning the camera on and off during shots over a period of 8 months caused a considerable amount of camera shake. Static reference points in the photograph appeared to move by up to 4 or 5mm between two photos. Because the real soil movements were smaller than this – less than 0.5mm – this represented a challenge during analysis. Plotting displacement vector fields was not achievable, nor were displacement contours within the sample.

The strain values recorded in this research are valid only for the achieved level of protection against moisture loss. Strains in perfectly sealed or poorly contained samples are expected to be different, as would be those in samples more or less disturbed by the tube driving process.

6.3 Extrusion Tests

6.3.1 Concluding Remarks

The four stored samples and two trial samples (BNC, BtNC) were extruded from their tubes, and this process was photographed to measure movements on the centreline and close to the wall. Strain paths were plotted and compared for elements from sampler top to the base of the specimen. It was observed that samples were compressed while still inside the tube, up to 5% in soil elements further than 1 tube diameter away from the piston and over 20% in soil closest to the piston. Because of this, it was expected that such elements would have undergone excessive deformations and it was recommended they be discarded as they would be unsuitable for laboratory testing. Tube geometry appeared to have little effect on strains experienced by the sample during extrusion, although soil with higher Overconsolidation Ratios was less affected than normally consolidated soil, which was consistent with results from the tube driving tests. The strains experienced during extrusion

were deemed sufficient to produce irrecoverable changes to the soil's properties, even provided a suitable method of reconsolidation was used.

6.3.2 Test Limitations

The main limitation of the extrusion test was the difference in length between samples – some were up to 15 mm longer than others. With hindsight, these should all have been trimmed identically after tube driving and before pouring the paraffin wax, or failing that, prior to the extrusion tests. This was not considered at the time, and since the strains experienced by the sample are linked to both distance from the piston and length of the sample, it is expected that differences in sample length will impact on the magnitudes which were measured.

6.4 Recommendations for Field Sampling and Laboratory Testing

6.4.1 Field Sampling

If using an open tube sampler, the engineer should be aware of the associated risks, above all the recovery of excess soil from under the sampler's walls. The tube's geometry is linked to the extent of sample disturbance, and the element causing the most distortion is the Area Ratio. To reduce disturbances, the AR of the tube should be as small as possible, under 16-17% if ground conditions allow for this. This will ensure that relative to the size of the specimen, little excess soil is forced into the sampler. In any case, the upper 3 tube diameters should be discarded, so that the soil used in laboratory tests has experienced only a limited strain cycle (up to -6% in extension, <2% in compression for an AR of 16-17%).

Longer samples could also be taken, provided a method is used to limit the amount of friction between the soil and sampler. The answer to this issue might be the use of gel-push samplers (Taylor and Cubrinovski, 2012).

Using a tube with a higher Inside Clearance Ratio can reduce the magnitude of the residual and extensive strains, since the diameter of the sample is closer to its original dimensions. While this can be helpful to reduce the effects of excess soil recovery, it may not have a significant impact since the specimen's structure will already have been distorted as the soil

passes the cutting edge which has a smaller inside diameter. In sensitive soils, where lateral expansion destroys the cementation bonds between particles, this is not an option.

The tube should be as sharp as possible, bearing in mind that if the tube is tapered over a significant portion of its length, this is similar to using a thinner tube, which is prone to damage during tube driving. 30° tapered over 10mm significantly reduces the magnitude of all strains experienced by the soil, and further reductions can be achieved with longer and thinner tapering.

6.4.2 Laboratory Procedures

Strains during extrusion are also non-negligible. Compression up to 5% was observed in specimens, which has the potential of introducing irrecoverable changes to the structure and hence to the properties of the sample. Friction is the main cause of these strains, and therefore this must be reduced. Again, a thin layer of low friction material such as foil or a polymer gel between the sampler and the specimen could be beneficial if:

- The loss in friction does not impede recovery of the sample during retrieval from the ground
- The use of an additional layer does not significantly alter the inside diameter of the tube, thus increasing the AR
- The layer does not react with the soil

Split samplers, where the tube comes apart in two parts surrounding the specimen, also exist. Their use is not recommended since disturbance is caused to the sample by other means during sampling. The development of a thinner tube fitting these requirements could be considered.

Extruding in the normal direction (direction opposite to the original flow of material into the sampler) could be beneficial since the specimen will experience less disturbance during extrusion (Chung *et al*, 2004), but also because the most disturbed part of the sample after tube driving (the top 2-3 tube diameters) will be in contact with the piston during extrusion, meaning that less of the sample will have to be discarded before laboratory testing.

6.5 Recommendations for Further Work

The limitations of each of the three set-ups used in this study were presented previously. These must be addressed before any further work is undertaken using similar equipment or to achieve similar goals. Using transparent soil and PIV is a labour-intensive methodology, with long preparation times and significant photo and data processing required before the data can be used. It has the advantage of being the cheapest technology available to look inside a body of soil – albeit artificial – and measure displacements, and should therefore be further investigated, developed and refined.

With regard to the model itself, its size should be as large as possible, bearing in mind that the time for consolidation will increase, and the transparency will be reduced. In any case, a deeper model than that used in this research is necessary for future works, as this would increase the usable data in any given test. Smaller tubes could have been used, but these also have disadvantages, such as having only a small area to study – and therefore less well defined vector fields.

The cameras and lenses used in this study were perfectly adequate, although models are continually becoming available with increased shooting rates and higher resolutions. While more photos with larger file size will be generated, personal computers are also developing at a fast rate so processing these large amounts of data should not be difficult. Lens distortion should be corrected for where large movements occur. Where soil remains close to its original position, this added work may not be necessary.

The tube should be better held in place to avoid being driven at an angle, and causing the soil to form a plug inside the tube. This affected many later tests and it was suspected that the O-ring connection deteriorated with repeated use and because of the contact with the oils forming part of the transparent soil. Due to space constraints in the already-built consolidation rig, the O-ring design was used, whereas if space had not been so limited, an alternative design with a tighter and longer connection would have been chosen (see Appendix A).

With regard to the extrusion test, for ease of use, it could be recommended using a motor to drive the piston, although this is not necessary. Chung *et al* (2004) studied the effect of the direction at which the sample is extruded from the tube. With a larger number of samples, this could also be investigated by comparing the magnitude of the strains generated during extrusion in both directions.

The monitoring tests would have benefited from a camera with a sensitive power button, rather than a switch. Flipping the on/off switch of the camera twice a week during the six months' monitoring period was sufficient to cause visible camera shake. In a set-up looking to measure minute strains, these apparent movements can be larger than those being observed and therefore the imprecise method of removing this camera shake may significantly affect the data. This did not impact on the strains calculated from the displacements since all displacements were similarly affected. It would, however, have been useful to be able to study displacement contour fields inside the tubes. Mains power could be considered at an extra cost, but H&S implications of leaving a power supply on for prolonged use must be investigated.

6.6 Ideas for Future Use of the White Light and PIV Set-Up

This section is divided into two parts: the future works which the author would have liked to carry out in this study, and those which can be done with the methodology and equipment developed through this research with minimal changes to the set-up.

6.6.1 Work to Improve this Study

As explained previously, the main limitation of the tube-driving tests was the number of tests which could be carried out. Repeating a number of these tests would increase confidence in the data generated from each of these. In particular, tests AtNC, BtNC and CtNC would be repeated, to validate the effect of tube geometry on the extent of disturbance. The "sharp" tubes used in this study had large angles cut over a limited length of the sampler. This was because it had been thought that the visibility through the rough part of the cut glass would be poor. It was found during testing that this was not the case, and in future tests, the length

over which the angle is applied could be longer to study the effect of more realistic sharp sampling tubes.

6.6.2 Work to Extend this Study

The PIV-white light set-up could be used to study a number of geotechnical problems at depth, or close to the surface. Existing physical models with limited size due to poor visibility in laser-PIV set-ups could benefit from this adapted methodology to obtain results less affected by boundary conditions. Future applications could include pile penetration, augering, tunnelling, soil anchors and slope stability problems.

Staying with sampling disturbance in open tubes, one option would be to study the effect of using a borehole fluid or mud on the excess recovery ratio. This could be modelled using unconsolidated slurry to support the surface of the soil not covered with the pressure plate. Developing this further, sampling disturbance in piston samplers could be investigated. This would require a fixed piston to be manufactured and installed to fit inside the tube's driving mechanism. The tolerance between the outer wall of the tube and the disc cut out of the pressure plate would have to be small to prevent soil escaping upwards during tube-driving.

References

Adrian, R.J. (1991). Particle Imaging Techniques for Experimental Fluid Mechanics. *Annual Review of Fluid Mechanics*, **23**, 261-304

Adrian, R. J. (2005). Twenty Years of Particle Image Velocimetry. *Experiments in Fluids*, **39** (2), 159-169.

Adrian, R.J., Westerweel, J. (2010). *Particle Image Velocimetry.* Cambridge University Press

Ahmed, M. & Iskander, M.G. (2012). Analysis of Tunnelling-Induced Ground Movements Using Transparent Soil Models, Journal of Geotechnical and Geoenvironmental Engineering, **137** (5), 525-535

Ahmed, M. & Iskander, M.G. (2012). Evaluation of Tunnel Face Stability by Transparent Soil Models, *Tunnelling and Underground Space Technology*, **27** (1), 101-110

Allersma, H.G.B (1988). Photoelastic Investigation of the Stress Distribution During Penetration, In: *Proceedings of 2nd European Symposium on Penetration Testing, Amsterdam*, 411-418

Baldwin, M. & Gosling, D. (2009). Technical Note: BS EN ISO 22475-1: Implications for Geotechnical Sampling in the UK, *Ground Engineering*, Issue: August 2009

Baldwin, M. & Gosling, D. (2010). Technical Note: Breaking New Ground, *Ground Engineering*, Issue: June 2010

Baligh, M.M. (1985). Strain Path Method, *Journal of Geotechnical Engineering*, **111** (9), 1108-1136

Baligh, M.M., Azzouz, A.S. & Chin, C.T. (1987). Disturbances due to Ideal Tube Sampling, *Journal of Geotechnical Engineering*, **113** (7), 739-757

Barnes, G. (2000). *Soil Mechanics*, 2nd Edition, Macmillan.

Baudet, B.A. & Ho, E.W.L. (2004). On the Behaviour of Deep-Ocean Sediments, *Géotechnique*, **54** (9), 571-580

Begemann, I. H. K. P. (1974). The Delft Continuous Soil Sampler. *Bulletin of the International Association of Engineering Geology,* **10** (1), 35-37.

Brown, D.C. (1966). Decentering Distortion of Lenses, *Photogrammetic Engineering,* **32** (3), 444-462

BS EN ISO 22475-1:2006 - Geotechnical Investigation and Testing — Sampling Methods and Groundwater Measurements — Part 1: Technical Principles for Execution

Budhu, M. & Wu, C.S. (1992). Numerical Analysis of Sampling Disturbances in Clay Soils, *International Journal for Numerical and Analytical Methods in Geomechanics,* **16**, 467-492

Chandler, R.J., Harwood, A.H. & Skinner, P.J. (1992). Sample Disturbance in London Clay, *Géotechnique*, **42** (4), 577-585

Chapman, T. (2008). The Relevance of Developer Costs in Geotechnical Risk Management, Proceedings of the 2nd British Geotechnical Association International Conference on Foundations- ICOF 2008. Brepress, Dundee

Chapman, T. & Marcetteau, A. (2004). Achieving Economy and Reliability in Piled Foundation Design for Building Pproject, *The Structural Engineer*, 2 June, 32-37

Chung, S.G., Kwag, J.M., Giao, P.H., Baek, S.H. & Prasad, K.N. (2004). A Study of Soil Disturbance of Pusan Clays with Reference to Drilling, Sampling and Extruding. *Géotechnique*, **54** (1), 61-65

Clayton, C.R.I., Hight, D.W. & Hopper, R.J. (1992). Progressive Destructuring of Bothkennar Clay : Implications for Sampling and Reconsolidation Procedures, *Géotechnique*, **42** (2), 219-239

Clayton, C.R.I., Matthews, M.C. & Simons, N.E. (1995). *Site Investigation: A Handbook for Engineers,* 2nd Edition, Oxford, GB, Blackwell Science

Clayton, C.R.I., Siddique, A. & Hopper, R.J. (1998). Effects of Sampler Design on Tube Sampling Disturbance – Numerical and Analytical Investigations, *Géotechnique*, **48** (6), 847-867

DeGroot, D.J., Poirier, S.E., & Landon, M.M. (2005). Sample Disturbance – Soft Clays, *Studia Geotechnica et Mechanica*, **27** (3-4), 91-105.

De Villiers, J.P., Leuschner, F.W. & Geldenhuys, R. (2008). Centri-Pixel Accurate Real-Time Inverse Distortion Correction, In : *Proceedings of International Society of Optics and Photonics*, **7266**

Eden, W.J. (1971). Sampler Trials in Overconsolidated Sensitive Clay, In: *Symposium on Sampling of Soil and Rock, ASTM STP 483*, 132-142

Fang, H-Y. (1991). *Foundation Engineering Handbook.* Chapman and Hall.

Georgiannou, V.N. & Hight, D.W. (1994). The Effects of Centreline Tube Sampling Strains on the Undrained Behavior of Two Stiff Overconsolidated Clays, *Geotechnical Testing Journal*, **17** (4), 475-487

Gosling, D. & Baldwin, M. (2010). Technical Note : Development of a Thin Wall Open Drive Tube Sampler (UT100), *Ground Engineering*, Issue: March 2010

Gribbon, K.T., Johnston, C.T. & Bailey, D.G. (2003). A Real-Time FPGA Implementation of a Barrel Distortion Correction Algorithm with Bilinear Interpolation, *Image and Vision Computing*, 408-413

Hajj, A. R. (1990). The Simulation of Sampling Disturbance and its Effects on the Deformation Behaviour of Clays, Thesis (PhD), University of Sheffield).

Heikkillä, J. (2000). Geometric Camera Calibration Using Circular Control Points, *IEEE Transactions on Pattern Analysis and machine Intelligence*, **22** (10), 1066-1077

Hight, D.W., Boëse, R., Butcher, A.P., Clayton, C.R.I. & Smith, P.R. (1992). Disturbance of the Bothkennar Clay Prior to Laboratory Testing, *Géotechnique*, **42** (2), 199-217

Hight, D.W. (1993). A Review of Sampling Effects in Clays and Sands, *Offshore Site Investigation and Foundation Behaviour*, **28**, 115-146

Hird, C.C. & Hajj, A.R. (1995). A Simulation of Tube Sampling Effects on the Stiffness of Clays, *Geotechnical testing Journal*, **18** (1), 3-14

Hird, C.C., Stanier, S.A. (2010). Modelling Helical Screw Piles in Clay using a Transparent Soil. In: *Proceedings of the 7th International Conference on Physical Modelling In Geotechnics Zurich*, **1**, 769-774

Hird, C.C., Ni, Q. & Guymer, I. (2010). Physical Modelling of Deformations around Piling Augers in Clay, *Géotechnique*, **61** (11), 993-999

Hopper, R.J. (1992). *The Effects and Implications of Sampling Clay Soils*, Thesis (PhD), University of Surrey

Hunt, R. E. (2005). *Geotechnical Engineering Investigation Handbook*. Crc Press.

Hvorslev, J. (1949). *Subsurface Exploration and Sampling of Soils for Civil Engineering Purposes*, Waterways Experimental Station, Vicksburg, USA.

Iskander, M. G., Lai, J., Oswald, C.J. & Mannheimer, R.J. (1994). Development of a Transparent Material to Model the Geotechnical Properties of Soils, *Geotechnical Testing Journal*, **17** (4), 425-433

Iskander, M.G., Liu, J. & Sadek, S. (2002). Transparent Amorphous Silica to Model Clay. *Journal of Geotechnical and Geoenvironmental Engineering*. **128** (3), 262-273

Iskander, M.G., Sadek, S. & Liu, J. (2003). Soil Structure Interaction in Transparent Synthetic Soils Using Digital Image Correlation. In: *Proceedings of TRB 2003 Session on Recent Advances in Modeling Techniques in Geomechanics*

Iskander, M. (2010). *Modelling with transparent soils*. Heidelberg

Iskander, M., Liu, J. (2010). Modelling Capacity of Transparent Soil. *Canadian Geotechnical Journal*, **47**, 451-460

Jamiolkowski, M. (1985). New Developments in Field and Laboratory Testing of Soils," State of the Art Report. In *Proceeding of the 11th International Conference on SMFE*, **1**, 57-153

Jardine, R. J., Potts, D. M., St John, H. D., & Hight, D. W. (1991). Some Practical Applications of a Non-linear Ground Model. In *Proceedings of the 10th European Conference on Soil Mechanics and Foundation Engineering, Florence,* **1**, 223-228

Kimura, T. & Saitoh, K. (1982). The Influence of Disturbance due to Sample Preparation on the Undrained Strength of Saturated Cohesive Soil, *Soils and Foundations*, **22** (4), 109-119

Kirkpatrick, W.M., & Khan, A.J. (1984). The Reaction of Clays to Sampling Stress Relief. *Géotechnique*, **34** (1), 29-42.

Kirkpatrick, W.M., Khan, A.J., & Mirza, A.A. (1986). The Effects of Stress Relief on some Overconsolidated Clays. *Géotechnique*, **36** (4), 511-525.

La Rochelle, P. & Lefebvre, G. (1971). Sampling Disturbance in Champlain Clays, In: *Symposium on Sampling of Soil and Rock, ASTM STP 483*, 143-163

La Rochelle, P., Sarrailh, J., Tavenas, F., Roy, M. & Leroueil, S. (1981). Causes of Sampling Disturbance and Design of a New Sampler for Sensitive Soils. *Canadian Geotechnical Journal,* **18**, 52-66

Lacasse, S., & Berre, T. (1988). Triaxial Testing Methods for Soils. *Advanced Triaxial Testing of Soil and Rock, ASTM STP, 977*, 264-289.

Ladd, C., & Lambe, T. (1963). The Strength of “Undisturbed” Clay Determined from Undrained Tests, In: *Symposium on Laboratory Shear Testing of Soils, ASTM STP 361*, 342-371

Ladd, C.C., & Foott, R. (1974). New design procedure for stability of soft clays. *Journal of the Geotechnical Engineering Division*, **100** (7), 763-786.

Lehane, B.M. & Gill, D.R. (2004). Displacement Fields Induced by Penetrometer Installation in an Artificial Soil, *International Journal of Physical Modelling in Geotechnics*, **4** (1), 25-36

Liu, J., Iskander, M.G. & Sadek, S. (2003). Consolidation and Permeability of Transparent Amorphous Silica, *Geotechnical Testing Journal*, **26** (4), 1-12

Liu, J. & Iskander, M. (2004). Adaptive Cross Correlation for Imaging Displacements in Soils. Journal of Computing in Civil Engineering, **18**, 46–57

Liu, J., Iskander, M.G. (2010). Modelling Capacity of Transparent Soil. *Canadian Geotechnical Journal*, **47** (4), 451-460

Long, M. (2001). Discussion: Tube Sampling Disturbance – Forgotten Truths and New Perspectives, *Geotechnical Engineering*, **149** (3), 195-200

Long, M. (2003). Sampling Disturbance Effects in Soft Laminated Clays, Geotechnical Engineering, **156** (4), 213-224

Long, M. (2006). Sample Disturbance Effects on Medium Plasticity Clay/Silt, *Geotechnical Engineering*, **159** (2), 99-111

Lunne, T., Berre, T., Andersen, K. H., Strandvik, S., & Sjursen, M. (2006). Effects of Sample Disturbance and Consolidation Procedures on Measured Shear Strength of Soft Marine Norwegian Clays. *Canadian Geotechnical Journal*, **43** (7), 726-750.

Lunne, T., & Long, M. (2006), Review of Long Seabed Samplers and Criteria for New Sampler Design. *Marine Geology*, **226** (1), 145-165.

Mannheimer, R.J. & Oswald, C.J. (1993). Development of Transparent Porous Media with Permeabilities and Porosities Comparable to Soils, Aquifers and Petroleum Reservoirs. *Ground Water*, **31** (5), 781-788

Melling, A. (1997). Tracer Particles and Seeding for Particle Image Velocimetry, *Measurement Science and Technology*, **8**, 1406-1416

Messerklinger, S., Springman, S.M. (2009). Economic Sampling and Extraction of Undisturbed, High Quality Samples in Normally Consolidated Lacustrine Clays Using a Large Diameter Tube, *Geotechnical and Geological Engineering,* **27** (2), 207-215

Miller, G.A. & Lutenegger, A.J. (1997). Influence of Pile Plugging on Skin Friction in Overconsolidated Clay, Journal of Geotechnical and Geoenvironmental Engineering, **123** (6), 525-533

Milovic, D.M. (1971). Effects of Sampling on Some Soil Characteristics, In: *Symposium on Sampling of Soil and Rock, ASTM STP 483*, 164-179

Nagaraj, T.S., Srinivasa Murthy B.R., Vatsala, A. & Joshi, R.C. (1990). Analysis of Compressibility of Sensitive Clays. *Journal of Geotehnical Engineering*, ASCE. **116** (1), 105-118

Nagaraj, T.S., Miura, N., Chung, S.G. & Nagendra Prasad, K. (2003). *Géotechnique*, **53** (7), 679-683

Nagendra Prasad, K., Trveni, S., Schanz, T. & Nagaraj, T.S. (2007). Sample Disturbance in Soft and Sensitive Clays: Analysis and Assessment, *Marine Georesources and Geotechnology*, **25**, 181-197

National Instruments (2013) NI Vision Concepts Help 372916P-01, In-Depth Discussion

NEDO (National Economic Development Office) (1988). *Faster Building for Commerce*. NEDO, London.

Ni, Q. Hird, C.C., Guymer, I. (2010). Physical Modelling of Pile Penetration in Clay using Transparent Soil and Particle Image Velocimetry", *Géotechnique*, **60** (2), 121-132

Paul, E.L., Atiemo-Obeng, V.A. & Kresta, S.M. (2004). Handbook of Industrial Mixing: Science and Practice, Volume 1, John Wiley and Sons

Prasad, A. K. (2000). Particle Image Velocimetry, *Current Science*, **79** (1), 51-60.

Raffel, M. (1998). *Particle Image Velocimetry, a Practical Guide*. Springer

Raymond, G.P., Townsend, D.L. & Lojkasek, M.J. (1971). The Effect of Sampling on the Undrained Properties of a Leda Soil. *Canadian Geotechnical Journal*, **8**, 546-557

Rostami, M., Ardeshir, A., Ahmadi, G. & Thomas, P.J. (2007). Development of a Low Cost and Safe PIV for Mean Flow Velocity and Reynolds Stress Measurements. International Journal of Engineering, **20** (2), 105-116

Rowe, P.W. (1971). Representative Sampling in Location, Quality and Size, In: *Symposium on Sampling of Soil and Rock, ASTM STP 483*, 77-106

Rowe, P.W. (1972). The Relevance of Soil Fabric to Site Investigation Practice, *Géotechnique*, **22** (2), 195-300

Sadek, S., Iskander, M. & Liu, J. (2002). Geotechnical Properties of Transparent Silica. *Canadian Geotechnical Journal*, **39** (1), 111-124

Sadek, S., Iskander, M. & Liu, J. (2003). Accuracy of Digital Image Correlation for Measuring Deformations in Transparent Media. *Journal of Computing in Civil Engineering,* **17** (2), 88–96.

Safaqah, O.A. & Riemer, M.F. (2005). Minimizing Sampling Disturbance using a new In-situ Device, *Soil Dynamics and Earthquake Engineering*, **26**, 153-161

Sagaseta, C., Whittle, A.J. & Santagata, M. (1997). Deformation Analysis of Shallow Penetration in Clay, *International Journal for Numerical and Analytical Methods in Geomechanics*, **21**, 687-719

Santagata, M.C. & Germaine, J.T. (2002). Sampling Disturbance Effects in Normally Consolidated Clays, *Journal of Geotechnical and Geoenvironmental Engineering,* **128** (12), 997-1006

Santagata, M.C. & Germaine, J.T. (2005). Effect of OCR on Sampling Disturbance of Cohesive Soils and Evaluation of Laboratory Reconsolidation Procedures, *Canadian Geotechnical Journal*, **42**, 459-474

Santagata, M., Sinfield, J.V. & Germaine, J. T. (2006). Laboratory Simulation of Field Sampling: Comparison with Ideal Sampling and Field Data. *Journal of Geotechnical and Geoenvironmental Engineering*, **132** (3), 351-362

Shih, S-W., Hung, Y-P. & Lin, W-S. (1993). When should we consider Lens Calibration in Camera Calibration, *Pattern Recognition*, **28** (3), 447-461

Siddique, A., (1990). *A Numerical and Experimental Study of Sampling Disturance*, Thesis (PhD), University of Surrey

Siddique, A., Clayton, C.R.I. & Hopper, R.J. (1999). The Effects of Varying Centreline Tube Sampling Disturbance on the Behavior of Reconstituted Clay, **22** (3), 245-256

Siddique, A., Farooq, S.M. & Clayton, C.R.I. (2000). Disturbances due to Tube Sampling in Coastal Soils, Journal of Geotechnical and Geoenvironmental Engineering, **126** (6), 568-575

Siddique, A., Ameen, S.F. & Islam, M.J. (2009). A Comparative Study on Engineering Properties of “Block” and “Tube” Samples of a Soft Clay, *Journal of Civil Engineering*, **37** (1), 11-30

Skempton, A.W. & Sowa, V.A. (1963). The Behaviour of Saturated Clays during Sampling and Testing, *Géotechnique*, **13** (4), 269-290

Stanier, S.A., Black, J.A. and Hird, C.C. (2012). Enhancing Accuracy and Precision of Transparent Synthetic Soil Modelling, *International Journal of Physical Modelling in Geotechnics,* **12** (4), 162-175

Sukolrat, J., Nash, D.F.T., & Benahmed, N. (2008). The Use of Bender Elements in the Assessment of Disturbance of Soft Clay Samples. In *Proceedings of the 3rd International Conference on Site Characterization (ISC'3), Taipei*

Tan, T.S., Lee, F.H., Chong, P.T., & Tanaka, H. (2002). Effect of Sampling Disturbance on Properties of Singapore Clay. *Journal of Geotechnical and Geoenvironmental Engineering*, **128** (11), 898-906

Tan, W.H., Lee, C.Y. & Sivadass, T. (2008). Behaviour of Clay-Steel Interfaces, In: *Proceedings of the International Conference on Construction and Building Technology 2008*, 11-20

Tanaka, M., Tanaka, H. & Shiwakoti, D.R. (2001). Sample Quality Evaluation of Soft Clays Using Six Types of Samplers, In: P*roceedings of the 11th International Offshore and Polar Engineering Conference, Stavanger,* 493-500

Tardif, J-P., Sturm, P., Trudeau, M. & Roy, S. (2009). Calibration of Cameras with Radially Symmetric Distortion, *IEEE Transactions on Pattern Analysis and Machine Intelligence*, **31** (9), 1552-1566

Tavenas, F., & Leroueil, S. (1977). Effects of Stresses and Time on Yielding of Clays. In *Proceedings of the 9th International Conference on Soil Mechanics and Foundation Engineering*, **1**, 319-326

Tavenas, F. & Leroueil, S. (1987). Laboratory and In-Situ Stress-Strain-Time Behavior of Soft Clays I: Laboratory Tests, In: *Proceedings of the International Conference of Geotechnical Engineering on Soft Soils*, City of Mexico, p7-38

Taylor, M.L. Cubrinovski, M. (2012). Application of New 'Gel-Push' Sampling Procedure to Obtain High Quality Laboratory Test Data for Advanced Geotechnical Analyses, In: *Proceedings from the 11th Australia – New Zealand Conference on Geomechanics, Melbourne*

Taylor, M.L. Cubrinovski, M. (2012). Characterisation of Ground Conditions in the Christchurch Central Business District: A Mid-Project Summary, In: *Proceedings from the 11th Australia – New Zealand Conference on Geomechanics, Melbourne*

Terzaghi, K. (1943). *Theoretical Soil Mechanics*, John Wiley and Sons, New York

Tyrrel, A. P., Lake, L. M. & Parsons, A. W. (1983). *An Investigation of the Extra Costs Arising on Highway Contracts*, TRRL Supplementary Report SR814, Transport and Road Research Laboratory, Crowthorne, Berks.

van Eekelen S. & van den Berg, P. (1995). Sample Disturbance, Numerical Model and Experiments, *International Journal of Rock Mechanics and Mining Sciences and Geomechanics Abstracts,* **32** (3) 115A-115A). Elsevier.

Vass, G. & Perlaki, T. (2003). Applying and Removing Lens Distortion in Post Production, Colorfront Ltd, Budapest

Wei, R.L., Yang, S.H. & Wang, N.X. (1994). Sampling Disturbance Effect on Strength of Soft Clay, In: *Proceedings of the 13th International Conference on Soil Mechanics and Foundation Engineering, New Delhi*, **3**, 321-324

Westerweel, J. (1997). Fundamentals of Digital Particle Image Velocimetry, *Measurement Science and Technology*, **8**, 1379-1392

White, D.J., Take, W.A. & Bolton, M.D. (2001). Measuring Soil Deformation in Geotechnical Models using Digital Images and PIV Analysis, In: *Proceedings of the 10th International Conference on Computer Methods and Advances in Geomechanics*. 997-1002

White, D.J., Take, W.A. (2002). GeoPIV, Particle Image Velocimetry Software for Use in Geotechnical Testing. *Cambridge University Engineering Department Technical Report, D-SOILS-TR322*

White, D.J., Take, W.A. & Bolton, M.D. (2003). Soil Deformation Measurement using PIV and Photogrammetry. *Géotechnique*, **53** (7), 619–631

White, D. J., & Bolton, M. D. (2004). Displacement and Strain Paths During Plane-Strain Model Pile Installation in Sand. *Géotechnique*, **54** (6), 375-397.

White, D.J., Randolph, M. & Thompson, B. (2005). An Image-Based Deformation Measurement System for the Geotechnical Centrifuge. *International Journal of Physical Modelling in Geotechnics*, **5** (3), 1-12

Willert, C.E., & Gharib, M. (1991). Digital Particle Image Velocimetry, *Experiments in Fluids*, **10** (4), 181-193.

Wu, C. S. (1991). *Mechanics of Sampling Disturbances in Clay Soils*, Thesis (PhD), University of Arizona

Yan, W.M., Ng, I.T. & Cheuk, C.Y. (2010). Displacement Field around an Open-Tube Sampling. In: *Proceedings of the 7th International Conference on Physical Modelling in Geotechnics, Zurich*, **1**, 411-416

Zhao, H., Ge, L & Luna, R. (2010). Low Viscosity Pore Fluid to Manufacture Transparent Soil. *Geotechnical testing Journal*. **33** (6), 1-6

Appendix A Design of Manufactured Parts

1- Consolidation Rig

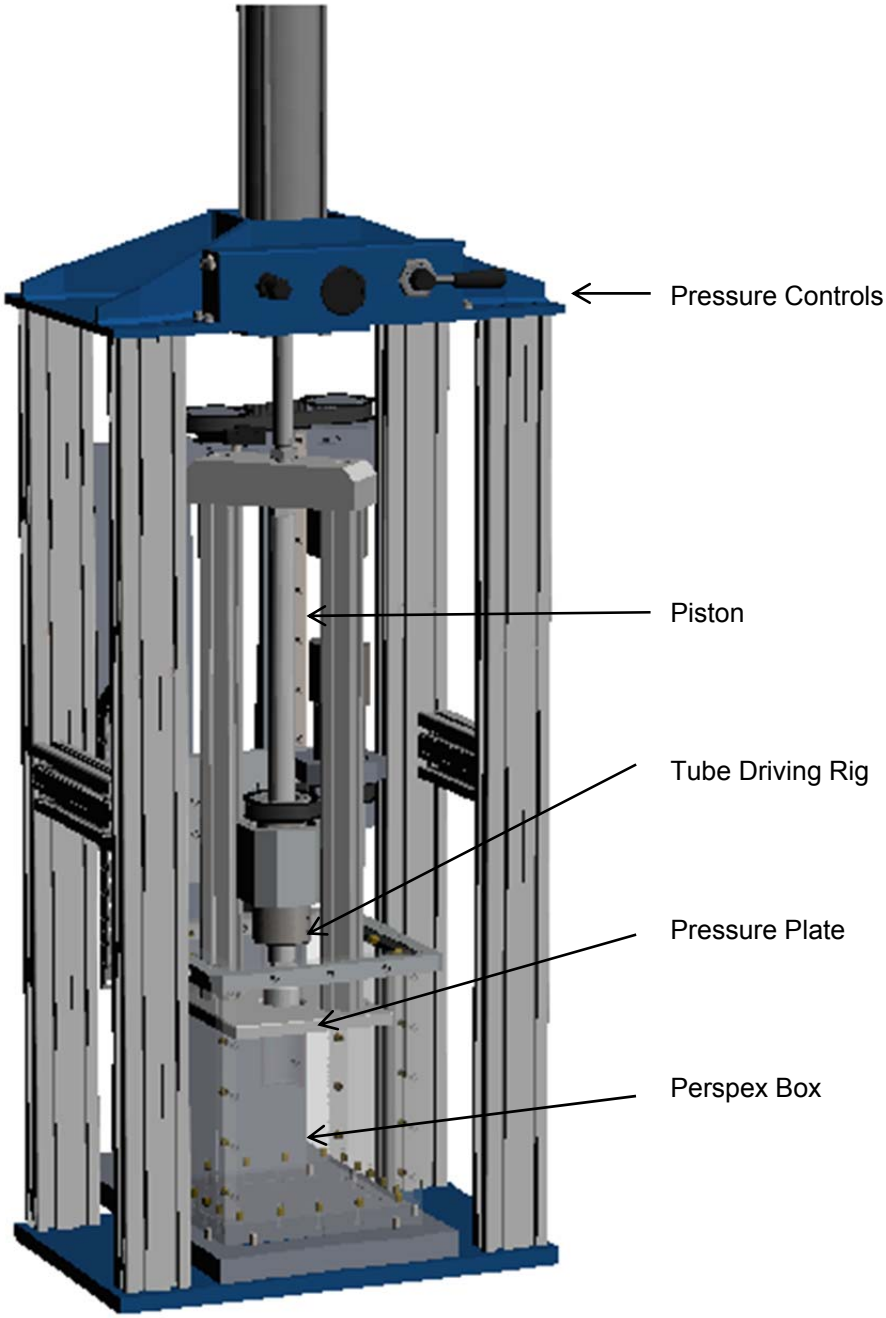

Figure A. 1 - Consolidation Rig

2- Perspex Box

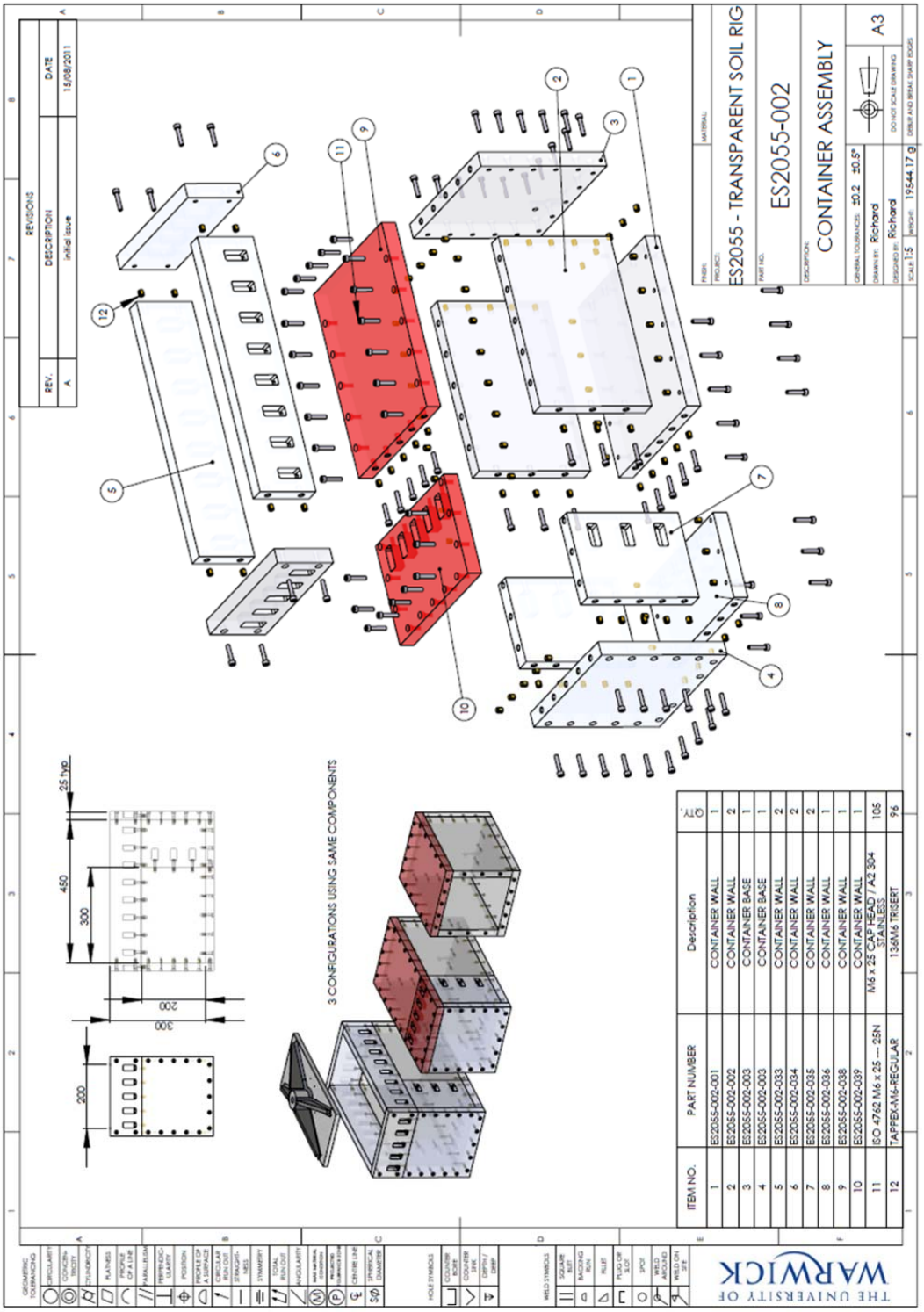

Figure A. 2 - Model Box

3- Tube Holder

Option C was chosen, although the connection between the tube and holder was made shorter. Future designs would benefit from an increased contact, and a regular replacement of the O-rings, which degrade in time and with contact with the oil which is a component of the transparent soil.

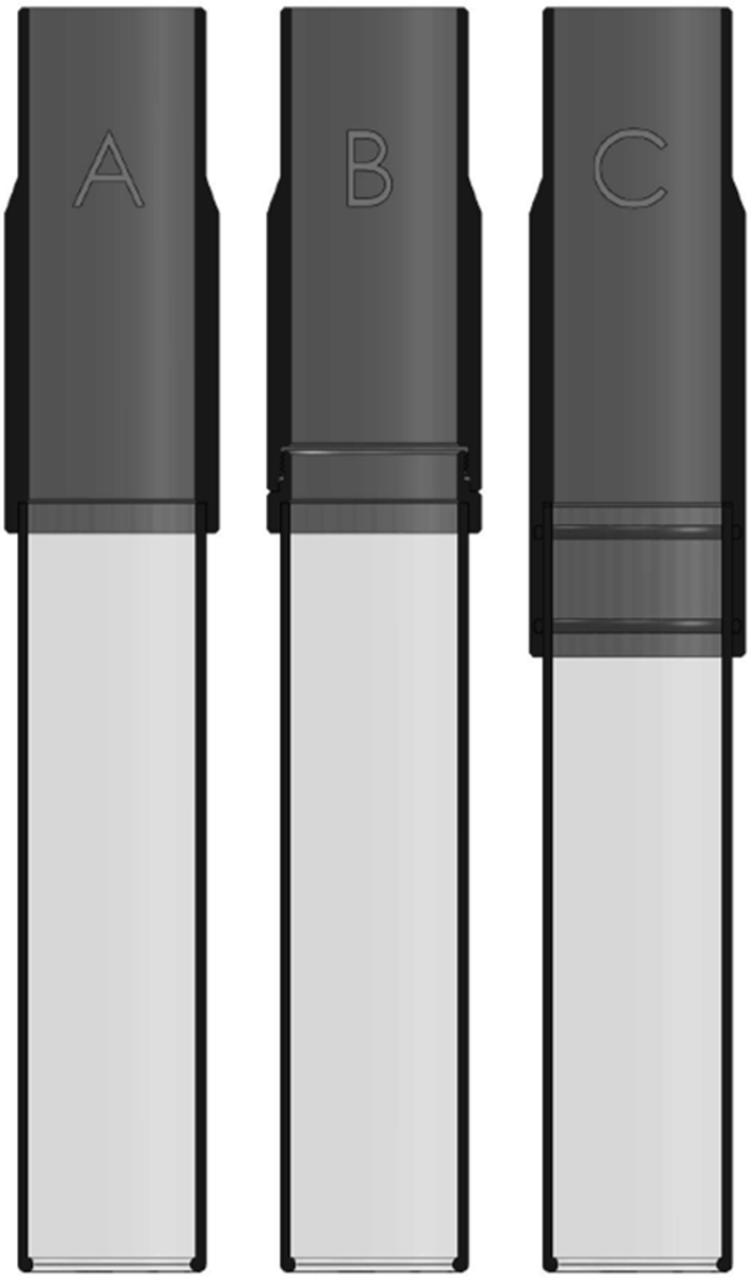

Figure A. 3 - Tube Holder

3- Monitoring Rig

The monitoring setup was covered with a blackout cloth, and the camera was fitted on its mount throughout the process to reduce camera shake. The charge lasted for the whole of the experiment, approximately nine months, when turned on twice a week to take a single photo.

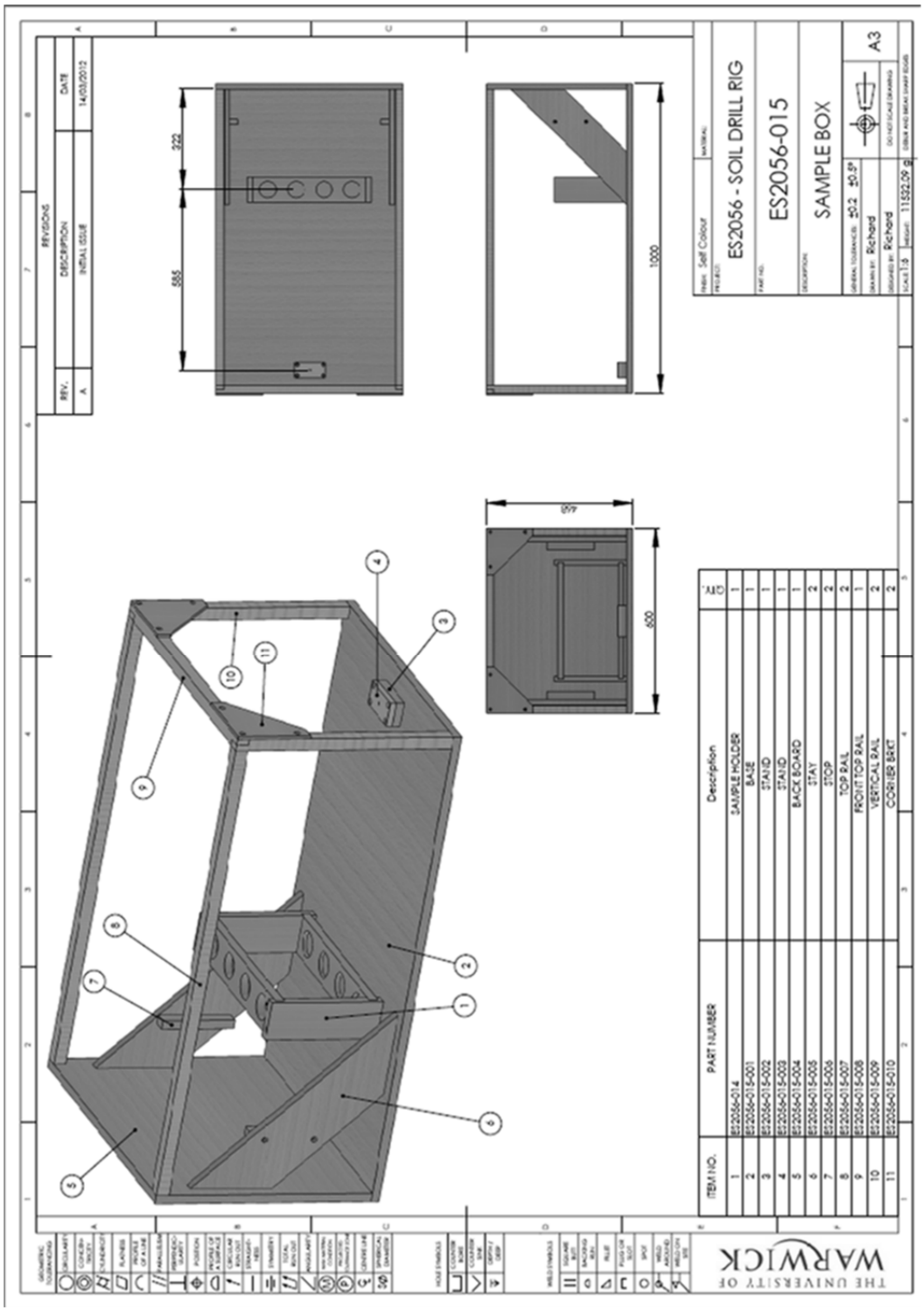

Figure A. 4 - Monitoring Rig

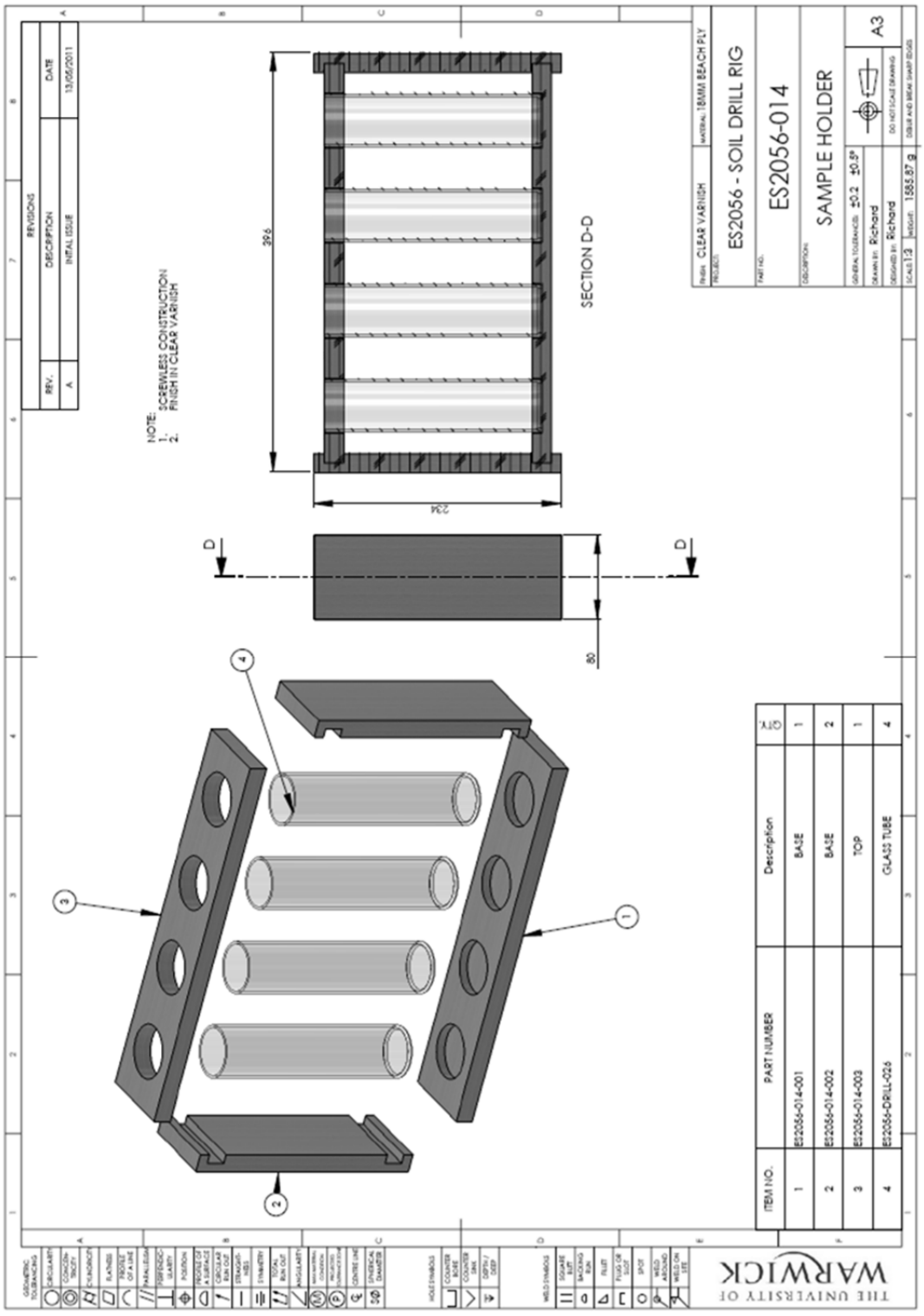

Figure A. 5 - Tube Holder

4- Extruder

The extruder was operated manually and was designed to clamp onto a universal mounting system.

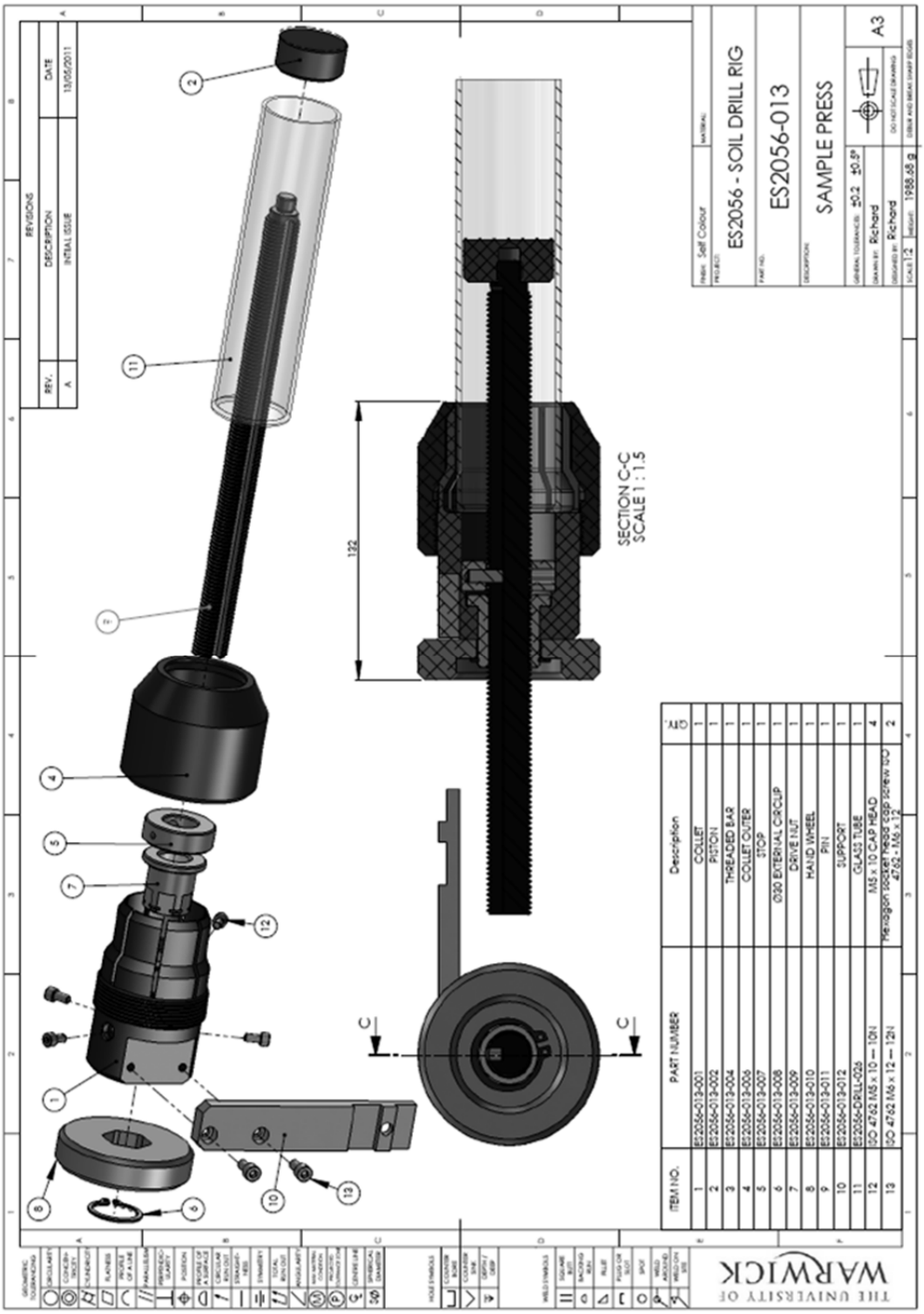

Figure A. 6 - Extrusion Apparatus

Appendix B Health and Safety: COSHH Forms

Aztec Oils Ltd
31-33 Intake Rd Bolsover, Chesterfield S44 6BB
SAFETY DATA SHEET
(Conforms to EC Directive 91/155/EEC)

Date of first Issue: October 1996
Date: 18th.October 2002

---

1. Identification **Code:** Tech15
Commercial name: **Technical White 15**

Emergency Telephone Number: **01246 823007**

---

2. Composition: Very Highly Refined Hydrocarbon Mineral oils.
CAS Registry number: 8042-47-5
EINECS Number: 232-455-8
Risk phrases: None required under present UK and EEC legislation.
Safety Phrases: N/A

---

3. Hazards Not classified as dangerous under current UK Health & Safety and Environmental Legislation when used in the application for which it is intended

---

4. First Aid Measures
Eye contact: Irrigate with plenty of cold water.
Skin contact: Wash off with copious amounts of soap and water.
Ingestion: If more than a few drops swallowed give patient water to drink. Do not induce vomiting and seek medical advice.
Inhalation: Remove to fresh air. If unconscious turn into the recovery position. Get medical help.

---

5. Fire Fighting Measures: Not considered flammable and does not constitute a fire hazard, but is inherently combustible.
Extinguishing Media: Carbon dioxide, dry powder, sand,earth,foam or water fog. Use fog of water spray to cool fire exposed surfaces.
Protective Equipment for Fire-fighters: Standard

---

6. Accidental Release Measures: Contain spillage in sand or sawdust. Dispose of according to Local Regulations. If allowed to enter drains and/or water courses, alert Local Water Authority.

---

7. Handling and Storage: Do not store in areas where food and drink are taken. Keep in tightly closed and clearly labelled containers. No smoking. Naked flames, hot elements or other ignition sources must not be present.

---

8. Exposure Control and Personal Protection:
In accordance with good industrial practice handle using gloves/gauntlets and standard eye protection.
OEL (Mineral oil mist) 5mg/m^3 8-hour TWA; 10mg/m^3 (STEL)

---

9. Physical and Chemical Properties
Physical form: Clear liquid
Colour: Colourless
Odour: None
pH of aqueous solution: N.A.

Flash Point: 186
Viscosity: 15 centistokes @ 40C
Flammability solid/gas: N.A.
Density: 0.843 @ 15.6C

---

10. Stability and Reactivity

Thermal decomposition: Stable under normal conditions of use.
Hazardous reactions: None under normal conditions of use. Avoid contact with strong oxidizing agents.

11a. Toxicological Data

The mineral oil components of these oils may be considered not to be essentially toxic in normal handling..

---

12. Ecological Information

Although not toxic to vertebrates and invertebrates, likely to harm aquatic life as films formed on water may affect oxygen transfer and damage organisms. Expected to biodegrade slowly.

---

13. Disposal Conditions: Dispose of according to a recognised method of chemical waste disposal.

---

14. Transport Information

UN Name: Not assigned.
IMDG Code/Class: Non hazardous
ICAO/IATA (Air) Class: Non Hazardous
RID/ADR Class:
ADNR Class:

---

15. Regulatory Information:

As far as is known not classified according to EEC Directives 67/548/EEC and 88/379/EEC

---

16. Other Information:

Date of first Issue: October 1996
Date: 18th.October 2002

---

1. Identification **Code:** n-Paraffin
Commercial name: **n-Paraffin C10-C13**

Emergency Telephone Number: **01246 823007**

---

2. Composition: C10-C13
CAS Registry number: 64771-71-7
Classification: Harmful
Risk phrases: R65-May cause lung damage if swallowed.
A combination of normal paraffins having carbon numbers predominantly greater than C10 and mainly in the C10-C13 range. Contains no substances classified as hazardous under Directive 67/548/EEC and other UK CHIP Regulations.

---

3. Hazards: On the basis of our knowledge, n-Paraffin C10-C13 is unlikely to be hazardous to man in normal use. It is substantially biodegradable in the aquatic environment.

---

4. First Aid Measures
Eye contact: Irrigate with plenty of cold water.
Skin contact: Wash off with copious amounts of soap and water.
Ingestion: If more than a few drops swallowed give patient water to drink. Do not induce vomiting and seek medical advice.
Inhalation: Remove to fresh air. If unconscious turn into the recovery position. Get medical help.

---

5. Fire Fighting Measures .
Extinguishing Media: Carbon dioxide, dry powder, sand, earth, foam or water fog.
Use fog of water spray to cool fire exposed surfaces.
Unsuitable Extinguishing Media: Do not use water jets.
Protective Equipment for Fire-fighters: Self-contained breathing apparatus must be employed in a Fire situation.

---

6. Accidental Release Measures: Treat any spillage as a fire hazard. Spray vapour or mist can be a potential fire or explosion hazard Contain spillage in sand or sawdust. Dispose of according to Local Regulations. If allowed to enter drains and/or water courses, alert Local Water Authority.

---

7. Handling and Storage: Do not store in areas where food and drink are taken. Keep in tightly closed and clearly labelled containers. Store in well ventilated conditions out of direct sunlight. No smoking. Naked flames, hot elements or other ignition sources must not be present.

---

8. Exposure Control and Personal Protection:
In accordance with good industrial practice handle using gloves/gauntlets and standard eye protection.
OEL Time weighted average(8 hours)- (1200mg/m3)

---

9. Physical and Chemical Properties
Physical form: Clear liquid
Colour: Colourless
Odour: None
pH of aqueous solution: N.A.
Flash Point: 65 .
Boiling Range 180-235 C
Melting Point-21 C

---

10. Stability and Reactivity

Stability: Stable at ambient temperatures.

Conditions to avoid: Must not be situated near sources of ignition.

Materials to avoid: Incompatible with strong oxidizing agents.

Hazardous decomposition products:

Thermal decomposition may lead to the formation of a multiplicity of compounds some of which may be hazardous. With incomplete combustion smoke and hazardous fumes and gases including carbon monoxide may be formed.

---

11. Toxicological Data

Toxicity following single exposure (orally, dermally or by inhalation) to n-Paraffin C10-C13 is of a low order.

With the use of good occupational hygiene any risk will be minimal.

---

12. Ecological Information

n-Paraffin C10-C13 components have log Pow values in the range 3.9 to greater than 6. May bioaccumulate; films formed on water may affect oxygen transfer and damage organisms.

---

13. Disposal Conditions: Dispose by incineration or by methods approved by local authority. Do not discharge into public drainage system, or marine or inland waterway.

---

14. Transport Information

UN Name: Not assigned.

IMDG Code/Class: Non hazardous

ICAO/IATA (Air) Class: Non Hazardous

RID/ADR Class:

ADNR Class:

---

15. Regulatory Information:

Labelling

Classified as dangerous under the 21st ATP of the Dangerous Substances Directive 67/548/EEC due to the aspiration hazard

Classification: Harmful

Symbol: St Andrews Cross

Risk Phrases: R65 Harmful: May cause lung damage if swallowed.

Safety Phrases: S2 Keep out of reach of children, S23-Do not breathe vapour, S24- Avoid contact with skin. S43-In case of fire use foam, dry powder, AAAF, CO2 –Never use water. S62- If swallowed do not induce vomiting: seek medical advice immediately and show this container or label.

Issue Date: 16.11.2001,
NA Edition No. 12 Product code: 0142/eng/07 Revsion Date: 27.10.2002 (EU)

1. IDENTIFICATION OF THE SUBSTANCE/PREPARATION AND THE COMPANY/UNDERTAKING
Identification of the substance/preparation
Product name Hydrated Amorphous Silica , Product code 0142
Use of the Substance Additive, Chemical intermediate
Supplier PPG Industries Inc. One PPG Place, Pittsburgh PA 15272, USA
Telephone ++1 412 434 2278, Telefax ++1 412 434 3193
Emergency telephone number ++1 304 843 1300 (USA)
Emergency telephone number ++32 1 458 4545 (Europe)

---

2. COMPOSITION/INFORMATION ON INGREDIENTS
Chemical name of the substance Silicon Dioxide- hydrated
Synonyms HiSil®, Lo-Vel®, Flo-Gard®, San-Sil®. Silene® Silica, chemically prepared.
EC-No. 231-545-4 CAS-No. 7631-86-9 / 112926-00-8
Hazardous impurities This product contains no crystalline silica (<0.01%, below detection limit)

---

3. HAZARDS IDENTIFICATION
Most important hazards Health injuries are not known or expected under normal use.
Specific hazards May cause eye or skin irritation with susceptible persons. May cause irritation of respiratory tract.

---

4. FIRST AID MEASURES
General advice
Immediate medical attention is not required. No hazards which require special first aid measures.
Inhalation: Move to fresh air. If symptoms persist, call a physician.
Skin contact: Wash off with soap and plenty of water.
Eye contact: Wash off with plenty of water. If eye irritation persists, consult a specialist.
Ingestion: Gently wipe or rinse the inside of the mouth with water. Give small amounts of water to drink. Never give anything by mouth to an unconscious person. Consult a physician if necessary.

---

5. FIRE-FIGHTING MEASURES
Suitable extinguishing media: The product itself does not burn.
Extinguishing media which must not be used for safety reasons: None.
Specific hazards: None.
Special protective equipment for firefighters: None.

---

6. ACCIDENTAL RELEASE MEASURES
Personal precautions: Ensure adequate ventilation.
Environmental precautions: No special environmental precautions required.
Methods for cleaning up: Pick-up and arrange disposal without creating dust. After cleaning, flush away traces with water.

---

7. HANDLING AND STORAGE
Technical measures/Precautions: Provide appropriate exhaust ventilation at places where dust is formed. Take measures to prevent the build-up of electrostatic charge.
Safe handling advice: Avoid dust formation.
Technical measures/Storage conditions: Keep in a dry place. Keep tightly closed.
Incompatible products: None.

---

8. EXPOSURE CONTROLS / PERSONAL PROTECTION
Occupational exposure controls
Exposure Limit Values: OSHA PEL 6 mg/ m3 (Total dust.) 8-hour TWA /1989), ACGIH 10 mg/m3 (Total dust.) 8h TWA OEL- Austria: MAK 4 mg/m3, JAN1999

Engineering measures to reduce exposure: Ensure adequate ventilation, especially in confined areas.
Personal protection equipment
Respiratory protection: Effective dust mask.
Hand protection: Rubber gloves / leather gloves. Break through time > 8h.
Eye protection: Tightly fitting safety goggles.
Skin and body protection: Lightweight protective clothing, boots, apron.
Hygiene measures: General industrial hygiene practice. When using do not eat or drink.
Environmental exposure controls No special environmental precautions required.

---

9. PHYSICAL AND CHEMICAL PROPERTIES
General Information
Form powder / granular Colour white Odour none.
Important Health Safety and Environmental Information pH 6.5 - 7.3 (5% suspension)
Boiling point/range not applicable
Decomposition temperature no data available
Flash point does not flash
Explosion limits not applicable
Vapour pressure none.
Vapor density not applicable
Bulk density no data available
Solubility Water solubility insoluble
Melting point/range no data available

---

10. STABILITY AND REACTIVITY
Stability Stable at normal conditions.Hazardous polymerisation does not occur.
Conditions to avoid Do not expose to temperatures above 800 °C
Materials to avoid None.
Hazardous decomposition products None.

---

11. TOXICOLOGICAL INFORMATION
Acute toxicity LD50/oral/rat > 5 g/kg (estimated).
Local effects Product dust may be irritating to eyes, skin and respiratory system.
Long term toxicity Health injuries are not known or expected under normal use.
Specific effects ARC Group III - Carcinogenicity classification not possible from current data.

---

12. ECOLOGICAL INFORMATION
Mobility Insoluble.
Persistence / degradability No data available.
Bioaccumulation No data available.
Ecotoxicity EC0/daphnia > 1000ppm EC0/4 days/Fish > 10,000ppm EC0/96h/Fish> 10,0ppm

---

13. DISPOSAL CONSIDERATIONS
Waste from residues / unused products Can be landfilled, when in compliance with local regulations.
Contaminated packaging Empty containers should be taken for local recycling, recovery or waste disposal.
Further information According to the European Waste Catalogue, Waste Codes are not product specific, but application specific. Waste codes should be assigned by the user based on the application for which the product was used.

---

14. TRANSPORT INFORMATION
Not classified as dangerous in the meaning of transport regulations.

---

15. REGULATORY INFORMATION
The product does not need to be labelled in accordance with EC directives or respective national laws.

Appendix C Evidence of Camera Shake

Camera shake was measured and used to correct the photos so that the apparent movement of elements within the image was reduced. The following graphs plot this movement around the original location of the patch, at (0, 0). The conversion factor to mm is approximately 1/11.

Tube Driving Tests, Pentax K20D Camera, 35mm Lens – Test 2CNC

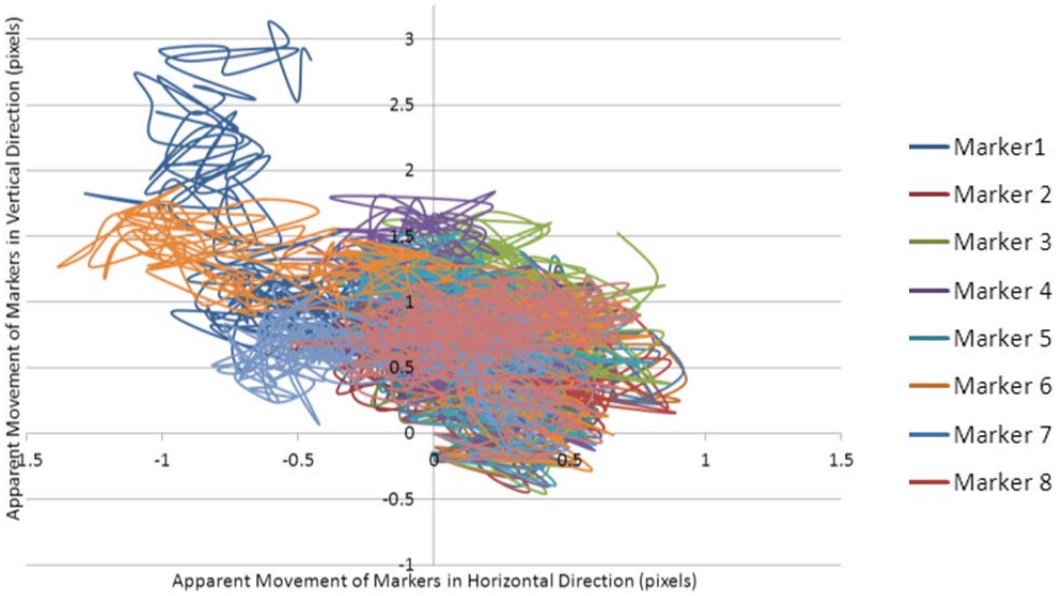

Figure C. 1 - Apparent Movement of Static Marker Points due to Camera Shake before Correction

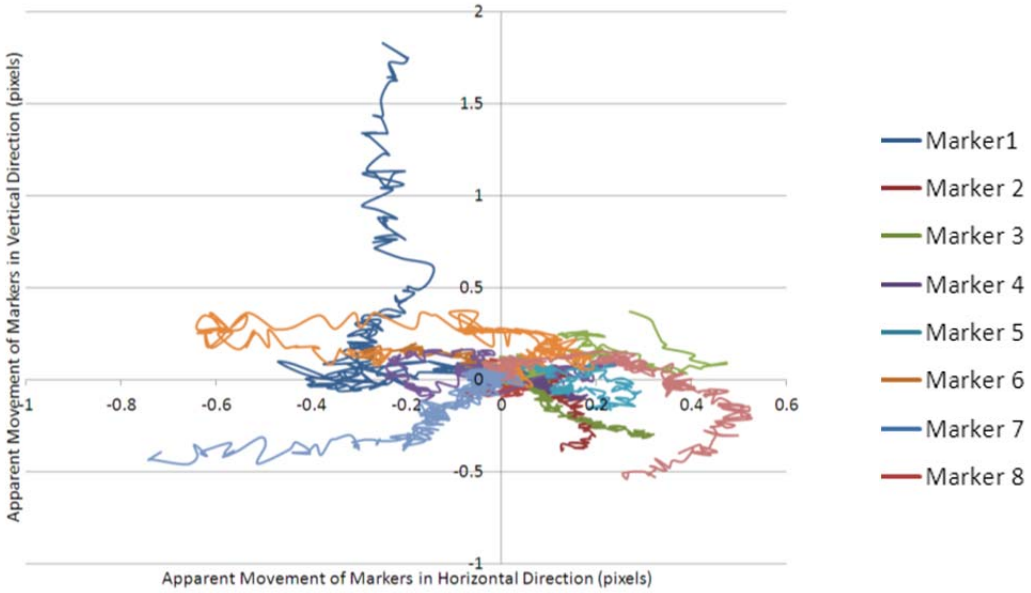

Figure C. 2 - Apparent Movement of Static Marker Points due to Camera Shake after Correction

Monitoring Tests, Pentax K-r Camera, 40mm Lens

The apparent movements for the Pentax K-r were more significant than in the two other cameras. This is due to use over a long period of time when the camera would be switched on twice weekly to take a single photograph. The action of switching on the camera caused apparent movements of up to ±40 pixels, or approximately 4mm, which was problematic since the studied displacements were smaller than this.

A study of the movements revealed that these were typical of a small (approx. 0.1°) rotation, which would not easily be corrected using image registration. By not correcting the data, strains could be calculated, but displacements would be erroneous.

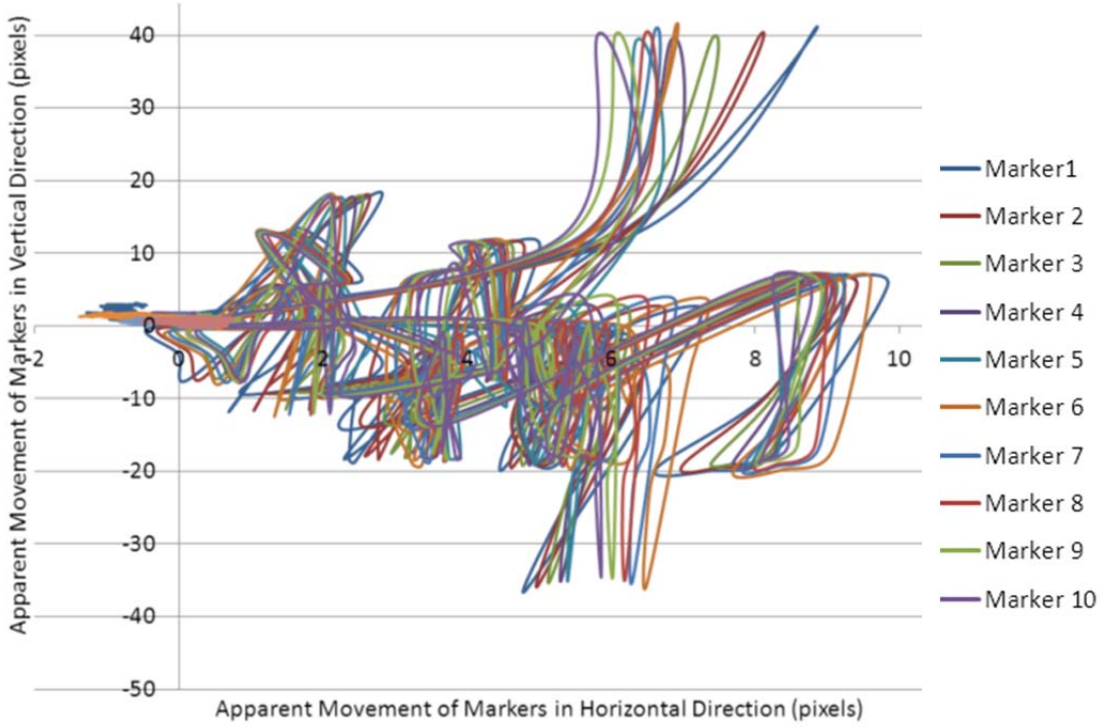

Figure C. 3 - Apparent Movement of Static Marker Points due to Camera Shake before Correction

Extrusion Tests, Canon EOS 6D Camera, 50 mm Lens – Test

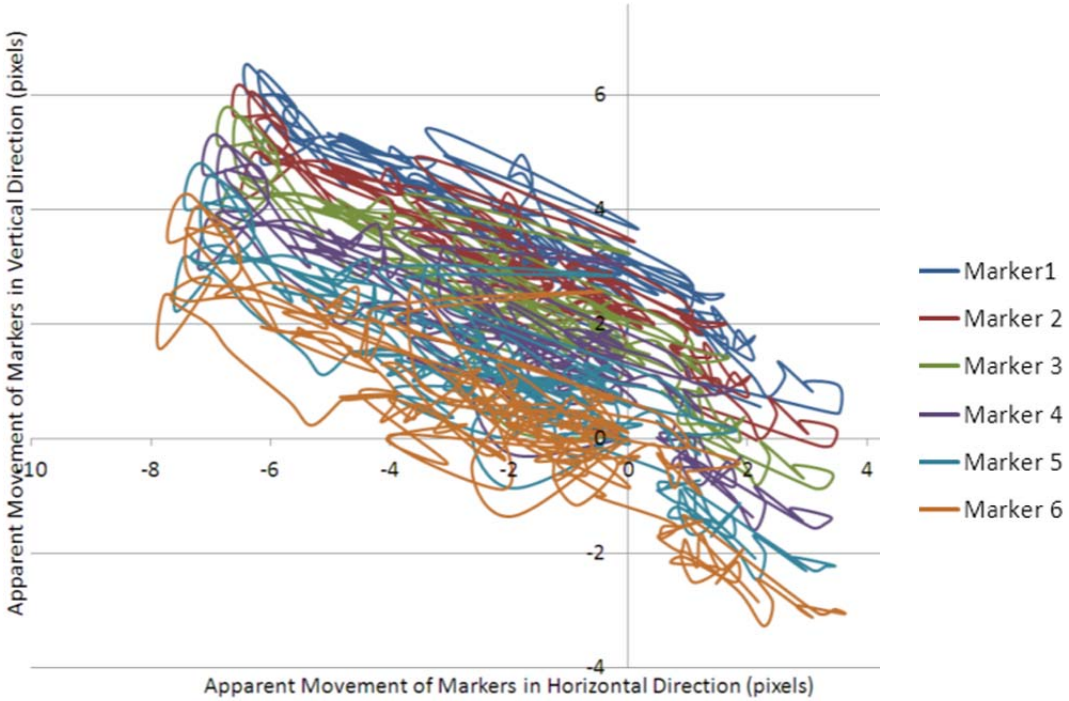

Figure C. 4 - Apparent Movement of Static Marker Points due to Camera Shake before Correction

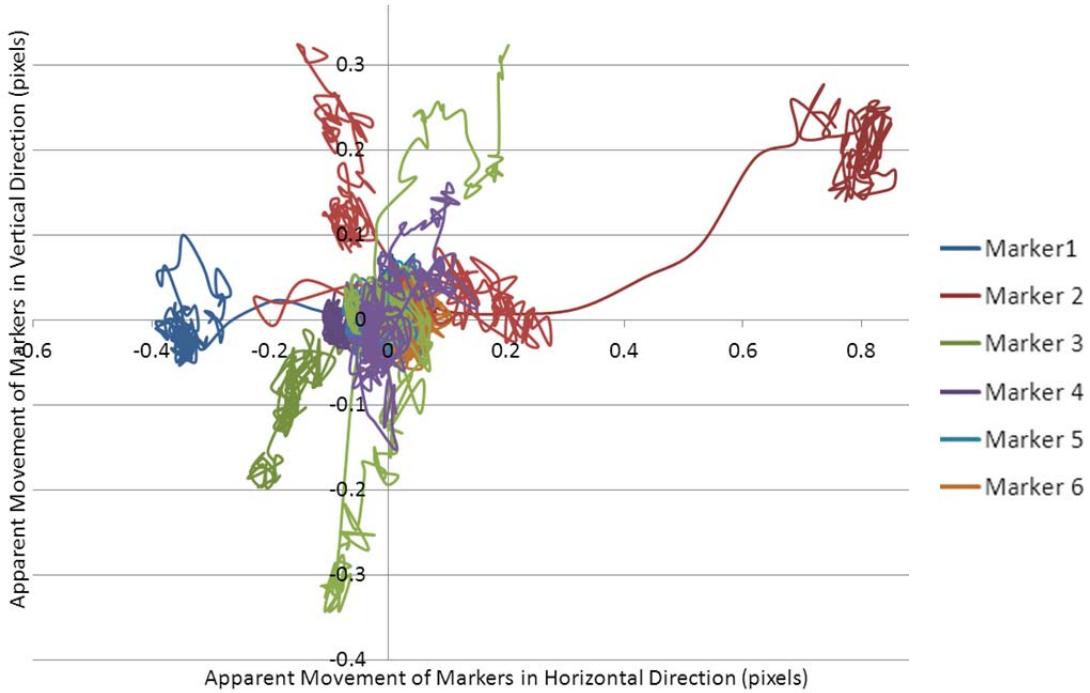

Figure C. 5 - Apparent Movement of Static Marker Points due to Camera Shake after Correction

Appendix D Correction for Optical Distortions

To study lens distortions, calibration plates can be used (White *et al*, 2003, Ni *et al*, 2010). A calibration plate (Appendix I) was made in the form of a sheet of marker points of 4mm diameter spaced at 10mm centres. It was created with Inkscape, an image processing program which allowed precise (to the pixel) designs of calibration sheets. This was printed and stuck to a 200x200x300 mm (L:W:H) rigid frame. This was photographed with the Pentax K20D using a 40mm fixed lens, under test conditions (hereafter referred to as Photo A, same set-up, same lighting, same camera to box distance), inside the empty Perspex box with its front side removed (this was just to ensure the frame was orthogonal to the camera), but also in the box filled with oil (Photo B, the oil has same RI as the transparent soil), for later use when determining the effect of refraction on distortion. A Matlab script by the creators of GeoPIV was used to calculate the coordinates of the centroid of each marker point to two decimal places, with some evidence of rounding. The spacings (in pixels) between each pair of points were calculated throughout the entire calibration sheet in x and y directions. Figure D. 1 represents a colour map for each direction, with green representing smaller spacings (average spacing minus 1.5 pixels: less magnification) and red for larger spacings (average spacing plus 1.5 pixels: highest magnification). Zones of highest x spacing were seen in two bands running down the entire length of the photograph, while the distribution of y spacings was more uniform (average spacing ± 0.5 pixels). The data does not fully resemble barrel distortion, since the spacings would be expected to be largest in the centre of the image, decreasing towards the edges of the image. Nor does it resemble pincushion distortion, since smaller distortions appear at the edges of the photograph. Overall it is closest to barrel at first glance. The average spacing between marker points for x and y directions was calculated and was found to differ by 0.15 pixels over a distance of 84 pixels. This points either to a printer or software issue when creating the calibration sheet, or to the possibility that the pixels in the camera are not completely square (White et al, 2003). Evidence of rounding to 0 decimal places was seen for many marker points, so the accuracy of the script is questionable.

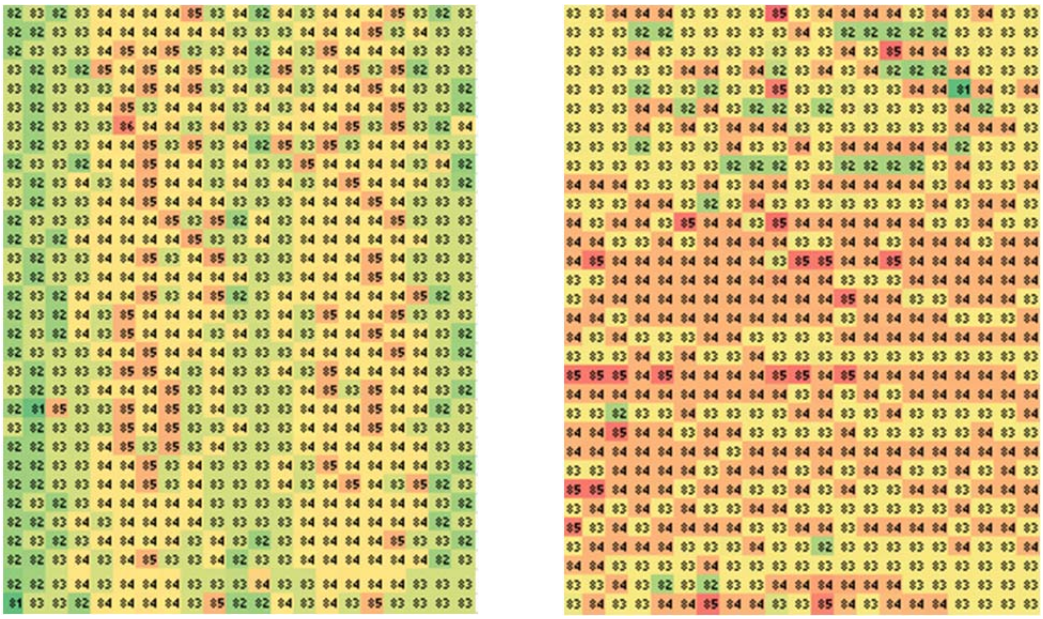

Figure D. 1 - Measured Spacings between marker Points for Air Only Photo in a) x direction, and b) y direction

Distortion can be measured by comparing the original (undistorted by the lens) position of each marker point with its position in the photograph, provided that the original position is known. In a photograph with linear magnification, the spacing between any pair of marker points can be measured and used to calculate the coordinates of all other points, as they are separated by a known number of pixels in x and y direction. Comparing the coordinates of the marker points with those recreated – if the behaviour is indeed linear – the difference will be zero, allowing for some noise in the data. If the behaviour is not linear, plotting the difference between these coordinates against the distance from the centre will reveal the distortion pattern in the image. The issue then is to select an appropriate value for spacing in the recreated matrix of coordinates, since distortion is suspected throughout the photograph, and no value can be taken as representative. Since spacings seem to decrease at higher distances from the image centre, the problem can be studied as barrel distortion, and one approach would be to take the spacing at the centre of the image. Selecting the average values for x and y spacings over the innermost 10 rows and columns of marker points, the distortions between the recreated coordinates and the measured coordinates are presented in Figure D. 2.

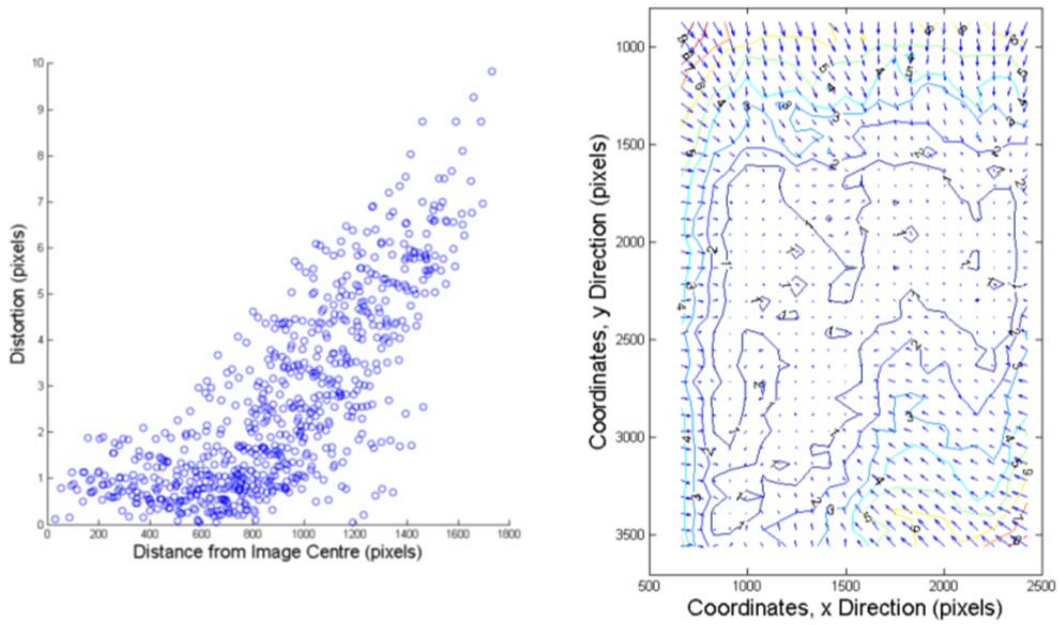

Figure D. 2 - Evidence of Barrel Distortion in Photo A from Calibration Plate

A comparison of Figure 3.20 and Figure D. 2 shows that the type of distortion is indeed barrel distortion and that the maximum distortion in the photograph, due to the lens, is 10 pixels inwards (i.e, the image edges shrink up to 10 pixels inwards). However, in the parts of the photograph where the displacement data is gathered – typically 1200<y<3400 (since that is where the soil is) – distortion vectors are inferior to 4 pixels, with the vast majority much smaller (dark blue and light blue contours in Figure D. 2). Since the magnitude of soil movement is relatively small (as will be seen in Chapter 4), it will not cross many contour boundaries and will therefore not be largely affected by lens distortion within the area of interest. A second check for barrel distortion is to look at a line within the image which is known to be straight in object-space, such as each row or column of marker points, and plot their coordinates to check whether they are still collinear. Figure D. 3 shows the curve for two outer columns and the bottom row of marker points and the evidence for barrel distortion is clear, which validates the evidence above. The behaviour is not the same in x and y directions, with more barrelling present in the x direction.

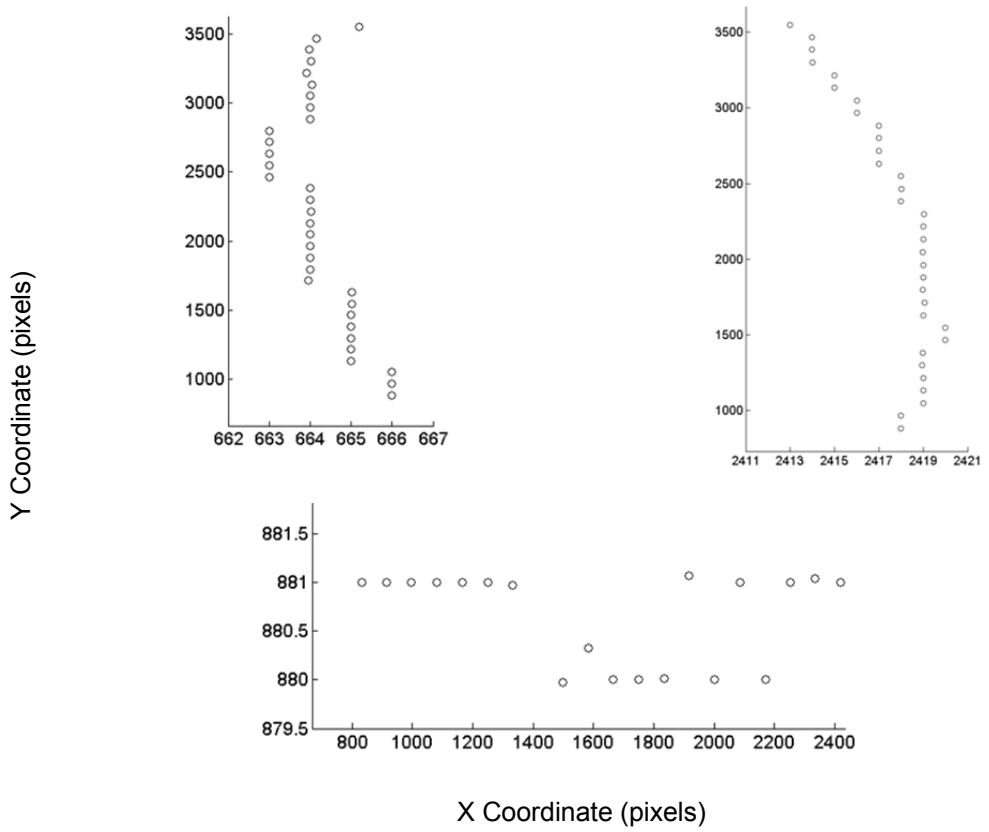

Figure D. 3 - Evidence of Barrelling of Straight Lines in Photo A

A final check was carried out on the marker points closest to where the tube's centreline would be driven, since this is where the need for accuracy is the highest. The spacings between markers were taken from the 11th column in Figure D. 1 and compared. These did not vary much with distance, but grouped around the average. The fact that most were close to a full integer (83 and 84) suggests the patch coordinates were rounded by the software, as stated previously, and since the spacing alternates between each value, the real spacing is most probably its average (83.5 pixels). The lack of variation supports the decision to ignore lens distortion since it will affect data on the centreline by less than 1 pixel, a magnitude in line with other sources of noise. Trying to correct for lens distortion would create another level of noise and it is doubtful whether the effort is warranted. Attempts were made using Equation 22 to correct the data but the results were not promising.

Appendix E Displacement Fields

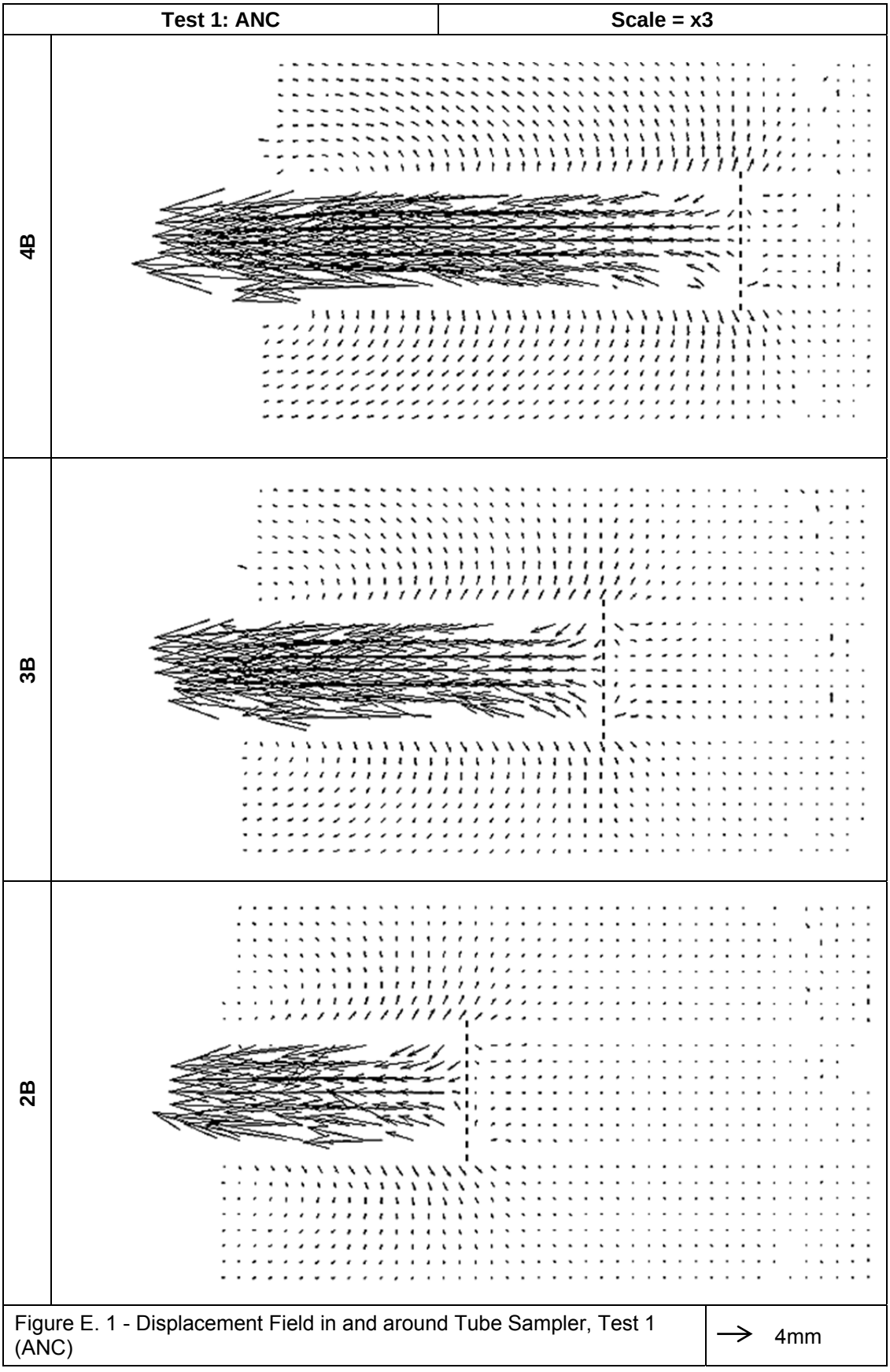

Figure E. 1 - Displacement Field in and around Tube Sampler, Test 1 (ANC)

Test 2: BNC - 1	Scale = x3

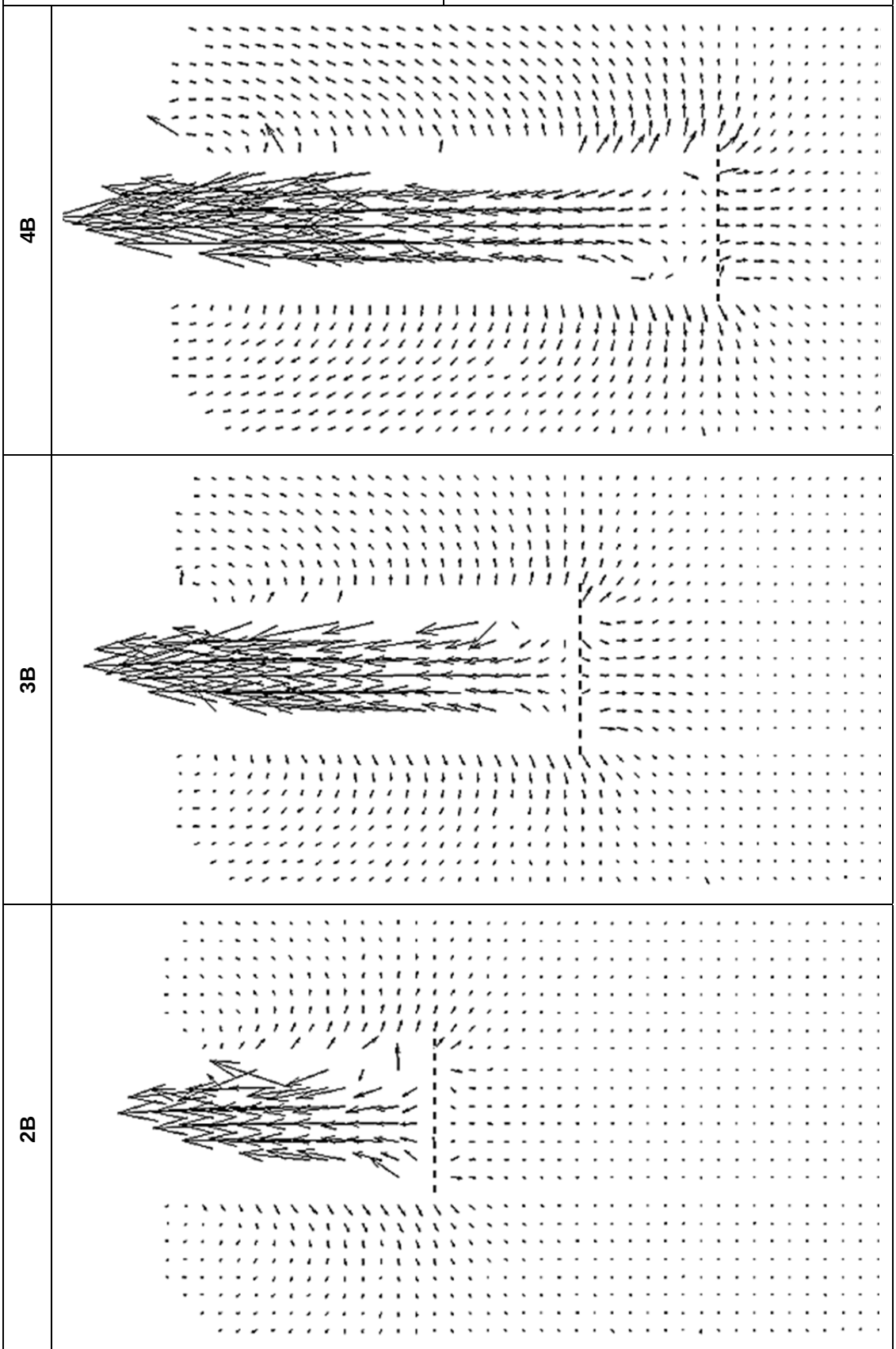

Figure E. 2 - Displacement Field in and around Tube Sampler, Test 2 (BNC - 1)

→ 4mm

Test 3: BNC - 2	Scale = x3

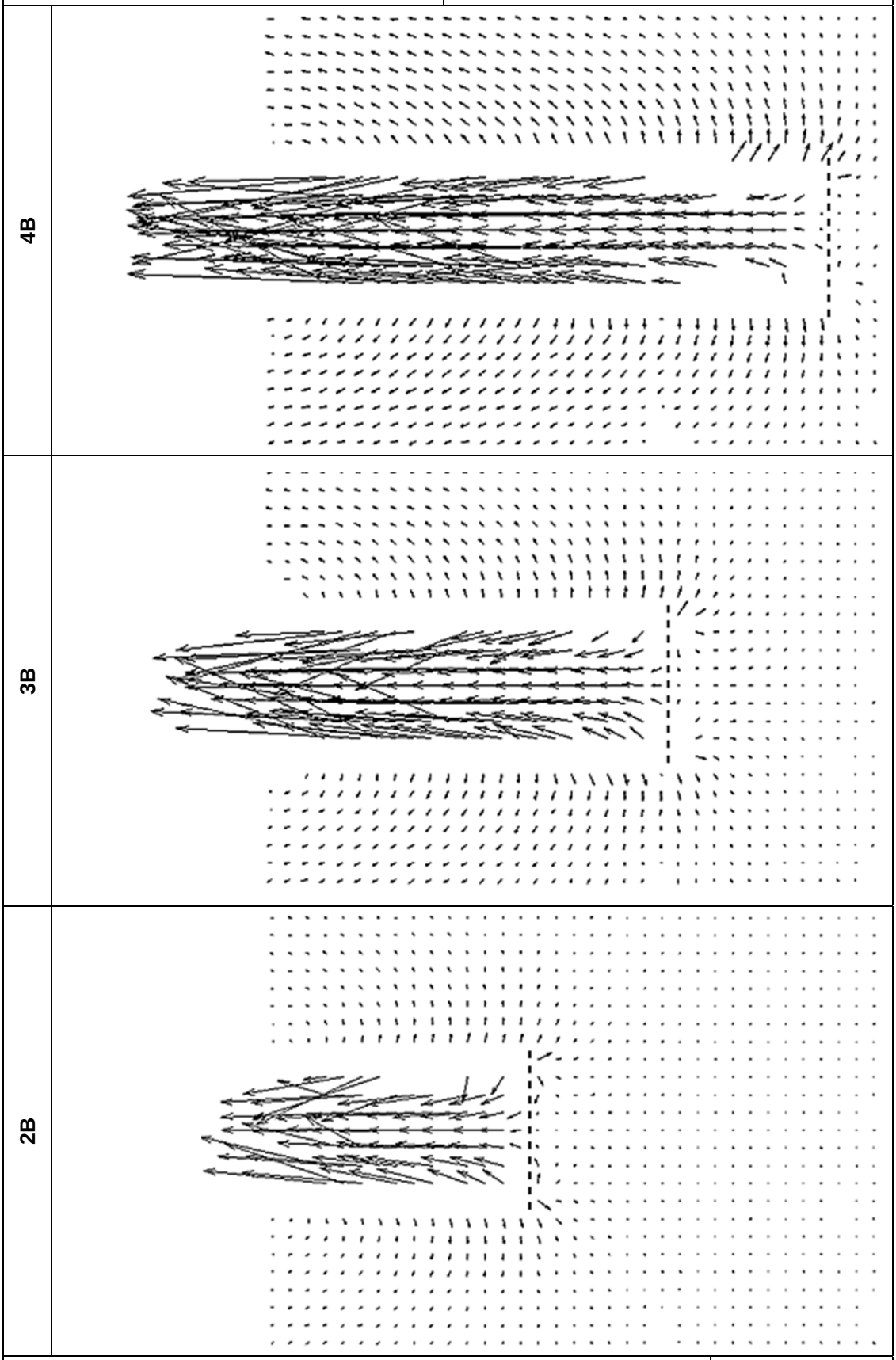

Figure E. 3 - Displacement Field in and around Tube Sampler, Test 3 (BNC - 2)

→ 4mm

Test 4: CNC	Scale = x3
4B	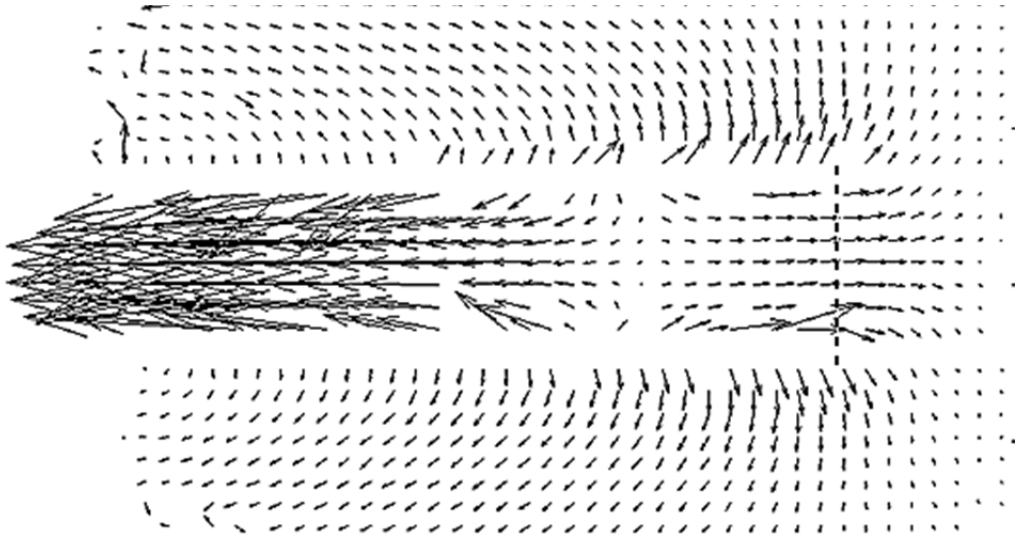
3B	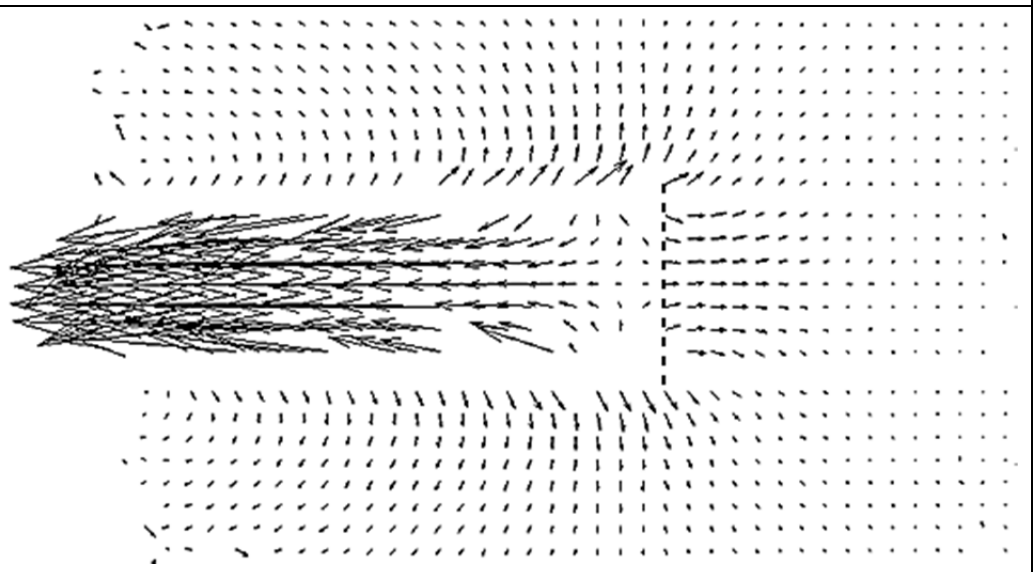
2B	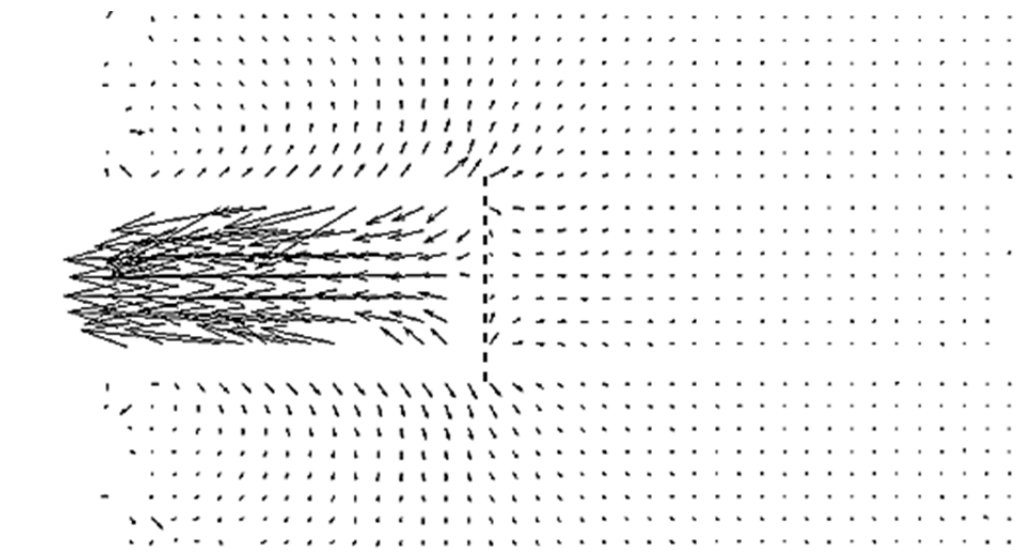

Figure E. 4 - Displacement Fields in and around Tube Sampler, Test 4 (CNC)

→ 4mm

Test 5: AtNC	Scale = x3
4B 3B 2B	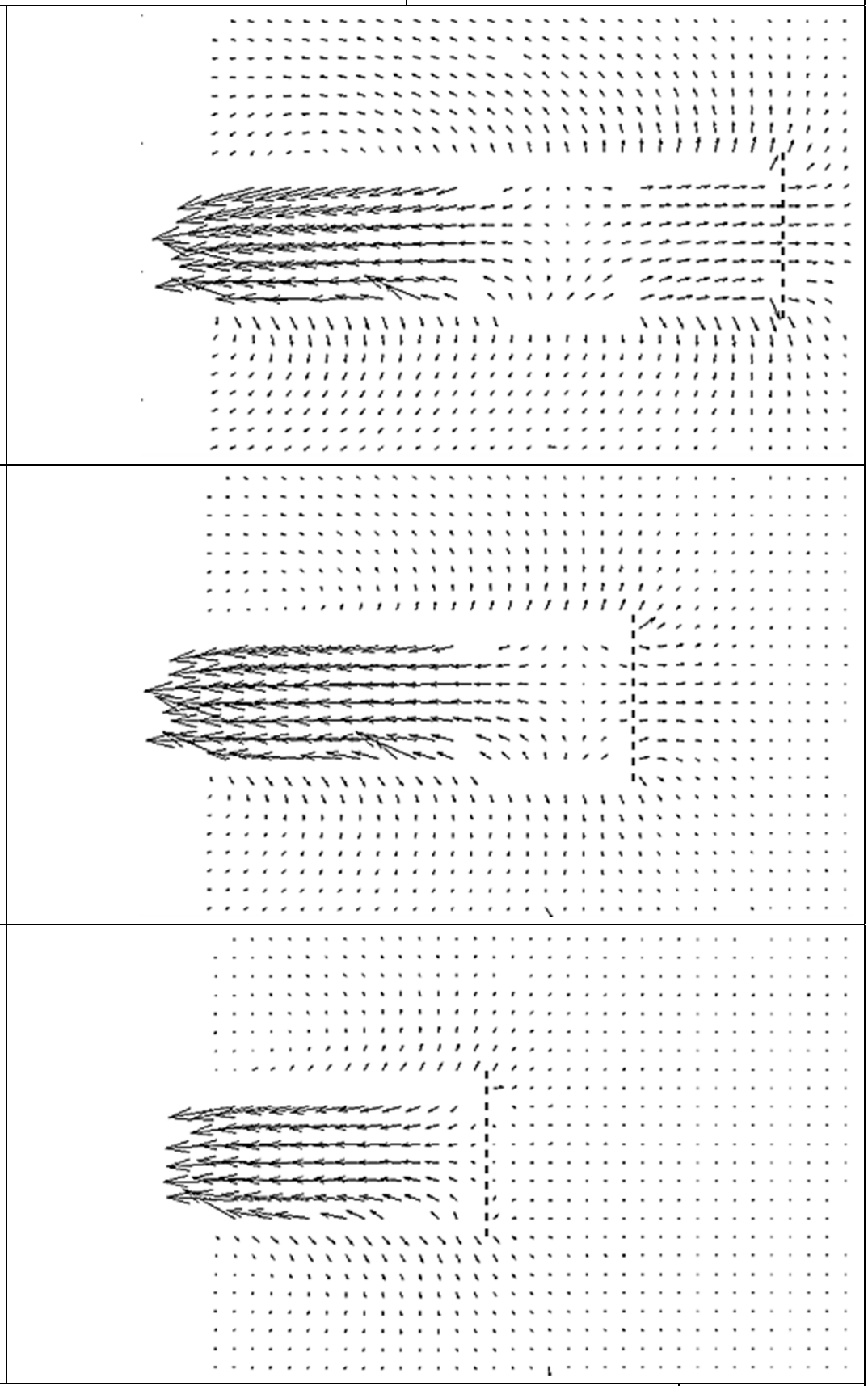
Figure E. 5 - Displacement Fields in and around Tube Sampler, Test 5 (AtNC)	→ 4mm

Test 6: BtNC	Scale = x3
4B 3B 2B	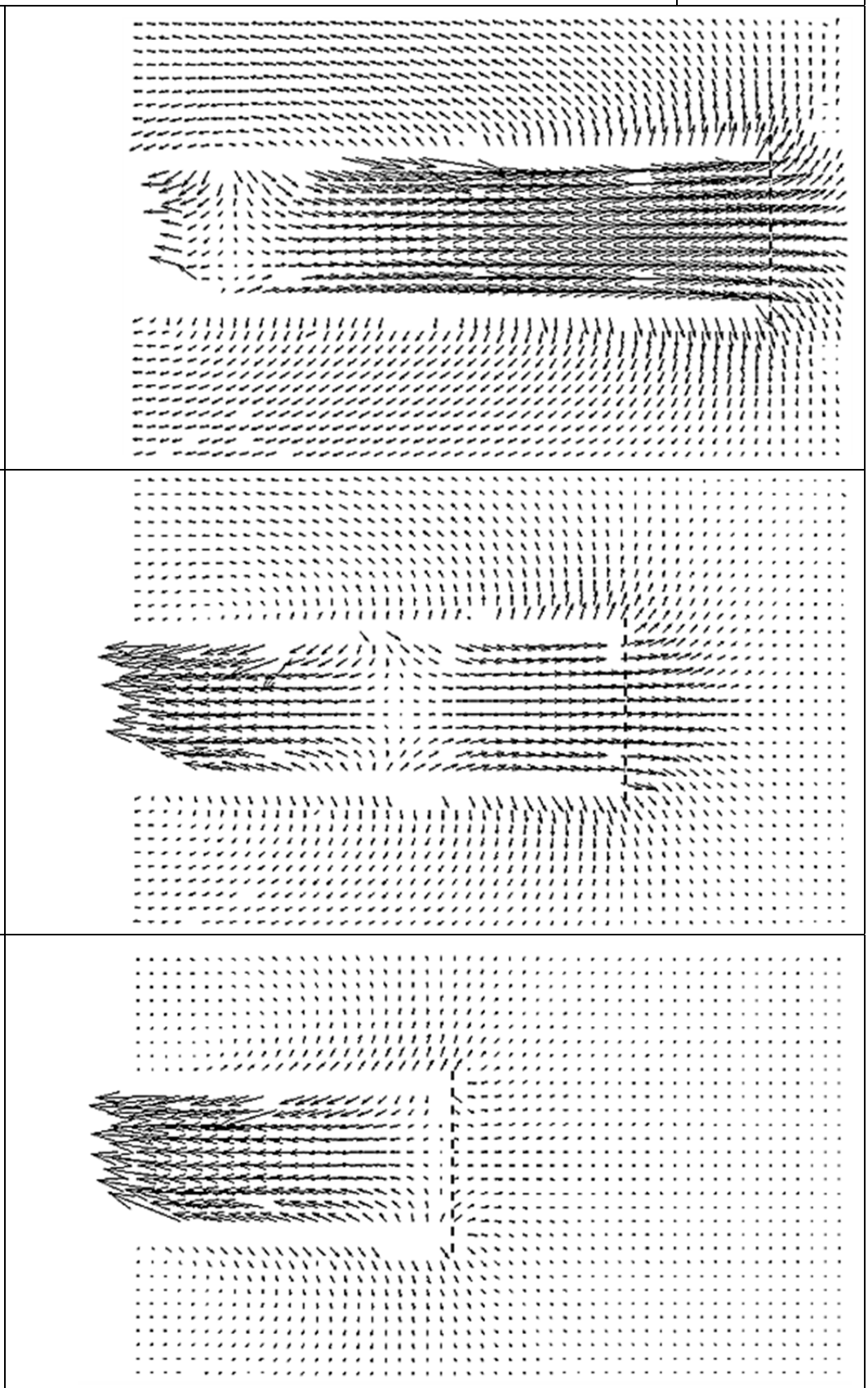
Figure E. 6 - Displacement Fields in and around Tube Sampler, Test 6 (BtNC)	→ 4mm

Test 7: CtNC	Scale = x3
4B	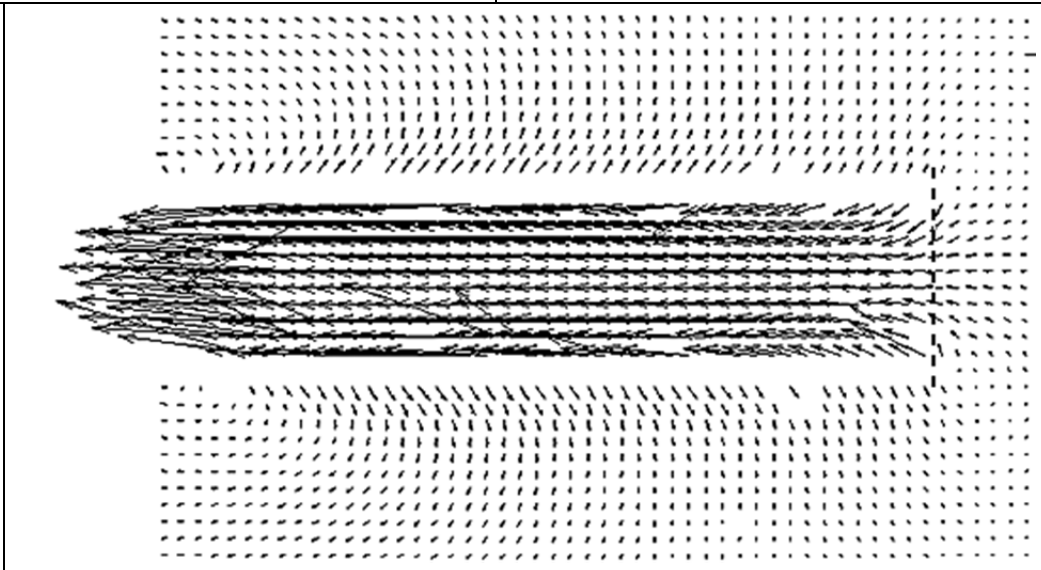
3B	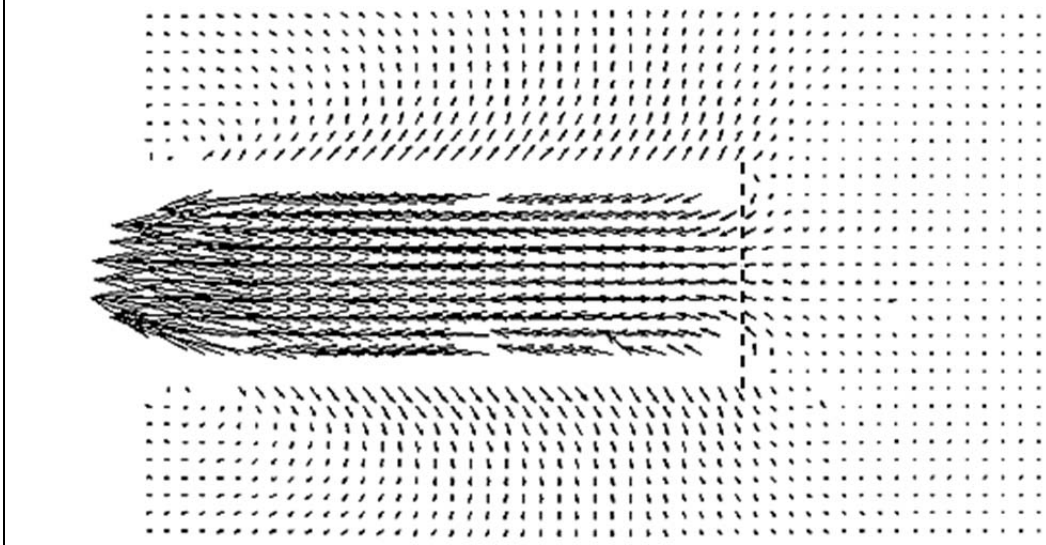
2B	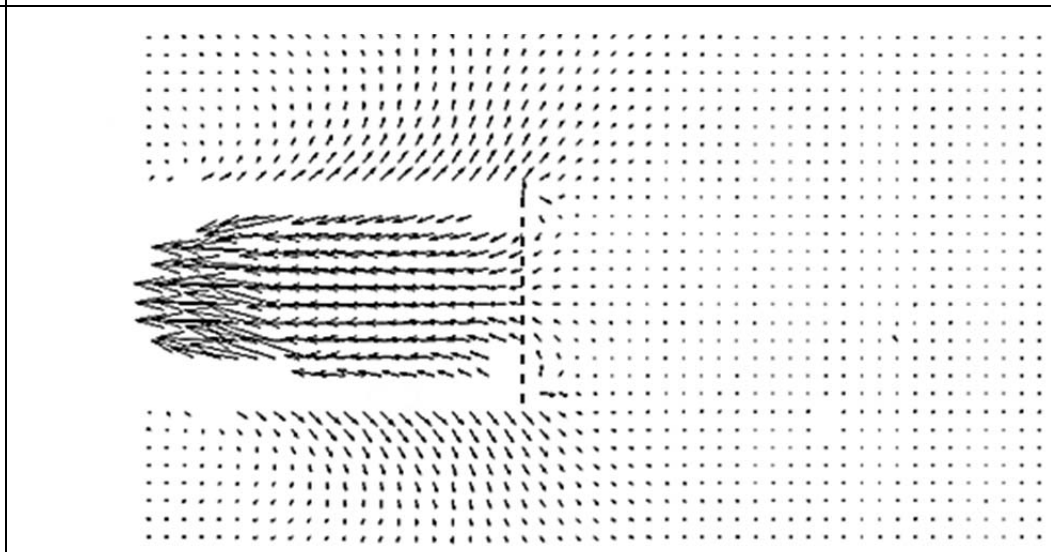
Figure E. 7 - Displacement Fields in and around Tube Sampler, Test 7 (CtNC)	→ 4mm

Test 8: AOC - 1	Scale = x3

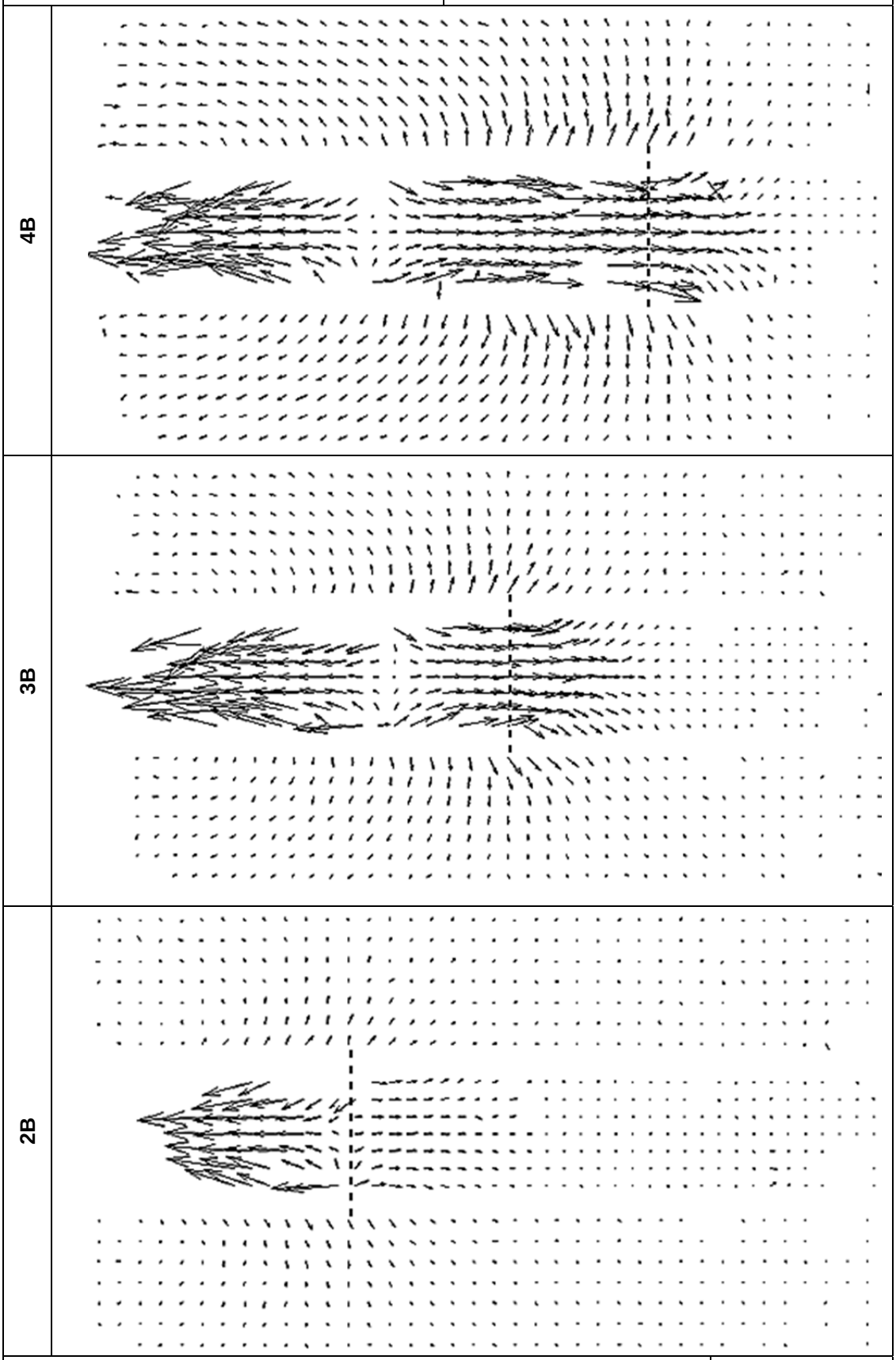

Figure E. 8 - Displacement Fields in and around Tube Sampler, Test 8 (AOC-1)

→ 4mm

Test 9: AOC - 2	Scale = x3

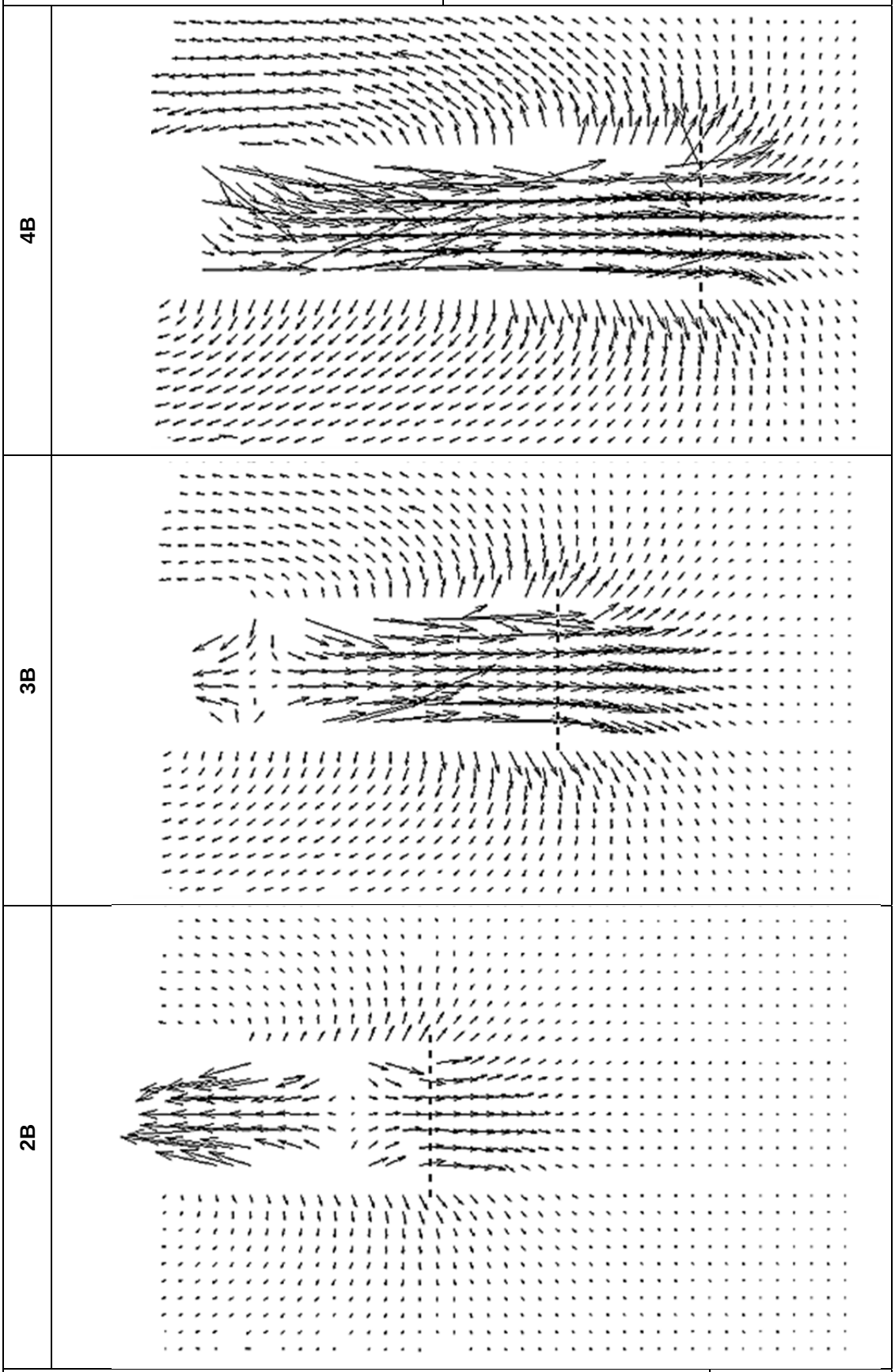

Figure E. 9 - Displacement Fields in and around Tube Sampler, Test 9 (AOC-2)

→ 4mm

Test 10: AOC - 3	Scale = x3

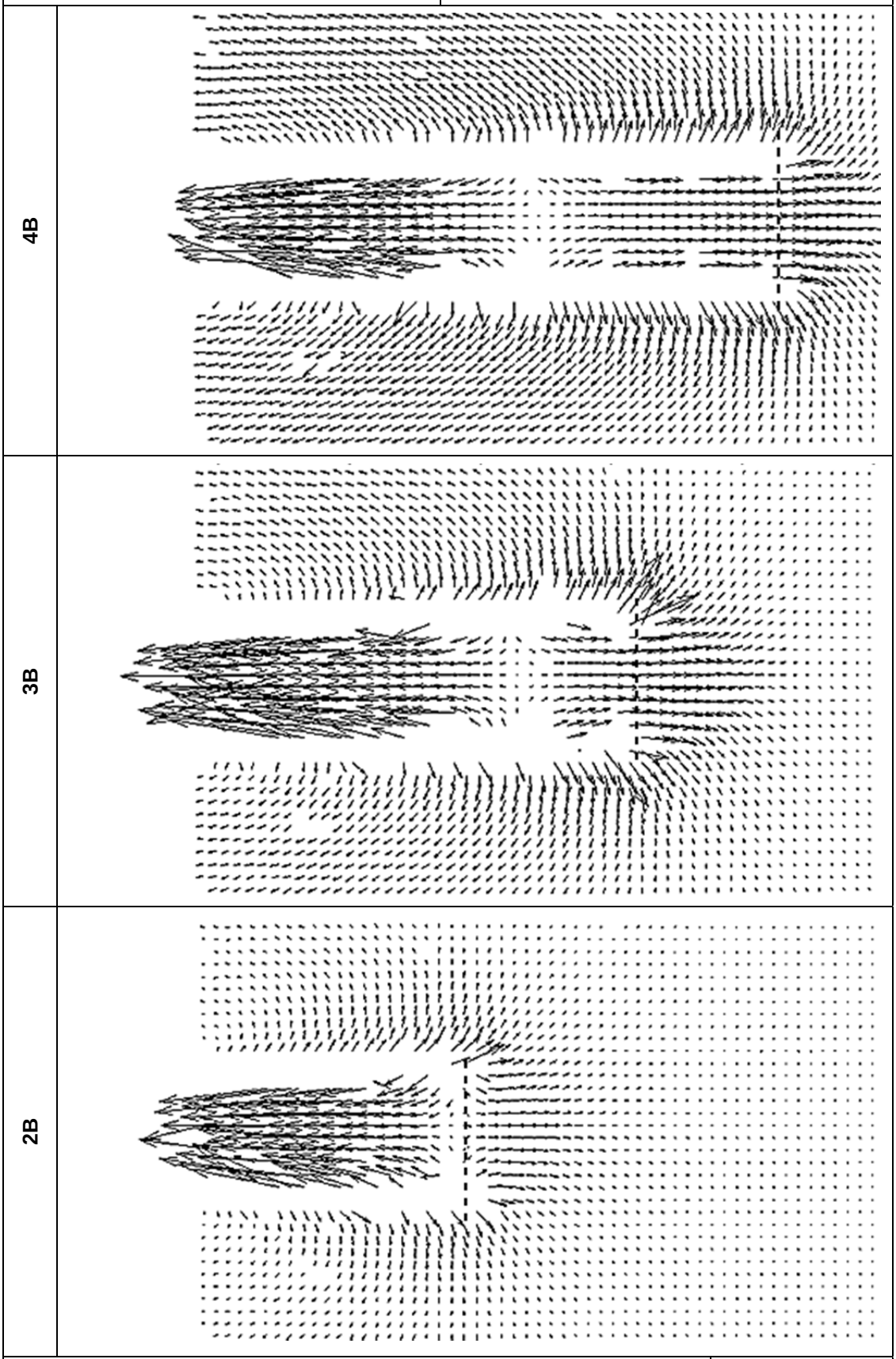

Figure E. 10 - Displacement Fields in and around Tube Sampler, Test 10 (AOC-3)

→ 4mm

Test 11: BOC	Scale = x3
4B	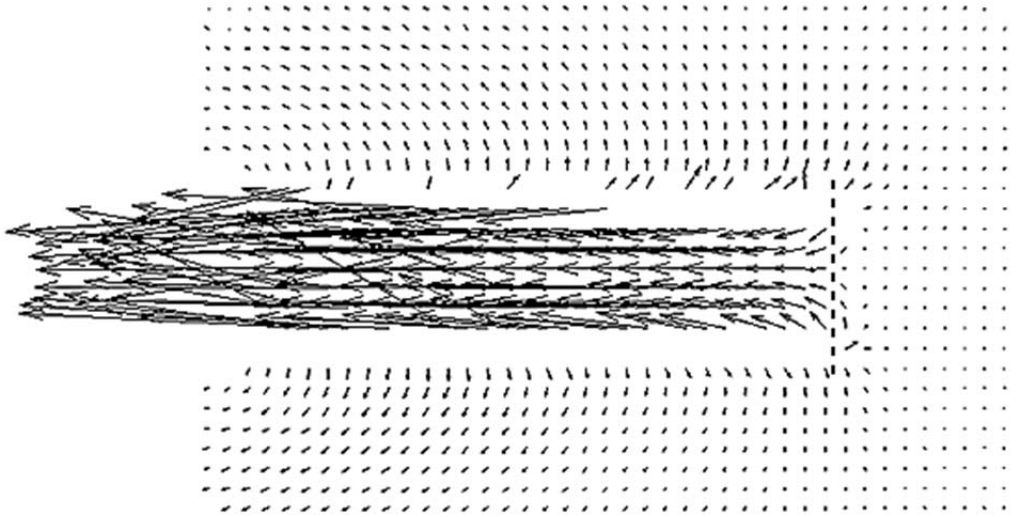
3B	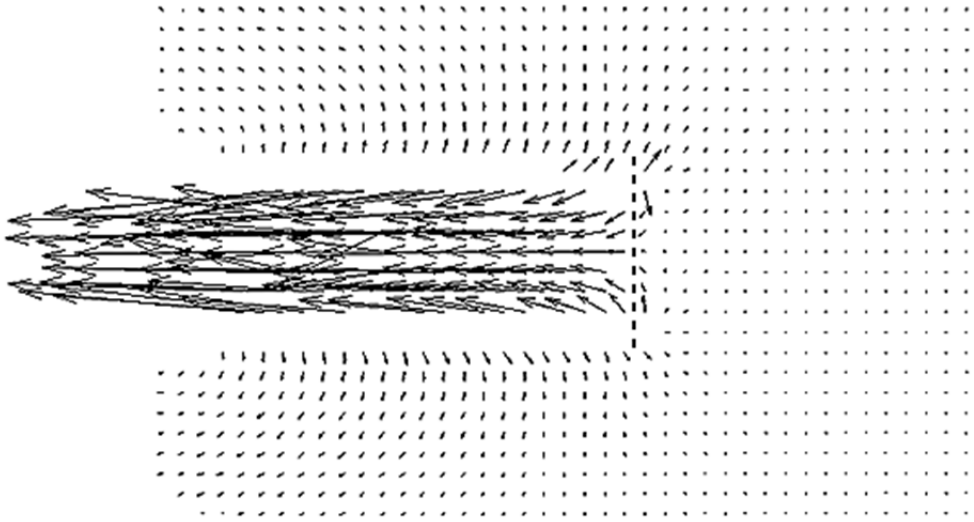
2B	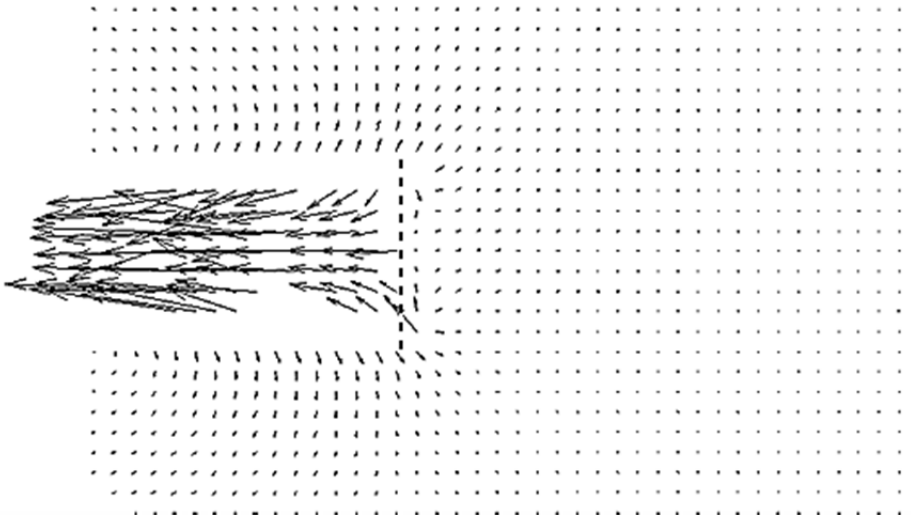

Figure E. 11 - Displacement Fields in and around Tube Sampler, Test 11 (BOC)

→ 4mm

Test 12: COC	Scale = x3

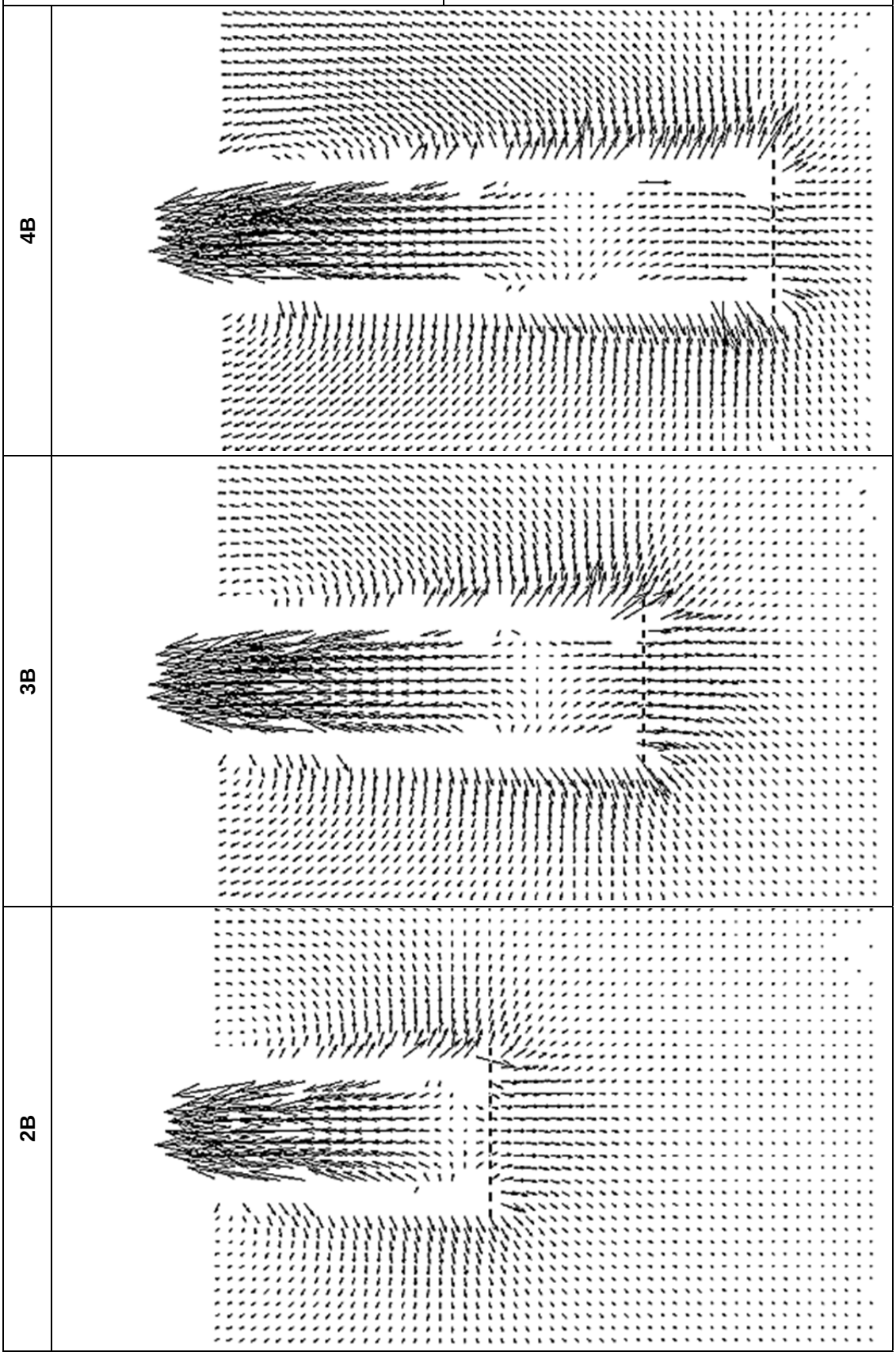

Figure E. 12 - Displacement Fields in and around Tube Sampler, Test 12 (COC)

→ 4mm

Appendix F Quadratic Trendlines

The graphs in this section were used to obtain a single value for the final position of each interrogation area at a tube penetration depth of 4 tube diameters. Data from 15 PIV runs at different Leapfrogs were plotted, wild vectors were removed if more than 2 standard deviations away from the median, and a quadratic trendline was applied to the remaining points to get the locations. All values are in pixels, since conversion only occurred at a later stage in the analysis. Residuals represent the difference between the trendline and the data points. In all low visibility tests (earlier tests using the first batches of technical white oil), the fit to the trendline is looser than in the tests when transparency is increased.

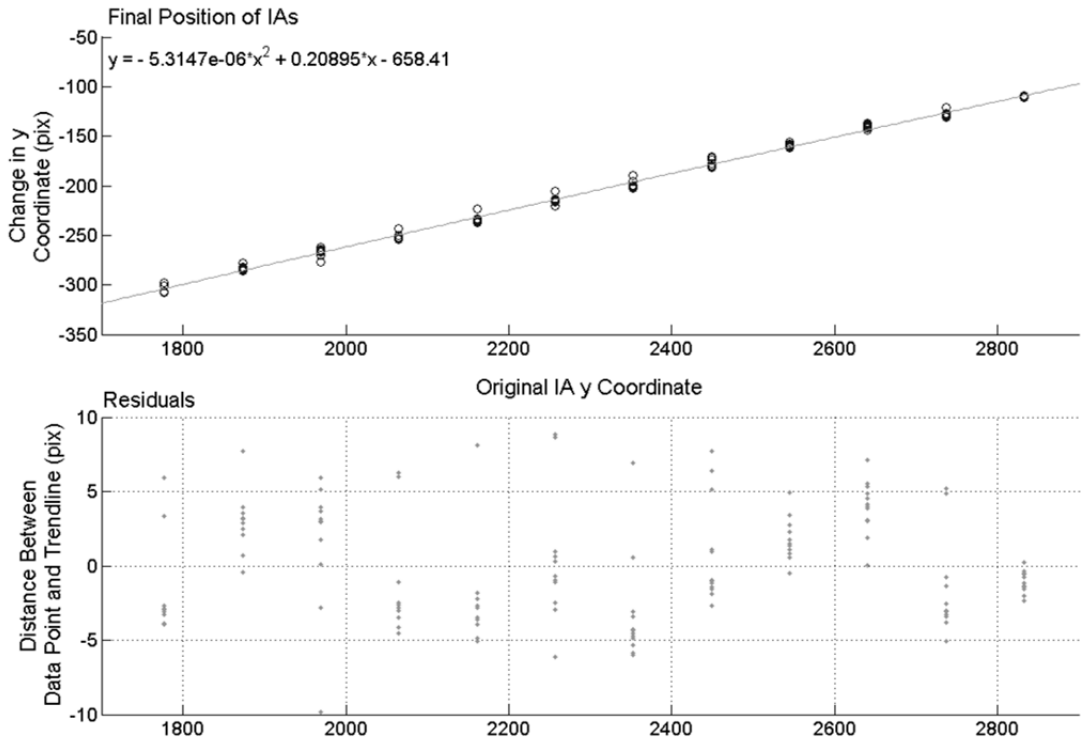

Figure F. 1 - Quadratic Trendline – Test 1 ANC

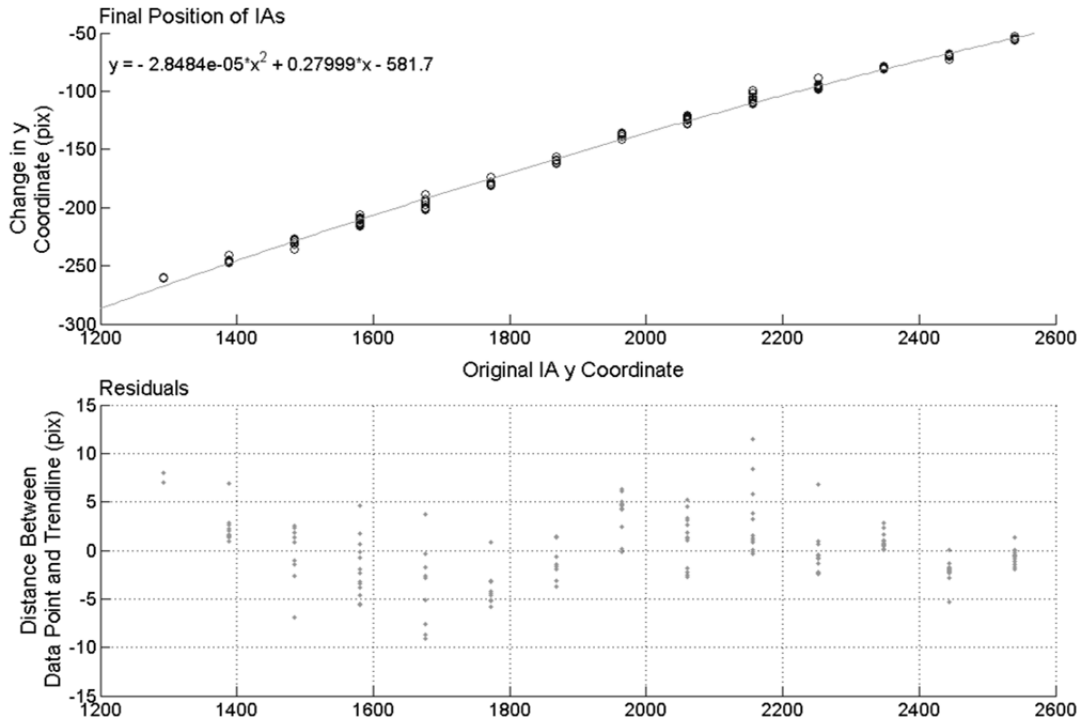

Figure F. 2 - Quadratic Trendline – Test 2 BNC-1

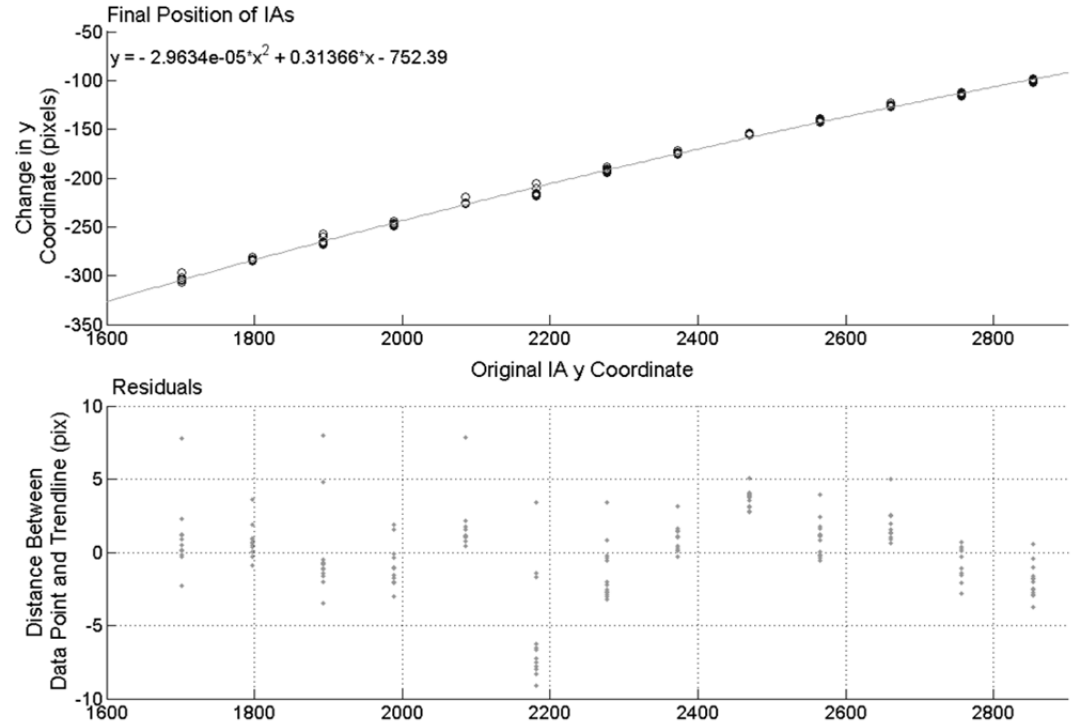

Figure F. 3 - Quadratic Trendline – Test 3 BNC-2

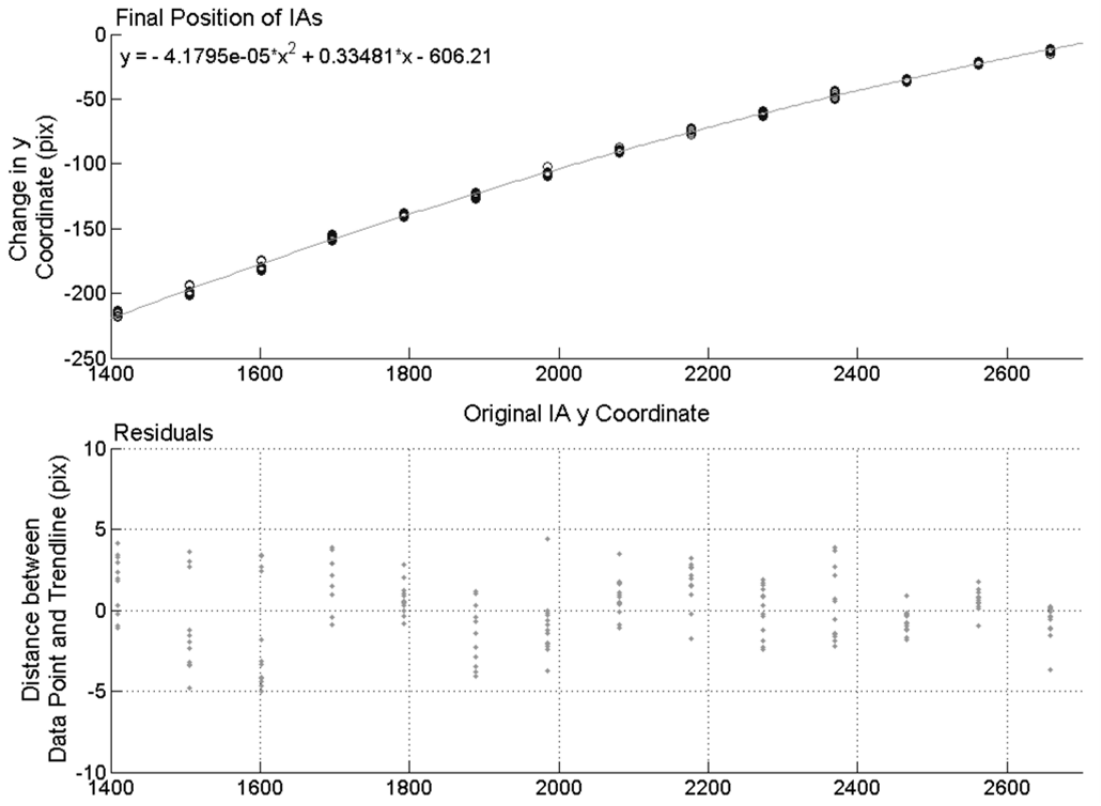

Figure F. 4 - Quadratic Trendline – Test 4 CNC

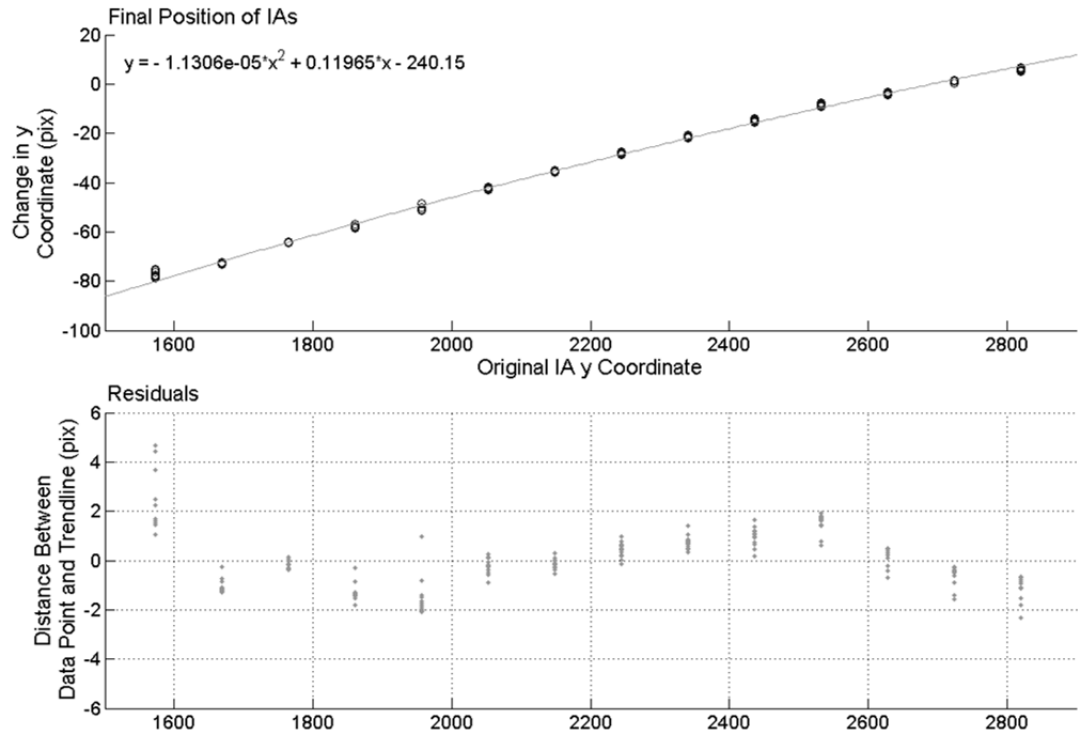

Figure F. 5 - Quadratic Trendline – Test 5 AtNC

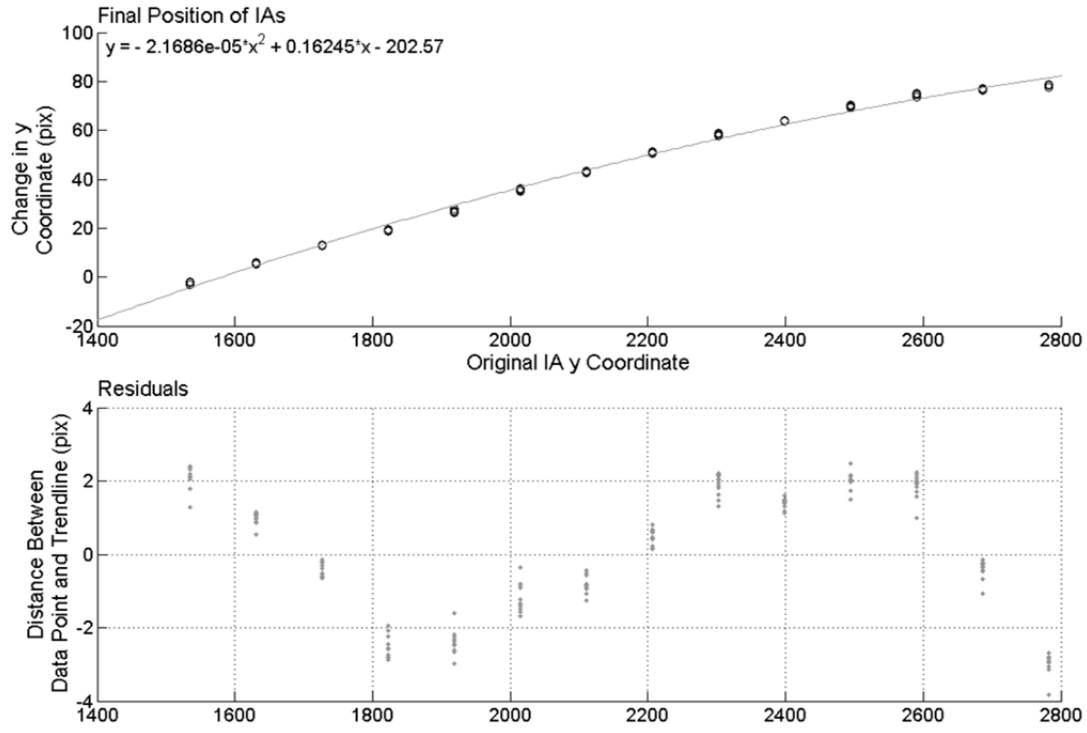

Figure F. 6 - Quadratic Trendline – Test 6 BtNC

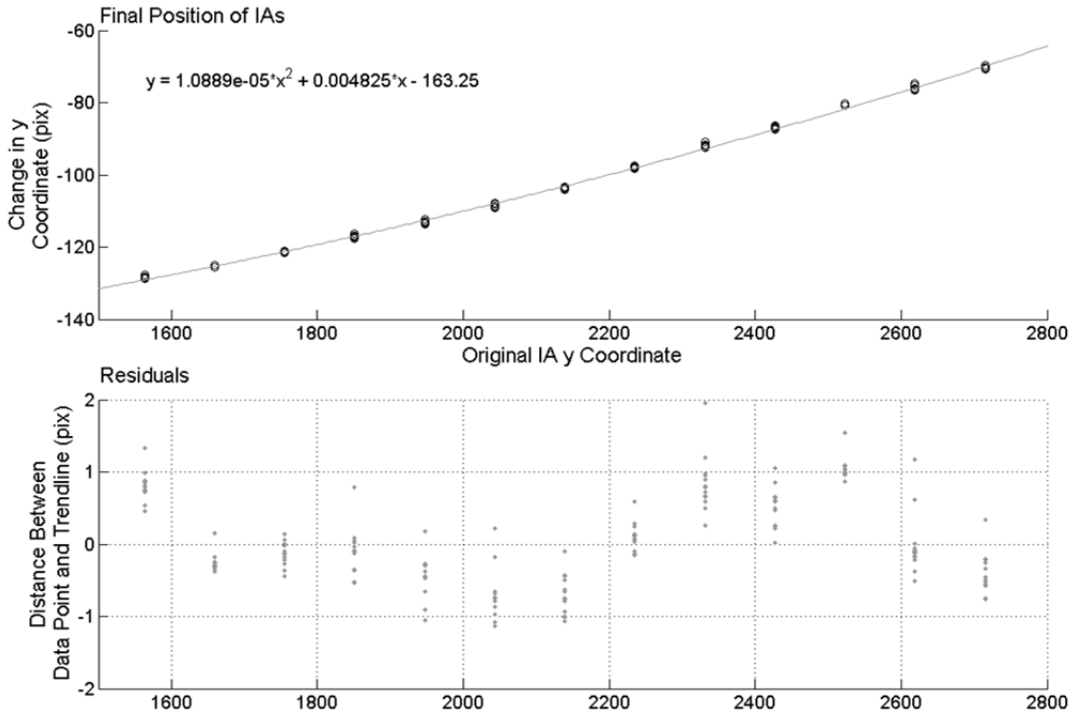

Figure F. 7 - Quadratic Trendline – Test 7 CtNC

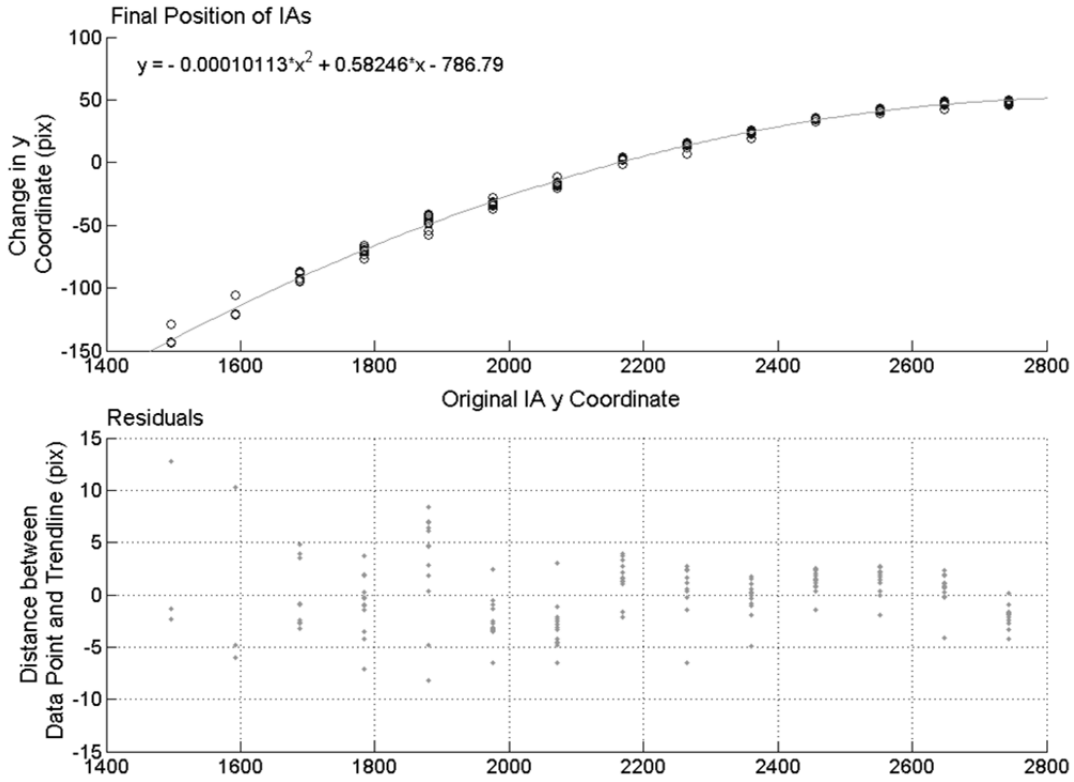

Figure F. 8 - Quadratic Trendline – Test 8 AOC-1

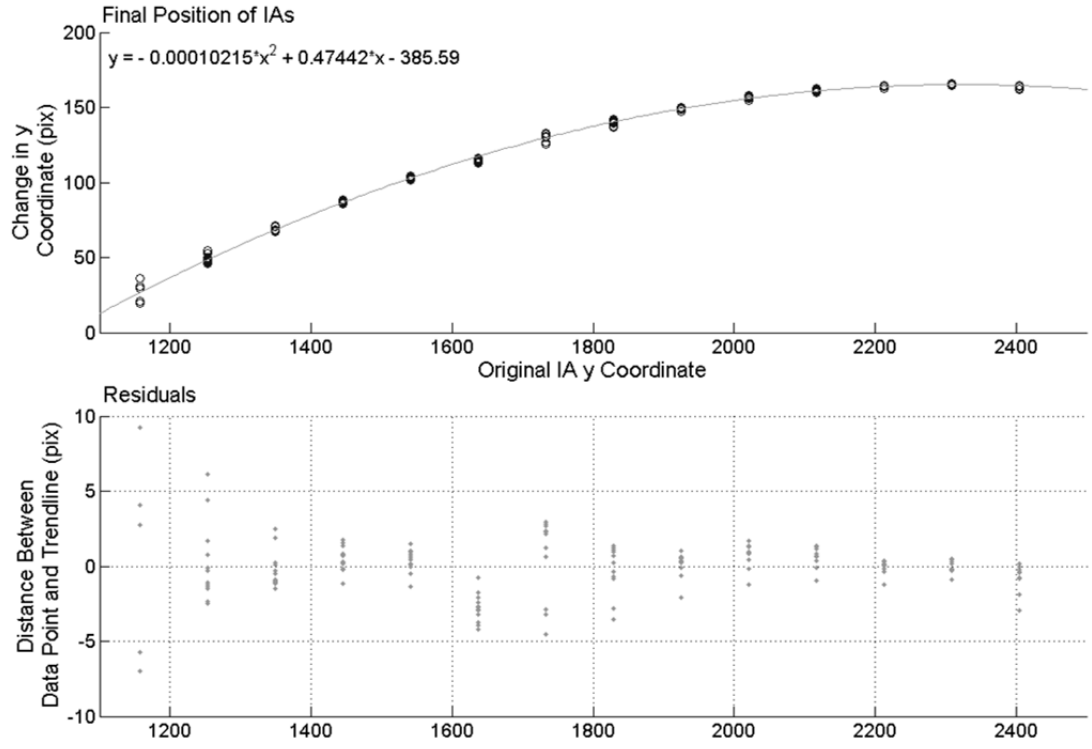

Figure F. 9 - Quadratic Trendline – Test 9 AOC-2

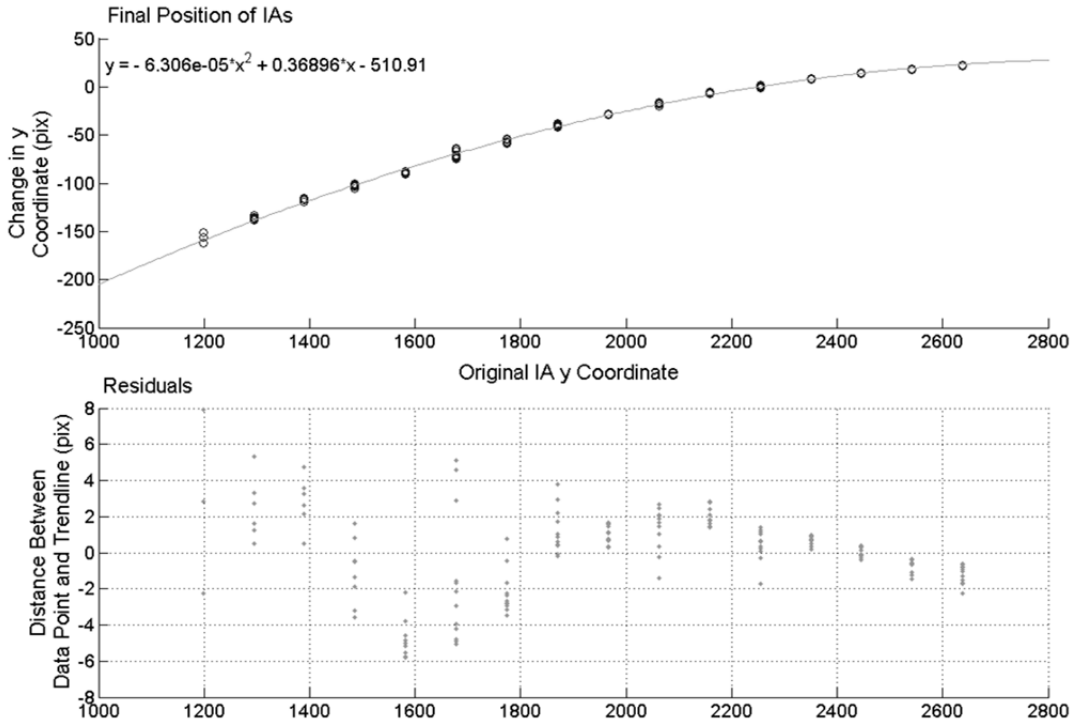

Figure F. 10 - Quadratic Trendline – Test 10 AOC-3

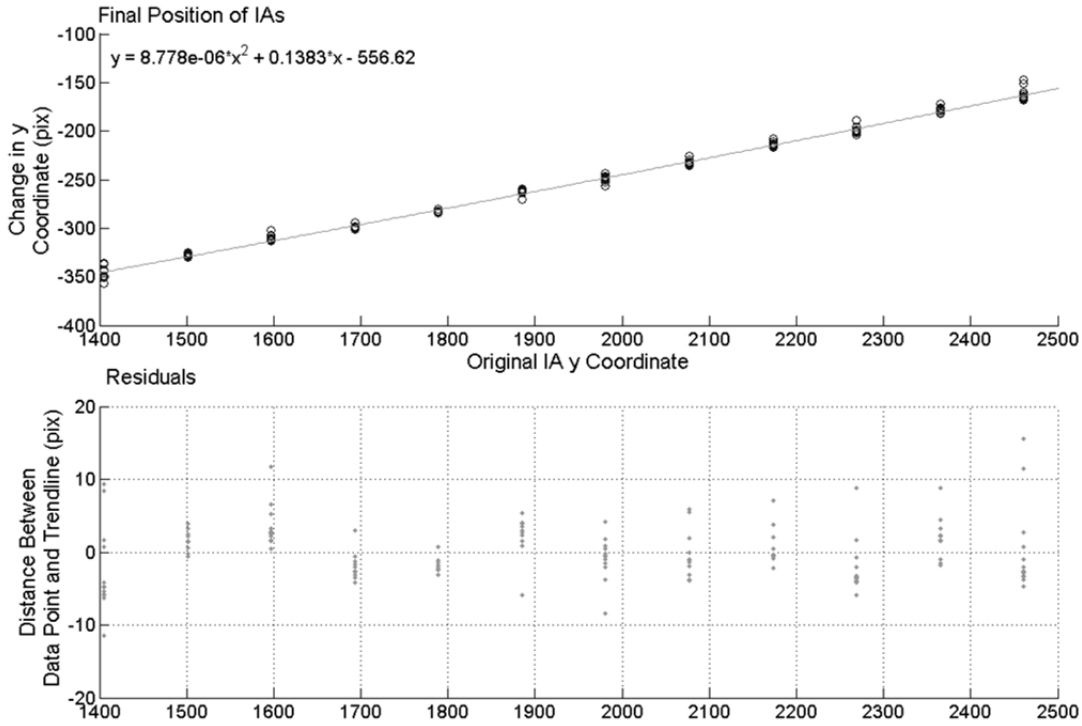

Figure F. 11 - Quadratic Trendline – Test 11 BOC

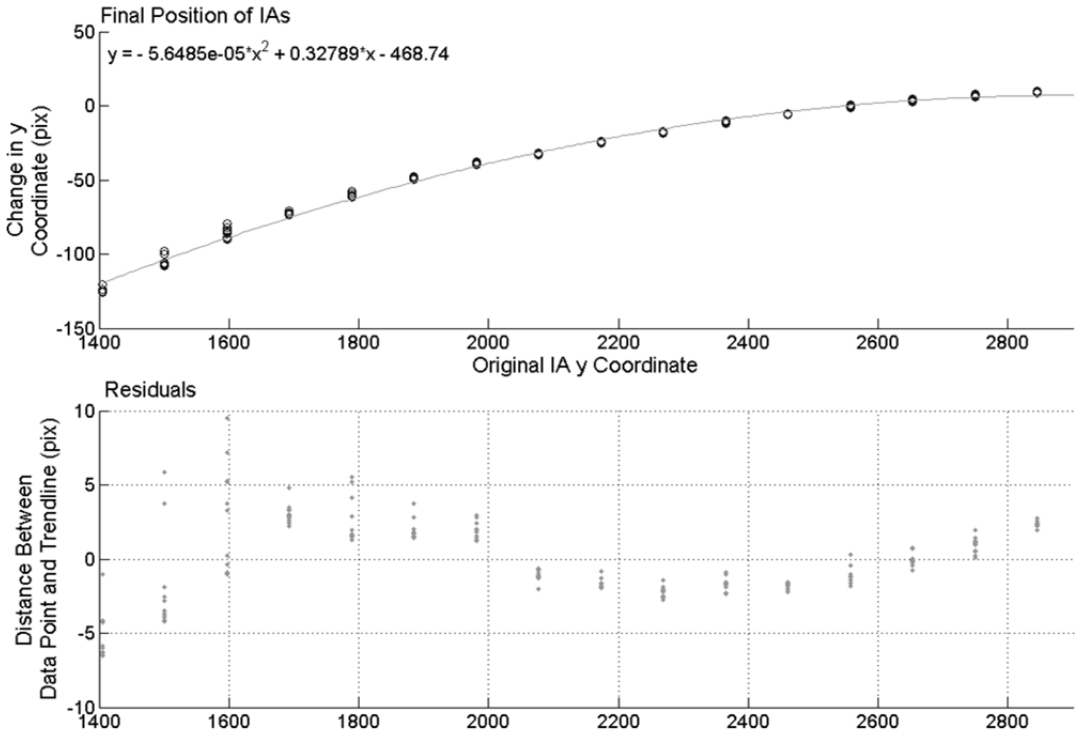

Figure F. 12 - Quadratic Trendline – Test 12 COC

Appendix G Centreline Displacement induced by Tube Sampling

Legend

Note: where upper IAs became hidden from view inside the tube holder, these curves have been removed from the graph due to wild vectors

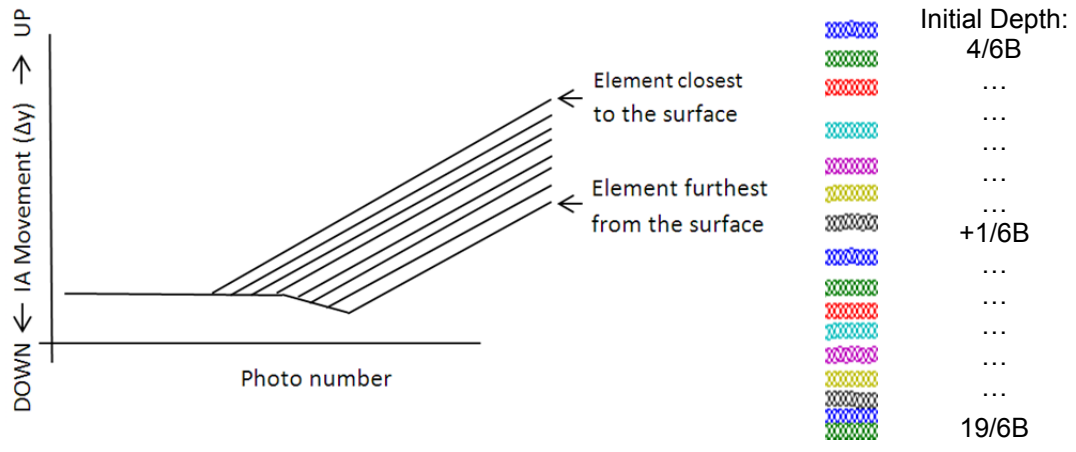

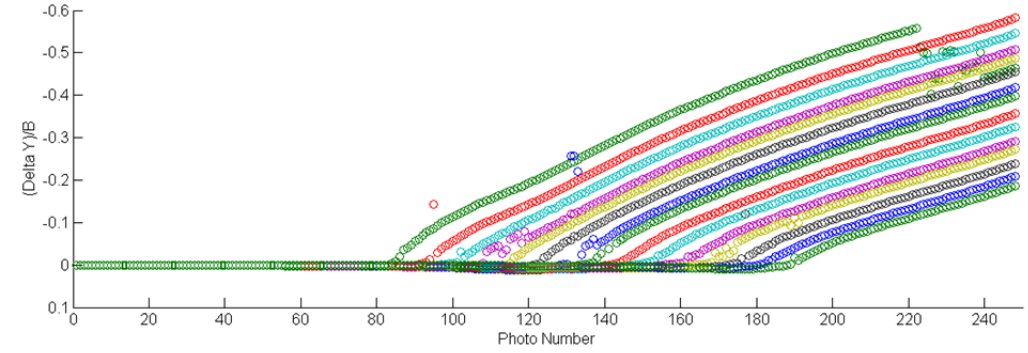

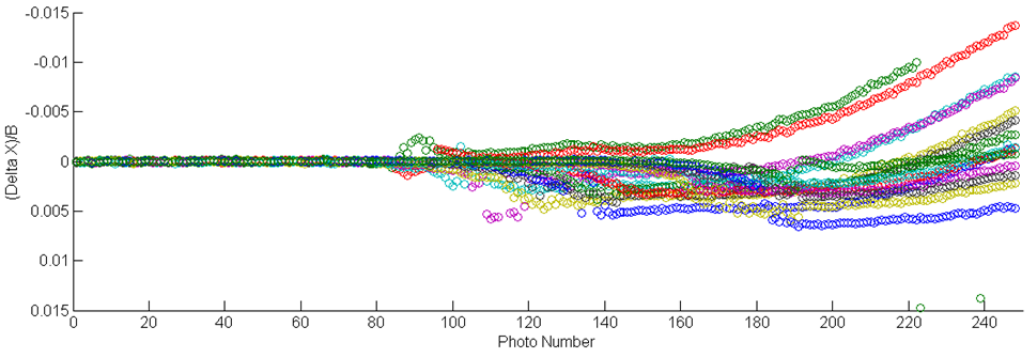

Figure G. 1 - IA Displacements over Time, Test ANC

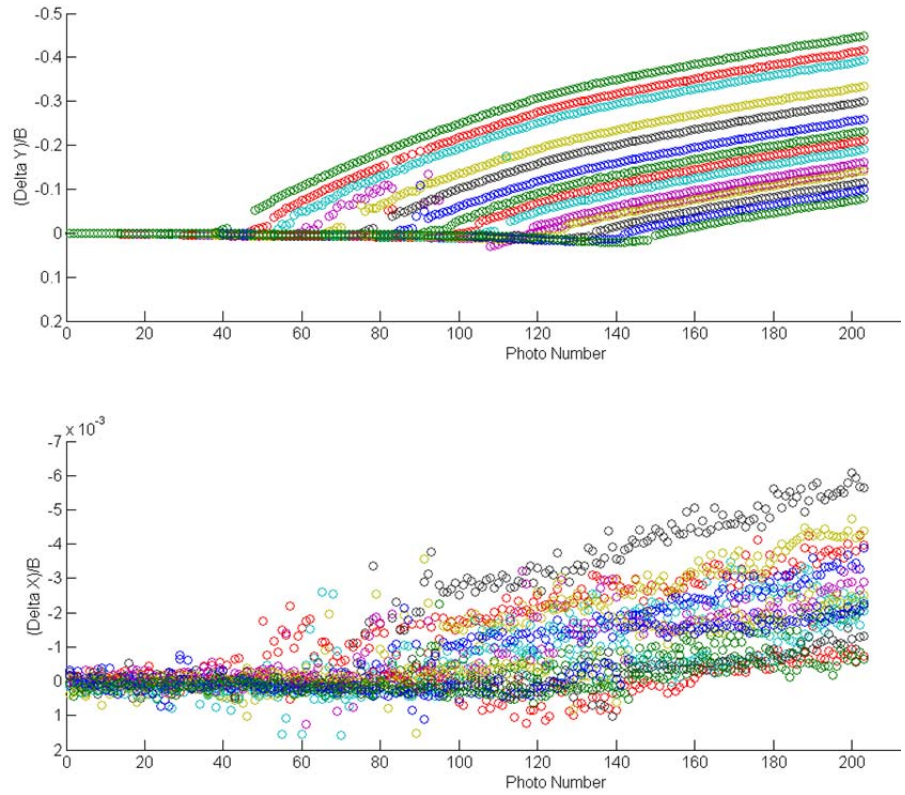

Figure G. 2 - IA Displacements over Time, Test BNC-1

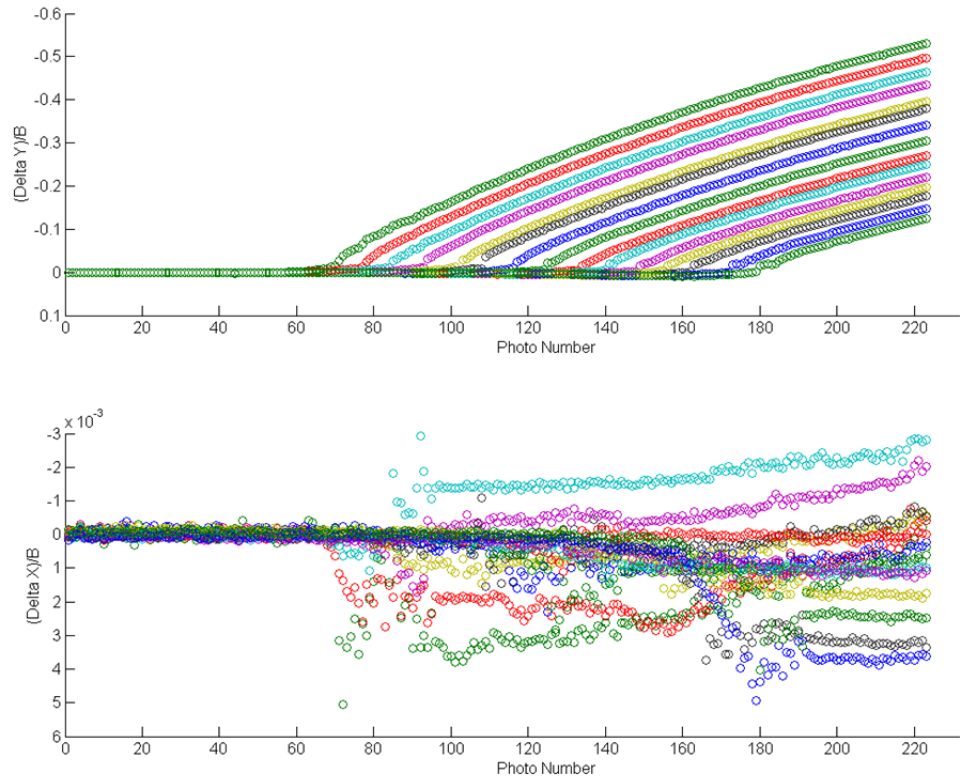

Figure G. 3 - IA Displacements over Time, Test BNC-2

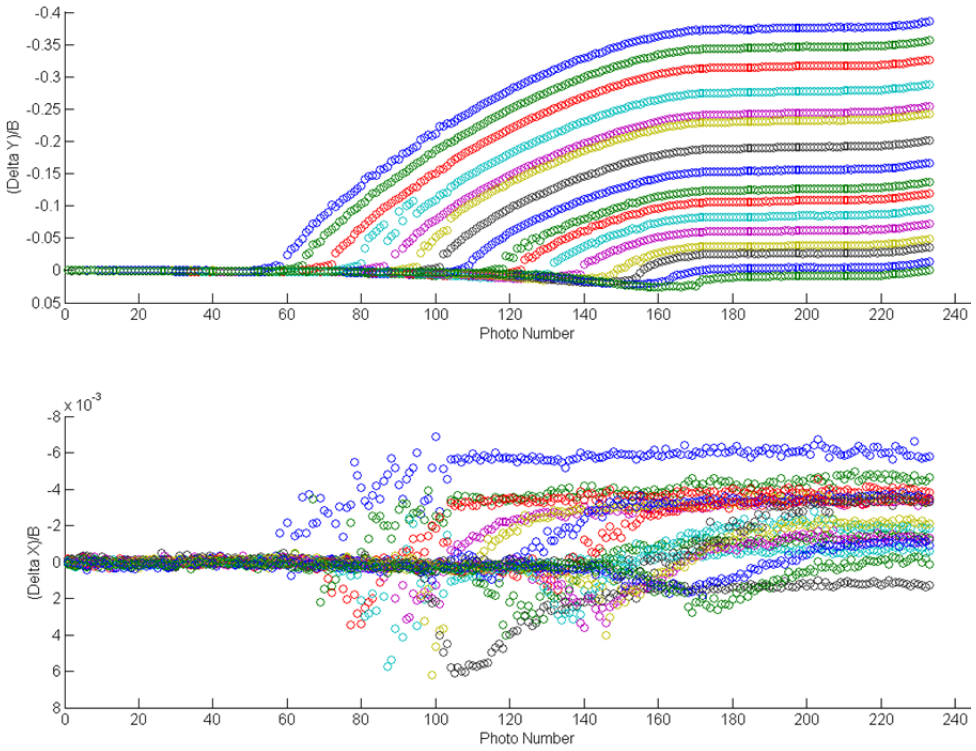

Figure G. 4 - IA Displacements over Time, Test CNC

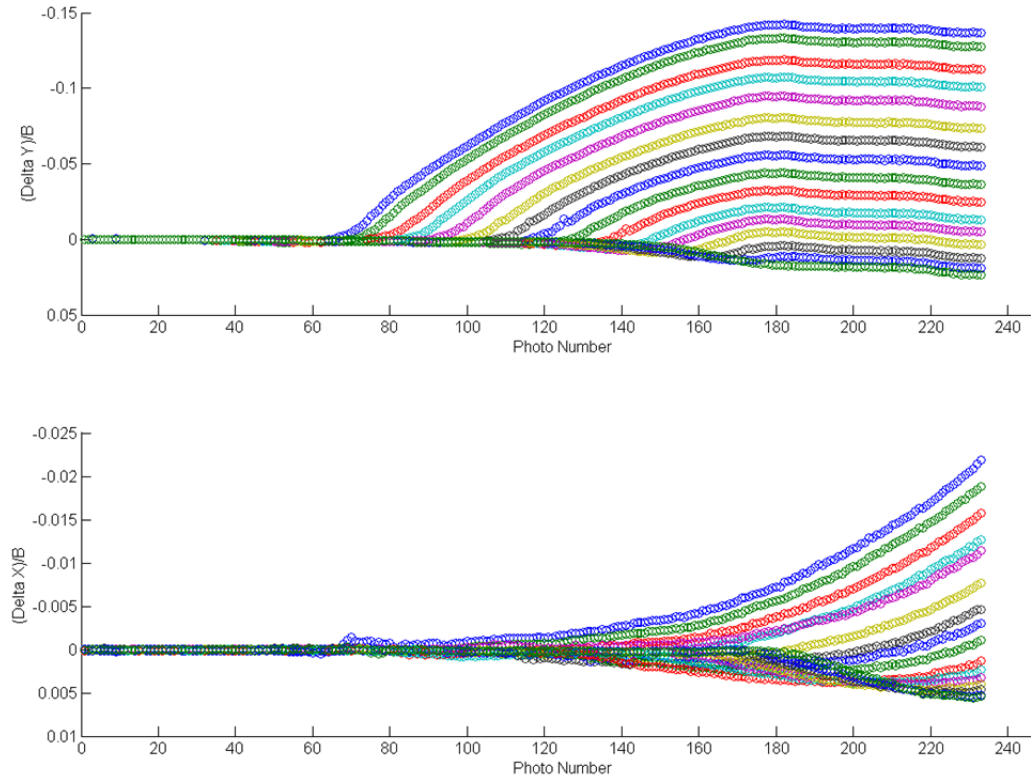

Figure G. 5 - IA Displacements over Time, Test AtNC

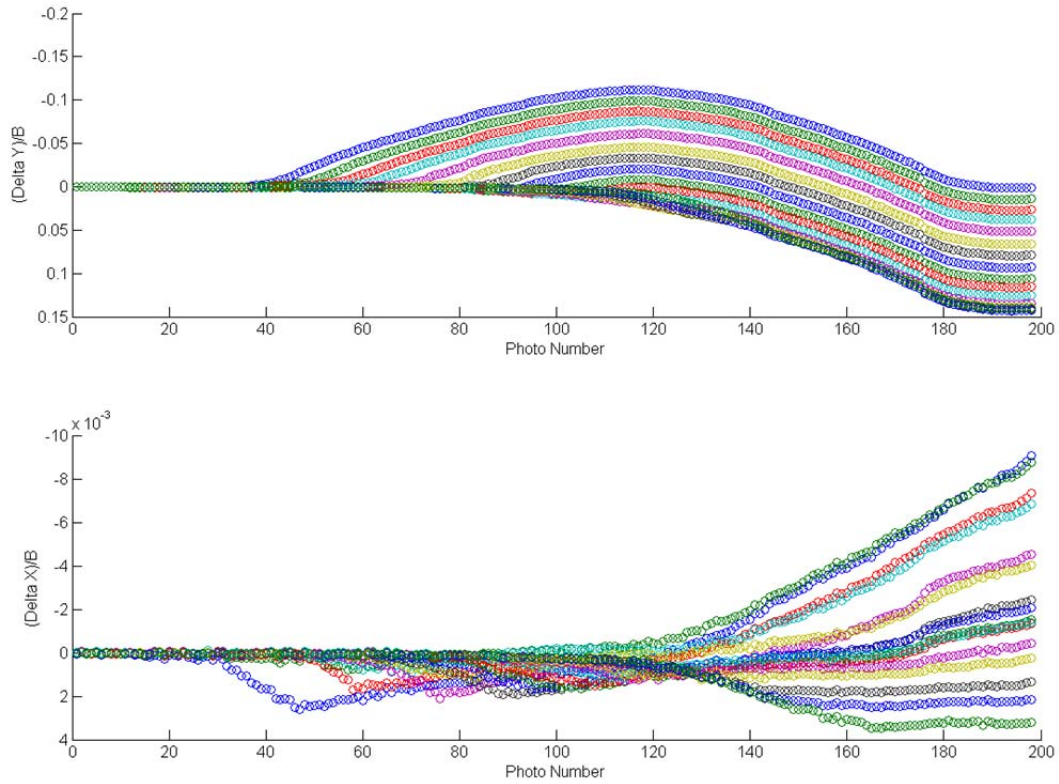

Figure G. 6 - IA Displacements over Time, Test BtNC

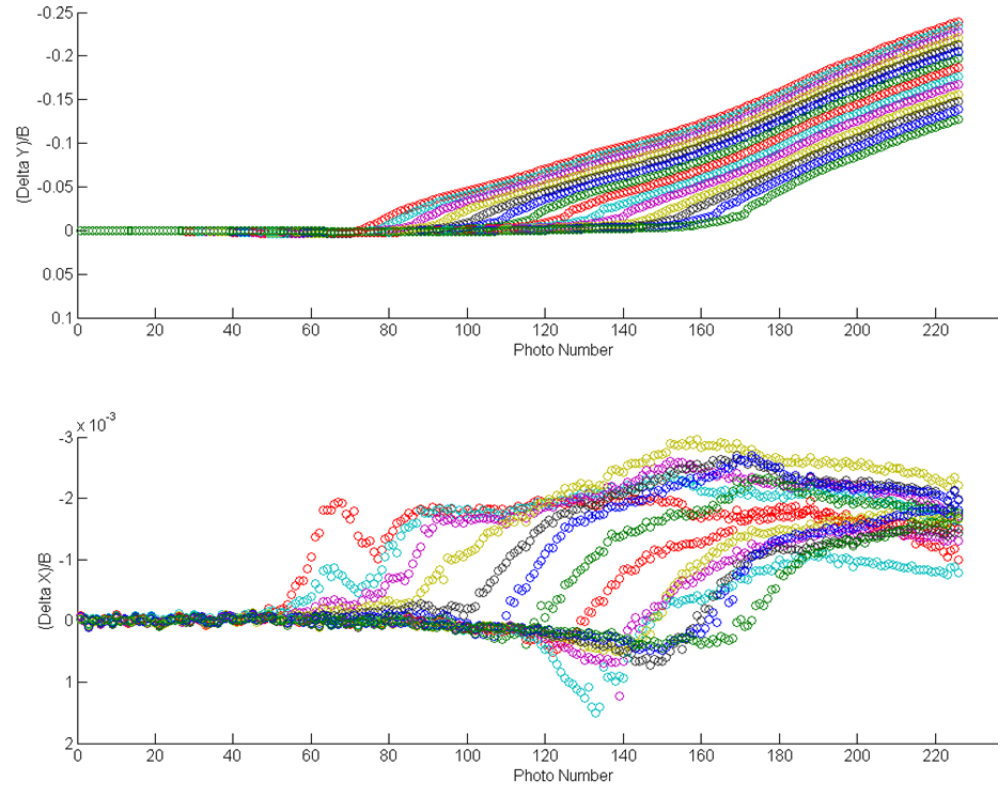

Figure G. 7 - IA Displacements over Time, Test CtNC

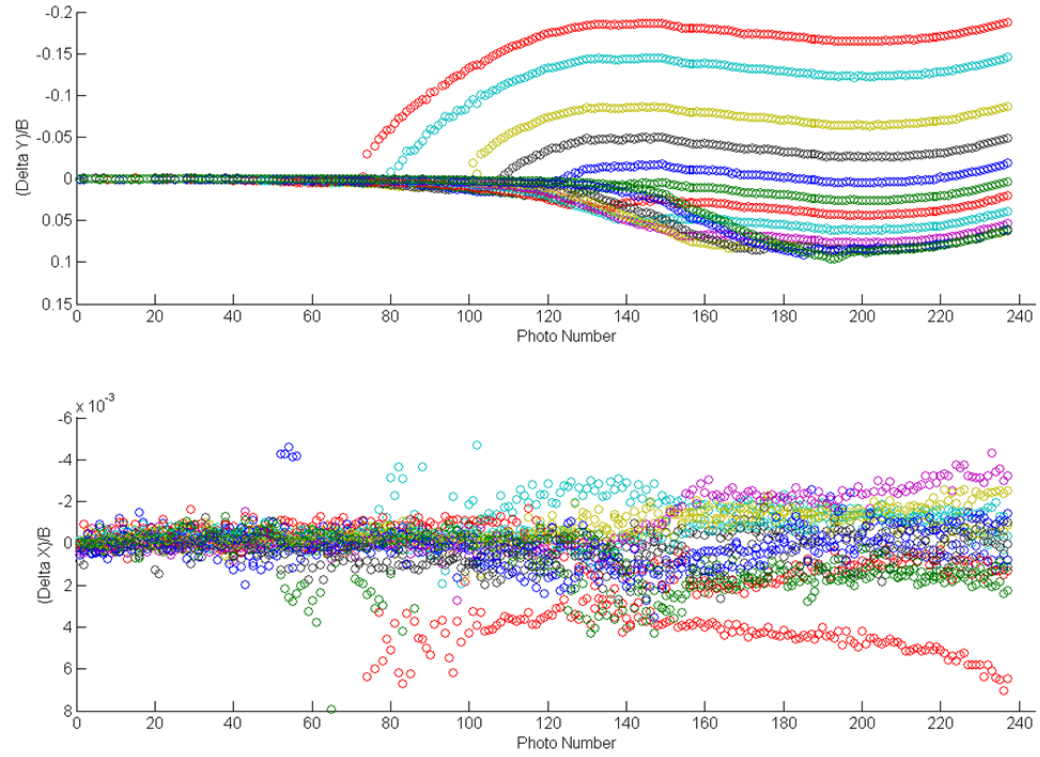

Figure G. 8 - IA Displacements over Time, Test AOC-1

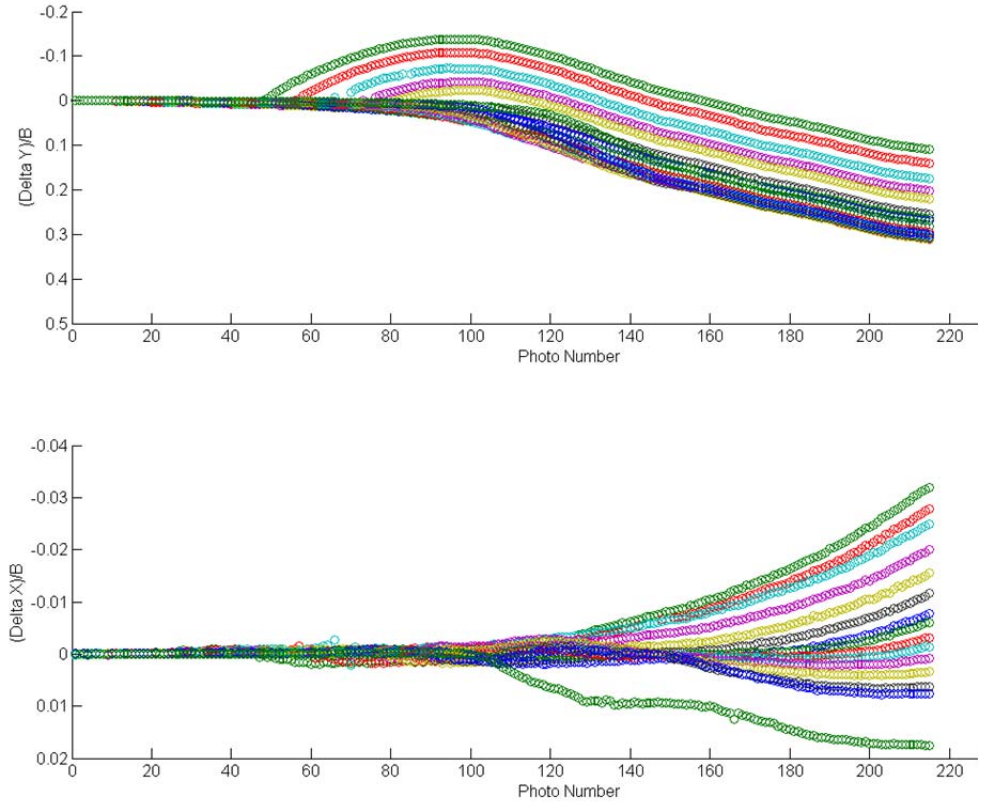

Figure G. 9 - IA Displacements over Time, Test AOC-2

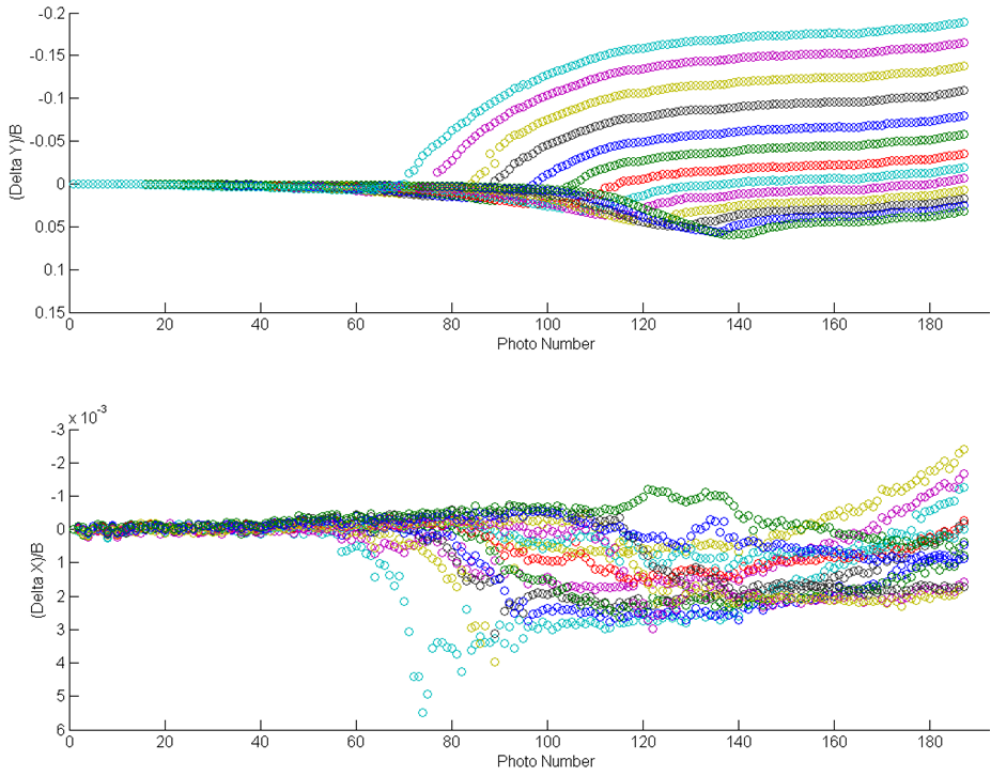

Figure G. 10 - IA Displacements over Time, Test AOC-3

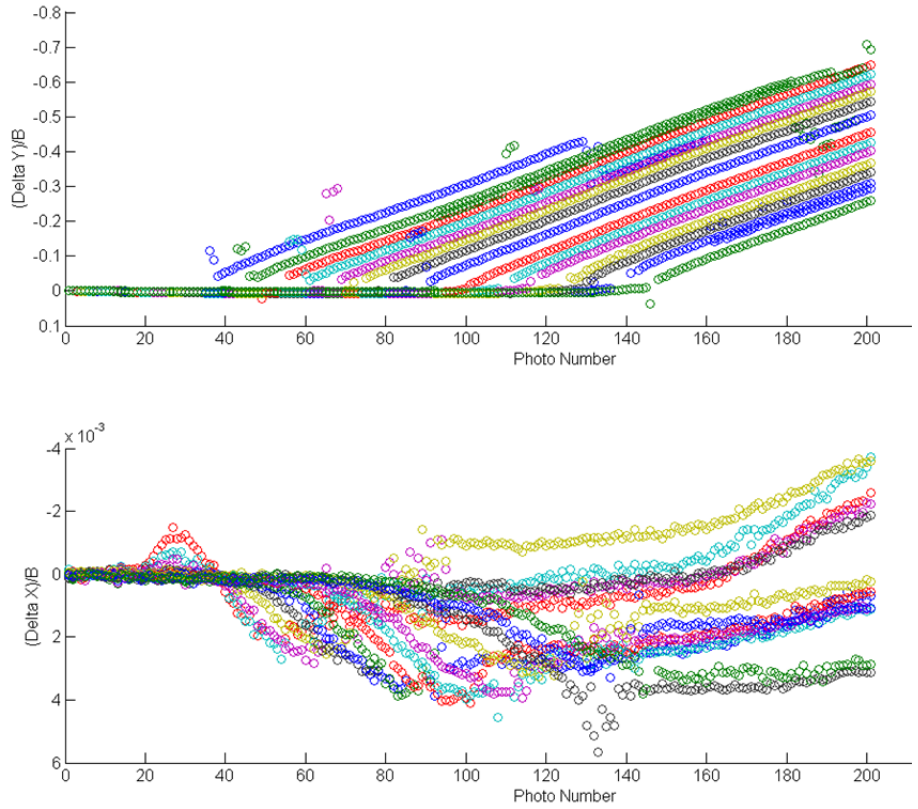

Figure G. 11 - IA Displacements over Time, Test BOC

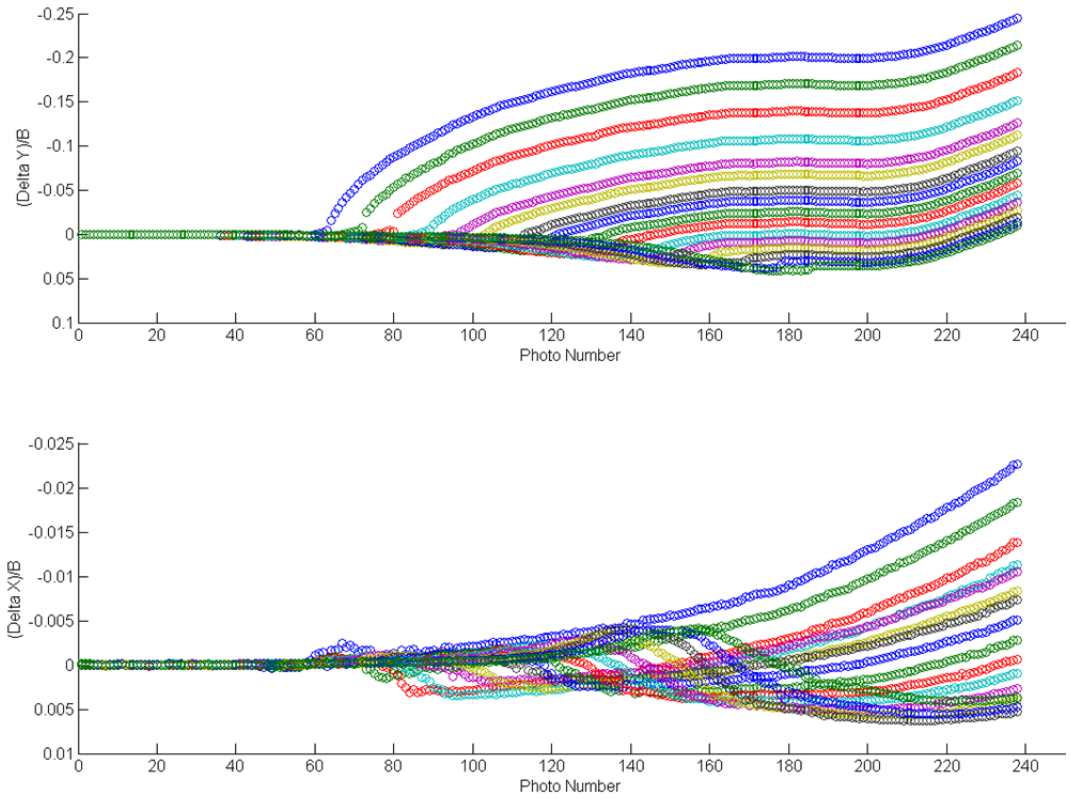

Figure G. 12 - IA Displacements over Time, Test COC

Appendix H Volumetric Strains during Tube Storage

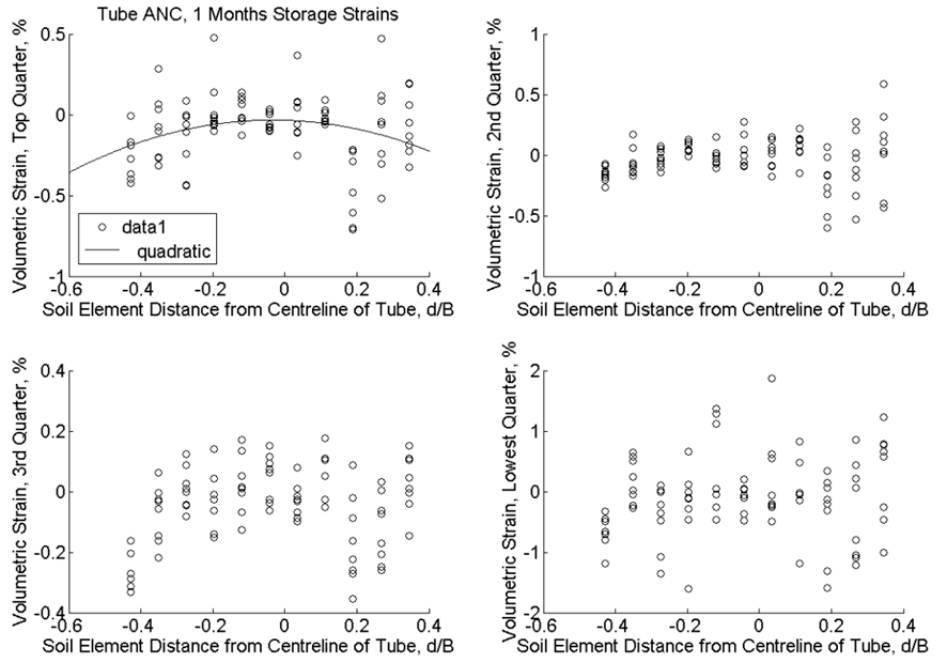

Figure H. 1 Volumetric Strains at 1 Month Storage Time, Tube ANC

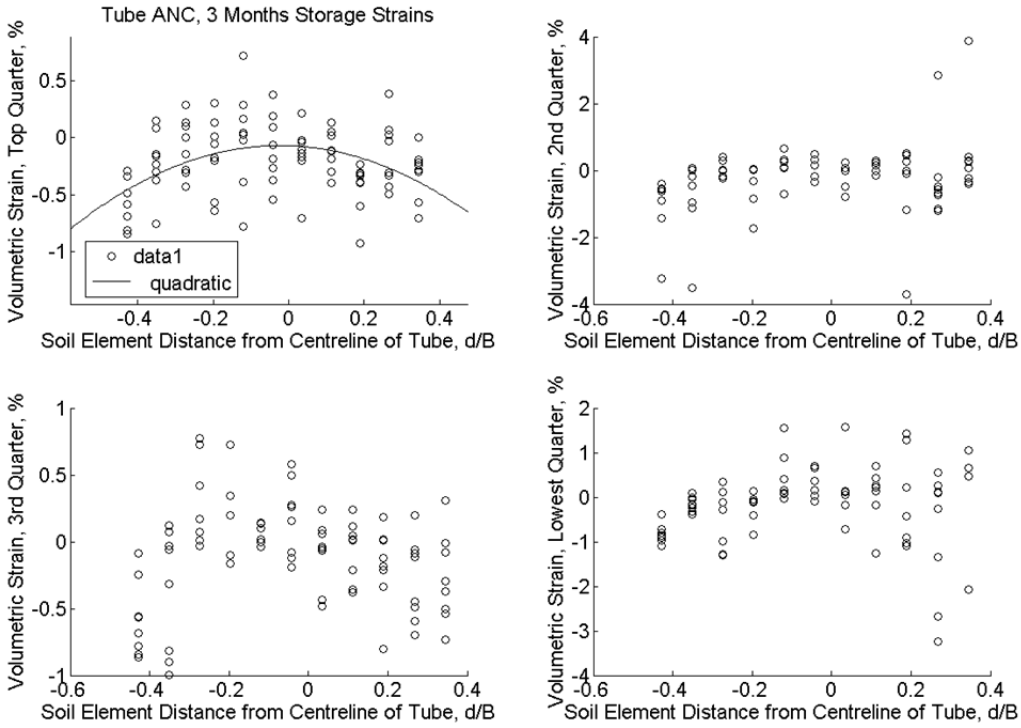

Figure H. 2 - Volumetric Strains at 3 Months Storage Time, Tube ANC

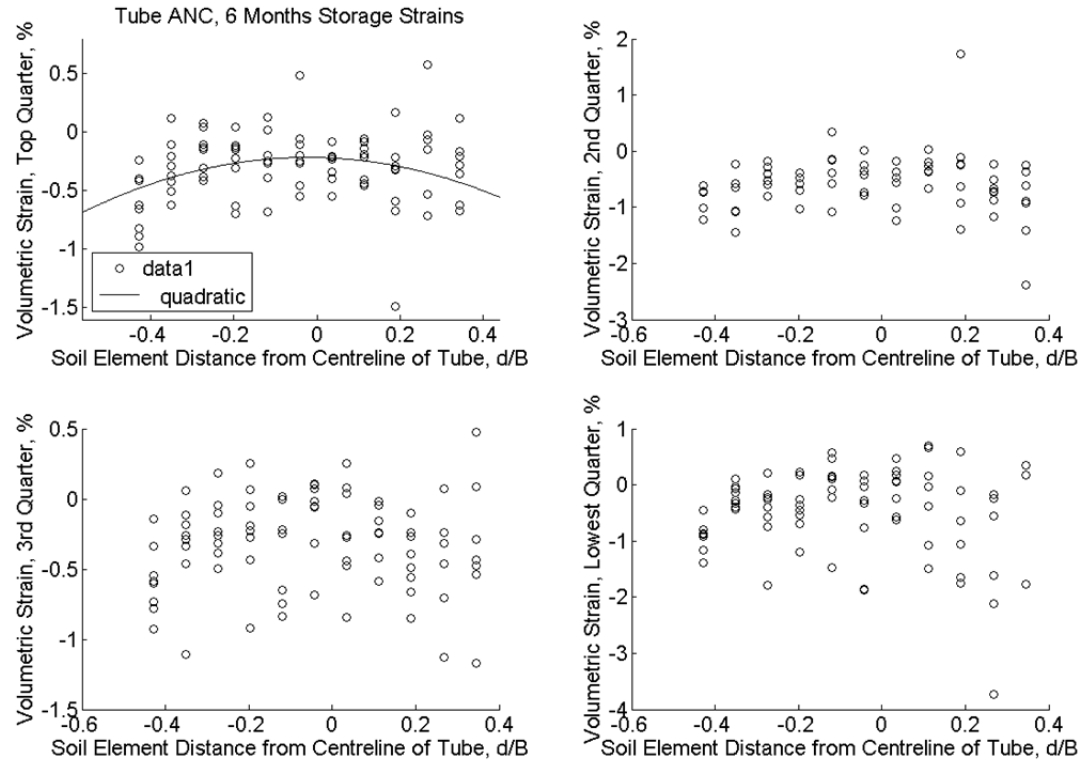

Figure H. 3 - Volumetric Strains at 6 Months Storage Time, Tube ANC

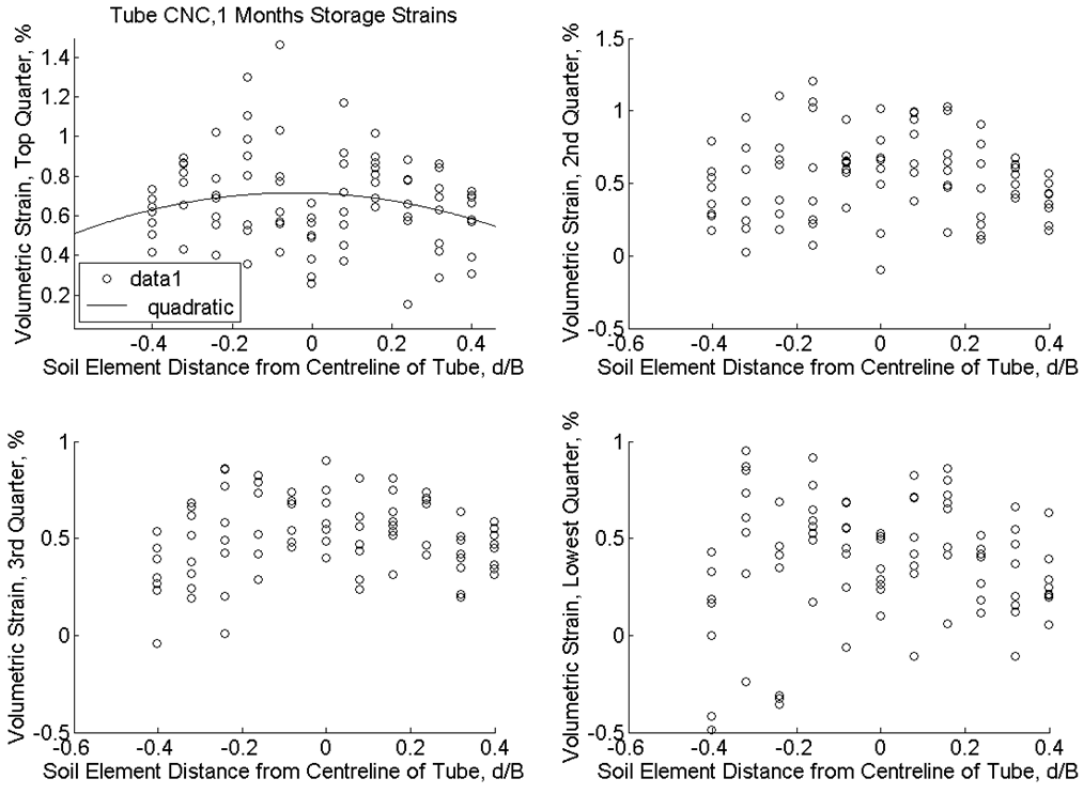

Figure H. 4 - Volumetric Strains at 1 Month Storage Time, Tube CNC

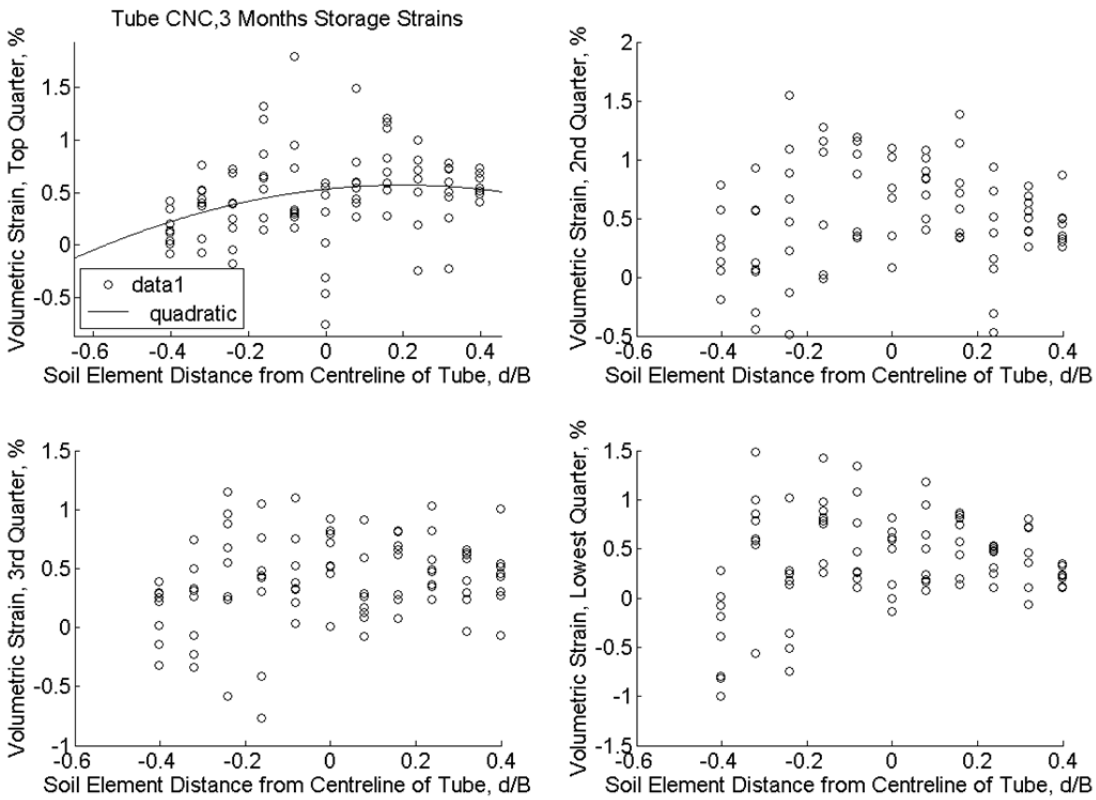

Figure H. 5 - Volumetric Strains at 3 Months Storage Time, Tube CNC

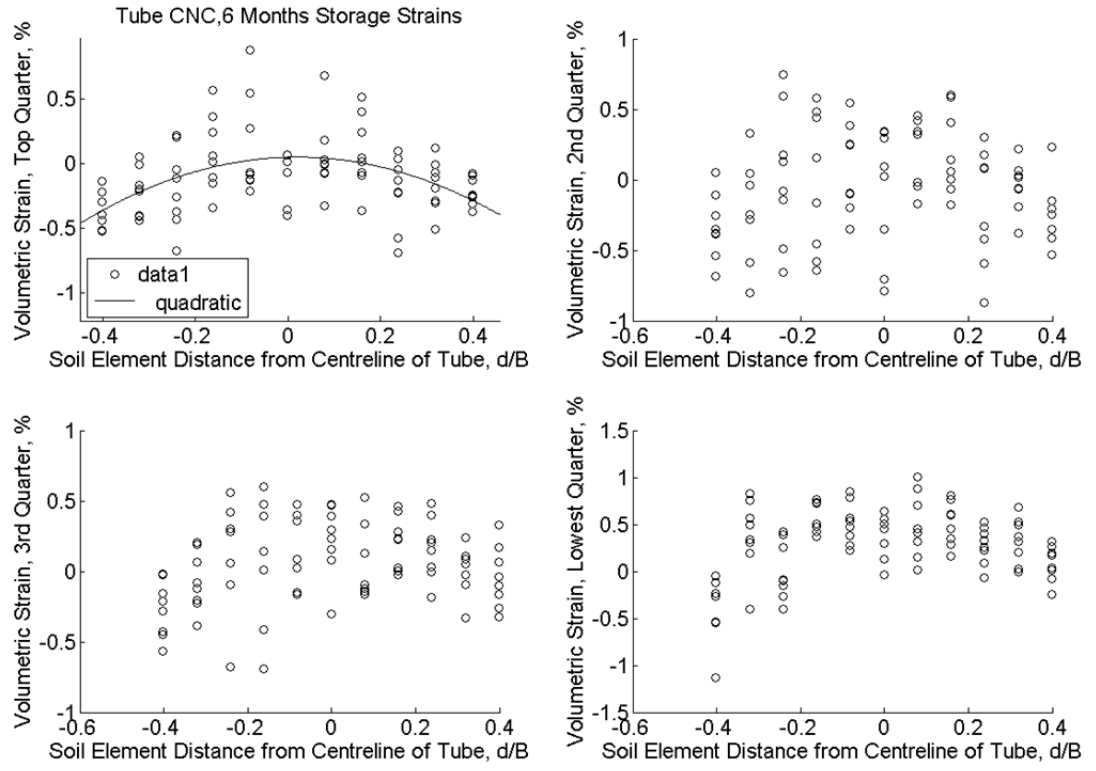

Figure H. 6 - Volumetric Strains at 6 Months Storage Time, Tube CNC

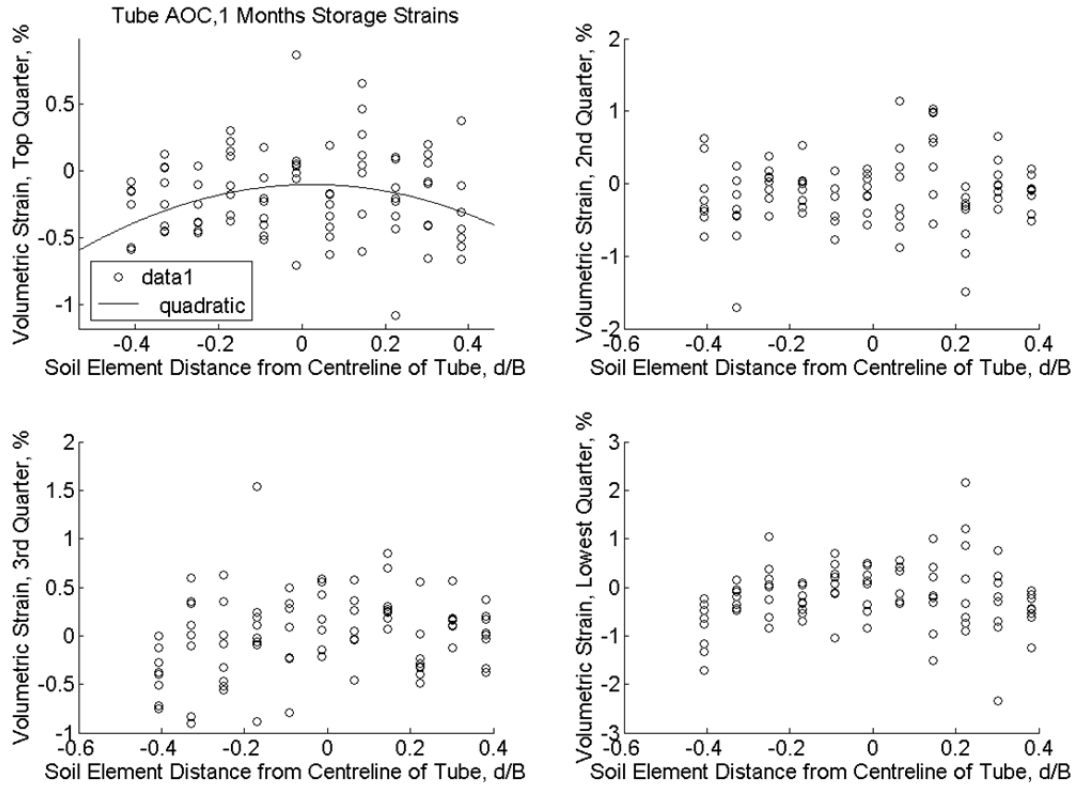

Figure H. 7 - Volumetric Strains at 1 Month Storage Time, Tube AOC

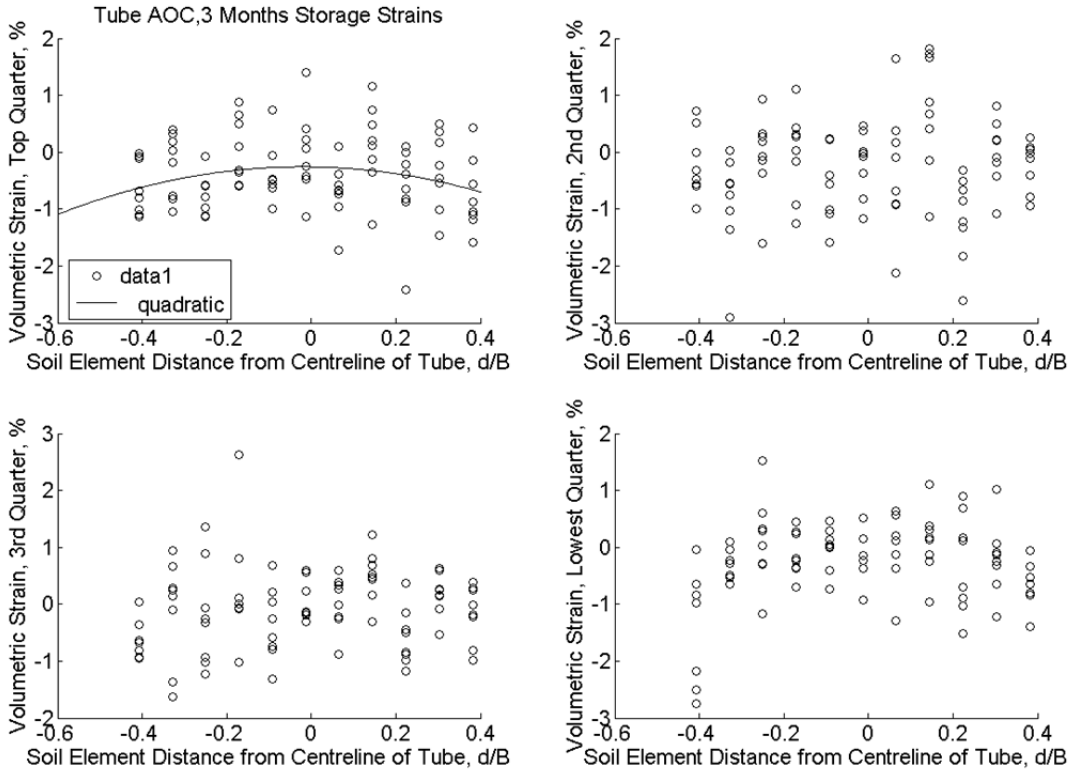

Figure H. 8 - Volumetric Strains at 3 Months Storage Time, Tube AOC

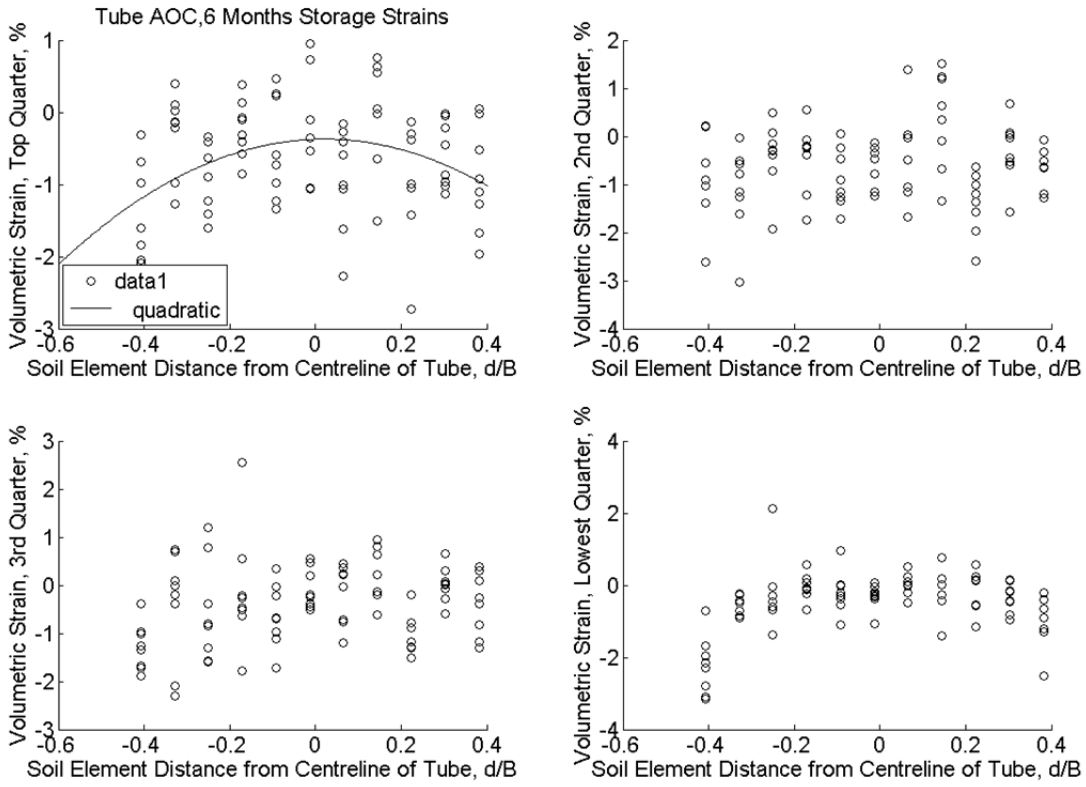

Figure H. 9 - Volumetric Strains at 6 Months Storage Time, Tube AOC

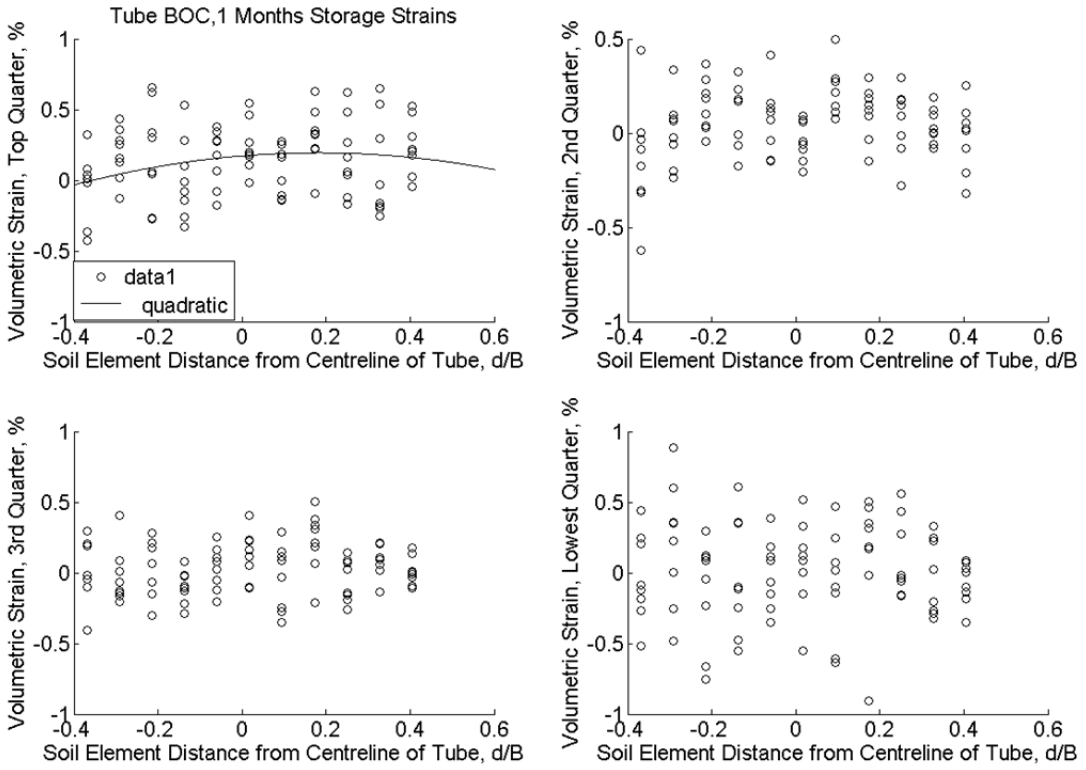

Figure H. 10 - Volumetric Strains at 1 Month Storage Time, Tube BOC

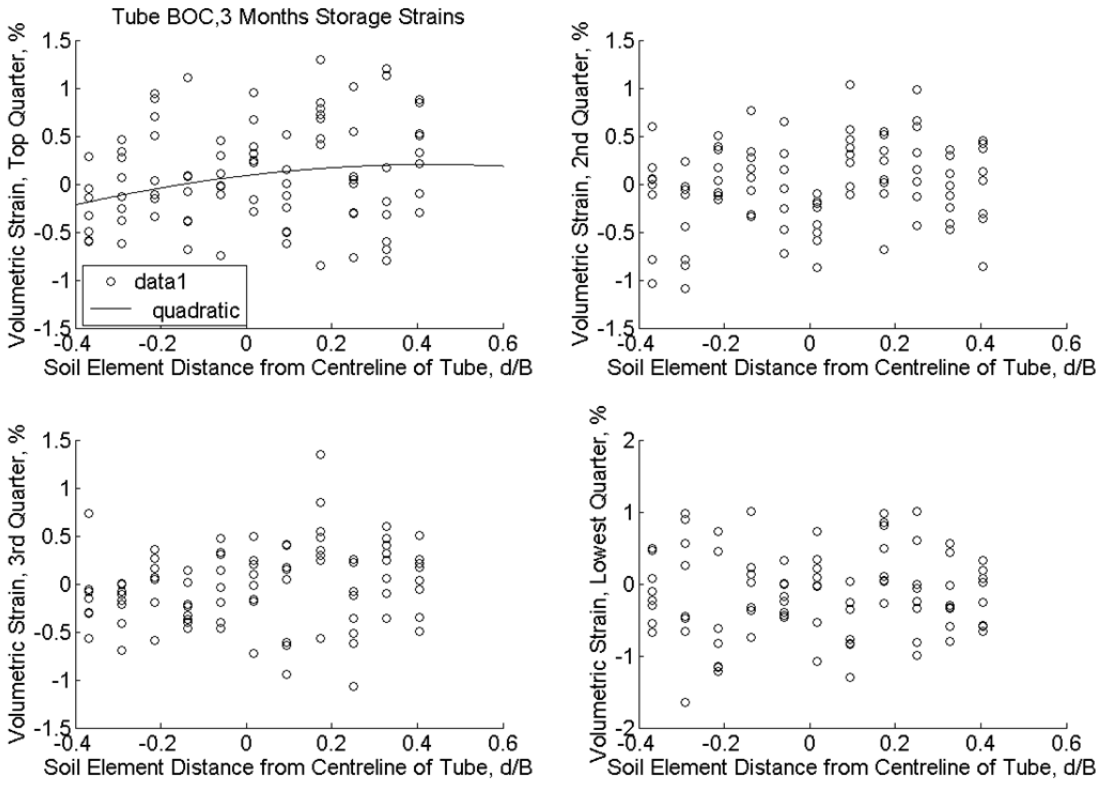

Figure H. 11 - Volumetric Strains at 3 Months Storage Time, Tube BOC

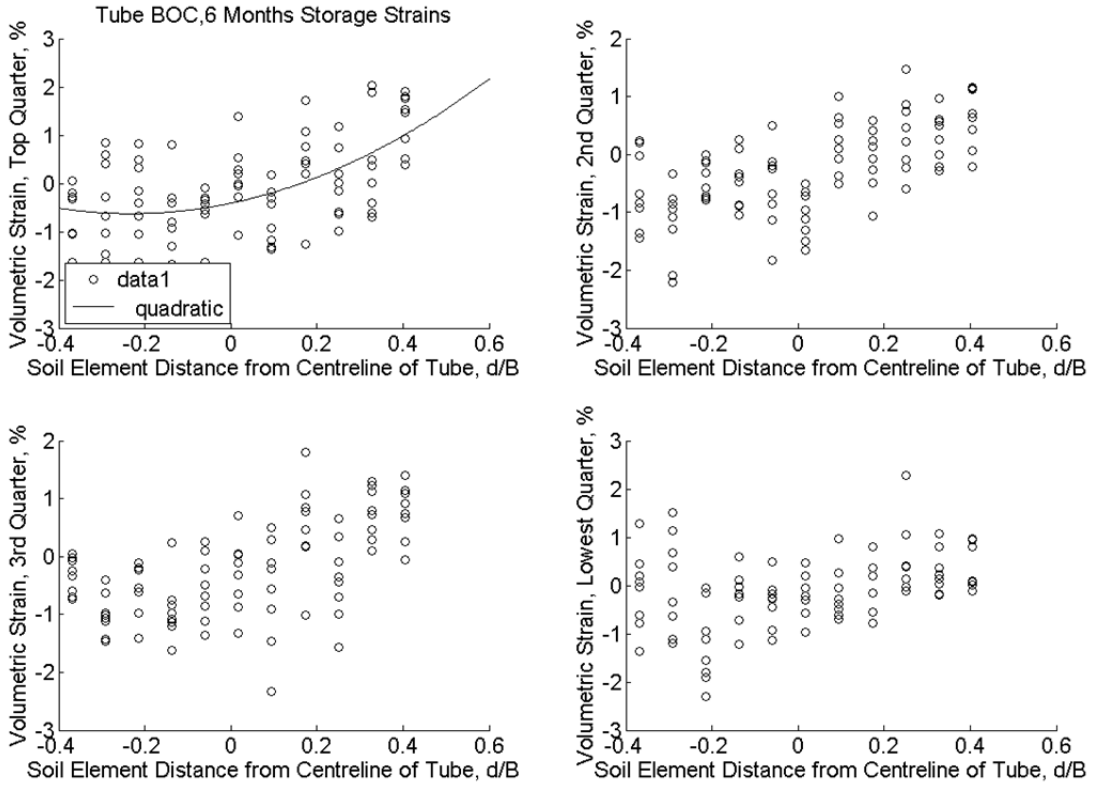

Figure H. 12 - Volumetric Strains at 6 Months Storage Time, Tube BOC

Appendix I Calibration Plate

A Calibration Plate was used to measure lens distortion. It was photographed through air only, and through all materials in the tube driving set-up. In the extrusion set-up, it was photographed in air only.

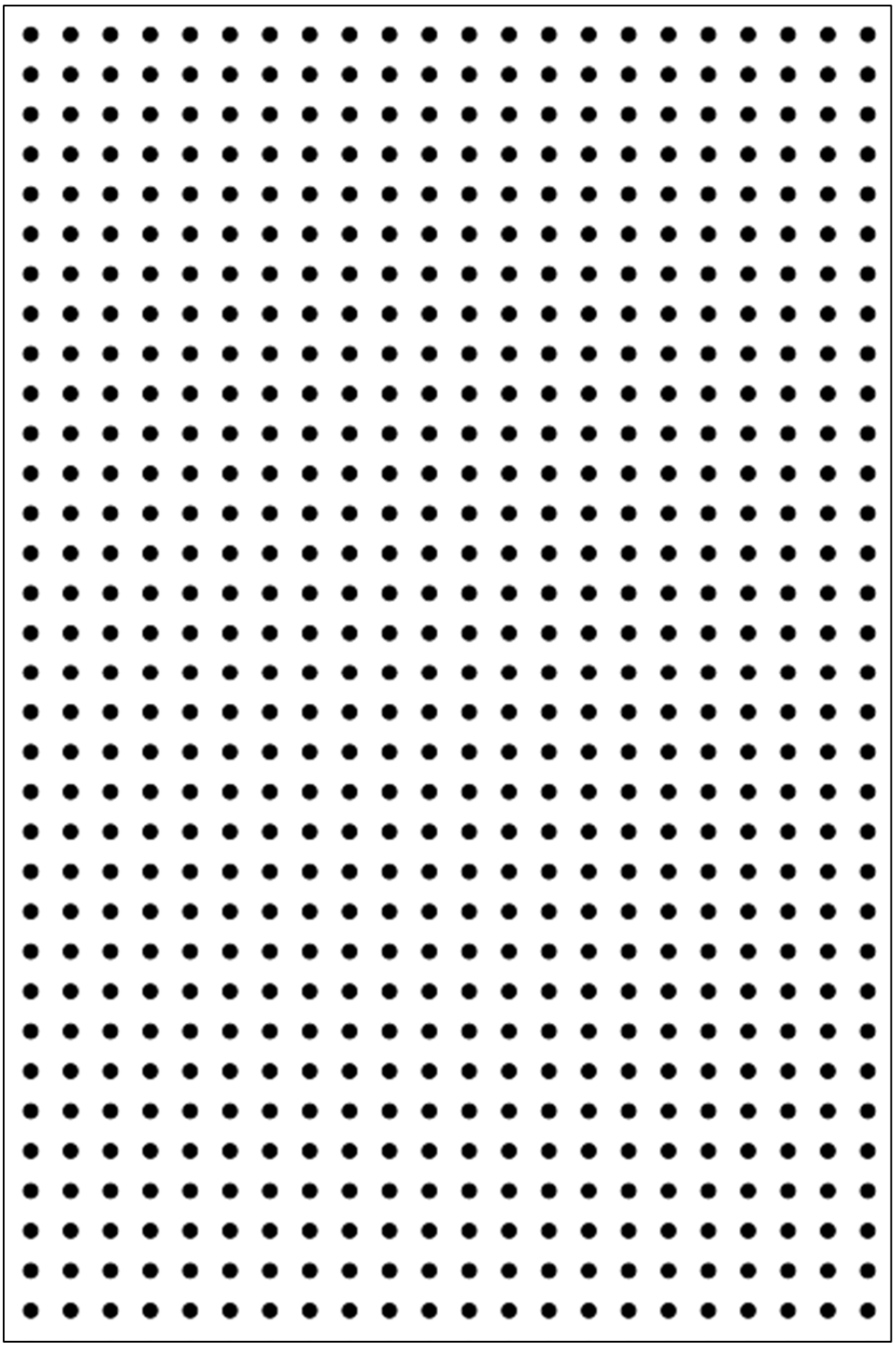

Figure I. 1 - Calibration Plate

Appendix J Scripts

Script 1: Calibration Model to calculate refraction caused in Tube Driving Tests – It was later found that this script could be simplified by treating the glass tube as a single sheet of glass acting at one constant depth into the model.

```
% Photo Calibration - Refraction only - Including tube (on
centreline only)
% This script calculates the initial position for each patch, for
which
% only the apparent position (after refraction) is known
% Eyre Hover, July 2013
% 1 - Create Matrix of apparent X, Y and Z positions

% In the end, we want to get a distortion as a function of distance
of the
% point to the centre of the image, so absolute coordinates do not
matter.
% By expressing all values relative to the centre of the image, the
process
% becomes more straightforward
x=0;
lengthx=length(x);
y=[-1500:50:1500];
lengthy=length(y);
z=(710+25+100)*11; % distance from camera to plane z=(camera to box
+ perspex thickness + soil thickness to plane) * pixels/mm at mid-
photo
XCoord=zeros(lengthy, lengthx);
YCoord=zeros(lengthy, lengthx);
ZCoord=zeros(lengthy, lengthx);
for i=1:lengthy
    for j=1:lengthx
        XCoord(i,j)=x(j); % final position, apparent, of patches
(what we see, distorted)
        YCoord(i,j)=y(i);
        ZCoord(i,j)=z;
    end
end
% 2 - Work out angles of all positions
Alpha1=zeros(lengthy, lengthx);
Beta1=zeros(lengthy, lengthx);
for i=1:lengthy
    for j=1:lengthx
    Alpha1(i,j)=atan((0-XCoord(i,j))/ZCoord(i,j));                  %
alpha is angle from camera axis in X DIRECTION (reference grid - X
and Z), seen from TOP
    Beta1(i,j)=atan((0-YCoord(i,j))/ZCoord(i,j));                   %
beta is angle from camera axis as seen from Y DIRECTION (reference
grid - Y and Z), seen from SIDE
    end
end
% 3 - Specify distances and material properties
RIair=1.00028;
RIperspex=1.495;
RIsoil=1.448;
RIglass=1.525;  %Borosilicate  glass,  RI=1.51-1.54  according  to
wikipedia
```

```
ZcameraTObox=(710)*11; % distance from camera to box z=(camera to
box) * pixels/mm at centreline
Zperspex=(25)*11;    % perspex thickness * pixels/mm at centreline
Zsoil=100*11;    % soil thickness * pixels/mm at centreline
ZCoordatBOX=Zsoil+Zperspex;
ZCoordatSOILend=Zsoil;
% 4 - 1st material boundary, air to perspex, 2nd material boundary,
perspex
% to soil
% angle is split into 2, alpha and beta
Alpha2=zeros(lengthy, lengthx);
Beta2=zeros(lengthy, lengthx);
for i=1:lengthy
    for j=1:lengthx
    Alpha2(i,j)=asin((RIair/RIperspex)*sin(Alpha1(i,j)));
% alpha is angle from camera axis in X DIRECTION (reference grid - X
and Z)
    Beta2(i,j)=asin((RIair/RIperspex)*sin(Beta1(i,j)));
% beta is angle from camera axis as seen from Y DIRECTION (reference
grid - Y and Z)
    end
end
XairTOboxINTERFACE=zeros(lengthy, lengthx);
YairTOboxINTERFACE=zeros(lengthy, lengthx);
XboxTOsoil=zeros(lengthy, lengthx);
YboxTOsoil=zeros(lengthy, lengthx);
for i=1:lengthy
    for j=1:lengthx
    XairTOboxINTERFACE(i,j)=(0-(z-ZCoordatBOX)*tan(Alpha1(i,j)));
    YairTOboxINTERFACE(i,j)=(0-(z-ZCoordatBOX)*tan(Beta1(i,j)));
    XboxTOsoil(i,j)=XairTOboxINTERFACE(i,j)-(ZCoordatBOX-
ZCoordatSOILend)*tan(Alpha2(i,j));
    YboxTOsoil(i,j)=YairTOboxINTERFACE(i,j)-(ZCoordatBOX-
ZCoordatSOILend)*tan(Beta2(i,j));
    end
end
% 5- this is the tricky part - into soil and through tube
TubeRadiusOut=26.06*11;
TubeRadiusIn=22.45*11;
Zglass=abs(TubeRadiusOut-TubeRadiusIn); % thickness of glass tube,
in y - z plane
Alpha3=zeros(lengthy, lengthx);
Beta3=zeros(lengthy, lengthx);
XatPlane=zeros(lengthy, lengthx); % this is where the light beam
ends up of there were no tube
YatPlane=zeros(lengthy, lengthx);
ZatPlane=zeros(lengthy, lengthx);
for i=1:lengthy
    for j=1:lengthx
    Alpha3(i,j)=asin((RIperspex/RIsoil)*sin(Alpha2(i,j)));
% alpha is angle from camera axis in X DIRECTION (reference grid - X
and Z)
    Beta3(i,j)=asin((RIperspex/RIsoil)*sin(Beta2(i,j)));
% beta is angle from camera axis as seen from Y DIRECTION (reference
grid - Y and Z)
    ZatPlane(i,j)=0;
    XatPlane(i,j)=XboxTOsoil(i,j)-(ZCoordatSOILend-
ZatPlane(i,j))*tan(Alpha3(i,j));
    YatPlane(i,j)=YboxTOsoil(i,j)-(ZCoordatSOILend-
ZatPlane(i,j))*tan(Beta3(i,j));
    end
```

```
end
% from here, the process is no longer straightforward through
parallel
% surfaces, but through curved class tube
%for each line, find the point at which the outer diameter of the
circle
%intersects the light line
X0=zeros(lengthy, lengthx); % this is the point where the light
touches the outside of the tube
Y0=zeros(lengthy, lengthx);
Z0=zeros(lengthy, lengthx);
Aa=zeros(lengthy, lengthx);
Bb=zeros(lengthy, lengthx);
Alpha3a=zeros(lengthy, lengthx);
radiusSlope=zeros(lengthy, lengthx);
for i=1:lengthy
    for j=1:lengthx
        pt2=[ZCoordatSOILend, XboxTOsoil(i,j),]; % point 1 on light
line - when emerges from perspex into box
        pt1=[ZatPlane(i,j), XatPlane(i,j) ]; % point 2 on light
line, when the light reaches the plane (no tube)
        a=(pt2(2)-pt1(2))/(pt2(1)-pt1(1)); % gives slope of line
from perspex to plane (no tube refraction)
        b=pt1(2)-a*pt1(1);
        % NOTE: circle equation = sqrt(radius^2-x^2), line equation=
a*x+b (values above),
        % solve for one equals the other
        eval(['A=''('   num2str(a)   '*z+'   num2str(b)   ')^2+z^2-'
num2str(TubeRadiusOut) '^2'';']);
        S=solve(A);
        z1=double(S(1));
        z2=double(S(2));
        x1=a*z1+b;
        x1=double(x1);
        x2=a*z2+b;
        x2=double(x2);
        if z1>=z2
            X0(i,j)=x1;
            Z0(i,j)=z1;
        else
            X0(i,j)=x2;
            Z0(i,j)=z2;
        end
        Y0(i,j)=YboxTOsoil(i,j)-(ZCoordatSOILend                    -
Z0(i,j))*tan(Beta3(i,j));
        Aa(i,j)=a;
        Bb(i,j)=b;
        if Z0(i,j)==0
            radiusSlope(i,j)=0;
            Alpha3a(i,j)=Alpha3(i,j);
        else
            radiusSlope(i,j)=X0(i,j)/Z0(i,j);
            Alpha3a(i,j)=atan(Aa(i,j))-atan(radiusSlope(i,j));
        end

    end
end
Alpha4=zeros(lengthy, lengthx);
Beta4=zeros(lengthy, lengthx);
Alpha4a=zeros(lengthy, lengthx);
for i=1:lengthy
```

```
    for j=1:lengthx
    Alpha4(i,j)=asin((RIsoil/RIglass)*sin(Alpha3a(i,j)));% alpha is
angle from camera axis in X DIRECTION (reference grid - X and Z)
    Beta4(i,j)=asin((RIsoil/RIglass)*sin(Beta3(i,j)));%   beta   is
angle from camera axis as seen from Y DIRECTION (reference grid - Y
and Z)
        if abs(atan(radiusSlope(i,j)))>=abs(Alpha4(i,j))
            if radiusSlope(i,j)>=0
                Alpha4a(i,j)=abs(abs(atan(radiusSlope(i,j)))-
abs(Alpha4(i,j)));
            else
                Alpha4a(i,j)=-abs((abs(atan(radiusSlope(i,j)))-
abs(Alpha4(i,j))));
            end
        else
            if radiusSlope(i,j)>=0
                Alpha4a(i,j)=-abs((abs(Alpha4(i,j))-
abs(atan(radiusSlope(i,j)))));
            else
                Alpha4a(i,j)=abs((abs(Alpha4(i,j))-
abs(atan(radiusSlope(i,j)))));
            end
        end
    end
end
 % find intersection point of line through tube and exit of tube
 X00=zeros(lengthy, lengthx); % this is the point where the light
touches the outside of the tube
Y00=zeros(lengthy, lengthx);
Z00=zeros(lengthy, lengthx);
Aaa=zeros(lengthy, lengthx);
Bbb=zeros(lengthy, lengthx);
delta=zeros(lengthy, lengthx);
 for i=1:lengthy
     for j=1:lengthx
         SecondLinePoint=[0,  X0(i,j)-Z0(i,j)*tan(Alpha4a(i,j))];  %
Check whether sign here is appropriate
         a=(X0(i,j)-SecondLinePoint(2))/(Z0(i,j)-
SecondLinePoint(1));
         b=SecondLinePoint(2)-a*SecondLinePoint(1);
         eval(['A=''('   num2str(a)   '*z+'   num2str(b)   ')^2+z^2-'
num2str(TubeRadiusIn) '^2'';']);
         delta(i,j)=(2*a*b)^2-4*(1+a^2)*(b^2-TubeRadiusIn^2);
         S=solve(A);
         if delta(i,j)<0
             X00(i,j)=0;
             Z00(i,j)=0;
             Y00(i,j)=0;
         elseif delta(i,j)==0
             z1=double(S);
             x1=a*z1+b;
             x1=double(x1);
             X00(i,j)=x1;
             Z00(i,j)=z1;
             Y00(i,j)=Y0(i,j)-(Z0(i,j)-Z00(i,j))*tan(Beta4(i,j));
         elseif delta(i,j)>0
             z1=double(S(1));
             z2=double(S(2));
             x1=a*z1+b;
             x1=double(x1);
             x2=a*z2+b;
```

```
            x2=double(x2);
            if z1>=z2
                X00(i,j)=x1;
                Z00(i,j)=z1;
                Y00(i,j)=Y0(i,j)-(Z0(i,j)-
Z00(i,j))*tan(Beta4(i,j));
            else
                X00(i,j)=x2;
                Z00(i,j)=z2;
                Y00(i,j)=Y0(i,j)-(Z0(i,j)-
Z00(i,j))*tan(Beta4(i,j));
            end
         end
        Aaa(i,j)=a;
        Bbb(i,j)=b;
     end
 end

% Find the equation of the line of light through the tube, then the
% equation of the inner radius to find alpha 5 (Beta 5 is equal to
Beta 4)
LightLinea=zeros(lengthy, lengthx);
LightLineb=zeros(lengthy, lengthx);
InnerRadiusa=zeros(lengthy, lengthx);
Alpha5=zeros(lengthy, lengthx);
Alpha6=zeros(lengthy, lengthx);
Beta6=zeros(lengthy, lengthx);
Alpha6a=zeros(lengthy, lengthx);
for i=1:lengthy
    for j=1:lengthx
        LightLinea(i,j)=(X0(i,j)-X00(i,j))/(Z0(i,j)-Z00(i,j));
        LightLineb(i,j)=X0(i,j)-LightLinea(i,j)*Z0(i,j);
        InnerRadiusa(i,j)=X00(i,j)/Z00(i,j);
        Alpha5(i,j)=atan(LightLinea(i,j))-atan(InnerRadiusa(i,j));
        Alpha6(i,j)=asin((RIglass/RIsoil)*sin(Alpha5(i,j)));
        Beta6(i,j)=asin((RIglass/RIsoil)*sin(Beta4(i,j)));
    end
end
% calculate final angle to normal
for i=1:lengthy
    for j=1:lengthx
        if abs(atan(InnerRadiusa(i,j)))>=abs(Alpha6(i,j))
            if InnerRadiusa(i,j)>=0
                Alpha6a(i,j)=abs(abs(atan(InnerRadiusa(i,j)))-
abs(Alpha6(i,j)));
            else
                Alpha6a(i,j)=-abs((abs(atan(InnerRadiusa(i,j)))-
abs(Alpha6(i,j))));
            end
        else
            if InnerRadiusa(i,j)>=0
                Alpha6a(i,j)=-abs((abs(Alpha6(i,j))-
abs(atan(InnerRadiusa(i,j)))));
            else
                Alpha6a(i,j)=abs((abs(Alpha6(i,j))-
abs(atan(InnerRadiusa(i,j)))));
            end
        end
    end
end
```

```
 % find original point on plane - 2 cases, previously we've ignored
if the
% light exits the tube - but on exterior it is possible that the
light
% remains within the glass, here, we pick up on this - if delta(i,j)
% negavive, then no intersection
XfinalPlane=zeros(lengthy, lengthx); % this is the point where the
light touches the plane, after all refractions
YfinalPlane=zeros(lengthy, lengthx);
ZfinalPlane=zeros(lengthy, lengthx); % by definition, plane is at
centre of coordinates
for i=1:lengthy
    for j=1:lengthx
        if delta(i,j)<0
            %no intersection
            XfinalPlane(i,j)=X0(i,j)-Z0(i,j)*tan(Alpha4a(i,j));
            YfinalPlane(i,j)=Y0(i,j)-Z0(i,j)*tan(Beta4(i,j));
        else
            XfinalPlane(i,j)=X00(i,j)-Z00(i,j)*tan(Alpha6a(i,j));
            YfinalPlane(i,j)=Y00(i,j)-Z00(i,j)*tan(Beta6(i,j));
        end
    end
end
% now compare point (real position) with its distorted location
XatPlaneNOrefraction=zeros(lengthy, lengthx); % i.e. the distorted
values, if the light went from plane to camera in a straight line
YatPlaneNOrefraction=zeros(lengthy, lengthx);
ZatPlaneNOrefraction=zeros(lengthy, lengthx);
for i=1:lengthy
    for j=1:lengthx
    XatPlaneNOrefraction(i,j)=-z*tan(Alpha1(i,j));
    YatPlaneNOrefraction(i,j)=-z*tan(Beta1(i,j));
    ZatPlaneNOrefraction(i,j)=0;
    end
end
deltaX=zeros(lengthy, lengthx);
deltaY=zeros(lengthy, lengthx);
Vectorlength=zeros(lengthy, lengthx);
for i=1:lengthy
    for j=1:lengthx
    deltaX(i,j)=XatPlaneNOrefraction(i,j)-XfinalPlane(i,j);        %
distorted position - real position
    deltaY(i,j)=YatPlaneNOrefraction(i,j)-YfinalPlane(i,j);
    Vectorlength(i,j)=sqrt((deltaX(i,j))^2+(deltaY(i,j))^2);
    end
end
% 7 - plot
figure1=figure(1);
for i=1:lengthy
    quiver(XCoord(i,:), YCoord(i,:), deltaX(i,:), deltaY(i,:), 0)
    hold all
end
grid on
axis equal
% 8 - mathematical solution
DistanceFromCentreDistorted=zeros(lengthy, lengthx); % from the
original photo, before calibration
for i=1:lengthy
    for j=1:lengthx
```

```
DistanceFromCentreDistorted(i,j)=sqrt((XCoord(i,j))^2+(YCoord(i,j))^
2);
    end
end
CompactedDfCd=DistanceFromCentreDistorted(1,:);
CompactedVl=Vectorlength(1,:);

for i=2:lengthy
    CompactedDfCd=[CompactedDfCd, DistanceFromCentreDistorted(i,:)];
    CompactedVl=[CompactedVl, Vectorlength(i,:)];
end
figure2=figure(2);
scatter(CompactedDfCd,CompactedVl)

figure3=figure(3);
for i=1:lengthy
    quiver(XatPlaneNOrefraction(i,:),  YatPlaneNOrefraction(i,:),  -
deltaX(i,:), -deltaY(i,:), 0)
    hold all
end
grid on
axis equal
% 9 - solution in terms of delta x and delta y
figure4=figure(4);
scatter( XCoord(1,:),-deltaX(1,:));
hold on
scatter( YCoord(:,1),-deltaY(:,1));
-----------------------------------------------------------------------
```

Script 2: Calculating Strain in Tube Driving Tests

```
% plottingCSP.m
% September 2012, Eyre Hover
% the purpose of this file is to collate and calculate the stresses
for one
% set of data, 4 columns per patch
% ADD LINE FOR COLUMN TITLES: image1, image 2, B, tube position,
position
% of patch, Z, Z/B, negative strain
% photo properties
clear all
clc
start=input('1st photo=');
finish=input('last photo=');
filequantity=finish-start;
% tube dimensions
B=input('value for B (pixels)=');
% loadings
eval(['A=load(''PIV_S'    num2str(start)    '_S'    num2str(finish)
'.txt'',''r'' );']); %variable
patchnumber=length(A(:,1));
spacing=A(2,3)-A(1,3);
TUBEPOS=PositionMatrixAOC1(:,2); % Change manually
% required files
DATAMATRIX=zeros(filequantity,  (4+4*(patchnumber-1)));  %predefines
size of matrix, to speed up process
DATAMATRIX(:,1)=DATAMATRIX(:,1)+  start;  %fills  column  1,  gives
original photo number
for n=start:1:(finish-1)
```

```
    DATAMATRIX(n+1-start,2)=n+1; % fills column 2, gives current
photo number
    DATAMATRIX(n+1-start,3)=B;   % fills column 3, gives value for B
    DATAMATRIX(n+1-start,4)=TUBEPOS(n+1-start,1);
    eval(['A=load(''PIV_S'    num2str(start)    '_S'    num2str(n+1)
'.txt'',''r'' );']); % loading data, 1 file per loop %variable
    for i=1:patchnumber-1
    eval(['strain'    num2str(i)    '=(A('    num2str(i+1)    ',7)-A('
num2str(i) ',7))*(-100)/spacing;' ]); % Note: strain is a function
of spacing, not patch size
    eval(['DATAMATRIX('  num2str(n+1-start)  ','  num2str(4+4*i)  ')=
strain' num2str(i); ]); % calculates negative strain line by line
    DATAMATRIX(n+1-start,1+4*i)=(A(i+1,3)+A(i,3))/2;  %  calculates
soil element location, as the average between the y values for the
patch centroids
    DATAMATRIX(n+1-start,2+4*i)=            DATAMATRIX(n+1-start,4)-
DATAMATRIX(n+1-start,1+4*i);  % calculates z, as defined by "tube
position-soil element centroid"
    DATAMATRIX(n+1-start,3+4*i)=        DATAMATRIX(n+1-start,2+4*i)/
DATAMATRIX(n+1-start,3);          % calculates z/B
    end
   end
save('DataMatrix1', 'DATAMATRIX'); % change manually
-----------------------------------------------------------------------
```

Script 3: Using Quadratic Curve to Generate New Mesh

```
RES=zeros(16, 5);
for i=1:16
    RES(i, 1)=i;        %patch number
    RES(i, 2)=1585+(i-1)*96;        %patch coordinate
    RES(i,  3)=(-5.3147)*(10^-6)*(RES(i,  2)^2)+0.20895*(RES(i,  2))-
658.41;         %patch delta y (displacement since beginning) – use
equation of quadratic trendline
end
for i=1:15
    RES(i, 4)=-(RES((i+1), 3)-RES((i), 3))*100/96;   %strain
end
for i=1:14
    RES(i, 5)=RES((i+1), 4)-RES((i), 4);    %delta strain, i.e. how
regularly spaced are the traces?
end
save('ResidualStrains1long', 'RES');
for i=1:16
    eval(['p' num2str(i) '=RES(i, 2)+RES(i, 3);']);
end
P=[p1, p2, p3, p4, p5, p6, p7, p8, p9, p10, p11, p12, p13, p14, p15,
p16];
xcoord=input('x coordinate= ');
PSiz=input('Patch size= ');
MESH=zeros(16, 9);
for i=1:16
    MESH(i, 1)=i;
end
MESH(:, 2)=0;
MESH(:, 3)=0;
MESH(:, 4)=xcoord;
for i=1:16
    MESH(i, 5)=P(i);
end
MESH(:, 6)=0;
```

```
MESH(:, 7)=0;
MESH(:, 8)=PSiz;
MESH(:, 9)=0;
fid=fopen('meshCNC.txt', 'w');%variable – enter name manually
fprintf(fid,'%%patch    uo  vo  uf  vf  du  dv  size    desc\n')
for i=1:16
fprintf(fid, '%4g \t %8.4f \t  %8.4f \t %8.4f \t %8.4f \t %8.4f \t
%8.4f \t %8.2f\t %8.2f\n', MESH(i,1:9))
end
fclose (fid)
```

Script 4 – Calculating Backwards CSP for Tube Driving Tests

```
% plottingCSP_BACK_updatedPatchLocation.m
% February 2013, Eyre Hover
% the purpose of this file is to collate and calculate the stresses
for one
% set of data, 4 columns per patch, backwards PIV run
% ADD LINE FOR COLUMN TITLES: image1, image 2, B, tube position,
position
% of patch, Z, Z/B, negative strain
% photo properties
start=input('1st photo=');
finish=input('last photo=');
filequantity=start-finish;
% tube dimensions
tubeB=input('value for B (pixels)=');
% loadings
eval(['A=load(''PIV_S'    num2str(start)    '_S'    num2str(finish)
'.txt'',''r'' );']);
patchnumber=length(A(:,1));
spacing=A(2,3)-A(1,3);
UPDATEDpos=[(1371+48):96:5000]; % original patch location in forward
analysis - enter manually
% required files
DATAMATRIXBACK=zeros(filequantity,           (4+4*(patchnumber-1)));
%predefines size of matrix, to speed up process
DATAMATRIXBACK(:,1)=start; %fills column 1, gives original photo
number
TUBEPOS=PositionMatrixAOC1(:,2);
[photonumber]=length(TUBEPOS);
TUBEPOS2=zeros(photonumber);
for i=1:photonumber
       TUBEPOS2(i)=TUBEPOS(sqrt((photonumber-i)^2)+1);
end
for n=start:-1:(finish+1);
    DATAMATRIXBACK(start-n+1,2)=n-1; % fills column 2, gives current
photo number
    DATAMATRIXBACK(start-n+1,3)=tubeB;     % fills column 3, gives
value for B
    DATAMATRIXBACK(start-n+1,4)=TUBEPOS2(start-n+1,1);
    eval(['A=load(''PIV_S'    num2str(start)    '_S'    num2str(n-1)
'.txt'',''r'' );']); % loading data, 1 file per loop
    load('ResidualStrains1long', 'RES'); %variable - enter manually

    for i=1:patchnumber-1;
    eval(['strain' num2str(i) '=RES(i, 4)+(A(' num2str(i+1) ',7)-A('
num2str(i) ',7))*(-100)/spacing;' ]); % Note: strain is a function
of spacing, not patch size
    eval(['DATAMATRIXBACK('  num2str(start-n+1)  ','  num2str(4+4*i)
')= strain' num2str(i); ]); % calculates negative strain line by
line
```

```
    DATAMATRIXBACK(start-n+1,1+4*i)=UPDATEDpos(i);    %    specifies
ORIGINAL patch location, specified by forwards mesh, as opposed to
quadratic calculated final patch locations
    DATAMATRIXBACK(start-n+1,2+4*i)=    DATAMATRIXBACK(start-n+1,4)-
DATAMATRIXBACK(start-n+1,1+4*i);   % calculates z, as defined by
"tube position-soil element centroid"
    DATAMATRIXBACK(start-n+1,3+4*i)=           DATAMATRIXBACK(start-
n+1,2+4*i)/ DATAMATRIXBACK(start-n+1,3);          % calculates z/B
    end
   end
save('DataMatrixBack1', 'DATAMATRIXBACK'); % enter manually
disp('Data Matrix created')
load('DatamatrixBack1', 'DATAMATRIXBACK');
[photonumber, colnumber]=size(DATAMATRIXBACK);
DATAMATRIXBACKandREVERSED=zeros(photonumber, colnumber);
for i=1:photonumber
    for j=1:colnumber
    DATAMATRIXBACKandREVERSED(i,
j)=DATAMATRIXBACK(sqrt((photonumber-i)^2)+1, j);
    end
  end
save('DATAMATRIXBACKandREVERSED1', 'DATAMATRIXBACKandREVERSED')
```

Script 5: Combining Forward and Backward CSPs

```
%CombineCSPHalves
%by Eyre Hover, February 2013
% HAVE DATAMATRIX (forward) OPEN TO INPUT VISUAL READINGS FOR Z/B=0
(take last negative)
load ('Datamatrix', 'DATAMATRIX');
load ('DATAMATRIXBACKandREVERSED', 'DATAMATRIXBACKandREVERSED');
[photonumber, colnumber]=size(DATAMATRIX);
COMBINEDdm=zeros(photonumber, colnumber);
%1- identical to CSP throughout
for i=1:photonumber
    COMBINEDdm(i, 1)=DATAMATRIX(i, 1);
    COMBINEDdm(i, 2)=DATAMATRIX(i, 2);
    COMBINEDdm(i, 3)=DATAMATRIX(i, 3);
    COMBINEDdm(i, 4)=DATAMATRIX(i, 4);
    for j=1:((colnumber-4)/4) %number of soil patches
        COMBINEDdm(i, 1+4*j)=DATAMATRIX(i, 1+4*j);
    end
end
%2- split data
%using visual cues, identify the point at which the tube passes the
patch,
%therefore z/B=0. This could be taken from CSPfile DATAMATRIX, in
forward
%matrix, as the last negative Z/B's line number
for i=1:((colnumber-4)/4)
    eval(['P' num2str(i) '=input(''Patch ' num2str(i) ', z/B=zero in
line '');']);
end
for i=1:((colnumber-4)/4)
    for j=1:eval(['P' num2str(i)])
        COMBINEDdm(j, 2+4*i)=DATAMATRIX(j, 2+4*i);
        COMBINEDdm(j, 3+4*i)=DATAMATRIX(j, 3+4*i);
        COMBINEDdm(j, 4+4*i)=DATAMATRIX(j, 4+4*i);
    end
    for j=(eval(['P' num2str(i)])+1):photonumber
        COMBINEDdm(j, 2+4*i)=DATAMATRIXBACKandREVERSED(j, 2+4*i);
        COMBINEDdm(j, 3+4*i)=DATAMATRIXBACKandREVERSED(j, 3+4*i);
```

```
        COMBINEDdm(j, 4+4*i)=DATAMATRIXBACKandREVERSED(j, 4+4*i);
    end
end
save('CombinedCSP11', 'COMBINEDdm')
-----------------------------------------------------------------------
```

Script 6: Calculating Volumetric Strains During Sample Storage

```
%MonitoringStrains.m

%Eyre Hover, January 2014

clear all
clc
colnumber=input('Number of columns: ');
rownumber=input('Number of rows: ');
patchsize=input('Patch Size: ');
centrelineX=input('X Centreline: ');
A=load('PIV_IMGP2448_IMGP2454.txt');  % enter manually
TubeWidth=input('Tube Width: ');
patchnumber=length(A(:, 1));
OriginalArea=patchsize^2;
for i=1:patchnumber-rownumber-1
    StrainData(i, 1)=i;
    StrainData(i, 2)=A(i+1, 4); % Point 1, X Coordinate
    StrainData(i, 3)=A(i+1, 5); % Point 1, Y Coordinate
    StrainData(i, 4)=A(i, 4); % Point 2, X Coordinate
    StrainData(i, 5)=A(i, 5); % Point 2, Y Coordinate
    StrainData(i, 6)=A(i+rownumber, 4); % Point 3, X Coordinate
    StrainData(i, 7)=A(i+rownumber, 5); % Point 3, Y Coordinate
    StrainData(i, 8)=A(i+rownumber+1, 4); % Point 4, X Coordinate
    StrainData(i, 9)=A(i+rownumber+1, 5); % Point 4, Y Coordinate

    StrainData(i,    10)=sqrt((    StrainData(i,    2)-StrainData(i,
6))^2+(StrainData(i, 3)-StrainData(i, 7))^2); %B1 length
    StrainData(i,    11)=sqrt((    StrainData(i,    2)-StrainData(i,
4))^2+(StrainData(i, 3)-StrainData(i, 5))^2); %a length
    StrainData(i,    12)=sqrt((    StrainData(i,    8)-StrainData(i,
6))^2+(StrainData(i, 9)-StrainData(i, 7))^2);  %c length

    if StrainData(i, 4)>=StrainData(i, 2)
    sideGradient1=atan((StrainData(i,               5)-StrainData(i,
3))/(StrainData(i, 4)-StrainData(i, 2)));
    else
    sideGradient1=atan((StrainData(i,               3)-StrainData(i,
5))/(StrainData(i, 2)-StrainData(i, 4)));
    end

    if sideGradient1>=0
        StrainData(i,13)=4*atan(1)-(sideGradient1-
atan((StrainData(i,    7)-StrainData(i,    3))/(StrainData(i,    6)-
StrainData(i, 2))));
    else
        StrainData(i,13)=4*atan(1)-(4*atan(1)-(atan((StrainData(i,
7)-StrainData(i,    3))/(StrainData(i,    6)-StrainData(i,    2)))-
sideGradient1));
    end
    if StrainData(i, 6)>=StrainData(i, 8)
    sideGradient2=atan((StrainData(i,               7)-StrainData(i,
9))/(StrainData(i, 6)-StrainData(i, 8)));
    else
```

```
    sideGradient2=atan((StrainData(i,               9)-StrainData(i,
7))/(StrainData(i, 8)-StrainData(i, 6)));
    end

     if sideGradient2>=0
        StrainData(i,14)=4*atan(1)-(sideGradient2-
atan((StrainData(i,    7)-StrainData(i,    3))/(StrainData(i,    6)-
StrainData(i, 2))));
    else
        StrainData(i,14)=4*atan(1)-(4*atan(1)-(atan((StrainData(i,
7)-StrainData(i,    3))/(StrainData(i,    6)-StrainData(i,    2)))-
sideGradient2));
    end

    StrainData(i,        15)=(StrainData(i,        10)*StrainData(i,
11)*sin(StrainData(i, 13)))/2;
    StrainData(i,        16)=(StrainData(i,        10)*StrainData(i,
12)*sin(StrainData(i, 14)))/2;
    StrainData(i, 17)=StrainData(i, 15)+StrainData(i, 16);
    StrainData(i,     18)=100*     (((sqrt(StrainData(i,     17)))^3-
(sqrt(OriginalArea))^3)/(sqrt(OriginalArea))^3);
    StrainData(i, 19)=A(i, 2)+patchsize/2-centrelineX;
end
FirstSequence=1:8;
SecondSequence=9:16;
ThirdSequence=17:24;
FourthSequence=25:32;
for i=1:10
FirstSequence=[FirstSequence, ((1+(i*rownumber))):(8+i*rownumber)];
SecondSequence=[SecondSequence,
((9+(i*rownumber))):(16+i*rownumber)];
ThirdSequence=[ThirdSequence,
((17+(i*rownumber))):(24+i*rownumber)];
FourthSequence=[FourthSequence,
((25+(i*rownumber))):(32+i*rownumber)];
end
subplot(2,  2,  1),  scatter(StrainData(FirstSequence,  19)/TubeWidth,
StrainData(FirstSequence, 18), 'k')
set(gca, 'FontSize', 16)
title('Tube CNC, 1 Month Storage Strains'); %enter manually
xlabel('Soil Element Distance from Centreline of Tube, d/B');
ylabel('Volumetric Strain, Top Quarter, %');
subplot(2,  2,  2),  scatter(StrainData(SecondSequence,  19)/TubeWidth,
StrainData(SecondSequence, 18), 'k')
set(gca, 'FontSize', 16)
xlabel('Soil Element Distance from Centreline of Tube, d/B');
ylabel('Volumetric Strain, 2nd Quarter, %');
subplot(2,  2,  3),  scatter(StrainData(ThirdSequence,  19)/TubeWidth,
StrainData(ThirdSequence, 18), 'k')
set(gca, 'FontSize', 16)
xlabel('Soil Element Distance from Centreline of Tube, d/B');
ylabel('Volumetric Strain, 3rd Quarter, %');
subplot(2,  2,  4),  scatter(StrainData(FourthSequence,  19)/TubeWidth,
StrainData(FourthSequence, 18), 'k')
set(gca, 'FontSize', 16)
xlabel('Soil Element Distance from Centreline of Tube, d/B');
ylabel('Volumetric Strain, Lowest Quarter, %');
```

Script 7: Calculating CSP during Extrusion

```
% March 2014, Eyre Hover
% ADD LINE FOR COLUMN TITLES: image1, image 2, B, tube position,
position of patch, Z, Z/B, negative strain
clear all
clc
% photo properties
start=input('1st photo=');
finish=input('last photo=');
TUBEPOS=input('tube position=');
filequantity=finish-start;
% tube dimensions
B=input('value for B (pixels)=');
PhotoCentreX=input('Photo Centre, X Coordinate= ');
PhotoCentreY=input('Photo Centre, Y Coordinate= ');
% loadings
eval(['A=load(''PIV_S' num2str(start, '%04.0f') '_S' num2str(finish,
'%04.0f') '.txt'',''r'' );']); %variable
patchnumber=length(A(:,1));
for i=1:patchnumber
      A(i, 10)=A(i, 2)-PhotoCentreX;        %distance from centre of
photo
      A(i, 12)=A(i, 2)-PhotoCentreY;        %distance from centre of
photo
      A(i, 11)=abs(A(i, 10));
      A(i, 13)=abs(A(i, 12));
    if A(i, 10)<=-650
        A(i,  2)=A(i,  2)-(5.2362*(10^-6)*(A(i,  11))^2-0.006839*A(i,
11)+2.3654);
    elseif A(i, 10)>-650 && A(i, 10)<=0
        A(i, 2)=A(i, 2);
    elseif A(i, 10)<=650 && A(i, 10)>0
        A(i, 2)=A(i, 2);
    elseif A(i, 10)>650
        A(i,  2)=A(i,  2)+(5.2362*(10^-6)*(A(i,  11))^2-0.006839*A(i,
11)+2.3654);
    end
     if A(i, 12)<=-650
        A(i,  3)=A(i,  3)-(5.2362*(10^-6)*(A(i,  13))^2-0.006839*A(i,
13)+2.3654);
    elseif A(i, 12)>-650 && A(i, 12)<=0
        A(i, 3)=A(i, 3);
    elseif A(i, 12)<=650 && A(i, 12)>0
        A(i, 3)=A(i, 3);
    elseif A(i, 12)>650
        A(i,  3)=A(i,  3)+(5.2362*(10^-6)*(A(i,  13))^2-0.006839*A(i,
13)+2.3654);
    end
end
for i=1:patchnumber-1
    originalcorrectedspacing(i)=sqrt((A(i+1,  2)-A(i,  2))^2+(A(i+1,
3)-A(i, 3))^2);
end
% required files
DATAMATRIX=zeros(filequantity,  (4+4*(patchnumber-1)));  %predefines
size of matrix, to speed up process
DATAMATRIX(:,1)=DATAMATRIX(:,1)+  start;  %fills  column  1,  gives
original photo number
for n=start:1:(finish-1)
    DATAMATRIX(n+1-start,2)=n+1;  %  fills  column  2,  gives  current
photo number
```

```
    DATAMATRIX(n+1-start,3)=B;   % fills column 3, gives value for B
    DATAMATRIX(n+1-start,4)=TUBEPOS;
    eval(['A=load(''PIV_S'     num2str(start,     '%04.0f')     '_S'
num2str(n+1, '%04.0f') '.txt'',''r'' );']); % loading data, 1 file
per loop %variable
    for i=1:patchnumber
        A(i,  10)=A(i,  4)-PhotoCentreX;  %distance  from  centre  of
photo
        A(i, 11)=abs(A(i, 10));
        A(i,  12)=A(i,  5)-PhotoCentreY;  %distance  from  centre  of
photo
        A(i, 13)=abs(A(i, 12));
        if A(i, 10)<=-650
        A(i,  4)=A(i,  4)-(5.2362*(10^-6)*(A(i,  11))^2-0.006839*A(i,
11)+2.3654);
        elseif A(i, 10)>-650 && A(i, 10)<=0
        A(i, 4)=A(i, 4);
         elseif A(i, 10)<=650 && A(i, 10)>0
        A(i, 4)=A(i, 4);
        elseif A(i, 10)>650
        A(i,  4)=A(i,  4)+(5.2362*(10^-6)*(A(i,  11))^2-0.006839*A(i,
11)+2.3654);
        end
          if A(i, 12)<=-650
        A(i,  5)=A(i,  5)-(5.2362*(10^-6)*(A(i,  13))^2-0.006839*A(i,
13)+2.3654);
        elseif A(i, 12)>-650 && A(i, 12)<=0
        A(i, 5)=A(i, 5);
         elseif A(i, 12)<=650 && A(i, 12)>0
        A(i, 5)=A(i, 5);
        elseif A(i, 12)>650
        A(i,  5)=A(i,  5)+(5.2362*(10^-6)*(A(i,  13))^2-0.006839*A(i,
13)+2.3654);
        end
    end


    for j=1: patchnumber-1
    eval(['strain'  num2str(j)  '=(sqrt((A('  num2str(j+1)  ',4)-A('
num2str(j) ',4))^2+(A(' num2str(j+1) ', 5)-A(' num2str(j) ', 5))^2)-
originalcorrectedspacing('             num2str(j)             '))*(-
100)/originalcorrectedspacing (' num2str(j) ');' ]); % Note: strain
is a function of spacing, not patch size
    eval(['DATAMATRIX('  num2str(n+1-start)  ','  num2str(4+4*j)  ')=
strain' num2str(j); ]); % calculates negative strain line by line
    DATAMATRIX(n+1-start,1+4*j)=(A(j+1,4)+A(j,4))/2;  %  calculates
soil element location, as the average between the x values for the
patch centroids
    DATAMATRIX(n+1-start,2+4*j)=            DATAMATRIX(n+1-start,4)-
DATAMATRIX(n+1-start,1+4*j);  % calculates z, as defined by "tube
position-soil element centroid"
    DATAMATRIX(n+1-start,3+4*j)=        DATAMATRIX(n+1-start,2+4*j)/
DATAMATRIX(n+1-start,3);          % calculates z/B
    end

end

save('DataMatrixExtrusionCentrelineCorrected', 'DATAMATRIX')
-----------------------------------------------------------------
```

Appendix K Project Costs

The following is an approximate breakdown of the material and equipment costs associated with this research. These are less than could be expected for a PIV system using a laser, which would also require a dedicated laser dark room and necessary protective equipment.

Item	Approximate Cost
Consolidation and Driving Rigs	£2000 plus technician time (4 months)
Two Perspex Boxes	£200 plus technician time (2 months)
Monitoring and Extrusion Rig	£100 plus technician time (1 months)
Vacuum Chamber	£500
Photographic Equipment	£1600
Glass Tubes	£80 for material and £200 for manufacture
Oil	£1500
Amorphous Silica	£600
Consumables (PPE, Glassware, Laboratory Equipment, etc)	£500